Understanding the role of mTORC1 and mTORC2 in embryonic and adult myogenesis

Inauguraldissertation

zur

Erlangung der Würde eines Doktors der Philosophie

vorgelegt der

Philosophisch-Naturwissenschaftlichen Fakultät

der Universität Basel

von

Nathalie Rion

aus Anniviers (VS), Schweiz

Basel, 2018

Genehmigt von der Philosophisch-Naturwissenschaftlichen Fakultät

auf Antrag von

Prof. Dr. Markus A. Rüegg

Prof. Dr. Christoph Handschin

Basel, den 12.12.2017

Prof. Dr. Martin Spiess

Table of Contents

1. Acknowledgements

First of all, I would like to thank Prof. Markus A. Rüegg for giving me the opportunity to perform my PhD thesis in his lab. During the last four years, it was a great pleasure for me to work on those projects with all its challenges, drawbacks and success. I highly appreciated his mentorship, guidance and support allowing me to learn and grow in the research and academic field. Thank you Markus for always having your door open for questions and concerns and for your personal support of my scientific career path!

Secondly, I would like to thank Prof. Christoph Handschin and Prof. Fiona Doetsch for accepting to be part of my PhD committee and for giving me critical advice. The fruitful discussions helped me to find the most interesting and promising paths in my projects and gave me a lot of personal guidance!

I thank Dr. Perrine Castets for her supervision and guidance especially in the beginning of my PhD. She taught me the important techniques and how to approach research questions, including how to organize and structure the projects most efficiently with a very high quality and ethical standard. Her supervision was not only restricted to the beginning of my PhD, she remained an extremely important mentor, who always found time to discuss results, give general advice and motivated me to exit from my comfort zone. Thank you very much Perrine, without you I would not stand at the same position as today!

Also my other lab members supported me during my PhD and made these four years a very pleasant and great experience! Thank you all for fruitful discussions, funny times and supporting gestures! Especially I would like to mention Dr. Shuo Lin, because he was a great help and very patient in supporting me in mouse experiments. I also would like to thank Malek Belguith, whom I supervised during his master thesis in our lab. It was a challenging experience for me, but I highly enjoyed working with you and learnt a lot from you! Additionally, I would like to mention my coffee gang and my lab buddy sitting next to me, thank you for the amazing time together! :-)

Lastly, I would like to thank my family and friends, who gave me a lot of support and motivation in the last years. Even though they did not understand the scientific part, they knew when and what support I needed during all the ups and downs in the last four years! Especially, William Duong stayed always at my side, listened to me, made me laugh after a challenging day and gave me a lot of personal and scientific advice! Thank you very much that I could always count on you, I would not have succeeded without you!!

2. List of abbreviations

4E-BP1	eIF4E binding protein 1
Akt	Protein kinase B
AMPK	AMP-activated protein kinase
aPKC	Atypical protein kinase C
bHLH	basic Helix-Loop-Helix (sequence motif)
BrdU	5-bromo-2'-deoxyuridine
Ctrl	Control
Ctx	Cardiotoxin (snake venom)
DEPTOR	DEP domain-containing mTOR-interacting protein
DTA	Diphtheria toxin
E	Embryonic day
EDL	Extensor Digitorum Longus (muscle)
EGFP	Enhanced green fluorescent protein
eIF2α	Eukaryotic translation initiation factor 2A
eIF4E / B / F / A	Eukaryotic translation initiation factor 4E / 4B / 4F / 4A
embMHC	Embryonic myosin heavy chain
FAP	Fibro-adipogenic progenitor
FGF	Fibroblast growth factor
FKBP12	FK506-binding protein 12
GAP	GTPase activating protein
Gastro	Gastrocnemius (muscle)
Grb10	Growth factor receptor-bound protein 10
GTPases	Small guanosine triphosphatases
H & E	Hematoxylin & Eosin (staining)
HGF	Hepatocyte growth factor
HSA	Human skeletal actin
IGF	Insulin-like growth factor
IL-6	Interleukin 6
IMP1	IGF2-mRNA binding protein 1
IRS1	Insulin-receptor substrate 1
LncRNA	Long non-coding RNA
M-cadherin	Myotubule cadherin
Mcam	Melanoma cell adhesion molecule
MEF	Mouse embryonic fibroblasts
Megf10	Multiple EGF like domains 10
miR	microRNA
mLST8	Mammalian lethal with SEC13 protein 8
MRF	Myogenic regulatory factor
MRF4	Myogenic regulatory factor 4
mSin1	Mammalian stress activated protein kinase interacting protein 1
mTOR	Mammalian / mechanistic target of rapamycin
mTORC1 / mTORC2	mTOR complex 1 / 2
Myf5	Myogenic factor 5

Myh3 / 7 / 8	Myosin heavy chain 3 / 7 / 8
Nfix	Nuclear factor I x
p38 α/β MAPK	p38 α/β mitogen-activated protein kinase
PAR	Partitioning defective
Pax3/7	Paired homeobox transcription factor 3/7
PCP	Planar cell polarity
PDCD4	Programmed cell death protein 4
PDGF	Platelet-derived growth factor
PDK1	Phosphoinositide dependent kinase 1
pH2AX	phospho-Histone H2A.X
PI3K	Phosphoinositide 3 kinase
PKCα	Protein kinase C α
PRAS40	Proline-rich Akt substrate 40 kDa
Protor 1 / 2	Protein observed with rictor 1 / 2
RAmKO	Raptor muscle knockout (HSA-Cre driven)
RAmyfKO	Raptor Myf5-Cre driven muscle knockout (muscle progenitors and precursors)
Raptor	Regulatory associated protein of mTOR
RAscKO	Raptor satellite cell knockout (Pax7-CreErt2 driven)
Rb	Retinoblastoma protein
Rheb	Ras homolog enriched in brain
Rictor	Rapamycin insensitive companion of mTOR
RImKO	Rictor muscle knockout (HSA-Cre driven)
RImyfKO	Rictor Myf5-Cre driven muscle knockout (muscle progenitors and precursors)
ROCK1	Rho-associated kinase 1
S6	40S ribosomal protein S6
S6K1	S6 kinase 1
SGK1	Serum- and glucocorticoid-regulated kinase1
shRNA	Small hairpin RNA
Sol	Soleus (muscle)
SPAR	Small regulatory polypeptide of amino acid response
SREBP	Sterol regulatory element-binding protein
TA	Tibialis anterior (muscle)
TNFα	Tumor necrosis factor α
TOR	Target of rapamycin
TSC1/TSC2	Tuberous sclerosis complex 1/2 complex
TSCmKO	TSC1 muscle knockout (HSA-Cre driven)
ULK1	Unc-51 like autophagy activating kinase 1
v-ATPase	Vacuolar H^+-ATPase
Vcam-1	Vascular cell adhesion molecule 1

3. Abstract

Myogenesis describes the formation of skeletal muscle fibers during embryogenesis and their regeneration of injury in the adult. The formation of myofibers includes the commitment of cell progenitors into the muscle lineage, their amplification and subsequent differentiation and fusion into multi-nucleated myotubes. The mammalian target of rapamycin (mTOR) assembles into two distinct complexes, termed complex 1 (mTORC1) and 2 (mTORC2), and controls cellular growth and metabolism, in response to nutrients and extracellular signals. The mTOR signaling pathway is crucial for homeostasis of mature skeletal muscle and mTOR deregulation in muscle results in progressive myopathies. Since myogenesis is determined by a complex regulatory network involving growth factors and external stimuli, I investigated the function of mTOR signaling in embryonic and adult myogenesis.

This PhD thesis describes the role of mTORC1 and mTORC2 in embryonic and adult myogenesis using genetically modified mice. Depletion of raptor, an essential protein of mTORC1, in muscle progenitors caused the mice to die perinatally because of severe defects in muscle development. I observed that mTORC1 was highly active in embryonic muscle progenitors and precursors and became downregulated in differentiating and fusing myocytes, suggesting a predominant role in muscle cell commitment and proliferation. Accordingly, raptor-depleted myoblasts showed severe defects in proliferation, most probably caused by reduced rates of protein synthesis. Furthermore, loss of mTORC1 reduced, but did not abolish differentiation of myoblasts. Thus, the myogenic process was still completed, but less efficiently, in the absence of mTORC1. To investigate the role of mTORC1 in adult myogenesis, depletion of raptor was induced in adult muscle stem cells, called satellite cells. mTORC1 depletion did not affect the quiescence of satellite cells but delayed their activation upon external stimuli. Furthermore, I established that satellite cells deficient for raptor proliferated and differentiated less efficiently, resulting in poor regeneration following muscle injury.

Mice deficient for mTORC2 signaling in developing muscle were viable and showed no histological and functional alterations of skeletal muscle. Moreover, depletion of rictor in embryonic muscle progenitors did not affect the number of satellite cells and their myogenic function in adult skeletal muscle upon injury. In particular, rictor-depleted satellite cells did not differ from control cells in their proliferation, differentiation and fusion capacity. However, the number of satellite cells decreased following repeated muscle injuries in the absence of mTORC2. Furthermore, the number of quiescent satellite cells declined during physiological aging in mutant mice, causing an impairment in the regenerative capacity at progressed age.

In conclusion, I established that mTORC1, but not mTORC2 signaling is required for the formation of skeletal muscle during embryogenesis and for the regeneration of the tissue following severe muscle damage. I found that loss of mTORC1 reduces protein synthesis and thereby limits the proliferation and differentiation capacity of myoblasts during embryonic and adult myogenesis. In contrast, mTORC2 is dispensable for the myogenic function of myoblasts to proliferate, differentiate and fuse, but is required for the maintenance of the muscle stem cell pool during aging and after muscle injury. Overall, these results are of major importance as they extent our knowledge about the distinct roles of mTORC1 and mTORC2 in the myogenic process and the maintenance of the muscle stem cell pool. As mTOR is a central regulatory hub, integrating the metabolic status of a cell and translating those signals into proteostatic processes, my work has established that these mTOR-controlled functions are important in muscle precursors. These results may open new avenues regarding pathological conditions, such as aging or metabolic muscle disorders, which have also been related to mTOR deregulation.

4. Introduction

Muscle is the most abundant tissue in the human body and is subdivided into skeletal, smooth and cardiac muscles. Skeletal muscle (simply referred to as muscle, in the following) corresponds to 40 % of the total body mass and is a type of striated muscle controlled by the somatic nervous system. The main function of muscle is to generate force necessary for locomotion and precise movements in the environment, and to control mechanical activity, including respiration and posture maintenance. Skeletal muscle is composed of differentiated, post-mitotic myofibers that consist of repetitions of actin and myosin filaments, which are responsible for its contractile properties. Since muscle is a metabolic organ that responds fast to its environment, muscle development, growth and regeneration occur throughout life of an organism. Myogenesis corresponds to the formation of skeletal muscle fibers during embryonic muscle development and during muscle regeneration in adult mice. Even though the mechanisms of myogenesis, including cell commitment, proliferation, differentiation and fusion, are similar at all developmental stages, the morphology and functionality of the generated muscles varies depending on the needs of the animal (Biressi et al., 2007). Since skeletal muscle is a highly plastic organ, its function is often compromised in pathological conditions, such as muscular dystrophies, which leads to an imbalance between muscle degeneration and regeneration and consequently in a decline in muscle homeostasis. During natural aging, muscles develop sarcopenia which is characterized by the loss in muscle mass and force (Evans and Campbell, 1993). Sarcopenia strongly affects muscle function and therefore results progressively in physical disability, a reduction in the quality of life and increases morbidity and mortality. Hence, it is of major importance to study and understand the pathways and mechanisms controlling skeletal muscle development, homeostasis and regeneration.

4.1 Skeletal muscle development during embryogenesis

All limb and trunk skeletal muscles originate, in vertebrates, from the paraxial mesoderm formed at early stages in the embryo (Comai and Tajbakhsh, 2014). The paraxial mesoderm gives rise by segmentation and epithelialization to somites which differentiate into 4 independent compartments on either side of the neural tube (Figure 1) (Deries and Thorsteinsdottir, 2016): 1) the ventral sclerotome which differentiates into axial bones; 2) the syndetome that gives rise to tendons and connective tissue; 3) the dorsal dermomyotome containing muscle and brown fat progenitors, endothelial cells and cells contributing to the dorsal dermis; and 4) the myotome which originates from muscle progenitors delaminating from the dorsomedial part of the dermomyotome. While the dorsomedial, epaxial part of the myotome forms the back and intercostal muscles, the

ventrolateral, hypaxial myotome generates the diaphragm, limb and abdominal muscles. Of note, head and neck muscles derive from the cranial mesoderm which lacks any signs of segmentation (Comai and Tajbakhsh, 2014).

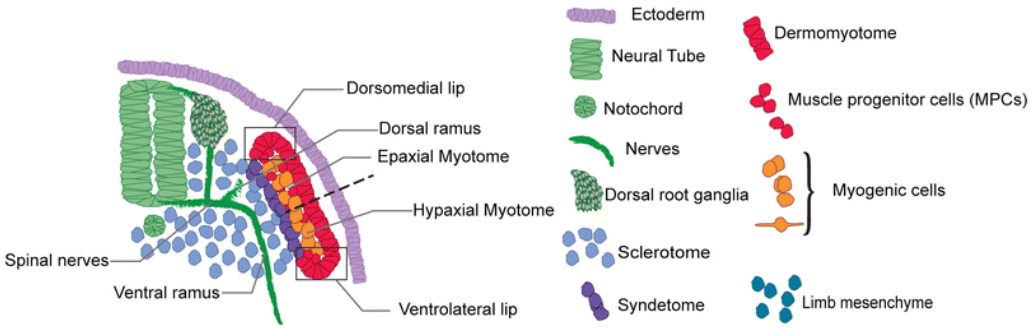

Figure 1. At E10.5, the somites have formed four different compartments: the sclerotome, syndetome, dermomyotome and myotome (Deries and Thorsteinsdottir, 2016).

Molecular regulation of embryonic myogenesis

Myogenesis is regulated by a network of transcription factors expressed in a cell autonomous manner and through cell-cell communication. The first metameric structures formed in embryo are the somites which are specified by local oscillations of gene expression and by morphogen gradients, including Notch, Wnt, fibroblast growth factors (FGF) and retinoic acid (Bentzinger et al., 2012). Prior to segmentation, at embryonic day (E) 8, cells in the paraxial mesoderm start to express Pax3, which belongs to the *Pax* family of transcription factors characterized by their paired domain allowing sequence-specific binding to DNA (Buckingham and Relaix, 2007). Pax3 and Pax7 are two *Pax* members that regulate skeletal muscle development, while other *Pax* genes are important for the development of other tissues, *e.g.* central nervous system, skeleton, thymus and kidney. Pax3 remains transcribed in somites and is restricted around E10 to the dorsomedial and ventrolateral dermomyotome, while being replaced in the central part of the dermomoytome by Pax7 (Murphy and Kardon, 2011). Pax3 expression is essential for the formation of hypaxial muscle of the trunk and for the delamination and migration of muscle progenitors from the dermomyotome in order to form limb muscle (Relaix et al., 2004). In contrast, Pax7 is dispensable for the formation of skeletal muscle since Pax3 is suggested to have a compensatory function during embryonic development (Hutcheson et al., 2009; Seale et al., 2000). However, ablation of Pax7-expressing cells affects later stages of muscle development, causing smaller muscle marked by a reduced number of myofibers formed. Importantly, Pax3- and Pax7-expressing progenitor cells (Figure 2) in the dermomyotome

are not yet committed into the muscle lineage, as they are still capable of downregulating Pax3/7 expression and acquiring a non-myogenic fate (Ben-Yair and Kalcheim, 2005; Esner et al., 2006). Final determination and differentiation into the muscle lineage is controlled by a family of basic-helix-loop-helix (bHLH) transcription factors termed myogenic regulatory factors (MRFs), including Myf5, MyoD, Myogenin and Mrf4. Those factors have been identified on their common expression pattern and their ability to convert non-muscle cells, *e.g*. fibroblasts, into cells capable to fuse into myotubes (Braun et al., 1990; Braun et al., 1989; Edmondson and Olson, 1989; Miner and Wold, 1990; Rhodes and Konieczny, 1989; Weintraub et al., 1991). While the basic domain of MRFs mediates DNA binding, the helix-loop-helix sequences form heterodimers with E proteins that are necessary for the recognition of genomic E boxes present in muscle-specific promoters (Massari and Murre, 2000). The skeletal muscle phenotype of *Myf5*- and *MyoD*-knockout mice was found to be normal (Braun et al., 1992; Rudnicki et al., 1992), suggesting that Myf5 and MyoD share redundant functions during myogenesis. Notwithstanding, *Myf5:MyoD* double-null mice completely lacked skeletal muscle tissue and *MyoG* expression (Rudnicki et al., 1993). Conditional cell ablation approaches, in which diphtheria toxin (DTA) expression was driven in Myf5- or MyoD-expressing cells, first suggested that Myf5 and MyoD independently regulate two functional cell lineages, which can compensate for each other to a large extent (Gensch et al., 2008; Haldar et al., 2008). However, a more recent report refutes this model, claiming that muscle formed in *Myf5^{Cre}-DTA* embryos, described by Gensch et al. and Haldar et al., were generated by non-targeted, escaper cells (Comai et al., 2014). Comai et al. rather found that ablation of Myf5-expressing cells results in severe muscle loss (Comai et al., 2014). Consistently, MyoD(iCre) embryos, expressing DTA in MyoD-expressing cells, showed severe defects in myogenesis accompanied with a loss of Myf5-positive cells, indicating that most muscle progenitors express both transcription factors (Wood et al., 2013). Myf5 and MyoD act as determination factors to commit progenitor cells into the

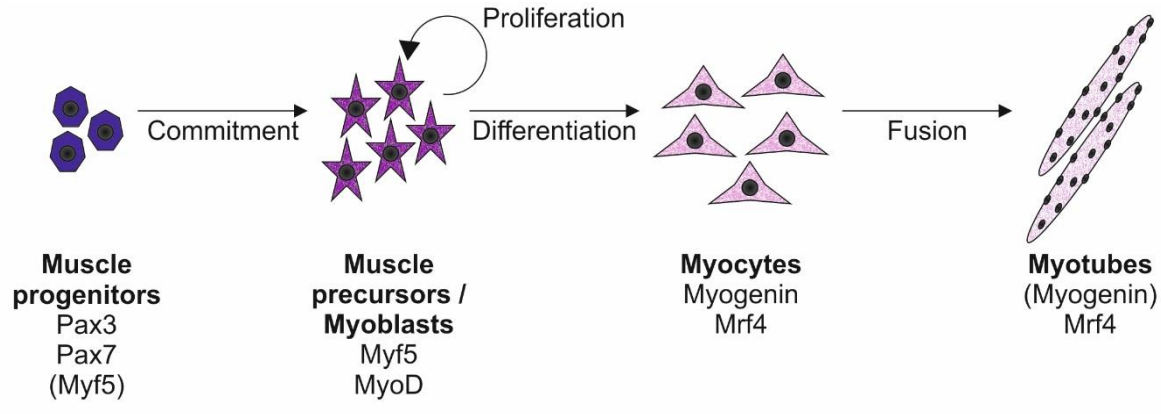

Figure 2. Hierarchy of transcription factors controlling the specification and differentiation of myogenic cells

muscle lineage and induce their transition into muscle precursors, also called myoblasts (Figure 2) (Bentzinger et al., 2012). Mechanistically, Myf5 specifies and initiates skeletal muscle determination by modifying chromatin at its binding sites prior to MyoD expression, but does not yet recruit polymerase II (Conerly et al., 2016). Subsequent expression of MyoD, which binds to the same sites as Myf5 and recruits polymerase II, robustly induces gene transcription for further muscle specification (Conerly et al., 2016). Before entering the differentiation program, muscle precursors undergo extensive proliferation, expanding the population of cells, which will ultimately form post-mitotic, multi-nucleated myotubes (Buckingham et al., 2003). Differentiating myogenic cells are termed myocytes (Figure 2) and are characterized by their elongated shape, their high capacity to fuse together and the expression of *MyoG* (Chal and Pourquie, 2017). *Myogenin*-null mice die perinatally due to severe defects in embryonic muscle development, evidenced by the accumulation of undifferentiated muscle precursors (Hasty et al., 1993; Nabeshima et al., 1993). Hence, myogenin has a unique function in controlling differentiation and subsequent fusion of myocytes. The last member of the MRF family, Mrf4, is genetically linked to *Myf5*; in most *Myf5:MyoD* double-null embryos, *Mrf4* expression is also affected (Kassar-Duchossoy et al., 2004). However, rescue of *Mrf4* expression in *Myf5:MyoD* double-null embryos restored embryonic myogenesis only to some extent (Kassar-Duchossoy et al., 2004), thus indicating that Mrf4 alone is not sufficient to robustly drive skeletal muscle formation autonomously. Interestingly, Mrf4 is the only MRF factor that remains expressed in differentiated, multi-nucleated myotubes (Hinterberger et al., 1991). Furthermore, it was suggested that Mrf4 is necessary for the downregulation of myogenin in postnatal skeletal muscle, therefore providing evidence for a role of Mrf4 in late stages of differentiation and in the maintenance of the differentiated state (Zhang et al., 1995).

Embryonic and fetal wave of myogenesis

During embryogenesis, the myogenic process occurs in successive waves and is therefore divided into embryonic and fetal myogenesis. In mice, embryonic myogenesis finishes around E14.5 with the generation of primary, embryonic myofibers as basic muscle pattern (Biressi et al., 2007). During the second wave of myogenesis, occurring between E14.5 and E17.5, secondary or fetal myofibers are generated and contribute to muscle growth and maturation by increasing the number of fibers and the size of primary fibers (Evans et al., 1994). Peri- and postnatal development of skeletal muscle is driven by muscle progenitors that divide at a slow rate and fuse to adjacent myofibers and by the growth of existing myofibers (Biressi et al., 2007). The switch from embryonic to fetal myogenesis is regulated by the transcription factor Nfix (nuclear factor I x) whose expression is induced by Pax7 in fetal muscle (Messina et al., 2010). Nfix represses embryonic genes and induces the

expression of genes important for fetal myogenesis, including skeletal muscle-specific isoforms of enzymes. Interestingly, primary myofibers express *Myh3*, encoding the embryonic isoform of myosin heavy chain (MHC), and *Myh7*, encoding the slow isoform, and thereby acquire the identity of slow myofibers (type I fibers). In contrast, secondary myofibers become fast, type II fibers, by preferentially expressing *Myh3* and *Myh8* (encoding the fast, perinatal isoform of MHC) (Biressi et al., 2007). *Myh7* is one particular embryonic gene that is directly repressed by Nfix after the transition between embryonic and fetal myogenesis (Messina et al., 2010).

4.2 Myogenesis in adult skeletal muscle

During fetal myogenesis, a portion of Pax3- and Pax7-expressing muscle progenitors retain their uncommitted state and acquire the fate of skeletal muscle stem cells, also termed satellite cells (Kassar-Duchossoy et al., 2005). Even though satellite cells are considered as MRF-negative cells, most of them transiently expressed MyoD prenatally (Kanisicak et al., 2009). During late fetal myogenesis, Pax3/Pax7-positive progenitors colonize nascent myofibers and change their transcriptional program by downregulating Pax3 and inducing the expression of Myf5 (Kassar-Duchossoy et al., 2005; Relaix et al., 2005). Notwithstanding, Pax7 remains constantly and highly expressed in quiescent satellite cells, hence serving as a widely used specific cell marker. In adult skeletal muscle, satellite cells remain quiescent, adopt their specific localization underneath the basal lamina and exhibit a high nucleus-to-cytoplasm ratio (Dumont et al., 2015). The main function of satellite cells is to provide progeny in order to regenerate muscle fibers upon stimuli from their environment, such as muscle damage. Accordingly, satellite cells turn into an activated state which is accompanied by metabolic and transcriptional changes promoting their proliferation and differentiation. Activated satellite cells pass through the myogenic process, which shows similarities to embryonic muscle development. Thus, the process of skeletal muscle regeneration is also termed adult myogenesis. Additionally, adult myogenesis includes satellite cell self-renewal, which corresponds to the return of a portion of activated satellite cells back into quiescence to ensure further rounds of degeneration / regeneration.

Molecular regulation of satellite cell quiescence

Quiescent satellite cells tightly associate to myofibers through adhesion molecules, such as M-cadherin, Mcam, Megf10, integrin α4β1 and Vcam-1 (Brohl et al., 2012). Defects in adhesion or spontaneous activation of satellite cells promote their migration and cause them to localize to the myofibrillar interstitial space. The microenvironment surrounding satellite cells is termed the niche, which supports the self-renewal of the stem cell pool and prevents

their activation (Jones and Wagers, 2008; Scadden, 2006). The niche is a complex network including blood vessels, stromal cells, soluble factors, extracellular matrix, neural inputs and adhesion molecules. One important, extrinsic mediator of satellite cell quiescence is the Notch signaling: myofibers express the Notch ligand Delta 1 and satellite cells the Notch receptor and the co-receptor syndecan-3 facilitating Notch signaling transduction (Bjornson et al., 2012; Mourikis et al., 2012; Pisconti et al., 2010). Inhibition of Notch components or syndecan-3 causes the satellite cells to exit quiescence and to differentiate spontaneously, leading to self-renewal impairments (Dumont et al., 2015). Maintenance of the quiescent state of satellite cells also requires the inhibition of signaling pathways promoting their proliferation. In particular, FGF2 has been shown to induce satellite cell activation (Jones et al., 2001; Sheehan and Allen, 1999; Yablonka-Reuveni et al., 1999). Quiescent satellite cells display high expression of sprouty1, which counteracts FGF2 signaling and thereby actively maintains their quiescent state (Chakkalakal et al., 2012; Shea et al., 2010). Quiescent satellite cells strongly express cyclin dependent-kinase inhibitors, *e.g.* p21, p27 and p57, while genes controlling DNA replication and cell cycle, such as cyclin A2, cyclin B1, cyclin E2 and survivin, are repressed (Cheung and Rando, 2013). The oncogene Dek also directly regulates myogenic progenitor proliferation: upon asymmetric cell division, Dek sequesters to the more committed, differentiated daughter cell (Cheung et al., 2012). Interestingly, *Dek* is post-transcriptionally suppressed by miR-489 in quiescent satellite cells in order to prevent activation. Additionally, quiescent satellite cells reduce their metabolism to a minimal level and mostly depend on fatty acid oxidation as an energy source. They undergo a metabolic switch during their transition to an activated state by using glycolysis to produce ATP rapidly (Ryall et al., 2015). Phosphorylation of the eukaryotic translation initiation factor 2A (eIF2α) in quiescent satellite cells leads to the repression of general mRNA translation, only allowing translation of specific mRNA selected dependent on their uORFs (Zismanov et al., 2016). Upon satellite cell activation, eiF2α is dephosphorylated, which induces protein synthesis required for their function in an activated state. In particular, *Myf5* mRNA is sequestered in RNA granules in quiescent cells, but is translocated to polysomes and thus translated upon activation of the cells (Crist et al., 2012). Interestingly, it was proposed that two distinct phases of quiescence exist: one being more dormant and the other one being closer to activation, called “alerted state”, which is characterized by an increase in cell size and a faster cell cycle entry (Rodgers et al., 2014). This alerted state of satellite cell is initiated upon a systemic injury, which induces hepatocyte growth factor (HGF) binding to cMet and consequently activation of mTORC1.

The process of muscle regeneration

Skeletal muscle regeneration is provoked in response to muscle damage either caused by direct trauma from extensive physical activity or induced by pathological conditions, such as neurological dysfunction or innate genetic defects. For successful restoration into a well-innervated, fully vascularized and contractile skeletal muscle, the extracellular matrix is required as a template for the formation of myofibers (Charge and Rudnicki, 2004). Skeletal muscle regeneration includes an initial phase of muscle degeneration accompanied by an inflammatory response and followed by a secondary phase defined by the restoration of myofibers. Skeletal muscle degeneration is initiated by complete necrosis of muscle fibers. Already during the phase of muscle degeneration and the boost of pro-inflammatory cytokines, quiescent satellite cells get activated by various signals released from the extracellular matrix (*e.g.* FGF2, HGF and nitric oxide) and start to express MyoD (myoblast state) (Charge and Rudnicki, 2004; Dumont et al., 2015). Myoblasts exhibit the capacity to undergo proliferation, which is controlled by signaling pathways and multiple factors that either increase cell cycle progression or repress premature differentiation. Interestingly, the first ~30 – 40 % of divisions are asymmetric, while afterwards, symmetric divisions ensure expansion of the pool of muscle precursors, and the maintenance of mother cells with stemness features (Le Grand et al., 2009; Yennek et al., 2014). During asymmetric cell divisions, the daughter cell attached to the basal lamina keeps its stem cell fate and remains Myf5-negative. In contrast, in the more committed, apical daughter cell, *Myf5* transcription is induced when Pax7 is methylated by the arginine methyltransferase Carm1 (Kawabe et al., 2012; Kuang et al., 2007; McKinnell et al., 2008). Interestingly, 10 % of Pax7-positive satellite cells have never expressed *Myf5*, suggesting that the satellite cell pool is heterogeneous and that some satellite cells have a higher propensity to contribute to the cell reservoir following activation (Kuang et al., 2007). Engraftment studies revealed that Myf5-negative satellite cells have a higher self-renewal potential (Kuang et al., 2007). Symmetric, planar division of Myf5-negative satellite cells is promoted by the planar cell polarity (PCP) pathway, which is considered as a non-canonical Wnt pathway, regulating cytoskeleton reorganization and gene expression (Le Grand et al., 2009). Satellite cell self-renewal is not only determined by asymmetric and symmetric cell division, but involves also satellite cell intrinsic signaling pathways and multiple extrinsic factors from the niche, which affect their return into quiescence and the maintenance of a stem cell fate. In parallel, regulation of cell commitment during asymmetric cell division also relies on specific signaling pathways and polarity proteins. It was reported that the partitioning defective (PAR) complex, consisting of PAR-3 and PAR-6, and the atypical protein kinase C (aPKC) polarize to the more committed cell, where they activate p38α/β MAPK signaling and thereby induce the transcription of *MyoD* (Troy et al., 2012). After several rounds of cell

divisions, MyoD-expressing myoblasts permanently exit the cell cycle and enter the differentiation program by inducing the expression of cell cycle inhibitors (*e.g.* p21 and p57), and upregulating *Myogenin* and *Mrf4* expression (Cornelison et al., 2000; Halevy et al., 1995; Hollenberg et al., 1993). Similar to embryonic myogenesis, differentiating myoblasts in regenerating adult skeletal muscle undergo cell-cell fusion to form multi-nucleated myotubes that mature into specialized, innervated myofibers (Dumont et al., 2015).

Efficient skeletal muscle regeneration not only depends on satellite cells, since non-myogenic cells like immune cells and fibro-adipogenic progenitors (FAPs) also contribute to the restoration of myofibers following muscle damage. Skeletal muscle resident leukocytes, such as mast cells, macrophages and circulating monocytes, sense metabolites, DNA, RNA and other molecules released by permeable, damaged muscle fibers and thereby get activated and secrete additional cytokines. These factors, *e.g.* TNFα, tryptase and IL-6, promote satellite cell activation and proliferation, as well as the recruitment of additional, circulating leukocytes (Chen et al., 2007; Duchesne et al., 2011; Serrano et al., 2008). After a first invasion of granulocytes, which clear muscle debris by phagocytosis, M1 macrophages accumulate and induce a pro-inflammatory phase and myoblast proliferation by repressing early differentiation (Dumont et al., 2015). Subsequently, M2 macrophages, corresponding to an anti-inflammatory response, mediate myoblast differentiation and myofiber growth. Skeletal muscle resident FAPs are initially stimulated upon muscle injuries to amplify and provide pro-myogenic cues promoting the regenerating phase (Joe et al., 2010; Uezumi et al., 2010). Subsequently, the differentiation of FAPs is repressed by the presence of restored myofibers. However, in skeletal muscle undergoing chronic degeneration and regeneration, *e.g.* in muscular dystrophies, or exhibiting an impaired regenerative capacity, the dynamics of FAPs is not repressed, hence causing them to differentiate into fibroblasts and adipocytes, which is often observed as fatty degeneration (Joe et al., 2010; Mozzetta et al., 2013; Uezumi et al., 2010).

Satellite cell function in aging

During physiological aging, skeletal muscles get sarcopenic, which is characterized by an atrophy of type II (fast) myofibers, an heterogeneity in fiber size, an accumulation of collagen-rich and fatty tissue, and a reduced oxidative capacity (Sousa-Victor and Munoz-Canoves, 2016). Sarcopenia is accompanied by a decline in the regenerative capacity of aged skeletal muscle (Brack and Munoz-Canoves, 2016). Even though over time satellite cells fuse and contribute to their adjacent myofibers in the absence of muscle damage, depletion of the satellite cell pool in young mice does not affect the maintenance of the cross-sectional area, therefore indicating that a deficiency in satellite cell homeostasis

during aging is not the main cause of sarcopenia (Fry et al., 2015; Keefe et al., 2015). The lower regenerative potential of aged skeletal muscle results partially from the decrease in satellite cell content during aging (Shefer et al., 2006; Sousa-Victor and Munoz-Canoves, 2016). The decline in the myogenic potential of aged satellite cells also correlates with a lower proliferation and differentiation efficiency. Furthermore, it was established that satellite cells switch from their reversible quiescent state into senescence during geriatric age, corresponding to an age of more than 24 months in mice (Sousa-Victor et al., 2014). Derepression of $p16^{INK4a}$ (Cdkn2a) contributes to satellite cell senescence by causing the de-phosphorylation of the retinoblastoma protein (Rb) and the repression of E2F target genes, hence leading to an irreversible cell cycle exit and the loss of self-renewal. Loss of proteostasis resulted in oxidative stress and ROS production, which was unraveled as the key epigenetic regulator of $p16^{INK4a}$ in aging satellite cells. Moreover, in senescent satellite cells, foci with the phosphorylated form of the histone H2AX (pH2AX), a biomarker for DNA damage, accumulate (Sousa-Victor et al., 2014). Recently, it was discovered that the autophagy flux, responsible for the turnover of proteins and organelles, is dysfunctional in aged satellite cells (Garcia-Prat et al., 2016). Age-dependent changes in the satellite cell niche also contribute to the loss of stem cell quiescence and function during physiological aging. Aged skeletal muscle fibers express increased levels of FGF2, which correlates with a decreased expression of the FGF signaling inhibitor sprouty1 in satellite cells (Chakkalakal et al., 2012; Shea et al., 2010). Consequently, FGF2 signaling drives aged satellite cells to exit quiescence and enter the myogenic program without replenishing the stem cell pool. Mechanistically, FGF stimulation in the aged niche chronically activates p38α/β MAPK signaling via the FGF receptor-1 (FGFR1) expressed in resident satellite cells, which prevents their asymmetric cell division (Bernet et al., 2014). Hence, two committed daughter cells are generated and the self-renewal capacity of aged satellite cells abrogated. Overall, several cell-intrinsic alterations and external signals derived from the niche, determine changes in the fate and function of satellite cells during physiological aging.

4.3 The mTOR signaling pathway

The mammalian (or mechanistic) target of rapamycin (mTOR) is a serine/threonine protein kinase that controls cellular growth and metabolism, by integrating environmental cues including amino acids, growth factors and cellular energy such as ATP. Rapamycin, clinically termed sirolimus, is generated by the bacteria *Streptomyces Hygroscopicus* and was discovered because of its toxic, anti-proliferative effect in yeast. Rapamycin forms a gain-of-function complex with the 12-kDa peptidyl-prolyl-isomerase FK506-binding protein

(FKBP12), which binds to the mediators TOR1 and TOR2 (Cafferkey et al., 1993; Kunz et al., 1993). Later, mTOR was identified as the homolog protein in mammals (Brown et al., 1994; Sabatini et al., 1994; Sabers et al., 1995). The catalytic subunit mTOR assembles into two structurally and functionally distinct complexes, termed mTOR complex 1 (mTORC1) and mTOR complex 2 (mTORC2) (Figure 3). Both complexes include mammalian lethal with sec-13 protein 8 (mLST8), DEP domain containing mTOR-interacting protein (DEPTOR) and Tti1/Tel2 complex (Laplante and Sabatini, 2012). mTORC1 additionally contains regulatory-associated protein of mTOR (raptor) and proline-rich Akt substrate 40 kDa (PRAS40), whereas rapamycin-insensitive companion of mTOR (rictor), mammalian stress-activated map kinase-interacting protein 1 (mSin1) and protein observed with rictor 1 and 2 (protor1/2) are specific of mTORC2 (Laplante and Sabatini, 2012). In mammals, rapamycin directly interacts and inhibits mTORC1, but not mTORC2 (Brown et al., 1994; Sabatini et al., 1994). However, prolonged rapamycin treatment also disrupts and affects mTORC2 (Lamming et al., 2012).

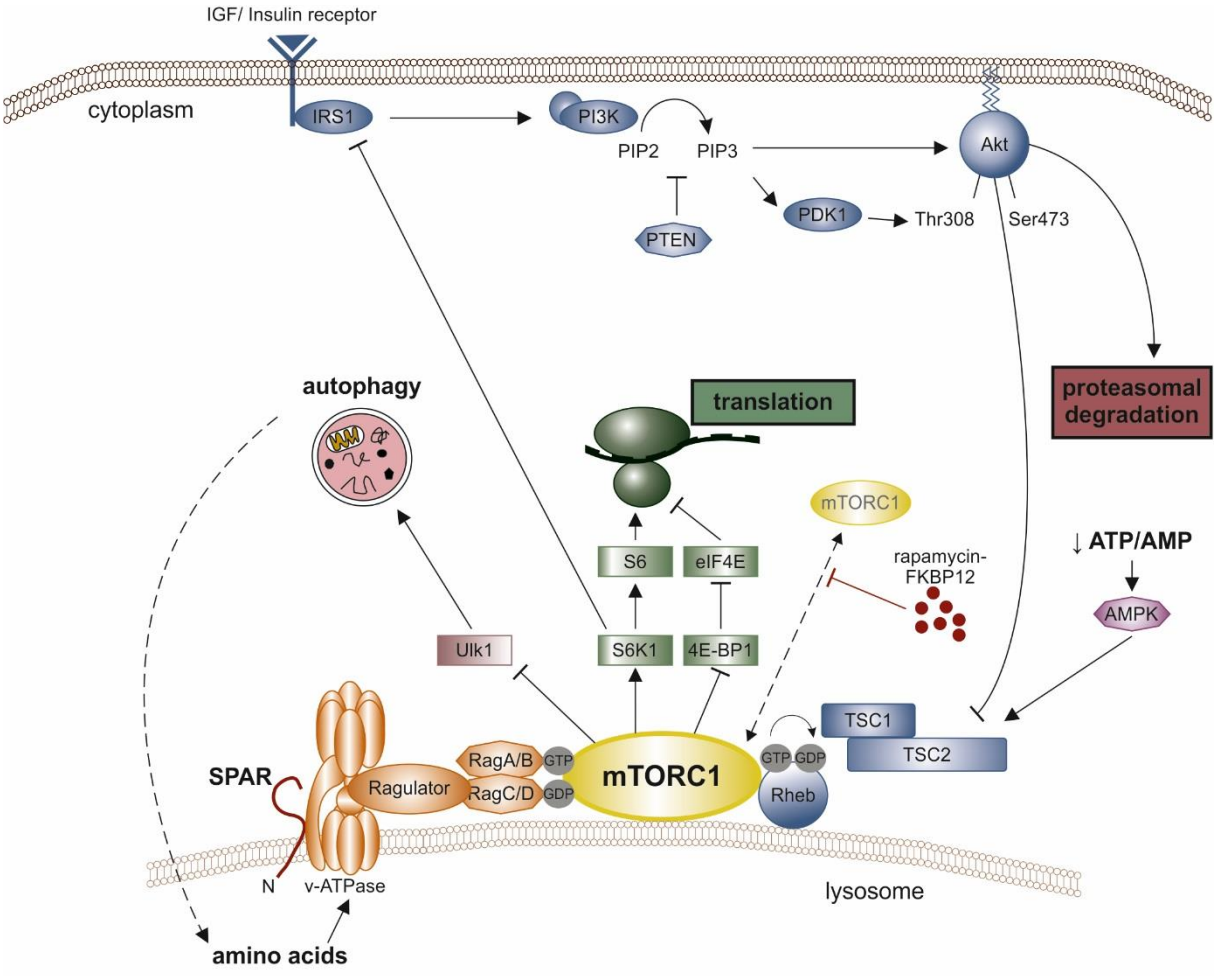

Figure 3. The mTORC1 signaling pathway

Upstream of mTORC1

As a key sensor of the nutritive status of the cell, several upstream pathways control mTORC1 activation. Binding of growth factors, including insulin and insulin-like growth factors (IGF), to the receptor tyrosine kinase on the cell surface promotes the intracellular recruitment and tyrosine phosphorylation of the adapter protein insulin-receptor substrate 1 (IRS1) and subsequent activation of the lipid kinase phosphatidylinositol-4,5-bisphosphate 3-kinase (PI3K) (Figure 3) (Laplante and Sabatini, 2009). Consequently, the serine/threonine protein kinase B (PKB/Akt) is recruited to the membrane, where the phosphoinositide-dependent kinase 1 (PDK1) phosphorylates its activation loop (at the Threonine 308) (Alessi et al., 1997; Stokoe et al., 1997; Wick et al., 2000). Akt phosphorylates tuberous sclerosis complex 2 (TSC2), which disrupts the interaction with TSC1 (tuberous sclerosis complex 1) and leads to their dissociation from the lysosomal membrane (Inoki et al., 2002; Manning et al., 2002; Menon et al., 2014; Potter et al., 2002). The TSC complex functions as a GTPase-activating protein (GAP) for the small GTPase termed Ras homolog enriched in brain (Rheb) (Inoki et al., 2003a; Tee et al., 2003). GTP-loaded Rheb stimulates the kinase activity of mTORC1 (Long et al., 2005) and thereby regulates mTORC1 downstream signaling in yet unknown mechanisms. Akt also activates mTORC1 independently from TSC1/2, by phosphorylating and inactivating PRAS40, which functions as an inhibitor through its binding to raptor (Sancak et al., 2007; Thedieck et al., 2007; Vander Haar et al., 2007; Wang et al., 2007). Moreover, mTORC1 activation is also controlled by the availability of cytosolic and intra-lysosomal amino acids *via* distinct mechanisms (Figure 3). Lysosomal amino acids, in particular arginine, are sensed by SLC38A9, a lysosomal transmembrane protein involved in amino acid transport and integrated into the vacuolar H^+-ATPase (v-ATPase), Ragulator and Rag GTPase complex (Jung et al., 2015; Rebsamen et al., 2015; Wang et al., 2015). V-ATPase, an ATP-driven proton pump controlling the acidification of the lysosomal lumen, directly interacts with the pentameric protein complex Ragulator that anchors Rag GTPases close to the lysosomal membrane (Shimobayashi and Hall, 2016). Amino acid stimulation weakens the interaction of the v-ATPase with Ragulator, consequently activating the heterodimeric protein Rag (Zoncu et al., 2011). The activated Rag complex, achieved by loading RagA/B with GTP and hydrolyzing RagC/D-GTP, recruits mTORC1 from the cytosol to the lysosomal membrane, where it encounters full activation by Rheb-GTP (Sancak et al., 2008). Another component in the amino acid-dependent activation of mTORC1 is the small regulatory polypeptide of amino acid response (SPAR), a polypeptide encoded by the conserved lncRNA LINC00961 acting upstream of the v-ATPase, Ragulator and Rag GTPase complex (Matsumoto et al., 2017). Lastly, mTORC1 reacts to stress conditions, *e.g.* low ATP levels or DNA damage, which are incompatible with cellular growth and metabolism (Figure 3).

Low energy levels upon starvation, resulting in a decreased ATP/AMP ratio, activate the stress responsive metabolic regulator AMP-activated protein kinase (AMPK); active AMPK inhibits mTORC1 signaling directly through the phosphorylation of raptor, as well as indirectly by phosphorylating and thereby activating TSC2 (Gwinn et al., 2008; Inoki et al., 2003b; Shaw et al., 2004).

Downstream of mTORC1

mTORC1 functions as a central regulator of cell growth by controlling key players in protein translation and degradation (Figure 3). Active mTORC1 phosphorylates the p70S6 Kinase 1 (S6K1, at the Threonine 389), which in turn activates several proteins involved in mRNA translation initiation, *e.g.* eIF4B, a protein associating with eIF4F and eIF4A and promoting ATP-dependent RNA unwinding before cap-dependent translation (Holz et al., 2005). Additionally, S6K1 promotes phosphorylation-dependent degradation of PDCD4, an inhibitor of eIF4A (Dorrello et al., 2006). The second major downstream substrate of mTORC1 is 4E-BP1, which represses 5'cap-dependent mRNA translation by sequestering eIF4E (Brunn et al., 1997; Gingras et al., 1999). Upon inhibitory phosphorylation by mTORC1, 4E-BP1 releases eIF4E allowing it to take part in the eIF4F complex and to direct ribosomes to the cap-structure of mRNAs. In addition to the role of mTORC1 in protein synthesis, mTORC1 negatively regulates protein catabolism, most notably autophagy. Autophagy is a cellular process degrading organelles and damaged proteins *via* the formation of autophagic vesicles (called autophagosomes), ultimately fusing with lysosomes. Autophagy is initiated upon activation of unc-51 like autophagy activating kinase 1 (ULK1), which complexes with ATG13, FIP2000 and ATG101 and induces autophagosome formation (Ganley et al., 2009; Hara et al., 2008; Hosokawa et al., 2009). mTORC1 phosphorylates and inactivates ULK1 (at Serine 757), thereby blocking autophagy induction and reducing protein turnover (Castets et al., 2013; Kim et al., 2011). Lastly, mTORC1 is also implicated in *de novo* lipid synthesis *via* the sterol responsive element binding protein (SREBP) (Duvel et al., 2010), in nucleotide synthesis that are required for DNA replication, and in ribosome biogenesis in growing and proliferating cells (Saxton and Sabatini, 2017).

Upstream of mTORC2

In contrast to mTORC1, mTORC2 is insensitive to nutrients, but it functions as an effector of the insulin / growth factor and PI3K signaling, which promotes the association of mTORC2 with ribosomes to activate its kinase activity (Zinzalla et al., 2011). Another mechanism of mTORC2 activation involves the phosphorylation of mSin1, a specific component of mTORC2, by Akt, hence serving as a positive feedback loop between Akt

and mTORC2 (Yang et al., 2015). Surprisingly, mTORC2 signaling is also regulated by mTORC1, since mTORC1 was found to activate the growth factor receptor-bound protein 10 (Grb10), an inhibitor of insulin / IGF-1 (Hsu et al., 2011; Yu et al., 2011). Additionally, S6K1, a direct mTORC1 target, phosphorylates and marks IRS1 for degradation, hence constituting a negative feedback loop reducing PI3K and mTORC2 signaling (Harrington et al., 2004; Shah et al., 2004).

Downstream of mTORC2

mTORC2 signaling plays a role in cellular metabolism and survival, by regulating several members of the protein kinase family. One such phosphorylation target of mTORC2 is the serine/threonine protein kinase 1 (SGK1, at the Serine 422), which regulates ion transport and cell survival (Garcia-Martinez and Alessi, 2008). mTORC2 has also been implicated in actin cytoskeleton organization *via* the phosphorylation of protein kinase C α (PKCα, at the Serine 657) (Jacinto et al., 2004; Sarbassov et al., 2004). The last well-described downstream target of mTORC2 is Akt, phosphorylated in the carboxyl-terminal hydrophobic motif (at the Serine 473). Upon phosphorylation by mTORC2, Akt is fully activated by phosphorylation in its activation loop (at the Threonine 308) by PDK1 (Sarbassov et al., 2005). The mTORC2 / Akt axis regulates lipogenesis and glucose homeostasis in insulin-stimulated tissues, *e.g*. liver and skeletal muscle (Hagiwara et al., 2012; Kumar et al., 2008; Yuan et al., 2012).

4.4 mTOR signaling in skeletal muscle

Skeletal muscle is metabolically highly active and quickly adapts its morphology in response to physiological conditions, but is often compromised upon a diseased state. To maintain skeletal muscle homeostasis, processes such as tissue regeneration and maintenance of muscle mass are of major importance. Since both processes require large amounts of nutrients and energy, mTOR is positioned as a central regulator of muscle health and function. Notably, skeletal muscle growth is based on hypertrophy, rather than an increase in number of fibers (Glass, 2005). Moreover, hypertrophy is induced upon mTORC1 activation, but reversed into atrophy with rapamycin treatment (Bodine et al., 2001; Izumiya et al., 2008; Pallafacchina et al., 2002; Rommel et al., 2001). Mouse skeletal muscles expressing human TSC1, which stabilizes the TSC1/2 complex and consequently inhibits mTORC1, develop an atrophic phenotype (Wan et al., 2006). Similarly, muscle cells depleted for S6K show normal differentiation and fusion, but *S6K*$^{-/-}$ myotubes are atrophic and do not respond to IGF-I or nutrient stimulation (Ohanna et al., 2005). Even though expression of a constitutively active form of Akt, leading to short-term activation of

mTORC1, causes hypertrophy in muscle fibers (Bodine et al., 2001), sustained activation of mTORC1 in skeletal muscle, achieved by conditional knockout of *TSC1* under the control of the *human skeletal actin (HSA)* promoter (TSCmKO), results in severe atrophy and in a late-onset myopathy (Castets et al., 2013). Mechanistically, sustained activation of mTORC1 inhibits autophagy induction through ULK1 inhibitory phosphorylation, resulting in the accumulation of damaged organelles. Furthermore, in TSCmKO muscle the rate of protein synthesis is strongly increased, thus provoking an unfolded protein response and ER-stress (Guridi et al., 2015). Interestingly, skeletal muscles deficient for mTORC1 signaling (RAmKO) are atrophic and also show a degenerative phenotype, resulting in a progressive muscular dystrophy causing premature death of the mice (Bentzinger et al., 2008; Romanino et al., 2011). In both TSCmKO and RAmKO mice, lean mass and muscle force are decreased, indicating that balanced mTORC1 signaling is necessary for homeostasis and function of adult skeletal muscle (Guridi et al., 2016). Notably, whole-body knockout of *mTOR* or *Rptor* affects viability in early stages of embryogenesis (Gangloff et al., 2004; Guertin et al., 2006; Murakami et al., 2004), confirming a central function of mTORC1 in cell, organ and body growth. Furthermore, it was demonstrated that shRNA-mediated knockdown of *Rptor* or *Rheb* in C2C12 myoblasts enhances differentiation, by releasing the negative feedback of mTORC1 onto IRS1, and thereby increasing Akt signaling (Ge et al., 2011). Inversely, rapamycin treatment of rat and mouse myoblasts prevents differentiation *in vitro* (Conejo et al., 2001; Coolican et al., 1997; Cuenda and Cohen, 1999). Consistently, *in vivo* application of rapamycin inhibits differentiation of myoblasts during skeletal muscle regeneration following muscle injury in rodents (Ge et al., 2009; Miyabara et al., 2010). Notably, mTORC1 downstream signaling is highly increased in regenerating compared to uninjured muscle (Matsumoto et al., 2017; Miyabara et al., 2010; Rodgers et al., 2014). Moreover, it was proposed that mTORC1 remains inactive in quiescent satellite cells, but that the signaling is induced in the G_{Alert} and activated states (Rodgers et al., 2014). Interestingly, SPAR, an upstream inhibitor of amino acid-induced mTORC1 signaling, is strongly down-regulated in skeletal muscle upon muscle injury and may thus contribute to mTORC1 activation in the tissue (Matsumoto et al., 2017). Several lines of evidence point to a potential role of mTORC1 in myogenesis: 1) in myoblasts proliferation and differentiation; 2) in the transition between quiescence and activation of satellite cells. The exact mechanisms how mTORC1 controls the formation of muscle fibers during development and regeneration of the tissue are yet to be identified.

In contrast, the function of mTORC2 in adult skeletal muscle is less described. Mice depleted for rictor in differentiated, mature myofibers (RImKO – *HSA* promoter) are viable, have a normal life-span and show no alteration in skeletal muscle morphology (Bentzinger

et al., 2008). Nonetheless, whole-body metabolism of RImKO mice is perturbed due to defective insulin-stimulated glucose transport in skeletal muscle, which results in glucose intolerance of mutant mice (Kumar et al., 2008). Simultaneously, RImKO mice undergo a re-partitioning of lean to fat mass and exhibit increased abundance of intramyocellular triglycerides, providing fat as a preferred energy substrate (Kleinert et al., 2016). Although glucose and lipid metabolism is altered in the absence of mTORC2, the signaling is dispensable for the maintenance of adult skeletal muscle function. However, these studies addressed the consequences of mTORC2 depletion only in mature fibers (Leu et al., 2003; Schwander et al., 2003), but did not include the investigation on the role of mTORC2 in skeletal muscle formation and the function of satellite cells. Remarkably, whole-body knockout of *Rictor* in mice causes embryonic lethality at E11.5, thus indicating that mTORC2 signaling is crucial for embryogenesis (Guertin et al., 2006; Shiota et al., 2006). Inactivation of *Rictor* in the Myf5-lineage, *i.e.* in progenitors acquiring the fate of skeletal muscle or brown adipocytes, revealed that mTORC2 signaling is required for brown fat differentiation and growth (Hung et al., 2014). Moreover, loss of mTORC2 signaling shifts brown fat metabolism towards a more oxidative and less lipogenic state. Interestingly, Hung et al. provide evidence that mTORC2 is dispensable for embryonic muscle development, since mutant skeletal muscle did not show any alterations at young age. Nevertheless, long-term consequences of mTORC2 inactivation in skeletal muscle and their resident stem cells remain to be studied in greater detail. In C2C12 myoblasts, shRNA-mediated knockdown of *Rictor* blocked terminal differentiation and fusion (Shu and Houghton, 2009). Mechanistically, mTORC2-induced phosphorylation of Akt (at the Serine 473) appears necessary for the downregulation of Rho-associated kinase 1 (ROCK1), which normally occurs during differentiation. Previously, ROCK1 has been implicated in actin cytoskeleton organization and was found to be active in proliferating myoblasts and downregulated during late differentiation and fusion (Nishiyama et al., 2004). Hence, detailed analysis of mTORC2 in the formation of muscle fibers, including proliferation, differentiation and fusion of myoblasts, and in satellite cell homeostasis needs further investigation.

5. Rationale and objectives of the thesis

Several lines of evidence pointed to a potent role of mTORC1 and mTORC2 in embryonic and adult myogenesis, although the exact mechanisms have not yet been identified. The overall objective of my PhD work was to decipher the roles of mTOR signaling in the myogenic process, and the consequences of its deregulation in muscle development and regeneration. The first specific aim was to identify the functions of mTORC1 and mTORC2 in embryonic myogenesis. For this purpose, I describe in detail the muscle phenotype of the two conditional knockout mouse models, generated in the lab, which were depleted for raptor or rictor in Myf5-expressing muscle progenitors, leading to inactivation of mTORC1 (RAmyfKO) or mTORC2 (RImyfKO), respectively, from the onset of muscle development. More specifically, I focused on the consequences of mTORC1 or mTORC2 inactivation in myogenesis and tested the proliferation, differentiation and fusion capacity of muscle precursors, *in vitro* and *in vivo*. I also addressed whether inactivation of mTOR signaling affected the viability of muscle cells. The second specific aim of my PhD work was to determine whether mTORC1 and mTORC2 have similar functions in adult myogenesis, which involves satellite cells that are derived from fetal muscle progenitors and are essential for muscle regeneration upon injury. To investigate the function of mTORC1 in myogenesis of adult mice, we induced raptor depletion in Pax7-expressing satellite cells (RAscKO). I first addressed whether inactivation of mTORC1 or mTORC2 has an impact on the maintenance of the quiescent satellite cell pool. Secondly, I analyzed the myogenic capacity of RImyfKO and RAscKO satellite cells, by activating them either in culture conditions or by provoking muscle damage *in vivo*. Additionally, both experimental approaches allowed me to study their capacity to return into quiescence. Lastly, I investigated whether mTORC2-deficient satellite cells and myofibers differ in the age-related changes. Hence, during my PhD work, I aimed to understand whether and how mTORC1 and mTORC2 signaling are involved in the dynamics and homeostasis of muscle progenitors and precursors and thereby in the formation and maintenance of muscle fibers during development and regeneration.

6. Results

6.1 Manuscript 1: "Loss of mTORC1 in muscle progenitors reduces proliferation and differentiation and impairs, but does not abolish, myogenesis"

Loss of mTORC1 in muscle progenitors reduces proliferation and differentiation and impairs, but does not abolish, myogenesis

Nathalie Rion[1], Perrine Castets[1], Shuo Lin[1], Leonie Enderle[2], Christopher Eickhorst[3] and Markus A. Rüegg[1]*

[1] Biozentrum, University of Basel, CH-4056 Basel, Switzerland

[2] Lunenfeld-Tanenbaum Research Institute/Mount Sinai Hospital, Toronto, ON M5G 1XM, Canada

[3] Institute of Biochemistry II, School of Medicine, Goethe University, 60598 Frankfurt am Main, Germany

* Corresponding author:

markus-a.ruegg@unibas.ch, Tel: +41 61 267 22 23, Fax: +41 61 267 22 08

Abstract

Myogenesis, corresponding to skeletal myofiber formation during embryogenesis and regeneration in the adult, is a highly complex process requiring growth factors and nutrients. The mammalian (or mechanistic) target of rapamycin (mTOR) functions as a central regulator of cell growth and metabolism in response to extracellular signals. mTOR assembles into two distinct complexes: mTOR complex 1 (mTORC1) and complex 2 (mTORC2). Since mTORC1, but not mTORC2 is crucial for homeostasis of adult skeletal muscle, we aimed to understand the raptor-dependent role of mTORC1 in embryonic and adult myogenesis. We generated mice depleted for raptor, an essential protein of mTORC1, in embryonic muscle progenitors and adult muscle stem cells using *Myf5*-Cre and *Pax7*-CreERT2 mice, respectively. mTORC1 inactivation in developing muscle causes perinatal lethality of the mice and impairs embryonic myogenesis. We determined that specifically mTORC1 affects proliferation and differentiation of muscle precursors, although raptor-depleted cells contribute to myofiber formation. Removal of mTORC1 from muscle stem cells abolishes their myogenic function during regeneration of the adult tissue upon injury. Defects in adult myogenesis result from a delay of muscle stem cells to enter activation and from their limited capacity to proliferate and differentiate in the absence of mTORC1. Thus, we established that mTORC1 signaling is crucial for embryonic and adult myogenesis.

Introduction

Skeletal muscle is the largest organ of the human body, accounting for approximately 40 % of the weight. Formation of skeletal muscle fibers, corresponding to the process of myogenesis, occurs in several steps and waves. Embryonic myogenesis is initiated in mesodermal progenitors, which reside in the dermomyotome and express the paired box protein-3 and -7 (Pax3 and Pax7). These cells become committed to the myogenic lineage by expressing myogenic regulatory factors (MRFs) Myf5, MyoD, Mrf4 or Myogenin. These myoblasts then become post-mitotic and fuse together in order to form multi-nucleated muscle fibers (Deries and Thorsteinsdottir, 2016). There are two waves of myogenesis, the embryonic wave that gives rise to primary myofibers, and the fetal wave (starting around E14.5 in mouse), which uses a distinct gene expression program, and results in secondary myofibers (Biressi et al., 2007a). Many of the steps and mechanisms of developmental myogenesis are also important upon injury-induced muscle regeneration, where quiescent Pax7-positive satellite cells become activated and give rise to myogenic cells that are capable of repairing the injured myofibers in a process termed adult myogenesis (Dumont et al., 2015).

The mammalian (or mechanistic) target of rapamycin (mTOR) is a protein serine/threonine kinase that assembles into two structurally and functionally distinct multi-protein complexes, mTOR complex 1 (mTORC1) and mTORC2 (Saxton and Sabatini, 2017). High doses of the name-giving drug rapamycin block mTORC1 instantaneously by the direct binding of the FKBP12-rapamycin complex. In contrast, mTORC2 signaling is attenuated only after prolonged exposure to rapamycin (Sarbassov et al., 2006), arguing that rapamycin is not complex specific. In contrast, the different functions of mTORC1 and mTORC2 can be dissected by selective removal of their essential components raptor and rictor, respectively. Whole-body and cell- / tissue-specific knockouts for *Rptor* and *Rictor*, have shown that mTORC1 senses nutrients and growth factors and functions as a central regulator of cell growth by balancing protein synthesis and protein degradation, whereas mTORC2 can affect cytoskeletal remodeling and cell survival (Saxton and Sabatini, 2017). Interestingly, whole-body knockouts of *Mtor*, *Rptor* and *Rictor* in mice are embryonic lethal (Gangloff et al., 2004; Guertin et al., 2006; Murakami et al., 2004). Moreover, the phenotype caused by the tissue-specific ablations of *Rptor* or *Rictor* largely differ between tissues. For example, ablation of *Rptor* or *Mtor* in skeletal muscle causes a very similar phenotype dominated by muscle atrophy and a severe myopathy that results in early death of the mice (Bentzinger et al., 2008; Risson et al., 2009). In contrast, skeletal muscle-specific *Rictor* knockout mice do not have an overt phenotype, but their muscles show metabolic changes; in particular, a greater reliance on lipids and an increased lipid content (Kleinert et al., 2016).

In those experiments, the targeted genes were eliminated by driving Cre expression under the control of the *human skeletal actin* (HSA) promoter causing recombination in myonuclei but not in myoblasts or satellite cells (Leu et al., 2003).

There is evidence that mTORC1 also affects myogenesis, although the data obtained from several studies using rapamycin (or rapalogs) are rather controversial. Rapamycin-mediated inhibition of mTORC1 abrogates proliferation of cultured C2C12 myoblasts prior to differentiation (Conejo and Lorenzo, 2001), although rapamycin does not affect satellite cell proliferation in adult mice after freeze-injury *in vivo* (Miyabara et al., 2010). Myoblasts deficient for the mTORC1 targets, S6 kinase 1 and S6 kinase 2, do not show any deficit in myoblast proliferation and fusion (Ohanna et al., 2005). There is also evidence that rapamycin abolishes myotube formation of C2C12 myoblasts (Coolican et al., 1997; Cuenda and Cohen, 1999; Pollard et al., 2014). The rapamycin-inhibited role of mTOR in early differentiation is independent of its kinase domain and has been postulated to be based on mTOR-dependent regulation of IGF-II expression (Erbay and Chen, 2001; Erbay et al., 2003). However, fusion and maturation of myotubes requires the kinase activity of mTOR during differentiation *in vitro* and during muscle regeneration *in vivo* (Ge et al., 2009; Park and Chen, 2005). The rapamycin-dependent inhibition of myotube formation is likely mediated through mTORC1 as loss of rictor in the Myf5-lineage does not affect embryonic myogenesis *in vivo* (Hung et al., 2014). However, knockdown of raptor enhances and raptor overexpression inhibits differentiation of cultured C2C12 myoblasts (Ge et al., 2011; Pollard et al., 2014), suggesting a role of a raptor-independent mTOR complex in myoblast fusion.

To resolve these open questions and to firmly determine the role of raptor-dependent mTORC1 in myogenesis, we depleted raptor from muscle progenitors and adult satellite cells using *Myf5*-Cre (Tallquist et al., 2000) and *Pax7*-CreERT2 (Murphy et al., 2011) mice, respectively. In developing muscle, mTORC1 depletion impairs embryonic myogenesis and results in perinatal lethality due to respiratory failure. We find that mTORC1 signaling largely affects proliferation and differentiation of muscle precursors, although raptor-depleted cells do contribute to muscle fibers. Removal of mTORC1 from adult satellite cells causes a severe deficit in muscle regeneration upon injury. This defect is largely due to a strong delay of the satellite cells to transit from quiescence to activation and a deficit in cell proliferation and differentiation. Our data thus show that mTORC1 signaling is crucial for embryonic and adult myogenesis.

Results

Depletion of raptor impairs muscle development

Mice in which the mTORC1-essential component raptor is eliminated in myofibers, die between the age of four to six months because of a severe myopathy (Bentzinger et al., 2008). In addition, whole-body knockouts for raptor die *in utero* (Guertin et al., 2006). As we were interested in the role of mTORC1 in myogenesis, we examined the activation state of mTORC1 in myogenic precursor cells and myotubes. We used embryonic day 11.5 (E11.5) pups and stained them for the phosphorylated form of S6, which is indicative of active mTORC1 (Saxton and Sabatini, 2017). The different cell types were identified by co-staining the cross-sections with specific antibodies against Pax7 for muscle progenitors, MyoD for myoblasts, myogenin for myocytes and embryonic myosin heavy chain (embMHC) for myotubes. While phospho-S6 staining was strong in $Pax7^+$ and $MyoD^+$ cells (Figure 1A, B), only a minority of $myogenin^+$ and $embMHC^+$ cells were also phospho-S6 positive (Figure 1C, D). These data indicate high mTORC1 activity in the proliferative phase of embryonic myogenesis and low activity during cell fusion and fiber maturation (Figure 1E).

To understand the role of mTORC1 in myogenesis, we generated mice that expressed Cre under the control of *Myf5* (Tallquist et al., 2000) and carried floxed alleles for *Rptor* (Bentzinger et al., 2008). The *Myf5* gene is expressed in progenitor cells of the somites starting at embryonic day 8 (E8) (Ott et al., 1991). Such mice, termed RAmyfKO (for raptor-*Myf5*-knockout; $Myf5^{+/Cre}; Rptor^{fl/fl}$), were born at the expected Mendelian ratio, appeared cyanotic (Figure 2A) and died immediately. RAmyfKO mice did not breathe and their lungs were not inflated (Figure S1A). The diaphragm muscle was thin (Figure S1A, B) and neuromuscular junctions did not form properly with motor nerves overshooting the sites of high acetylcholine receptor (AChR) density in mutant mice (Figure S1C). Moreover, many non-synaptic AChR clusters were visible in RAmyfKO mice. In contrast, mice depleted for rictor (Bentzinger et al., 2008) in Myf5-expressing progenitors (Tallquist et al., 2000), termed RImyfKO mice (for rictor-*Myf5*-knockout; $Myf5^{+/Cre}; Rictor^{fl/fl}$), were viable and showed a normal overall muscle histology at young age (Figure 2B), indicating that mTORC2 is not required for embryonic muscle development. Examination of embryos at different ages revealed that the body weight of RAmyfKO mice was reduced compared to controls (Ctrl; $Myf5^{+/+}; Rptor^{fl/fl}$) as early as E13.5 (Figure 2C). In contrast, embryos heterozygous for the targeted *Rptor* allele ($Myf5^{+/Cre}; Rptor^{+/fl}$ - termed Het-RAmyfKO) were indistinguishable from Ctrl embryos and did not show any change in body weight (Figure S2A). The weight reduction of E18.5 RAmyfKO embryos was not based on an overall reduction in body size compared to Ctrl (Figure S2B). In particular, the length of the long bones was not altered (Figure S2C). The smaller size of the rib cage in RAmyfKO embryos, in turn, could be based

on the changes in myotomal development (Vinagre et al., 2010). Examination of skeletal muscles at E18.5 by H & E and by immunofluorescence staining revealed that their size was much smaller in RAmyfKO embryos, but the different muscle groups were still present (Figure 2D, E). The observation that muscle still formed in RAmyfKO embryos was supported by real-time PCR when mRNA was specifically isolated from muscle tissue of E18.5 embryos. Transcript levels of all the myogenic regulatory factors, with the exception of *Myf5*, were the same in RAmyfKO and Ctrl embryos (Figure 2F). The approximately 50 % reduction in *Myf5* expression is based on the inactivation of one copy of the *Myf5* gene in *Myf5*$^{+/Cre}$ mice (Figure S2D). Similar to the myogenic regulatory factors, expression levels of skeletal muscle markers, such as *Myh3* (coding for embMHC) and *Des* (coding for desmin), were not altered in mutant embryos (Figure 2F). These results indicate that the muscles of RAmyfKO embryos successfully passed the myogenic process. As Myf5 is also expressed in brown adipose tissue, we also examined this tissue and found a strong reduction in RAmyfKO embryos (Figure S2E), indicating that raptor depletion in brown adipocytes results in a similar loss as in skeletal muscle. Non-targeted tissue, such as liver, did not show any change in the amount of raptor and of S6 phosphorylation, indicating that mTORC1 signaling in RAmyfKO liver was not affected (Figure S2F, Table S1). Besides the loss of skeletal muscle, we also observed an increased accumulation of fat droplets in the muscle tissue of E18.5 RAmyfKO embryos compared to Ctrl (Figure 2G). Thus, in summary, depletion of raptor, but not of rictor, during myogenesis results in loss of muscle tissue. However, muscles are formed in RAmyfKO embryos, albeit at much lower efficacy than in Ctrl.

The observation that muscles can still form in RAmyfKO embryos could be explained in two ways: either mTORC1-deficient myoblasts are not viable and their loss is compensated by the expansion of non-targeted myoblasts or raptor-depleted myoblasts still contribute to the muscle lineage but at a significantly lower efficacy. To distinguish between those possibilities, we first examined the phosphorylation status of the mTORC1 target S6 by immunofluorescence to test for successful recombination in the different cell populations. At E11.5, Pax7-positive cells in RAmyfKO mice were negative for the phosphorylated form of S6 (Figure S3A, S3E), indicative of the lack of mTORC1 activity. A very similar loss of phospho-S6 was found in MyoD-, myogenin-, and embMHC-positive cells (Figure S3B-E). As shown in Figure 1, Pax7- and MyoD-positive cells express high levels of phospho-S6 in Ctrl embryos at the same age. Thus, these experiments are evidence for the successful depletion of raptor in RAmyfKO muscle at this particular developmental stage. Next, we analyzed the size of Pax7- and embMHC-positive structures in Ctrl and RAmyfKO embryos as hints for the function of raptor in primary myogenesis. Transverse cross-sections were

prepared from the hindlimb region of E11.5 embryos. In E11.5 embryos, the area covered by Pax7-positive progenitors was similar between Ctrl and mutant embryos (Figure 3A), while there was a tendency of fewer embMHC-positive myotubes in RAmyfKO embryos (Figure 3B). This trend towards smaller areas covered by myogenic cells was confirmed in E13.5 embryos and affected both Pax7- and embMHC-positive cells (Figure 3C, D). Quantification of the size of the myotome (embMHC-positive cells) revealed a significant size difference of this structure at E13.5 in RAmyfKO compared to Ctrl embryos (Figure 3E). As additional evidence for the relative contribution of myogenic cells to the entire embryo, quantitative real-time PCR on whole-body RNA extracts (normalized to the levels of β-actin mRNA) was performed (Figure 3F). Interestingly, at E11.5, *Pax7* expression was not altered in mutant compared to Ctrl embryos, while markers for myogenic precursor cells and mature muscle fibers were lower. At E13.5, *Pax7* expression was also lower in RAmyfKO embryos than in Ctrl (Figure 3F). The effect of mTORC1 inactivation on myogenic cells seemed not to be due to apoptosis as we could not detect any increase in the number of TUNEL-positive cells in E12.5 mutant mice compared to Ctrl (Figure 3G). Overall, these results indicate that mTORC1 contributes to primary myogenesis by affecting early stages of cell commitment, proliferation and differentiation. In addition, these results provide evidence that this effect becomes more pronounced at later stages of development. Strikingly, however, RAmyfKO embryos still contained differentiated primary myotubes (indicated by the presence of embMHC-positive regions). The finding that those structures were smaller than in Ctrl embryos indicate a slowing down of myogenesis.

RAmyfKO embryos contain myogenic cells that escape Cre-mediated raptor depletion

To address the question whether myogenic cells, that escaped recombination of the *Rptor* alleles, also contributed to the development of primary myotubes, we used an EGFP-expressing reporter mouse to follow Cre-mediated recombination. In this mouse line, called mR26CS^{EGFP}, the chick actin promoter drives expression of EGFP in the *ROSA26* locus. Expression of EGFP in the absence of Cre is prevented by an upstream stop codon that is flanked by loxP sites. Successful recombination by Cre results in high levels of EGFP in the targeted cells (Tchorz et al., 2012). While hindlimb muscles of Ctrl embryos (*Myf5*$^{+/+}$; *Rptor*$^{fl/fl}$; *mR26CS*$^{EGFP/+}$) did not express EGFP, all muscle fibers in Het-RAmyfKO embryos, carrying one floxed *Rptor* allele (*Myf5*$^{Cre/+}$; *Rptor*$^{fl/+}$; *mR26CS*$^{EGFP/+}$), were positive for EGFP (Figure 4A). The intensity of the EGFP staining varied between different muscle fibers of Het-RAmyfKO muscle (Figure 4A; middle). Importantly, hindlimb muscle of RAmyfKO embryos with the *Rptor* gene floxed at both alleles (*Myf5*$^{Cre/+}$; *Rptor*$^{fl/fl}$; *mR26CS*$^{EGFP/+}$) showed a mosaic expression of EGFP (Figure 4A; right). In contrast to Het-RAmyfKO

embryos, muscle of RAmyfKO embryos also contained fibers that were negative for EGFP, indicating that those fibers did not express the Cre recombinase at any time and thus continue to express raptor. Consistent with this, EGFP-negative muscle fibers were often also positive for phospho-S6, whereas EGFP-positive fibers were largely negative (Figure S4A). This result therefore suggests that cells that continue to express raptor, have a competitive advantage over cells in which mTORC1 is inactive. To quantify this effect, we isolated myogenic cells from the entire hindleg and foreleg of E18.5 embryos by FACS and determined the relative proportion of EGFP-positive and EGFP-negative cells (Figure S4B). As expected, Ctrl cells, which do not express Cre, were EGFP-negative, demonstrating that the floxed stop cassette for EGFP is not leaky (Figure 4B). In Ctrl EGFP^{+} muscles, that express Cre from the *Myf5* locus (*Myf5*$^{Cre/+}$; *Rptor*$^{+/+}$; *mRS26*$^{EGFP/+}$), more than 80 % of the cells also expressed EGFP. This value was very similar to cells isolated from Het-RAmyfKO embryos, demonstrating that haplo-insufficiency of raptor did not have any effect on myoblast generation. In stark contrast, however, only approximately 23 % of the myogenic cells isolated from RAmyfKO embryos were EGFP-positive, showing that loss of raptor results in a substantial increase of non-recombined myoblasts (Figure 4B). The freshly sorted cells were also genotyped using primers that specifically detect the targeted locus in *Rptor* gene (see scheme in Figure 4C). As control, we included embryos that were heterozygous for the floxed *Rptor* allele but were negative for Cre (*Myf5*$^{+/+}$; *Rptor*$^{fl/+}$; *mR26CS*$^{EGFP/+}$). Genomic DNA from myoblasts isolated from those mice contained both, the floxed and the wild-type allele of *Rptor* (Figure 4D; Ctrl EGFP^{-}; upper panel) and were negative for the recombined *Rptor* allele (Figure 4D; lower panel). The same result was obtained from EGFP-negative myoblasts of Het-RAmyfKO embryos (Figure 4D, Het-RAmyfKO EGFP^{-}). Importantly, EGFP-positive myoblasts from either Het-RAmyfKO mice (Het-RAmyfKO EGFP^{+}) or RAmyfKO mice (RAmyfKO EGFP^{+}) did not contain any floxed allele for *Rptor* (Figure 4D; upper panel), but were positive for the PCR product of the *Rptor* allele after recombination (Figure 4D; lower panel). In contrast, EGFP-negative myoblasts from RAmyfKO embryos were positive for the floxed *Rptor* allele (Figure 4D; RAmyfKO EGFP^{-}; upper panel). The presence of the recombined *Rptor* allele in the RAmyfKO EGFP^{-} myoblasts (lower panel) is probably due to contamination by EGFP-positive cells. In summary, these data show that expression of EGFP in the RAmyfKO embryos coincides with successful recombination of the floxed *Rptor* allele. Thus, the presence of EGFP-positive RAmyfKO myoblasts and of EGFP-positive muscle fibers argues that the myogenic process can progress in the absence of raptor.

Loss of mTORC1 affects proliferation and differentiation of myoblasts

As a next step, we aimed to directly address the function of mTORC1 in FACS-isolated myoblasts from E18.5 embryos with the different genotypes. Cells were additionally separated into EGFP-positive and EGFP-negative populations, were plated at the same density and cultured under growth conditions for 2 days. As mTORC1 is a key regulator of translation initiation, we measured the overall rate of protein synthesis using the surface sensing of translation (SUnSET) method (Goodman and Hornberger, 2013). Newly synthesized proteins were labeled with puromycin for 30 min and then stained with antibodies to puromycin (Figure 5A). As negative control, Ctrl cells were treated for 10 min with the protein synthesis inhibitor cycloheximide prior to the addition of puromycin. Control cells and EGFP-positive myoblasts from Het-RAmyfKO embryos incorporated puromycin to a similar extent, whereas puromycin incorporation was significantly lower in EGFP-positive myoblasts derived from RAmyfKO embryos (Figure 5A, B). Measurement of proliferation by a one-hour pulse with 5-bromo-2'-deoxyuridine (BrdU) revealed a highly significant impairment in EGFP-positive RAmyfKO myoblasts (Figure 5C, D). The efficacy to transit from proliferation to differentiation and the overall fusion capacity of RAmyfKO myoblasts was tested by switching from proliferation to differentiation medium. Fourteen hours after the medium change, the percentage of cells that still proliferated was low and it did not change between the genotypes (Figure 5E). However, fusion of RAmyfKO $EGFP^+$ myoblasts was lower than in Ctrl $EGFP^-$ or Het-RAmyfKO $EGFP^+$ cells after 72 hours (Figure 5F). This difference was significant for the fusion index, but only slightly altered for the relative number of myonuclei per myotube (Figure 5G). To confirm that the function of mTOR in proliferation and differentiation of myoblasts is specific for mTORC1, we analyzed the myogenic potential of mTORC2-deficient primary myoblasts isolated from 2 – 3 week-old RImyfKO mice. As expected, RImyfKO primary myoblasts lacked rictor expression and phosphorylation of Akt (at the Serine 473), a mTORC2 downstream substrate (Figure S5A, Table S2). Similar to mTORC2 inactivation in adult skeletal muscle (Bentzinger et al., 2008), we observed that total PKCα protein levels and its phosphorylated form (at the Serine 657) are reduced in RImyfKO myoblasts. In contrast, we confirmed that RImyfKO myoblasts exhibit normal mTORC1 signaling, shown by the phosphorylation of the S6 protein (at the Serine 235/236) (Figure S5A, Table S2). The proliferation capacity, measured by BrdU incorporation, of RImyfKO myoblasts was unchanged compared to Ctrl (Figure S5B, C). Similarly, the efficacy to transit from proliferation to differentiation was normal in mutant myoblasts (Figure S5D). Furthermore, after 48 hours of differentiation no difference in the fusion index and relative number of nuclei per myotube were detected between both genotypes (Figure S5E-G). These results show that mTORC1, but not mTORC2, is

important for proliferation and differentiation of myoblasts, consistent with the view that both of those processes require active protein synthesis (Pallafacchina et al., 2013).

mTORC1 signaling in adult muscle stem cells

Recent evidence showed that activation of satellite cells is paralleled by increased mTORC1 signaling (Rodgers et al., 2014). In particular, activation of mTORC1 is necessary and sufficient for the transition of satellite cells from a quiescent to an "alert" state. However, it is not known whether mTORC1 function is still necessary in the quiescence state and how mTORC1 signaling would affect muscle regeneration. To address these questions and to overcome any possible compensatory mechanisms, we generated a new mouse model (*Pax7*$^{Cre\text{-}ERT2/+}$*; Rptor*$^{fl/fl}$*; mR26CS*$^{EGFP/EGFP}$) that allowed selective depletion of raptor in satellite cells upon administration of tamoxifen (tmx) and monitoring of the cells by their expression of EGFP. These mice, called RAscKO, were analyzed 10 or 90 days after tmx injection (Figure 6A). Mice that were not injected with tamoxifen, did not express EGFP (Figure S6A), demonstrating that the mouse model was not leaky. In agreement with others (Murphy et al., 2011), tmx injection for 5 consecutive days resulted in the expression of EGFP in the vast majority of Pax7-positive satellite cells after 10 days (Figure 6B). Quantification by FACS showed that more than 84% of the satellite cells expressed EGFP (Figure S6B). Like in RAmyfKO myoblasts, PCR on genomic DNA isolated from the EGFP-positive satellite cells showed successful recombination of the floxed *Rptor* alleles in RAscKO cells (Figure S6C). Examination of the number of satellite cells in *tibialis anterior* (TA) muscle 10 or 90 days after tmx injection, did not reveal any significant change in their number compared Ctrl mice (Figure 6C). These data indicate that mTORC1 activity is not essential to maintain the satellite pool under homeostatic conditions.

Our finding that embryonic myogenesis is strongly impaired in RAmyfKO mice suggested that muscle regeneration in the adult may also be affected by inactivation of mTORC1 in satellite cells. To test this hypothesis, recombination of *Rptor* was induced by tmx injection and after 7 days, cardiotoxin was injected into the TA and *extensor digitorum longus* (EDL) muscles followed by 15 days recovery (see scheme in Figure 6D). Whereas the weights of the contralateral EDL and TA muscles were indistinguishable between RAscKO and Ctrl mice, the injured RAscKO muscle failed to regain a similar weight as regenerating Ctrl muscle (Figure 6E). Examination of muscles by H & E staining showed no difference between Ctrl and RAscKO mice in the contralateral leg (Figure 6F, left). However, a very obvious and dramatic difference between genotypes was observed in the injured legs (Figure 6F, right). While Ctrl muscle had fully regenerated, indicated by the presence of centronucleated myofibers, only few, small myofibers, containing centralized myonuclei,

were present in regenerating RAscKO mice (Figure 6F). Consistent with poor regeneration, RAscKO muscle were rich in collagen (Sirius Red positive, Figure 6G, left), indicative of fibrosis, and showed accumulation of Oil Red O-positive lipids (Figure 6G, right). Thus, mTORC1 signaling in satellite cells is important for proper regeneration of muscle fibers. Nevertheless, the presence of centrally nucleated myofibers suggested that raptor-depleted satellite cells can contribute to regenerating muscle fibers. Indeed, all the regenerating, embMHC^{+} myofibers in cardiotoxin-treated muscle from RAscKO mice were also EGFP-positive, whereas fibers in the contralateral, non-injured muscle were EGFP-negative (Figure 6H). Notably, almost all myofibers in regenerating Ctrl muscle downregulated embMHC expression 15 days post-injury (Figure 6H). These data indicate that raptor-depleted satellite cells can fuse although their efficacy is greatly diminished.

As noted, mice heterozygous for the floxed alleles of *Rptor* (Het-RAmyfKO) do not show any overt muscle phenotype. To test whether challenging of muscle would reveal a haplo-insufficiency, we conducted the same cardiotoxin experiment as described above in such Het-RAmyfKO mice. As expected, skeletal muscles of Het-RAmyfKO mice express only about half of the amount of raptor (Figure S7A, Table S3). As a consequence, phospho-S6 and phospho-4E-BP1 tended to be reduced, indicating that mTORC1 activity is also reduced. Fifteen days after cardiotoxin injury, we could not detect any difference in muscle fiber regeneration between Ctrl and Het-RAmyfKO mice, shown by body and muscle weight (Figure S7B), and the overall histology of the regenerated muscle (Figure S7C). Moreover, the number of satellite cells in the injured and non-injured muscles was the same in Het-RAmyfKO and Ctrl mice (Figure S7D, E). Thus, dampening of mTORC1 activity by approximately half does not affect successful muscle regeneration.

Activation is delayed in raptor-depleted satellite cells

To examine the proliferation and differentiation capacity of raptor-depleted satellite cells, we isolated single muscle fibers from EDL muscle of Ctrl and RAscKO mice, 90 days after tmx treatment. At time zero (T0), the number of Pax7-positive cells per muscle fiber was not significantly different in RAscKO mice from Ctrl (Figure 7A). In RAscKO mice, the Pax7-positive cells also expressed EGFP (98.07 ± 0.50%; n = 5, 20-30 myofibers per animal), confirming that all EGFP-positive satellite cells were also negative for raptor. At T0, none of the Pax7-positive satellite cells also expressed MyoD (Figure 7A, E). After 24 hours of culture (T24h), satellite cells become activated, indicated by the expression of MyoD (Dumont et al., 2015). Indeed, in Ctrl mice, the majority of Pax7-positve cells were also MyoD-positive, whereas a larger proportion of cells from RAscKO mice were Pax7 positive, but MyoD-negative (Figure 7B, E), indicating a delay in activation. After 48 hours (T48h),

some satellite cells became Pax7-negative and MyoD-positive, indicating their differentiation in the myogenic lineage (Figure 7E). At 72 hours (T72h), fibers from Ctrl mice contained three different populations of myogenic cells, *i.e.* cells ($Pax7^+$; $MyoD^-$) that became quiescent satellite cells to replenish the pool, still activated satellite cells ($Pax7^+$; $MyoD^+$) and differentiating myoblasts ($Pax7^-$; $MyoD^+$). In contrast, fibers isolated from RAscKO mice largely contained activated satellite cells ($Pax7^+$; $MyoD^+$) and only a very small percentage of quiescent cells ($Pax7^+$; $MyoD^-$) and differentiating myoblasts ($Pax7^-$; $MyoD^+$) (Figure 7C, E). Importantly, the number of myogenic cells increased exponentially in fibers isolated from Ctrl mice, whereas the number of myogenic cells remained low in cultured fibers isolated from RAscKO mice (Figure 7D). In summary, these results show that activation of raptor-depleted satellite cells is delayed and that they proliferate much slower than Ctrl cells. The finding that transcription factors driving muscle differentiation are still induced in RAscKO satellite cells, is in agreement with our results that muscle fibers do form in RAscKO mice upon cardiotoxin injury.

Isolation of satellite cells by FACS and subsequent cultivation revealed a significant slowing of proliferation in RAscKO cells (Figure S8A). In addition, RAscKO satellite cells formed fewer myotubes with often lower number of myonuclei when grown in differentiation medium for 4 days (Figure S8B), indicating an impairment in their fusion capacity. In summary, mTORC1 is not essential for the maintenance of $Pax7^+$ cells in the quiescent state, but the signaling is crucial for proliferation, differentiation and fusion. Nevertheless, in spite of mTORC1 being inactive, our results indicate that raptor-depleted myoblasts and satellite cells make use of an alternative pathway to partially overcome the mTORC1 deficit.

Discussion

mTORC1 signaling has been positioned as a central regulator of skeletal muscle homeostasis and growth at adult age. In most studies, *HSA-Cre* mice were used to drive Cre expression in differentiating myotubes and mature muscle fibers (Leu et al., 2003). Hence, to study the function of mTORC1 in muscle development, we generated mice depleted for raptor, the essential component of mTORC1, in Myf5-expressing cells (RAmyfKO). Myf5 is first detected at E8 in muscle progenitors and precursors in the dermomyotome. RAmyfKO embryos were perinatal lethal due to respiratory failure and exhibited strongly reduced skeletal muscle mass. In contrast, RImyfKO mice, characterized by the loss of mTORC2 signaling in Myf5$^+$ muscle progenitors and precursors, were viable and did not show any alteration in muscle histology at young age. Hence, we provide evidence that mTORC1, but not mTORC2, is essential for embryonic muscle development.

mTORC1, but not mTORC2, signaling is crucial for proliferation of myoblasts during myogenesis

Consistent to the current view, we found that inactivation of mTORC1 reduced protein synthesis in proliferating embryonic myoblasts. Initiation of the translational machinery is controlled by S6K1 and 4E-BP1, which are the main downstream substrates of mTORC1 (Saxton and Sabatini, 2017). Since protein synthesis is highly induced during the G1/S phase of the cell cycle (Cuyas et al., 2014), we analyzed whether loss of mTORC1 signaling in myogenic cells had an impact on their proliferation. Indeed, we provide evidence that mTORC1, according to the phosphorylation of the downstream S6 protein, was active in Pax7$^+$ progenitor and MyoD$^+$ precursor cells and the signaling decreased in Myogenin$^+$ myocytes and embMHC$^+$ myotubes, indicating that mTORC1 has a predominant function in proliferating cells during embryonic myogenesis. Concomitantly, we observed that the capacity of raptor-depleted myoblasts to proliferate was strongly reduced. Simultaneously, no increase in programmed cell death was detected upon the loss of mTORC1 in muscle progenitors and precursors. Consequently, the limited proliferation capacity of mTORC1-deficient myoblasts resulted in a reduced number of cells passing the myogenic process. Consistent with our findings, a regulatory function of mTORC1 in proliferation has also been demonstrated in other cell types, *e.g.* in β-cells of the pancreas or in mouse embryonic fibroblasts (MEF) (Blandino-Rosano et al., 2017; Dowling et al., 2010). Interestingly, even though protein synthesis is low during the G_2/M transition mTORC1 signaling remains hyperactive at this stage of the cell cycle (Bonneau and Sonenberg, 1987; Fan and Penman, 1970; Heesom et al., 2001). The increase in mTORC1 function during mitosis was shown to be mediated through the phosphorylation of raptor by the cyclin-dependent kinase 1 (CDK1), which promotes IRES-dependent mRNA translation (Ramirez-Valle et al., 2010).

Thus, this suggests that mTORC1 signaling mediates its effect on proliferation through various mechanisms. However, we confirmed that the regulatory function of mTORC1 on proliferation is independent of mTORC2 signaling, since rictor-deficiency in myoblasts did not affect their proliferation capacity and their potential to form myotubes *in vitro* and *in vivo*.

Raptor-depleted myoblasts contribute to the formation of myofibers

Remarkably, in hindlimbs of E18.5 RAmyfKO embryos all muscles were formed and normally expressed the myogenic regulatory factors, even though they were clearly smaller. In spite of alterations in myofiber formation in E11.5 and E13.5 RAmyfKO embryos, raptor-depleted myoblasts contributed to the myogenic process as confirmed by the introduction of an EGFP reporter in *Myf5-Cre* expressing cells. We detected $EGFP^+$ myofibers, lacking S6 phosphorylation and thereby mTORC1 activity, in E18.5 RAmyfKO and regenerating RAscKO muscles. Consistently, mTORC1-deficient myoblasts isolated from RAmyfKO embryos or RAscKO mice formed multi-nucleated myotubes *in vitro*, even though their fusion efficiency was decreased. Previously, it was shown that mTOR, independent of its kinase activity, controls the early stages of differentiation (Erbay and Chen, 2001; Ge et al., 2009). Additionally, several studies demonstrated that inhibition of mTORC1 signaling through rapamycin reduces the differentiation capacity of rat and mouse myoblasts *in vitro* and *in vivo* (Ge and Chen, 2012). Surprisingly, we provide evidence that in E11.5 Ctrl embryos mTORC1 signaling is absent in newly formed myofibers, suggesting that mTORC1 is not required after the fusion process during the embryonic wave of myogenesis. During embryonic and fetal myogenesis, myofibers mainly increase in size through myonuclear addition, but they undergo a general maturation and hypertrophic phase after birth (White et al., 2010). Therefore, it could be that mTORC1 signaling plays different roles in myofibers depending on the developmental stage. In summary, we provide evidence that mTORC1 signaling is not absolutely required for differentiation and fusion of muscle progenitors. Hence, inactivation of mTORC1 in muscle progenitors and precursors does not cause a complete blockage of the myogenic process.

Loss of mTORC1 in developing muscle causes partial compensation by non-recombined, raptor-expressing myoblasts

Despite the presence of $EGFP^+$, raptor-depleted myofibers, RAmyfKO muscles were also composed of EGFP-negative fibers, suggesting that those derived from $EGFP^-$, non-Cre-expressing cells and exhibited wild-type characteristics. It has been shown that *Cre* expression in the *Myf5* locus is not faithful with the endogenous *Myf5* expression, therefore leading to the generation of $Myf5^+$, but non-targeted myogenic cells (Comai et al., 2014). Furthermore, it was demonstrated that ablation of Myf5-expressing cells in Myf5-Cre//DTA

embryos stimulates non-targeted escaper cells to compensate and contribute to muscle formation during embryonic development (Comai et al., 2014; Gensch et al., 2008; Haldar et al., 2008). Similarly, we observed an expansion of non-recombined, $EGFP^-$ myoblasts upon the loss of mTORC1 in the *Myf5*-lineage, indicative of a partial compensation for the counter-selection of $EGFP^+$, raptor-depleted myoblasts. Strikingly, the EGFP expression in RAmyfKO muscle followed a heterogeneous patterning, leading to the hypothesis that $EGFP^+$, raptor-depleted myofibers mainly derived from the primary, embryonic wave of myogenesis. In line, we determined that almost all muscle progenitors and precursors of E11.5 RAmyfKO embryos were indeed deficient for mTORC1 signaling. Subsequently, the compensatory phenotype of non-targeted cells likely stems from the secondary, fetal wave of myogenesis, leading to the formation of $EGFP^-$, wild-type fibers. Interestingly, fast muscles, *e.g.* the EDL muscle of RAmKO mice, in which recombination of *Rptor* is induced in differentiating myofibers from E9.5 (Schwander et al., 2003), display signs of slow, *Myh7*-expressing fibers (Bentzinger et al., 2008). Those myofibers either acquire a slow phenotype upon a fiber type switch at adult age or originate from changes in the transition between the embryonic and fetal wave of myogenesis as primary myofibers express only the slow (*Myh7*) and embryonic (*Myh3*) isoforms of myosin heavy chain, while secondary myofibers acquire the fate of fast fibers by upregulating *Myh8* (Biressi et al., 2007b). In summary, defects upon inactivation of mTORC1 in progenitor and precursor cells lead to a partial compensation by non-targeted cells contributing to muscle formation in RAmyfKO hindlimbs.

Restoration of myofibers following muscle injury requires mTORC1

To increase recombination efficiency and recapitulate the function of mTORC1 in the myogenic process occurring during muscle regeneration of the adult tissue, we induced raptor depletion in Pax7-expressing cells (RAscKO). Satellite cells, characterized by their specific Pax7 expression, share similar characteristics to their embryonic counterpart during development as they originate from $Pax3/7^+$, MRF^- cells generated during fetal myogenesis (Kassar-Duchossoy et al., 2005). Abrogation of raptor, leading to inactivation of mTORC1, in Pax7-expressing cells did not affect the quiescent stem cell pool of RAscKO mice under homeostatic conditions, indicating that loss of mTORC1 signaling does not provoke apoptosis of satellite cells. Consistently, it was demonstrated that quiescent satellite cells in adult muscle exhibit low mTORC1 activity, however the signaling is induced upon an alerted stage (G_{Alert}), characterized by a faster cell cycle entry upon a systemic injury (Rodgers et al., 2014). Furthermore, the transition into an activated state depends on the induction of general mRNA translation, which is necessary for the expression of Myf5 and MyoD, both promoting the myogenic process (Crist et al., 2012; Zismanov et al., 2016).

During muscle regeneration, activated satellite cells are marked by high mTORC1 (Rodgers et al., 2014), indicating that the signaling plays a predominant role in activated rather than quiescent satellite cells. Indeed, we observed that mTORC1-deficient satellite cells show a delay in the transition from quiescence into activation, since an increased proportion of RAscKO satellite cells lacked MyoD expression after 24 h in culture. Nevertheless, RAscKO satellite cells entered the activated state at later time points, proposing that the delay in MyoD expression was due to reduced rates of protein synthesis in the absence of mTORC1 signaling. Despite the ability of raptor-depleted satellite cells to enter an activated state, their regenerative capacity was severely impaired in the absence of mTORC1. The regenerative failure of raptor-depleted satellite cells was most likely caused by their deficiency to proliferate in conditions of reduced rates of protein synthesis. Additionally, a decrease in the fusion efficiency of raptor-depleted satellite cells affected the restoration of myofibers, resulting only in small, embMHC$^+$ myofibers formed in regenerating RAscKO muscle. Interestingly, large areas were infiltrated with collagens and lipids in injured RAscKO muscle, suggesting that fibroblast and adipocyte differentiation further suppressed the regeneration process. Fibroblasts and adipocytes infiltrating muscle undergoing chronic degeneration and regeneration, originate from fibro-adipogenic progenitors (FAPs), whose differentiation is repressed in healthy muscle by the presence of restored myofibers (Mozzetta et al., 2013; Uezumi et al., 2010). In summary, we provide evidence that loss of mTORC1 signaling in satellite cells does not prevent their transition from quiescence into activation, however severely impairs their capacity to regenerate skeletal muscle due to defects in proliferation and differentiation.

Disruption of mTORC1 signaling in muscle fibers affects NMJ formation and maintenance

The strong muscle weakness in RAmyfKO embryos was likely the cause for the respiratory failure and subsequent lethality at birth. However, it remains unclear whether the deficits in the formation of neuromuscular junctions (NMJ) contributed to the respiratory failure of RAmyfKO embryos. Similar to the innervation defects in the diaphragm of RAmyfKO embryos, RAmKO mice also show extrasynaptic AChR clusters in the diaphragm muscle (Bentzinger et al., 2008). Interestingly, deteriorations in skeletal muscle fibers, such as inhibition of autophagy, were found to impact on neuromuscular synaptic function and stability (Carnio et al., 2014). In skeletal muscle of RAmKO mice, autophagy is constantly induced and the flux with the subsequent degradation steps is decreased (Castets et al., 2013). Therefore, it may well be that impairments in the autophagy flux provoke alterations in mTORC1-deficient myofibers and thereby cause changes in their neuromuscular synapses. Nevertheless, loss of autophagy in Myf5$^+$ cells does not affect the viability of

mice, as well as embryonic muscle development, even though adult mice display an atrophic phenotype in skeletal muscle (Martinez-Lopez et al., 2013). Hence, possible alterations in the autophagy pathway upon mTORC1 inactivation in muscle progenitors and precursors of RAmyfKO and RAscKO mice may not be the main cause for the defects observed in myogenesis.

In summary, our data demonstrate that coordinated mTORC1 signaling is crucial for the formation of skeletal muscle during embryogenesis and regeneration of the adult tissue. We provide evidence that mTORC1 activity is tightly controlled during the myogenic process and that loss of the signaling strongly affects proliferation and differentiation of muscle precursors. Given our observations, it is important to understand the activity and the function of mTORC1 in every step of the myogenic process, as the signaling is often deregulated in muscle pathologies and skeletal muscle aging.

Material and Methods

Key Resources Table

REAGENT or RESOURCE	SOURCE	IDENTIFIER
Antibodies		
Rabbit monoclonal anti-phospho-S6 ribosomal protein (Ser235/236)	Cell Signaling Technology	Cat#4858S; RRID: AB_916156
Rabbit polyclonal anti-phospho-S6 ribosomal protein (Ser235/236)	Cell Signaling Technology	Cat#2211S; RRID: AB_331679
Mouse monoclonal anti-Pax7	DSHB	Cat#PAX7; RRID: AB_528428
Rabbit polyclonal anti-MyoD1 (clone c-20)	Santa Cruz	Cat#sc-304; RRID: AB_631992
Mouse monoclonal anti-MyoD1 (clone 5.8A)	BD Bioscience	Cat#554130; RRID: AB_395255
Mouse monoclonal anti-Myogenin	DSHB	Cat#f5d; RRID: AB_2146602
Mouse monoclonal anti-myosin (embryonic)	DSHB	Cat#F1.652; RRID: AB_528358
Rabbit polyclonal anti-desmin	Abcam	Cat#ab15200; RRID: AB_301744
Rabbit polyclonal anti-laminin	Abcam	Cat#ab11575; RRID: AB_298179
Chicken polyclonal anti-GFP Tag	Thermo Fisher Scientific	Cat#A10262; RRID: AB_2534023
Rat monoclonal anti-BrdU [BU1/75 (ICR1)]	Abcam	Cat#ab6326; RRID: AB_305426

Mouse monoclonal anti-Puromycin (clone 12D10)	Millipore	Cat#MABE343 ; RRID: AB_2566826
Rabbit polyclonal anti-Synaptophysin	Dako	Cat#A0010; RRID: AB_2315411
Rabbit polyclonal anti-Neurofilament 200	Sigma	Cat#N4142; RRID: AB_477272
Rabbit monoclonal anti-Raptor	Cell Signaling Technology	Cat#2280S; RRID: AB_10694695
Rabbit monoclonal anti-S6 ribosomal protein (clone 5G10)	Cell Signaling Technology	Cat#2217S; RRID: AB_331355
Rabbit polyclonal anti-phospho-4E-BP1 (Ser65)	Cell Signaling Technology	Cat#9451S; RRID: AB_330947
Rabbit polyclonal anti-4E-BP1	Cell Signaling Technology	Cat#9452S; RRID: AB_10693791
Mouse monoclonal anti-α-Actinin	Sigma	Cat#A7732; RRID: AB_2221571
Rabbit polyclonal anti-Pan-Actin	Cell Signaling Technology	Cat#4968S; RRID: AB_10695740
Rabbit monoclonal anti-Rictor	Cell Signaling Technology	Cat#9476S; RRID: AB_10612959
Rabbit polyclonal anti-phospho-PKCα (Ser657)	Santa Cruz	Cat#sc-12356; RRID: AB_2168557
Rabbit polyclonal anti-PKCα	Cell Signaling Technology	Cat#2056S; RRID: AB_2284227

Rabbit monoclonal anti-phospho-Akt (Ser473)	Cell Signaling Technology	Cat#4058S; RRID: AB_331168
Rabbit polyclonal anti-Akt	Cell Signaling Technology	Cat#9272S; RRID: AB_329827
Mouse monoclonal anti-Integrin α-7 (clone 3C12)	MBL International Corporation	Cat#K0046-3; RRID: AB_592046
Rat monoclonal PE anti-CD11b	eBioscience	Cat#12-0112-81; RRID: AB_465546
Rat monoclonal PE anti-CD45	eBioscience	Cat#12-0451-81; RRID: AB_465667
Rat monoclonal biotin anti-CD34	eBioscience	Cat#13-0341-81; RRID: AB_466424
Rat monoclonal PE anti-Ly-6A/E	BD Biosciences	Cat#553108; RRID: AB_394629
Mouse monoclonal PE anti-CD31	BD Biosciences	Cat#555027; RRID: AB_395657
Biological Samples		
Freshly-sorted muscle progenitor cells or muscle satellite cells	This paper	N/A
Chemicals, Peptides, and Recombinant Proteins		
Alcian Blue	Sigma	005500
Alizarin Red	Sigma	A5533
Cardiotoxin	Latoxan	L8102
Puromycin	Sigma	P8833
Cycloheximide	Sigma	C7698
BrdU	Sigma	B5002
Dispase II	Roche	04942078001
Collagenase B	Roche	11088831001

Trypsin 2.5 %, no phenol red	Fisher Scientific	15090046
Tamoxifen	Sigma	T5648
Oil Red O	Sigma	O0625
Direct Red 80	Sigma	365548
Penicillin-Streptomycin	Thermo Fisher Scientific	15140122
Matrigel	BD Biosciences	354234
Chicken embryo extract (CEE)	MP Biomedicals / US Biological Life Sciences	92850145 / C3999
Collagenase A	Roche	10103586001
FGF-basic (AA 10-155) recombinant human protein	Thermo Fisher Scientific	PHG0023
RNase-free DNase	Qiagen	79254
PhosSTOP	Roche	04 906 837 001
cOmplete Mini, EDTA-free	Roche	11836170001
Proteinase K	Qiagen	19131
α-Bungarotoxin Alexa-488	Thermo Fisher Scientific	B13422
APC-Cy7 Streptavidin	BD Biosciences	5554063
Cy3 Streptavidin	Jackson Immuno Research Laboratories	016-160-084
Biotin-AffiniPure Goat anti-Mouse IgG1, Fcγ subclass 1 specific	Jackson Immuno Research Laboratories	115-065-205
IgG-free, protease-free BSA	Jackson Immuno Research Laboratories	001-000-162
Critical Commercial Assays		
In Situ Cell Death Detection Kit, Fluorescein	Roche	11684795910
Pierce BCA Protein Assay Kit	Thermo Fisher Scientific	23227
RNeasy Mini Kit	Qiagen	74104
iScript cDNA Synthesis Kit	Bio-Rad	170-8891
Power SYBR Green PCR Master Mix	Applied Biosystems	4367659

Experimental Models: Organisms/Strains		
Mouse: *Pax7*$^{tm1(cre/ERT2)GAKA}$*/J*	Jackson Laboratory	JAX: 017763
Mouse: *Gt(ROSA)26Sor*$^{tm8(CAG-EGFP)Npa}$	(Tchorz et al., 2012)	N/A
Mouse: *Myf5*$^{tm3(cre)Sor}$*/J*	Jackson Laboratory	JAX: 007845
Mouse: *Rptor*^{tm1Rueg}	(Bentzinger et al., 2008)	N/A
Software and Algorithms		
FlowJo V10	FlowJo	https://www.flowjo.com/
ImageJ-win64	National Institutes of Health	https://imagej.nih.gov/ij/download.html
GraphPad Prism 7	Graph Pad	https://www.graphpad.com/
StepOne Software v2.3	Thermo Fisher Scientific	https://www.thermofisher.com/
Other		
Cryostat CM1950	Leica	N/A
Microscope IX81 with camera XM10 and SC30	Olympus	N/A
Stereomicroscope M60 with camera IC80 HD	Leica	N/A
Fluorescence microscope DM5000 B	Leica	N/A
Microscope DMi8 with camera C11440	Leica / Hamamatsu	N/A
Confocal Microscope TCS SPE	Leica	N/A
FACSAria IIIu (cell sorter)	BD Bioscience	N/A
Step One Plus	Applied Biosystems	N/A
Fusion Fx7	Vilber Lourmat	N/A

Contact for Reagent and Resource Sharing

Further information and requests for resources and reagents should be directed to and will be fulfilled by the Lead Contact, Markus A. Rüegg (markus-a.ruegg@unibas.ch).

Experimental Model and Subject Details

Mouse Models

RAmyfKO and RAscKO mice were generated by crossing *Rptor*-floxed mice (Bentzinger et al., 2008) with transgenic mice expressing *Cre recombinase* under the control of the *Myf5* promoter that were obtained from Jackson Laboratories (Tallquist et al., 2000) or mice expressing Cre in the *Pax7* locus (Murphy et al., 2011), respectively. Both mouse models were additionally crossed with mR26CS-EGFP mice (Tchorz et al., 2012). RImyfKO mice were generated by crossing *Rictor*-floxed mice (Bentzinger et al., 2008) with *Myf5*-Cre mice (Tallquist et al., 2000). Genotyping and recombination PCR for the conditional *Rptor* or *Rictor* allele, *Cre recombinase* knock-in in the *Myf5* or *Pax7* locus and mR26-CS-EGFP transgene expression was performed as described (Bentzinger et al., 2008; Murphy et al., 2011; Tallquist et al., 2000; Tchorz et al., 2012). To induce raptor depletion in Pax7-expressing cells, intraperitoneal tamoxifen (2.5 mg/day) injections were administered in corn oil to 2 – 3 month-old mice for five consecutive days. For the analysis of adult mice, only male mice were used. All mice were maintained in a licensed animal facility with a fixed 12 h dark-light cycle and allowed food and water *ad libitum*. All animal studies were performed under the guidelines and the law of the Swiss authorities and regularly controlled and approved by the veterinary office.

Primary Cultures

RAmyfKO primary muscle progenitors or RAscKO satellite cells were isolated by FACS and RImyfKO primary myoblasts as described previously (Rosenblatt et al., 1995). Primary myoblasts were maintained in Glutamax Dulbecco's modified Eagle's medium (DMEM Glutamax) supplemented with 10 % horse serum (HS), 20 % fetal bovine serum (FBS), 1 % chicken embryo extract (CEE), 1 % penicillin-streptomycin (pen/strep) and 0.5 ng/ml β-fibroblast growth factor on Matrigel-coated cell culture dishes in 37 °C incubator with 5 % CO_2. For induction of myogenic differentiation, an equal number of cells were plated at higher density and incubated with DMEM Glutamax with 4 % HS, 1 % CEE and 1 % penicillin / streptomycin one day after FACS isolation. To test the proliferation capacity of myoblasts, the same number of cells were incubated in proliferation medium for 48 h or in differentiation medium for 14 h and 7.67 ug/ml Bromodeoxyuridine (BrdU, Sigma) was added for 1 h. To analyze the rates of protein synthesis the cells were incubated with 1 µM puromycin (Sigma) with or without 100 ug/ul cycloheximide (Sigma) for 30 min. Cells were fixed with 4 % paraformaldehyde (PFA, Fluka Chemika), washed with PBS pH7.4, 0.1 M glycine and kept frozen for subsequent immunostaining.

Method Details

Skeleton staining

E18.5 embryos were skinned, macerated and stained with Alcian Blue (cartilage, Sigma) and Alizarin Red (ossified bones, Sigma). The detailed protocol was previously described (Schneider, 2013). The stained skeleton was imaged using the stereomicroscope M60 (Leica) and the camera IC80 HD (Leica).

Cardiotoxin injury

2 – 3 month-old mice were anesthetized by intraperitoneal injection of Ketamine (111 mg/kg, Ketalar) and Xylzine (22 mg/kg, Rompun). The *tibialis anterior* (TA) and *extensor digitorum longus* (EDL) muscles of one left leg were injected with 150 µl of 6.7 µg Cardiotoxin (Latoxan) to induce complete muscle necrosis. The other leg was untreated and served as the contralateral control. The mice were treated with the analgesic 0.1 mg/kg Buprenorphine, twice a day for at least three days. The TA and EDL muscles were dissected 15 days after injury for subsequent histology or immunofluorescent staining.

Isolation of embryonic and adult muscle progenitors by FACS

To obtain embryonic myogenic cells by FACS isolation the protocol was adapted from (Pasut et al., 2013). In brief, hindlimb and foreleg muscles of E18.5 embryos were dissected and minced. Digestion of the tissue was started by transferring the muscle pieces into PBS with Collagenase B (2.5 U/ml, Roche) and Dispase II (2.5 U/ml, Roche) at 37 °C for 40 min with repeated trituration using a FBS-coated pipette. Digestion was stopped by the addition of 2 volumes of 10 % FBS. The cell suspension was filtered with a 70 µm cell strainer (Corning) and centrifuged two times at 239 g for 5 min. Adult muscle stem cells were isolated from hindlimb and foreleg muscles of 3 month-old mice 10 days after tamoxifen treatment according to a protocol modified from (Garcia-Prat et al., 2016). The muscles were minced and digested in PBS with 0.16 % Collagenase B (Roche) and 0.125% Trypsin (Gibco) at 37 °C under rotating conditions. After 25 min, the supernatant was collected, enzyme-inactivated with 0.25 volume of FBS and filtered with a 70 µm cell strainer (Corning). The remaining muscle pieces were again digested at 37 °C under rotating conditions. This procedure was repeated 4 times until the entire muscle was digested. The collected cell suspension was centrifuged at 60 g for 10 min to remove big pieces, the pellet washed and re-centrifuged. All the supernatant was centrifuged at 500 g for 15 min to collect all the isolated cells. Single cells were incubated with the following antibodies: anti-Integrin α-7 (MBL International Corporation), biotin anti-CD34 (eBioscience), PE anti-CD11b (eBioscience), PE anti-CD45 (eBioscience), PE anti-Ly-6A/E (BD Biosciences), PE anti-CD31 (BD Biosciences), APC-Cy7 Streptavidin (BD Biosciences) and Alexa647 anti-

mouse IgG1 (Molecular Probes). Additionally, DAPI was used as viability marker. Embryonic (Integrin α-7$^+$/CD11b$^-$/CD45$^-$/Sca1$^-$/CD31$^-$) and adult (Integrin α-7$^+$/CD34$^+$/CD11b$^-$/CD45$^-$/Sca1$^-$/CD31$^-$) myogenic cells were sorted by FACSAria IIIu cell sorter (BD Biosciences). Cells expressing EGFP were sorted based on their endogenous fluorescence.

Single fiber isolation

Single myofibers were isolated from the EDL muscle of 3 month-old mice 90 days after tamoxifen treatment by enzymatic digestion and trituration as previously described (Rosenblatt et al., 1995). In brief, the EDL was carefully dissected and digested in DMEM Glutamax (Gibco) supplemented with 1 mg/ml Collagenase A (Roche) and 1 % penicillin-streptomycin (Thermo Fisher Scientific) for 1.5 h at 37 °C and 5 % CO_2. Loose muscle bundles were transferred into DMEM Glutamax, 1 % pen/strep and triturated and cleaned into single myofibers. Fibers analyzed at T0 were immediately fixed with 4 % PFA. Fibers kept in culture for up to 72 h were transferred into DMEM Glutamax, 1 % pen/strep, 10 % HS, 1 % CEE and fixed with 4 % PFA at the time points indicated. Fibers were washed with PBS, permeabilized for 6 min with PBS, 0.5 % Triton-X100 and washed again. The fibers were then incubated in blocking solution (10 % HS, 10 % goat serum, 0.35 % Carrageenan – Sigma, PBS) for 30 min and primary antibodies were added overnight at 4 °C. Fibers were washed in PBS, 0.025 % Tween-20 (Sigma) and incubated with the secondary antibodies for 1.5 h. Following washing steps, the fibers were collected with a smoothened glass, horse serum-coated glass pipette and transferred on Non-Superfrost glass slides coated with 84 % acetone, 16 % (3-aminopropyl)triethoxysilane (Sigma). The fibers were mounted with Vectashield Dapi mounting medium. Primary antibodies and the dilution factors used were listed below: anti-Pax7 (Pax7, supernatant, DSHB, 1:100), anti-MyoD1 clone c-20 (sc-304, Santa Cruz, 1:100).

Histology

Mouse embryos were isolated at the embryonic stage of interest and equilibrated in 30 % Sucrose/PBS overnight at 4 °C. Embryos were embedded and frozen in Tissue-Tek (Sakure Finetek) and serially sectioned into 12 µm sections on a cryostat (CM1950, Leica). Only sections from embryos that were frozen and cut in the same orientation, were compared. Muscles from adult mice were dissected and frozen in liquid nitrogen-cooled isopentane. Consecutive cryosections of 8 µm were prepared. Embryos or adult muscles expressing EGFP were fixed in 4 % paraformaldehyde (PFA) overnight or in 2 % PFA for 2 h, respectively, and were incubated in 20 % sucrose overnight prior to freezing. General histology on sections was performed using hematoxylin and eosin staining (Merck) followed

by sequential dehydration with 70 %, 90 %, 100 % ethanol and 100 % xylene. For oil red O staining, sections were fixed with 4 % PFA for 1 h and stained with Oil Red O (Sigma; 5 mg/ml in 60 % triethyl-phosphate, Sigma) for 30 min. Then the sections were washed with running tap water and mounted in 10 % glycerol. Collagens were stained with a Picro-Sirius Red solution (Direct Red 80, Sigma; 1 mg/ml in 1.3 % aqueous solution of picric acid, Sigma) for 1 h followed by washing in 0.5 % acidic water for 30 min. The slides were mounted after dehydration in 100 % ethanol and after clearing in xylene.

Immunostaining

Cross-sections or cells were fixed with 4 % PFA for 6 min, washed in PBS pH7.4, 0.1 M glycine for neutralization and permeabilized with pre-cooled methanol for 6 min. Antigen retrieval was achieved by warming the sections in 0.01 M citric acid (Sigma) just below the boiling point. The samples were blocked in 3 % IgG-free BSA (Jackson Immuno Research Laboratories) supplemented with 0.05 mg/ml AffiniPure Mouse IgG, Fab Fragment (Jackson Immuno Research Laboratories). The primary antibodies with the according dilution listed below, were incubated overnight at 4 °C. The samples were washed with PBS and incubated with the corresponding secondary antibodies for 1.5 h at room temperature. After 3 times washing, the samples were mounted with Vectashield Dapi (Vector Laboratories). Immunostaining for EGFP and phospho-S6 ribosomal protein (Ser235/236) were performed without methanol treatment and antigen retrieval, instead 0.5 % Triton X-100 (Sigma) was added to the blocking solution for permeabilization. Apoptotic nuclei were immunolabeled using the "*In Situ* Cell Death Detection Kit, Fluorescein" (Roche) according to manufacturer's protocol. Whole-mount immunostaining of diaphragms from E17.5 embryos was performed by fixing the tissue with 1 % PFA, 0.1 M sodium phosphate pH7.3 at 4 °C. The diaphragms were rinsed in PBS and incubated in 0.1 M glycine pH7.3 for 15 min. After washing, the tissue was permeabilized and blocked in 2 % BSA (Sigma), 4 % goat serum, 0.5 % Triton X-100 (Sigma), PBS. The primary antibody was incubated overnight in 2 % BSA, 4 % NGS, PBS. After washing 3 times for 1 h, the secondary antibody was incubated overnight. The washing was repeated and the samples sequentially post-fixed in 1 % PFA, 100 % methanol and mounted in citifluor (Electron Microscopy Sciences). Primary antibodies and the dilution factors used were listed below: anti-phospho-S6 ribosomal protein (Ser235/236) (4858S, CST, 1:100), anti-Pax7 (Pax7, supernatant, DSHB, 1:50), anti-MyoD1 (554130, BD Bioscience, 1:500), anti-Myogenin (f5d, supernatant, DSHB, 1:50), anti-Myosin embryonic (F1.652, biosupe, DSHB, 1:1'200), anti-Desmin (ab15200, Abcam, 1:300), anti-Laminin (ab11575, Abcam, 1:300), anti-GFP (A10262, Thermo Fisher Scientific, 1:400), anti-BrdU (ab6326, Abcam, 1:300), anti-Puromycin

(MABE343, Millipore, 1:1'000), anti-Synaptophysin (A0010, Dako, 1:200), anti-Neurofilament (N4142, Sigma, 1:8'000).

Immunoblotting

Quadriceps muscles from 3 month-old mice were frozen in liquid nitrogen and powdered on dry ice. Hindlimb and foreleg muscles from E18.5 embryos were minced and snap-frozen in liquid nitrogen. Proliferating primary myoblasts were collected after trypsination, washed in cold PBS and snap-frozen as pellet in liquid nitrogen. Samples were lysed in cold RIPA buffer (50 mM Tris-HCl pH8, 150 mM NaCl, 1 % NP-40, 0.5 % sodium deoxycholate, 0.1 % SDS, 1 % Triton X-100, 10 % glycerol, ddH_2O) supplemented with phosphatase and protease inhibitor cocktail tablets (Roche), incubated on ice for 2 h and sonicated two times for 15 sec. Afterwards, the lysate was centrifuged at 16'000 g for 30 min at 4 °C. The cleared lysates were used to determine total protein amount using the Pierce BCA Protein Assay Kit (Thermo Fisher Scientific) according to manufacturer's protocol. Proteins were separated on 4 – 12 % Bis-Tris Protein Gels (NuPage Novex, Thermo Fisher Scientific) and transferred to nitrocellulose membrane (Whatman). The membrane was blocked with 5 % BSA, 0.1 % Tween-20, TBS for 1 h at room temperature. The primary antibody diluted in the blocking solution was incubated overnight at 4 °C with continuous shaking. The membranes were washed three times for 15 min with TBST (0.05 % Tween-20, TBS) and incubated with the secondary horseradish peroxidase-conjugated antibody for 1.5 h at room temperature. After washing with TBST, proteins were visualized by chemiluminescence (KPL). Primary antibodies and dilution factors used were listed below: anti-Raptor (2280S, CST, 1:1'000), anti-phospho-S6 ribosomal protein (Ser235/236) (2211S, CST, 1:1'000), anti-S6 ribosomal protein (2217S, CST, 1:1'000), anti-phospho-4E-BP1 (Ser65) (9451S, CST, 1:1'000), anti-phospho-4E-BP1 (9452S, CST, 1:1'000), anti-Pan-Actin (4968S, CST, 1:1'000), anti-α-Actinin (A7732, Sigma, 1:5'000), anti-Rictor (9476S, CST, 1:1'000), anti-PKCα (2056S, CST, 1:1'000), anti-phospho-PKCα (Ser657) (sc-12356, Santa Cruz, 1:500), anti-Akt (9272S, CST, 1:1'000), anti-phospho-Akt (Ser473) (4058S, CST, 1:1'000).

RNA extraction and qRT-PCR

Total RNA were extracted from whole E11.5 and E13.5 embryos or from hindlimb and foreleg muscles of E18.5 embryos using the RNeasy Mini Kit (Qiagen) according to manufacturer's protocol. RNA was transcribed into cDNA using the iScript cDNA Synthesis Kit (Bio-Rad). Selected genes were amplified and detected using the Power SYBR Green PCR Master Mix (Applied Biosystems) and the relative gene expression was determined with the Step One software and normalized to ***β-actin*** expression. All qPCR primers were listed in Table S3.

Quantification and Statistical Analysis

All experiments were performed on a minimum of 3 independent biological samples indicated by the n-number (n). In all graphs, data are represented as the mean value and the respective standard error of the mean (SEM, error bars). Student's *t* test was employed when two groups were compared to evaluate statistical significance. One or two-way ANOVA with Tukey's multiple comparisons test was used in comparisons of more than two groups. P-values lower than 0.05 are considered statistically significant.

Data and Software availability

A list of software used in this study can be found in the Key Resources Table.

References

Bentzinger, C.F., Romanino, K., Cloetta, D., Lin, S., Mascarenhas, J.B., Oliveri, F., Xia, J., Casanova, E., Costa, C.F., Brink, M.*, et al.* (2008). Skeletal muscle-specific ablation of raptor, but not of rictor, causes metabolic changes and results in muscle dystrophy. Cell Metab *8*, 411-424.

Biressi, S., Molinaro, M., and Cossu, G. (2007a). Cellular heterogeneity during vertebrate skeletal muscle development. Dev Biol *308*, 281-293.

Biressi, S., Tagliafico, E., Lamorte, G., Monteverde, S., Tenedini, E., Roncaglia, E., Ferrari, S., Ferrari, S., Cusella-De Angelis, M.G., Tajbakhsh, S.*, et al.* (2007b). Intrinsic phenotypic diversity of embryonic and fetal myoblasts is revealed by genome-wide gene expression analysis on purified cells. Dev Biol *304*, 633-651.

Blandino-Rosano, M., Barbaresso, R., Jimenez-Palomares, M., Bozadjieva, N., Werneck-de-Castro, J.P., Hatanaka, M., Mirmira, R.G., Sonenberg, N., Liu, M., Ruegg, M.A.*, et al.* (2017). Loss of mTORC1 signalling impairs beta-cell homeostasis and insulin processing. Nat Commun *8*, 16014.

Bonneau, A.M., and Sonenberg, N. (1987). Involvement of the 24-kDa cap-binding protein in regulation of protein synthesis in mitosis. J Biol Chem *262*, 11134-11139.

Carnio, S., LoVerso, F., Baraibar, M.A., Longa, E., Khan, M.M., Maffei, M., Reischl, M., Canepari, M., Loefler, S., Kern, H.*, et al.* (2014). Autophagy impairment in muscle induces neuromuscular junction degeneration and precocious aging. Cell Rep *8*, 1509-1521.

Castets, P., Lin, S., Rion, N., Di Fulvio, S., Romanino, K., Guridi, M., Frank, S., Tintignac, L.A., Sinnreich, M., and Ruegg, M.A. (2013). Sustained activation of mTORC1 in skeletal muscle inhibits constitutive and starvation-induced autophagy and causes a severe, late-onset myopathy. Cell Metab *17*, 731-744.

Comai, G., Sambasivan, R., Gopalakrishnan, S., and Tajbakhsh, S. (2014). Variations in the Efficiency of Lineage Marking and Ablation Confound Distinctions between Myogenic Cell Populations. Dev Cell *31*, 654-667.

Conejo, R., and Lorenzo, M. (2001). Insulin signaling leading to proliferation, survival, and membrane ruffling in C2C12 myoblasts. J Cell Physiol *187*, 96-108.

Coolican, S.A., Samuel, D.S., Ewton, D.Z., McWade, F.J., and Florini, J.R. (1997). The mitogenic and myogenic actions of insulin-like growth factors utilize distinct signaling pathways. J Biol Chem *272*, 6653-6662.

Crist, C.G., Montarras, D., and Buckingham, M. (2012). Muscle satellite cells are primed for myogenesis but maintain quiescence with sequestration of Myf5 mRNA targeted by microRNA-31 in mRNP granules. Cell Stem Cell *11*, 118-126.

Cuenda, A., and Cohen, P. (1999). Stress-activated protein kinase-2/p38 and a rapamycin-sensitive pathway are required for C2C12 myogenesis. J Biol Chem *274*, 4341-4346.

Cuyas, E., Corominas-Faja, B., Joven, J., and Menendez, J.A. (2014). Cell cycle regulation by the nutrient-sensing mammalian target of rapamycin (mTOR) pathway. Methods Mol Biol *1170*, 113-144.

Deries, M., and Thorsteinsdottir, S. (2016). Axial and limb muscle development: dialogue with the neighbourhood. Cell Mol Life Sci *73*, 4415-4431.

Dowling, R.J., Topisirovic, I., Alain, T., Bidinosti, M., Fonseca, B.D., Petroulakis, E., Wang, X., Larsson, O., Selvaraj, A., Liu, Y.*, et al.* (2010). mTORC1-mediated cell proliferation, but not cell growth, controlled by the 4E-BPs. Science *328*, 1172-1176.

Dumont, N.A., Bentzinger, C.F., Sincennes, M.C., and Rudnicki, M.A. (2015). Satellite Cells and Skeletal Muscle Regeneration. Compr Physiol *5*, 1027-1059.

Erbay, E., and Chen, J. (2001). The mammalian target of rapamycin regulates C2C12 myogenesis via a kinase-independent mechanism. J Biol Chem *276*, 36079-36082.

Erbay, E., Park, I.H., Nuzzi, P.D., Schoenherr, C.J., and Chen, J. (2003). IGF-II transcription in skeletal myogenesis is controlled by mTOR and nutrients. J Cell Biol *163*, 931-936.

Fan, H., and Penman, S. (1970). Regulation of protein synthesis in mammalian cells. II. Inhibition of protein synthesis at the level of initiation during mitosis. J Mol Biol *50*, 655-670.

Gangloff, Y.G., Mueller, M., Dann, S.G., Svoboda, P., Sticker, M., Spetz, J.F., Um, S.H., Brown, E.J., Cereghini, S., Thomas, G.*, et al.* (2004). Disruption of the mouse mTOR gene leads to early postimplantation lethality and prohibits embryonic stem cell development. Mol Cell Biol *24*, 9508-9516.

Garcia-Prat, L., Martinez-Vicente, M., Perdiguero, E., Ortet, L., Rodriguez-Ubreva, J., Rebollo, E., Ruiz-Bonilla, V., Gutarra, S., Ballestar, E., Serrano, A.L.*, et al.* (2016). Autophagy maintains stemness by preventing senescence. Nature *529*, 37-42.

Ge, Y., and Chen, J. (2012). Mammalian target of rapamycin (mTOR) signaling network in skeletal myogenesis. J Biol Chem *287*, 43928-43935.

Ge, Y., Wu, A.L., Warnes, C., Liu, J., Zhang, C., Kawasome, H., Terada, N., Boppart, M.D., Schoenherr, C.J., and Chen, J. (2009). mTOR regulates skeletal muscle regeneration in vivo through kinase-dependent and kinase-independent mechanisms. Am J Physiol Cell Physiol *297*, C1434-1444.

Ge, Y., Yoon, M.S., and Chen, J. (2011). Raptor and Rheb negatively regulate skeletal myogenesis through suppression of insulin receptor substrate 1 (IRS1). J Biol Chem *286*, 35675-35682.

Gensch, N., Borchardt, T., Schneider, A., Riethmacher, D., and Braun, T. (2008). Different autonomous myogenic cell populations revealed by ablation of Myf5-expressing cells during mouse embryogenesis. Development *135*, 1597-1604.

Goodman, C.A., and Hornberger, T.A. (2013). Measuring protein synthesis with SUnSET: a valid alternative to traditional techniques? Exerc Sport Sci Rev *41*, 107-115.

Guertin, D.A., Stevens, D.M., Thoreen, C.C., Burds, A.A., Kalaany, N.Y., Moffat, J., Brown, M., Fitzgerald, K.J., and Sabatini, D.M. (2006). Ablation in mice of the mTORC components raptor, rictor, or mLST8 reveals that mTORC2 is required for signaling to Akt-FOXO and PKCalpha, but not S6K1. Dev Cell *11*, 859-871.

Haldar, M., Karan, G., Tvrdik, P., and Capecchi, M.R. (2008). Two cell lineages, myf5 and myf5-independent, participate in mouse skeletal myogenesis. Dev Cell *14*, 437-445.

Heesom, K.J., Gampel, A., Mellor, H., and Denton, R.M. (2001). Cell cycle-dependent phosphorylation of the translational repressor eIF-4E binding protein-1 (4E-BP1). Curr Biol *11*, 1374-1379.

Hung, C.M., Calejman, C.M., Sanchez-Gurmaches, J., Li, H., Clish, C.B., Hettmer, S., Wagers, A.J., and Guertin, D.A. (2014). Rictor/mTORC2 loss in the Myf5 lineage reprograms brown fat metabolism and protects mice against obesity and metabolic disease. Cell Rep *8*, 256-271.

Kassar-Duchossoy, L., Giacone, E., Gayraud-Morel, B., Jory, A., Gomes, D., and Tajbakhsh, S. (2005). Pax3/Pax7 mark a novel population of primitive myogenic cells during development. Genes Dev *19*, 1426-1431.

Kleinert, M., Parker, B.L., Chaudhuri, R., Fazakerley, D.J., Serup, A., Thomas, K.C., Krycer, J.R., Sylow, L., Fritzen, A.M., Hoffman, N.J.*, et al.* (2016). mTORC2 and AMPK differentially regulate muscle triglyceride content via Perilipin 3. Mol Metab *5*, 646-655.

Leu, M., Bellmunt, E., Schwander, M., Farinas, I., Brenner, H.R., and Muller, U. (2003). Erbb2 regulates neuromuscular synapse formation and is essential for muscle spindle development. Development *130*, 2291-2301.

Martinez-Lopez, N., Athonvarangkul, D., Sahu, S., Coletto, L., Zong, H., Bastie, C.C., Pessin, J.E., Schwartz, G.J., and Singh, R. (2013). Autophagy in Myf5+ progenitors regulates energy and glucose homeostasis through control of brown fat and skeletal muscle development. EMBO reports *14*, 795-803.

Miyabara, E.H., Conte, T.C., Silva, M.T., Baptista, I.L., Bueno, C., Jr., Fiamoncini, J., Lambertucci, R.H., Serra, C.S., Brum, P.C., Pithon-Curi, T.*, et al.* (2010). Mammalian target of rapamycin complex 1 is involved in differentiation of regenerating myofibers in vivo. Muscle Nerve *42*, 778-787.

Mozzetta, C., Consalvi, S., Saccone, V., Tierney, M., Diamantini, A., Mitchell, K.J., Marazzi, G., Borsellino, G., Battistini, L., Sassoon, D.*, et al.* (2013). Fibroadipogenic progenitors mediate the ability of HDAC inhibitors to promote regeneration in dystrophic muscles of young, but not old Mdx mice. EMBO Mol Med *5*, 626-639.

Murakami, M., Ichisaka, T., Maeda, M., Oshiro, N., Hara, K., Edenhofer, F., Kiyama, H., Yonezawa, K., and Yamanaka, S. (2004). mTOR is essential for growth and proliferation in early mouse embryos and embryonic stem cells. Mol Cell Biol *24*, 6710-6718.

Murphy, M.M., Lawson, J.A., Mathew, S.J., Hutcheson, D.A., and Kardon, G. (2011). Satellite cells, connective tissue fibroblasts and their interactions are crucial for muscle regeneration. Development *138*, 3625-3637.

Ohanna, M., Sobering, A.K., Lapointe, T., Lorenzo, L., Praud, C., Petroulakis, E., Sonenberg, N., Kelly, P.A., Sotiropoulos, A., and Pende, M. (2005). Atrophy of S6K1(-/-) skeletal muscle cells reveals distinct mTOR effectors for cell cycle and size control. Nat Cell Biol *7*, 286-294.

Ott, M.O., Bober, E., Lyons, G., Arnold, H., and Buckingham, M. (1991). Early expression of the myogenic regulatory gene, myf-5, in precursor cells of skeletal muscle in the mouse embryo. Development *111*, 1097-1107.

Pallafacchina, G., Blaauw, B., and Schiaffino, S. (2013). Role of satellite cells in muscle growth and maintenance of muscle mass. Nutr Metab Cardiovasc Dis *23 Suppl 1*, S12-18.

Park, I.H., and Chen, J. (2005). Mammalian target of rapamycin (mTOR) signaling is required for a late-stage fusion process during skeletal myotube maturation. J Biol Chem *280*, 32009-32017.

Pasut, A., Jones, A.E., and Rudnicki, M.A. (2013). Isolation and culture of individual myofibers and their satellite cells from adult skeletal muscle. J Vis Exp, e50074.

Pollard, H.J., Willett, M., and Morley, S.J. (2014). mTOR kinase-dependent, but raptor-independent regulation of downstream signaling is important for cell cycle exit and myogenic differentiation. Cell Cycle *13*, 2517-2525.

Ramirez-Valle, F., Badura, M.L., Braunstein, S., Narasimhan, M., and Schneider, R.J. (2010). Mitotic raptor promotes mTORC1 activity, G(2)/M cell cycle progression, and internal ribosome entry site-mediated mRNA translation. Mol Cell Biol *30*, 3151-3164.

Risson, V., Mazelin, L., Roceri, M., Sanchez, H., Moncollin, V., Corneloup, C., Richard-Bulteau, H., Vignaud, A., Baas, D., Defour, A.*, et al.* (2009). Muscle inactivation of mTOR causes metabolic and dystrophin defects leading to severe myopathy. J Cell Biol *187*, 859-874.

Rodgers, J.T., King, K.Y., Brett, J.O., Cromie, M.J., Charville, G.W., Maguire, K.K., Brunson, C., Mastey, N., Liu, L., Tsai, C.R.*, et al.* (2014). mTORC1 controls the adaptive transition of quiescent stem cells from G0 to G(Alert). Nature *510*, 393-396.

Rosenblatt, J.D., Lunt, A.I., Parry, D.J., and Partridge, T.A. (1995). Culturing satellite cells from living single muscle fiber explants. In Vitro Cell Dev Biol Anim *31*, 773-779.

Sarbassov, D.D., Ali, S.M., Sengupta, S., Sheen, J.H., Hsu, P.P., Bagley, A.F., Markhard, A.L., and Sabatini, D.M. (2006). Prolonged rapamycin treatment inhibits mTORC2 assembly and Akt/PKB. Mol Cell *22*, 159-168.

Saxton, R.A., and Sabatini, D.M. (2017). mTOR Signaling in Growth, Metabolism, and Disease. Cell *168*, 960-976.

Schneider, S. (2013). Skeletal examination by double staining for ossified bone and cartilaginous tissue. Methods Mol Biol *947*, 215-221.

Schwander, M., Leu, M., Stumm, M., Dorchies, O.M., Ruegg, U.T., Schittny, J., and Muller, U. (2003). Beta1 integrins regulate myoblast fusion and sarcomere assembly. Dev Cell *4*, 673-685.

Tallquist, M.D., Weismann, K.E., Hellstrom, M., and Soriano, P. (2000). Early myotome specification regulates PDGFA expression and axial skeleton development. Development *127*, 5059-5070.

Tchorz, J.S., Suply, T., Ksiazek, I., Giachino, C., Cloetta, D., Danzer, C.P., Doll, T., Isken, A., Lemaistre, M., Taylor, V.*, et al.* (2012). A modified RMCE-compatible Rosa26 locus for the expression of transgenes from exogenous promoters. PLoS One *7*, e30011.

Uezumi, A., Fukada, S., Yamamoto, N., Takeda, S., and Tsuchida, K. (2010). Mesenchymal progenitors distinct from satellite cells contribute to ectopic fat cell formation in skeletal muscle. Nat Cell Biol *12*, 143-152.

Vinagre, T., Moncaut, N., Carapuco, M., Novoa, A., Bom, J., and Mallo, M. (2010). Evidence for a myotomal Hox/Myf cascade governing nonautonomous control of rib specification within global vertebral domains. Dev Cell *18*, 655-661.

White, R.B., Bierinx, A.S., Gnocchi, V.F., and Zammit, P.S. (2010). Dynamics of muscle fibre growth during postnatal mouse development. BMC Dev Biol *10*, 21.

Zismanov, V., Chichkov, V., Colangelo, V., Jamet, S., Wang, S., Syme, A., Koromilas, A.E., and Crist, C. (2016). Phosphorylation of eIF2alpha Is a Translational Control Mechanism Regulating Muscle Stem Cell Quiescence and Self-Renewal. Cell Stem Cell *18*, 79-90.

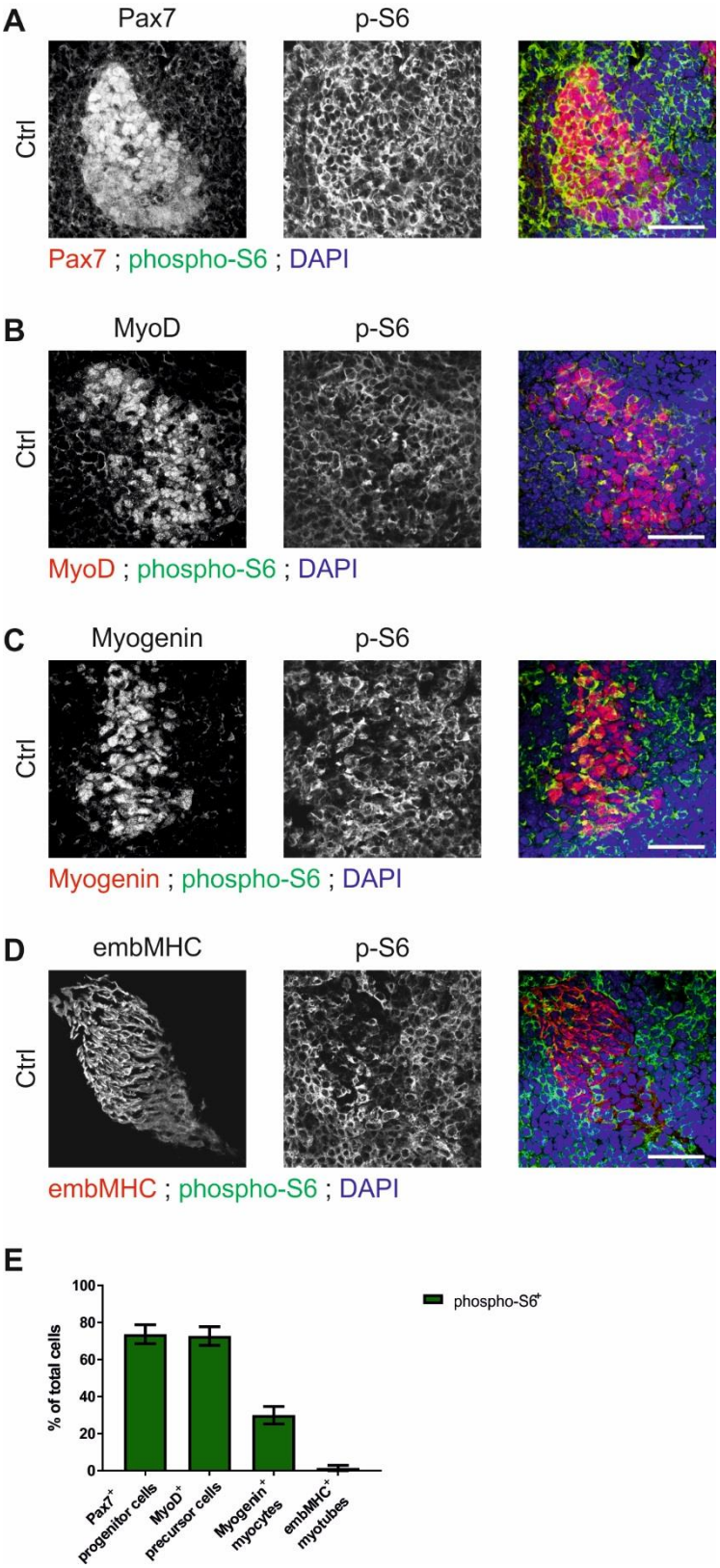

Figure 1. During embryonic myogenesis mTORC1 is active in proliferation, but the signaling is decreased during differentiation and fusion

(A - D) Immunostaining against phospho-S6 Ser235/236, indicative of mTORC1 activity, and Pax7 (A), MyoD (B), Myogenin (C), embMHC (D) on transverse cross-sections of Ctrl embryos at embryonic day (E) 11.5. Scale bar, 50 µm.
(E) Quantification of the percentage of phospho-S6^{+} progenitor cells (Pax7^{+}), precursor cells (MyoD^{+}), myocytes (Myogenin^{+}) and myotubes (embMHC^{+}) (n = 3).
Data represented as mean ± SEM.

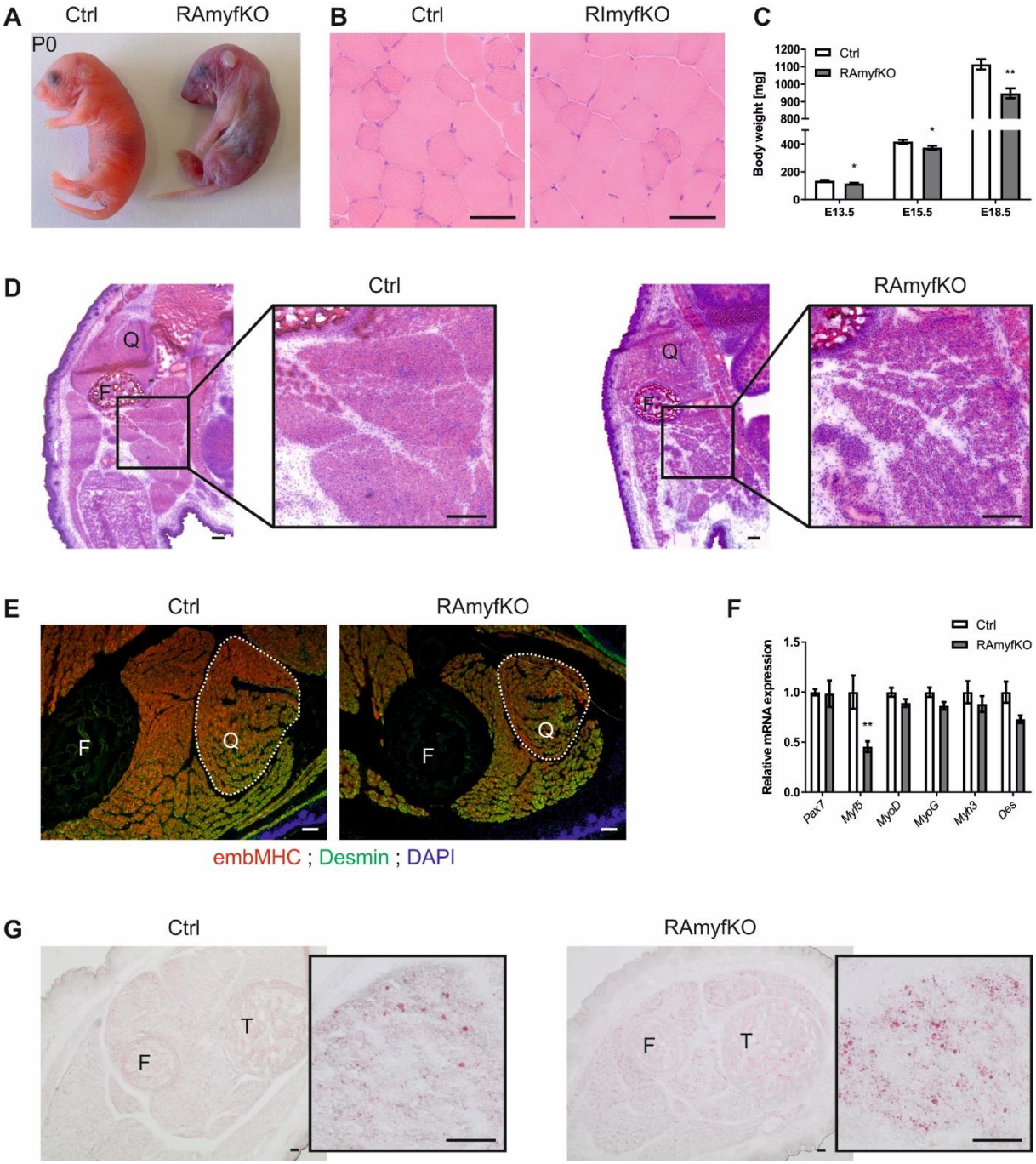

Figure 2. Ablation of raptor severely impairs embryonic muscle development

(A) Photograph of Ctrl (*Myf5*$^{+/+}$*; Rptor*$^{fl/fl}$) and RAmyfKO (*Myf5*$^{+/Cre}$*; Rptor*$^{fl/fl}$) pups at post-natal day 0 (P0).

(B) Hematoxylin and eosin (H&E) staining on TA muscle cross-sections of 2 month-old Ctrl (*Myf5*$^{+/+}$*; Rictor*$^{fl/fl}$) and RImyfKO (*Myf5*$^{+/Cre}$*; Rictor*$^{fl/fl}$) mice. Scale bar, 50 µm.

(C) The body weight of Ctrl and RAmyfKO embryos was measured at embryonic day (E) 13.5, 15.5 and E18.5 (n ≥ 7).

(D) H&E coloration of transverse cross-sections through the whole embryo at E18.5. F, femur; Q, quadriceps muscle. Scale bar, 200 µm.

(E) Immunostaining for embryonic myosin heavy chain (embMHC; red) and desmin (green) on transverse cross-sections of E18.5 Ctrl and RAmyfKO quadriceps muscle. F, femur; Q, quadriceps muscle (delineated with a dotted line). Scale bar, 100 µm.
(F) Relative mRNA levels of *Pax7*, *Myf5*, *MyoD*, *MyoG*, *Myh3* and *Des* was measured by RT-qPCR in hindlimb RNA extracts of E18.5 embryos. Normalization to β-actin (n = 5).
(G) Lipids were visualized by Oil Red O staining on hindlimb cross-sections of E18.5 Ctrl and RAmyfKO embryos. Fat droplets (red) accumulated between myofibers of RAmyfKO embryos. F, femur; T, tibia. Scale bar, 50 µm.
Data represented as mean ± SEM. * $p < 0.05$, ** $p < 0.01$, Student's *t* test.

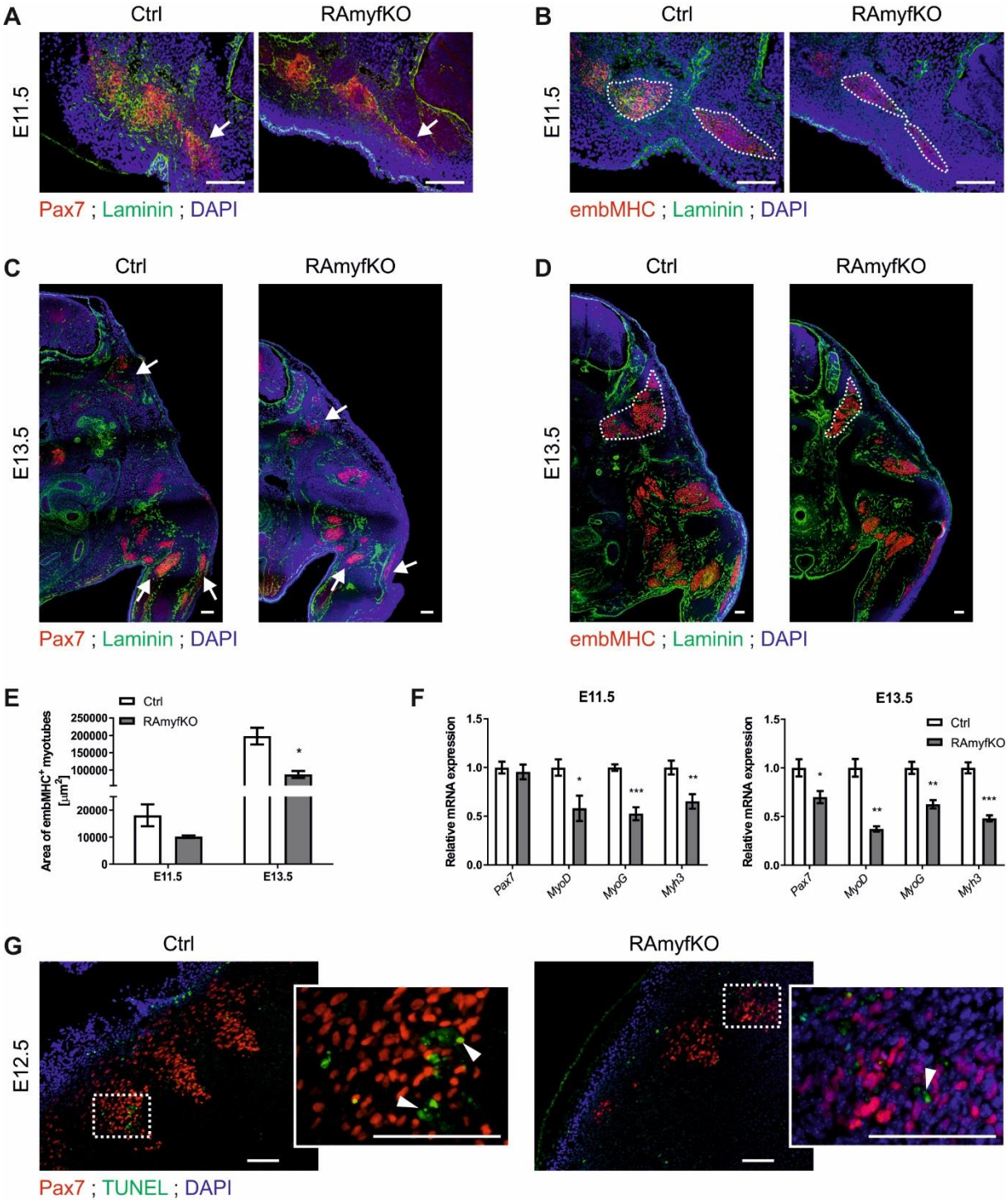

Figure 3. Less myotubes are formed in the absence of raptor expression

(A - D) Immunostaining against Pax7 (progenitor cells, red, A and C) or embMHC (myotubes, red, B and D) and laminin (green) on transverse cross-sections of E11.5 (A, B) or E13.5 (C, D) Ctrl and RAmyfKO embryos. Arrows point to $Pax7^+$ progenitors in the dermomyotome and the hindlimbs and the dotted line labels the myotome containing $embMHC^+$ myotubes. Scale bar, 100 µm.

(E) The area of the myotome was measured by the embMHC staining on cross-sections of E11.5 and E13.5 embryos (n = 3-4).

(F) Relative mRNA levels of *Pax7*, *MyoD*, *MyoG* and *Myh3* was measured by RT-qPCR of whole-embryo RNA extracts at E11.5 and E13.5. Normalization to β-actin (n = 5).
(G) Immunostaining against Pax7 (red) and TUNEL (green) on transverse cross-sections of E12.5 Ctrl and RAmyfKO embryos. $TUNEL^+$ nuclei (arrowhead) were detected in Ctrl and RAmyfKO embryos, but they did not co-localize with Pax7-expressing progenitors. Scale bar, 100 µm.
Data represented as mean ± SEM. * $p < 0.05$, ** $p < 0.01$, *** $p < 0.001$, Student's *t* test.

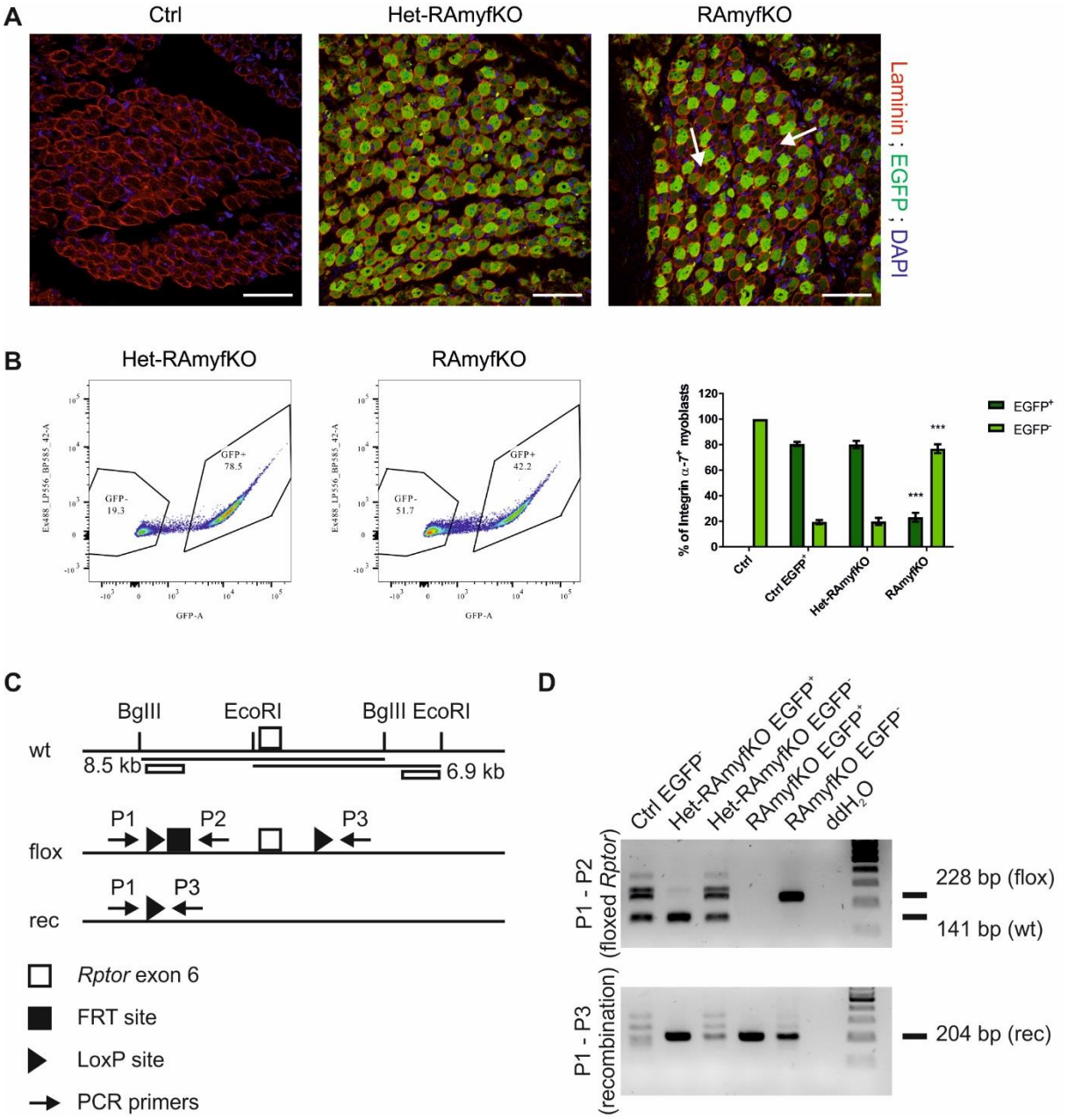

Figure 4. Loss of mTORC1 in the Myf5-lineage causes partial compensation by non-recombined, raptor-expressing myoblasts

(A) Immunolabeling against laminin (red) and green fluorescent protein (EGFP, green) on hindlimb cross-sections of E18.5 embryos. The arrow point to EGFP$^-$ myofibers detected in RAmyfKO muscles. Scale bar, 50 µm.

(B) Myogenic cells (Integrin α-7$^+$ / CD45$^-$ / CD11b$^-$ / Sca1$^-$ / CD31$^-$) were isolated from foreleg and hindlimb muscles of E18.5 embryos by FACS sorting and analyzed for their intrinsic EGFP expression. A representative FACS blot of myogenic cells isolated from Het-RAmyfKO and RAmyfKO embryos, are displayed. The percentage of EGFP$^+$ or EGFP$^-$ normalized to the total number of Integrin α-7$^+$ myoblasts was quantified and compared between Ctrl (*Myf5*$^{+/+}$; *Rptor*$^{fl/fl}$; *mR26CS*$^{+/EGFP}$), Ctrl EGFP$^+$ (*Myf5*$^{+/Cre}$; *Rptor*$^{+/+}$;

mR26CS$^{+/EGFP}$), Het-RAmyfKO (*Myf5*$^{+/Cre}$*; Rptor*$^{+/fl}$*; mR26CS*$^{+/EGFP}$) and RAmyfKO (*Myf5*$^{+/Cre}$*; Rptor*$^{fl/fl}$*; mR26CS*$^{+/EGFP}$) embryos (n = 4-8).

(C) Schematic presentation of wild-type, floxed and recombined alleles of *Rptor*. Primers used for PCR are indicated as P1, P2 and P3. wt: wild-type allele of *Rptor*, flox: floxed allele containing loxP sites, rec: *Rptor* alleles after recombination by Cre.

(D) PCR analysis was performed on FACS-isolated myogenic cells using primers to amplify a sequence from the wild-type (wt) or floxed (flox) *Rptor* allele (P1 – P2) or to detect a sequence from the recombined (rec) *Rptor* allele (P1 – P3). In Het-RAmyfKO EGFP^{+} and RAmyfKO EGFP^{+} cells the recombination product (204 bp) was detected and the band for the floxed sequence (228 bp) in *Rptor* was lost using primers P1 – P2 due to successful recombination (n = 3).

Data represented as mean ± SEM. *** $p < 0.001$, two-way ANOVA with Sidak's multiple comparisons test.

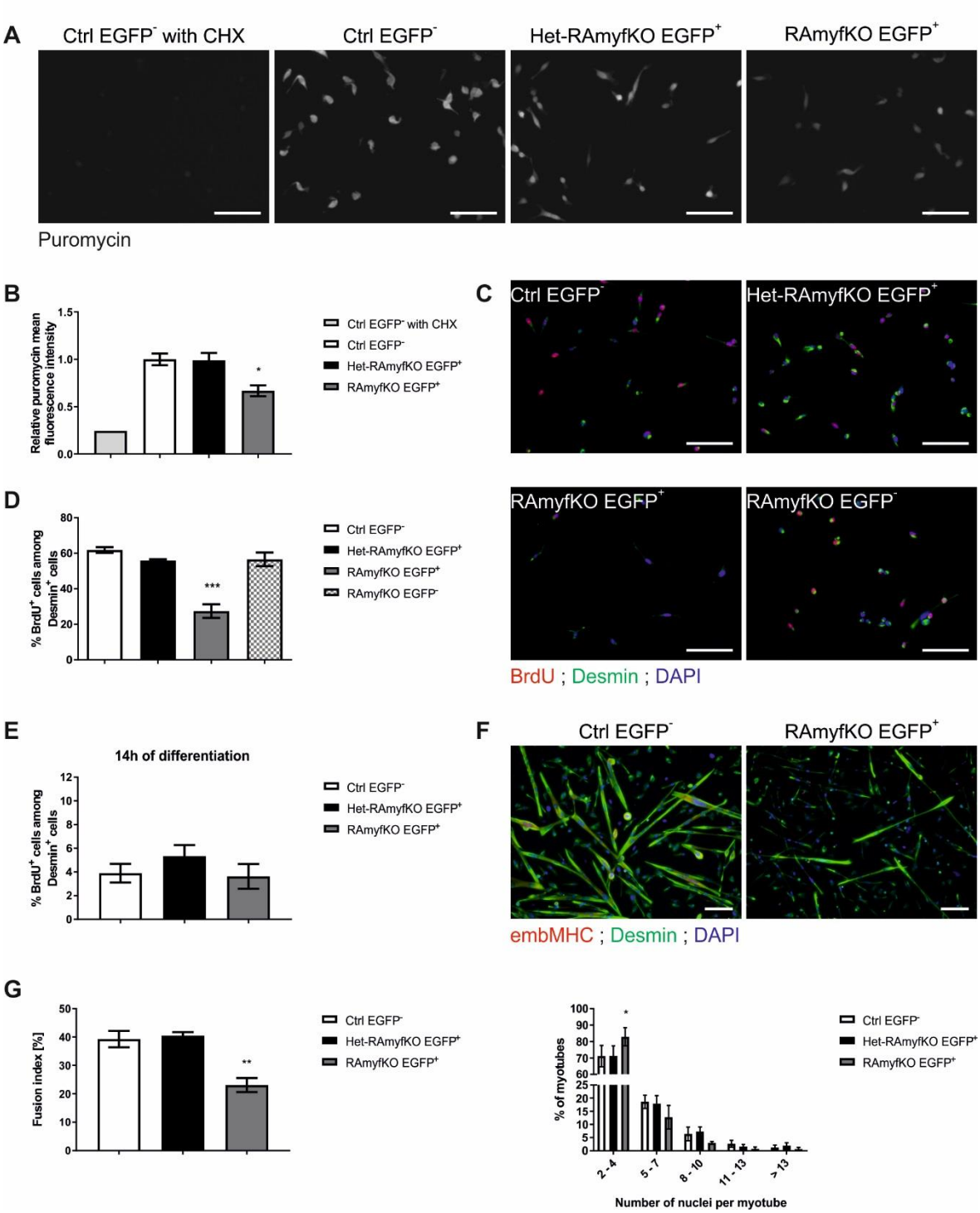

Figure 5. mTORC1 signaling is critical for proliferation, differentiation and fusion of embryonic myoblasts *in vitro*

FACS-isolated Integrin α-7^{+} / Lin^{-} myogenic cells from E18.5 embryos were plated at the same density for all genotypes and cultured in growth or differentiation media.

(A) Directly after FACS-isolation the myogenic cells were cultured in growth media for 48 hours (h) and incubated with puromycin only or in combination with cycloheximide (CHX) for 30 min. Puromycin incorporation, indicative of the rate of protein synthesis, was visualized by immunostaining against puromycin. Scale bar, 100 µm.

(B) Rates of protein synthesis was reported as the mean puromycin fluorescence intensity relative to Ctrl (n = 4).
(C) Immunostaining against BrdU (red) and desmin (green) visualizes the myoblasts in the S-phase of the cell cycle during the 1 h pulse. Scale bar, 100 µm.
(D and E) The percentage of $BrdU^+$ / $Desmin^+$ myoblasts after 48 h of proliferation (D, n = 3-4) or after 14 h of differentiation (E, n = 4-5) was quantified.
(F) Immunostaining against embMHC (red) and desmin (green) on myotubes after 3 days of differentiation. Scale bar, 100 µm.
(G) The fusion index and size distribution were assessed after 3 days of differentiation (n = 3).
Data represented as mean ± SEM. * $p < 0.05$, *** $p < 0.001$, one-way ANOVA with Tukey's multiple comparisons test.

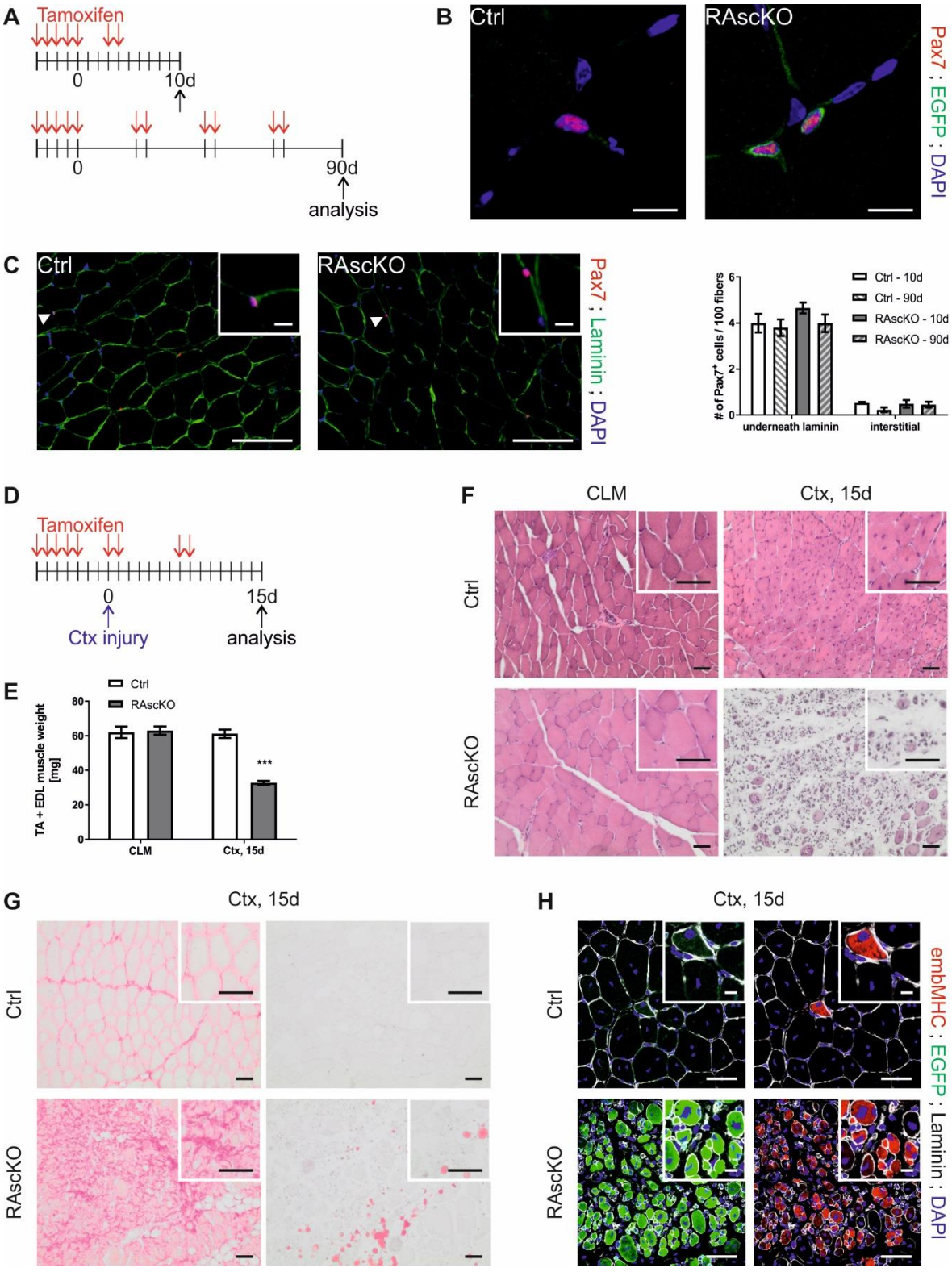

Figure 6. Raptor expression is essential for the restoration of muscle fibers following muscle injury

(A) Experimental scheme for (B and C). Tamoxifen was administered for 5 consecutive days to 3 month-old mice and the muscles harvested 10 or 90 days after the treatment. For long-term studies, tamoxifen injection was repeated every month.

(B) Immunostaining against Pax7 (red) and EGFP (green) on TA muscle cross-sections from 3 month-old Ctrl and RAscKO mice 10 days after tamoxifen treatment. Scale bar, 10 µm.

(C) Immunostaining against Pax7 (red) and laminin (green) on TA muscle cross-sections from 3 month-old mice 10 days after tamoxifen treatment. Arrowheads point to quiescent $Pax7^+$ satellite cells lying underneath the basal lamina. The number of $Pax7^+$ satellite cells in the TA muscle were counted and normalized to 100 myofibers 10 or 90 days after the tamoxifen treatment (n = 3-5). Scale bar, 100 µm and 10 µm at higher magnification.

(D) Experimental scheme for (E - H). Cardiotoxin (Ctx) injury was applied to the TA and EDL muscle of 3 month-old mice 3 days after the tamoxifen treatment. Analysis of muscles was performed 15 days post-injury (Ctx, 15d). The contralateral muscle (CLM) was not injured.

(E) The muscle weight of the uninjured and injured TA and EDL was measured 15 days after Ctx-injury (n = 3).

(F) H&E coloration on CLM and Ctx, 15d TA cross-sections of Ctrl and RAscKO mice. Centralized nuclei are characteristics of regenerating fibers.

(G) Sirius Red coloration (red, left panel) on regenerating TA muscles visualizes the collagens in the extracellular matrix between myofibers of Ctrl mice and additional accumulation in the fibrotic tissue of RAscKO mice. Oil red O staining (red, right panel) stains lipid droplets in the regenerating muscle of RAscKO mice. Scale bar, 50 µm.

(H) Immunostaining against EGFP (green, left panel) or embryonic myosin heavy chain (embMHC, red, right panel) and laminin (white) on regenerating TA muscle of Ctrl and RAscKO mice 15 days post-injury. In regenerating Ctrl muscle only very few $embMHC^+$ myofibers were detected. Almost all $EGFP^+$ myofibers in regenerating RAscKO muscle were positive for embMHC. Scale bar, 50 µm and 10 µm at higher magnification.

Data represented as mean ± SEM. ** $p < 0.01$, *** $p < 0.001$, Student's *t* test.

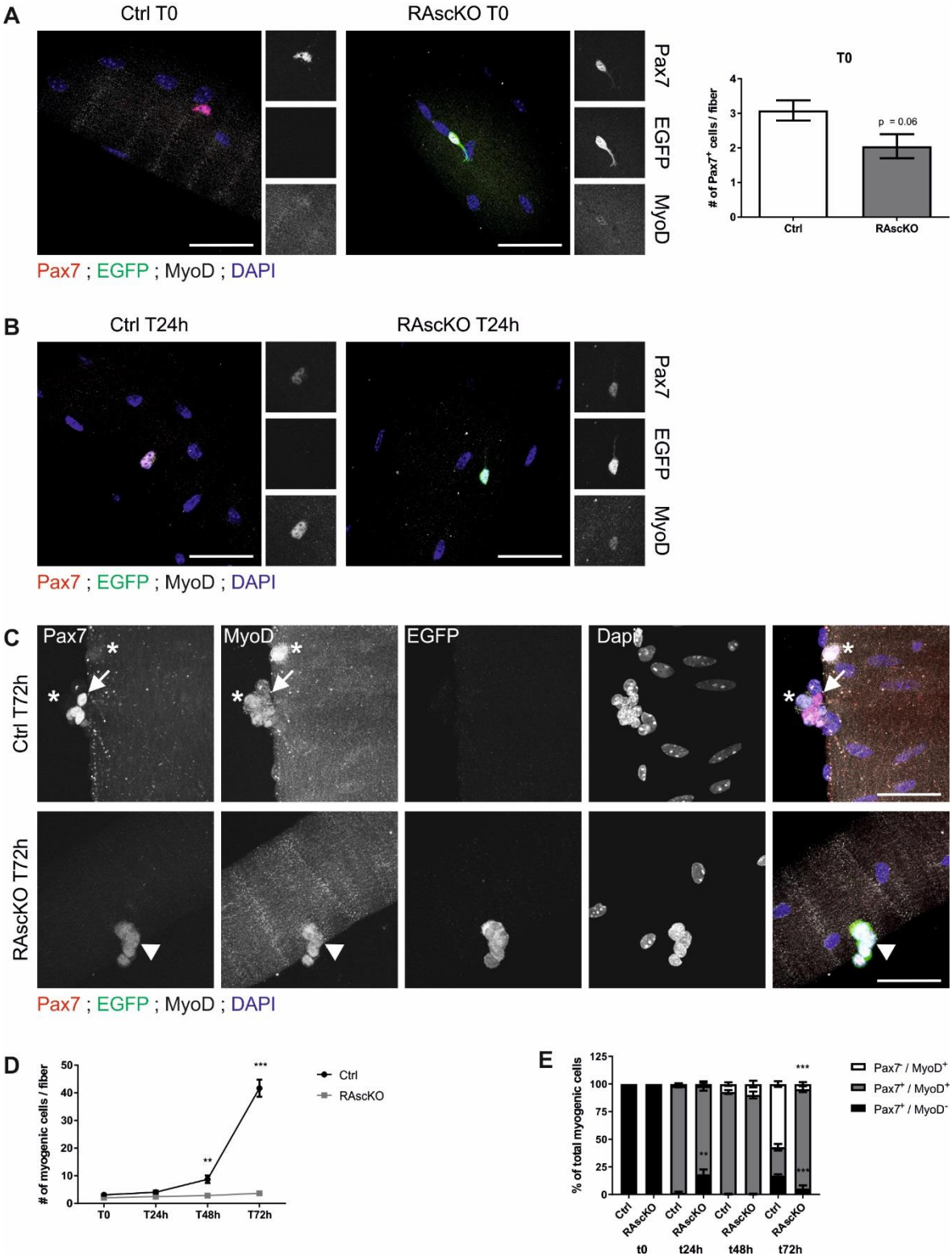

Figure 7. Loss of mTORC1 delays activation of quiescent satellite cells

Single myofibers were isolated from Ctrl and RAscKO EDL muscle 90 days after tamoxifen treatment and their associated satellite cells analyzed directly after isolation (T0) or after 24, 48 or 72 h of culture (T24, T48, T72h).

(A) Immunostaining against Pax7 (red), EGFP (green) and MyoD (grey) on quiescent satellite cells associated to isolated Ctrl and RAscKO myofibers at T0. The number of $Pax7^+$

cells normalized per fiber was counted (n = 4-5, 20-30 myofibers per animal). Scale bar, 50 µm.

(B and C) Immunostaining against Pax7 (red), EGFP (green), MyoD (grey) on satellite cells associated to myofibers after 24 h (B) or 72 h (C) of culture. At T24h, Ctrl satellite cells express MyoD in their activated state (B). At T72h, Ctrl satellite cells (C) have formed clones containing cells expressing Pax7 only (returning into quiescence, arrow) or cells expressing MyoD only (differentiating, asterix). Cells expressing both Pax7 and MyoD remain in an activated state (arrowhead). Scale bar, 50 µm.

(D) The number of myogenic cells normalized per fiber was quantified at T0, T24h, T48h and T72h (n = 4-5, 20-30 myofibers per animal).

(E) The number of Pax7- and / or MyoD-positive cells were quantified and normalized to the total number of myogenic cells on single isolated myofibers at T0, T24h, T48h and T72h (n = 4-5, 20-30 myofibers per animal).

Data represented as mean ± SEM. ** $p < 0.01$, ** $p < 0.01$, *** $p < 0.001$, Student's *t* test.

Supplemental data

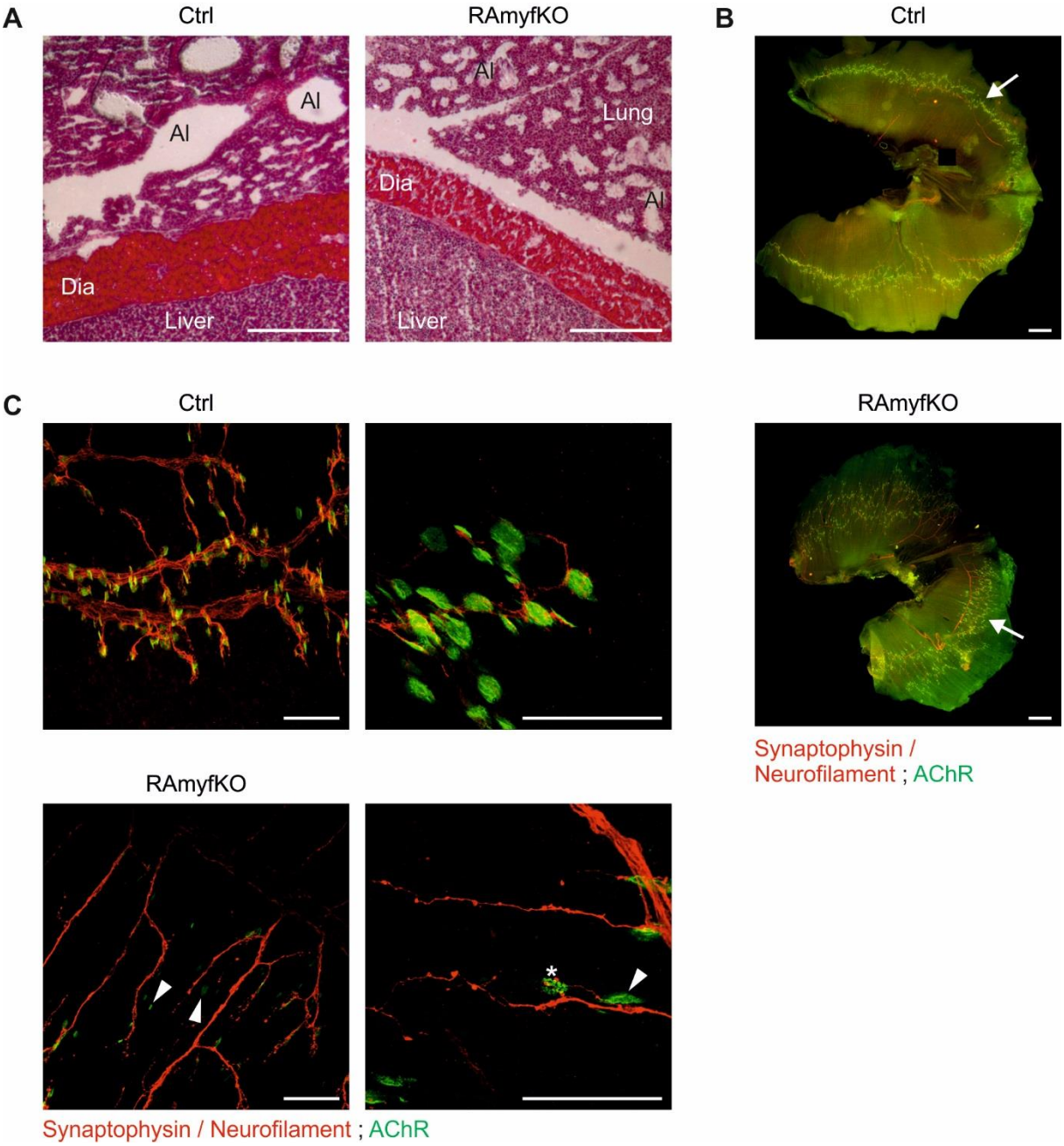

Supplementary Figure 1. RAmyfKO embryos die perinatally due to respiratory failure

(A) H&E coloration on longitudinal cross-sections of newborn pups (P0) in the region of the lung, diaphragm (Dia) and liver. The alveolar spaces (Al) are smaller and the interstitial mesenchyme thicker in RAmyfKO lungs, indicating that their lungs were not inflated. Scale bar, 500 µm.

(B and C) Whole-mount staining for synaptophysin / neurofilament (red) visualizes the phrenic nerve and fluorescently labeled α-bungarotoxin stains acetylcholine receptor clusters (AChR, green) on diaphragms of E17.5 embryos. In RAmyfKO diaphragms the

innervation zone is enlarged and disorganized (B, arrow), since motor neurons overshoot the innervation zone and many AChR clusters are not innervated (C, arrowhead). Fragmented postsynaptic AChR clusters in RAmyfKO diaphragms are indicated with a star. Scale bar, 500 µm (B) and 50 µm (C).

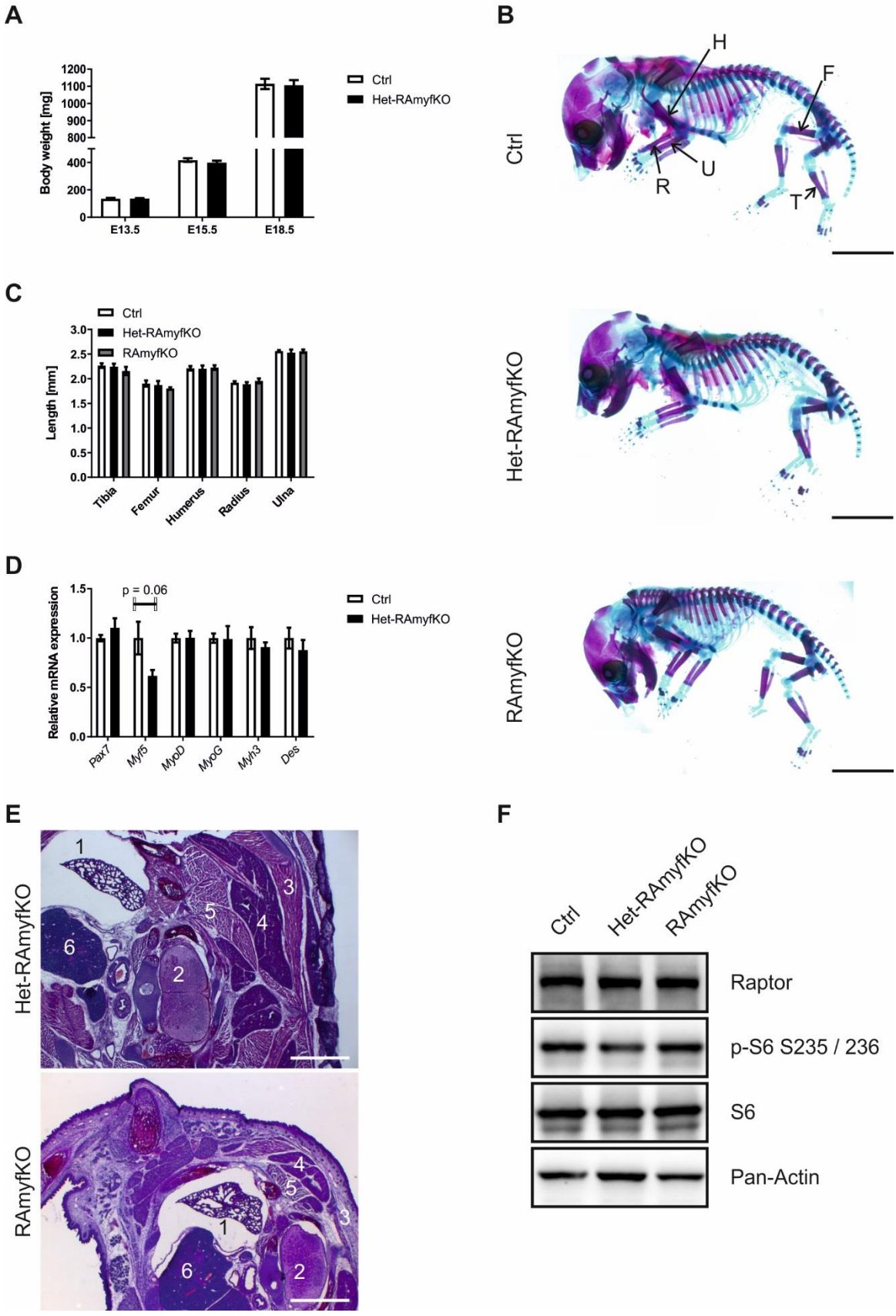

Supplementary Figure 2. 50 % reduction of raptor protein levels does not affect embryonic muscle development

(A) The body weight of Ctrl (*Myf5*$^{+/+}$; *Rptor*$^{fl/fl}$) and Het-RAmyfKO (*Myf5*$^{+/Cre}$; *Rptor*$^{+/fl}$) embryos was measured at E13.5, E15.5 and E18.5 (n = 4-12).

(B and C) Alcian blue (cartilage) and alizarin red (ossified bones) staining of E18.5 embryos (B). T, tibia; F, femur; H, humerus; R, radius; U, ulna. Scale bar, 5 mm. The length of the respective bones was measured (n = 3-4) (C).

(D) RT-qPCR analysis on E18.5 hindlimb muscle RNA extracts for the indicated genes. Normalization to β-actin (n = 5).

(E) H&E coloration of transverse cross-sections through the upper part of E18.5 embryos. 1, lung; 2, spinal cord; 3, trapezius muscle; 4, brown fat; 5, semispinalis muscles; 6, thymus. Scale bar, 1000 µm.

(F) Western blot analysis on liver extracts of E18.5 Ctrl, Het-RAmyfKO and RAmyfKO embryos using antibodies against the proteins indicated. Equal amount of protein was loaded in each lane. Antibodies to Pan-actin was used as loading control (n = 3-4).

Data represented as mean ± SEM. Student's *t* test and one-way ANOVA with Tukey's multiple comparisons test.

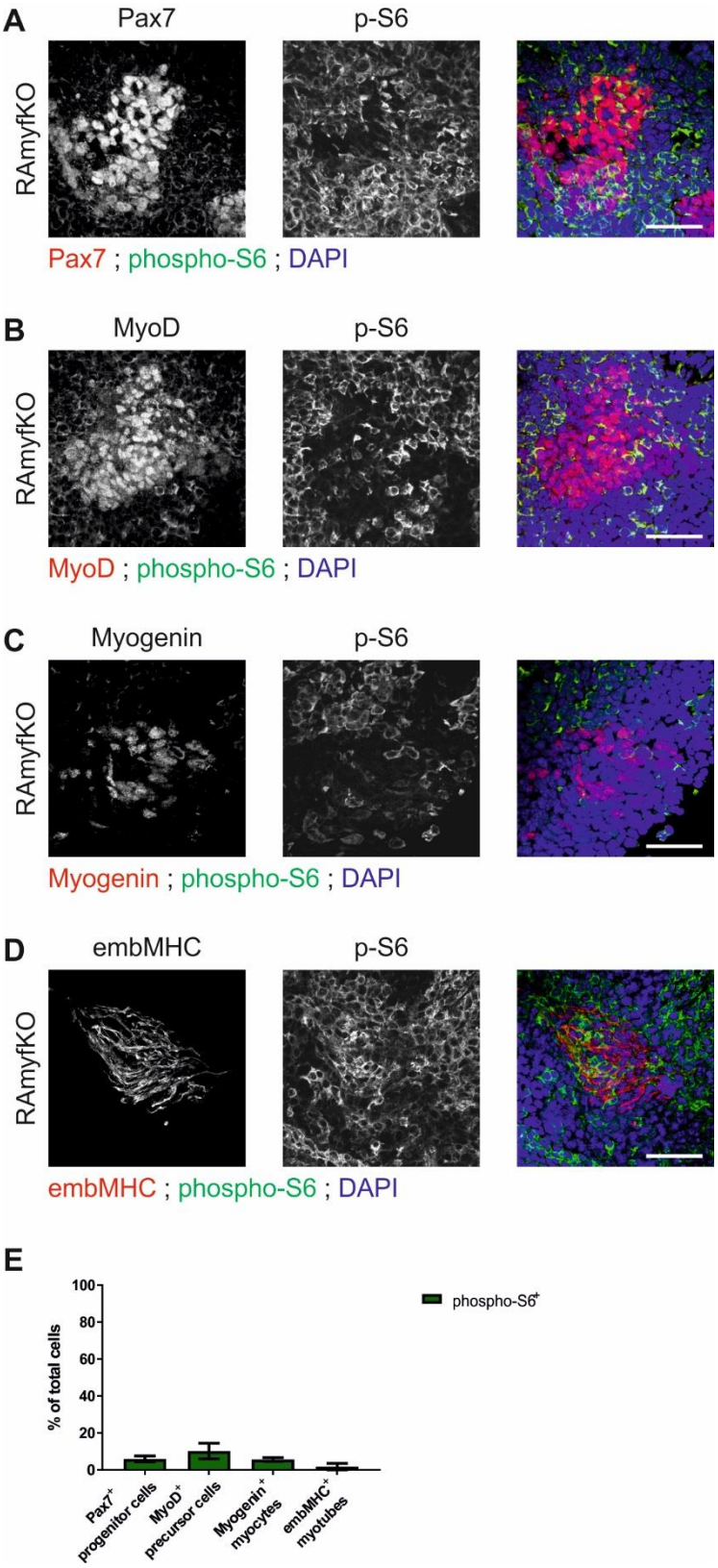

Supplementary Figure 3. mTORC1 activity is absent in muscle progenitors, precursors, myocytes and myotubes of E11.5 RAmyfKO embryos

(A - D) Immunostaining against phospho-S6 Ser235/236 and Pax7 (A), MyoD (B), Myogenin (C), embMHC (D) on transverse cross-sections of E11.5 RAmyfKO embryos. Scale bar, 50 µm.

(E) Quantification of the percentage of phospho-S6^{+} progenitors (Pax7^{+}), precursors (MyoD^{+}), myocytes (Myogenin^{+}) and myotubes (embMHC^{+}) (n = 3).

Data represented as mean ± SEM.

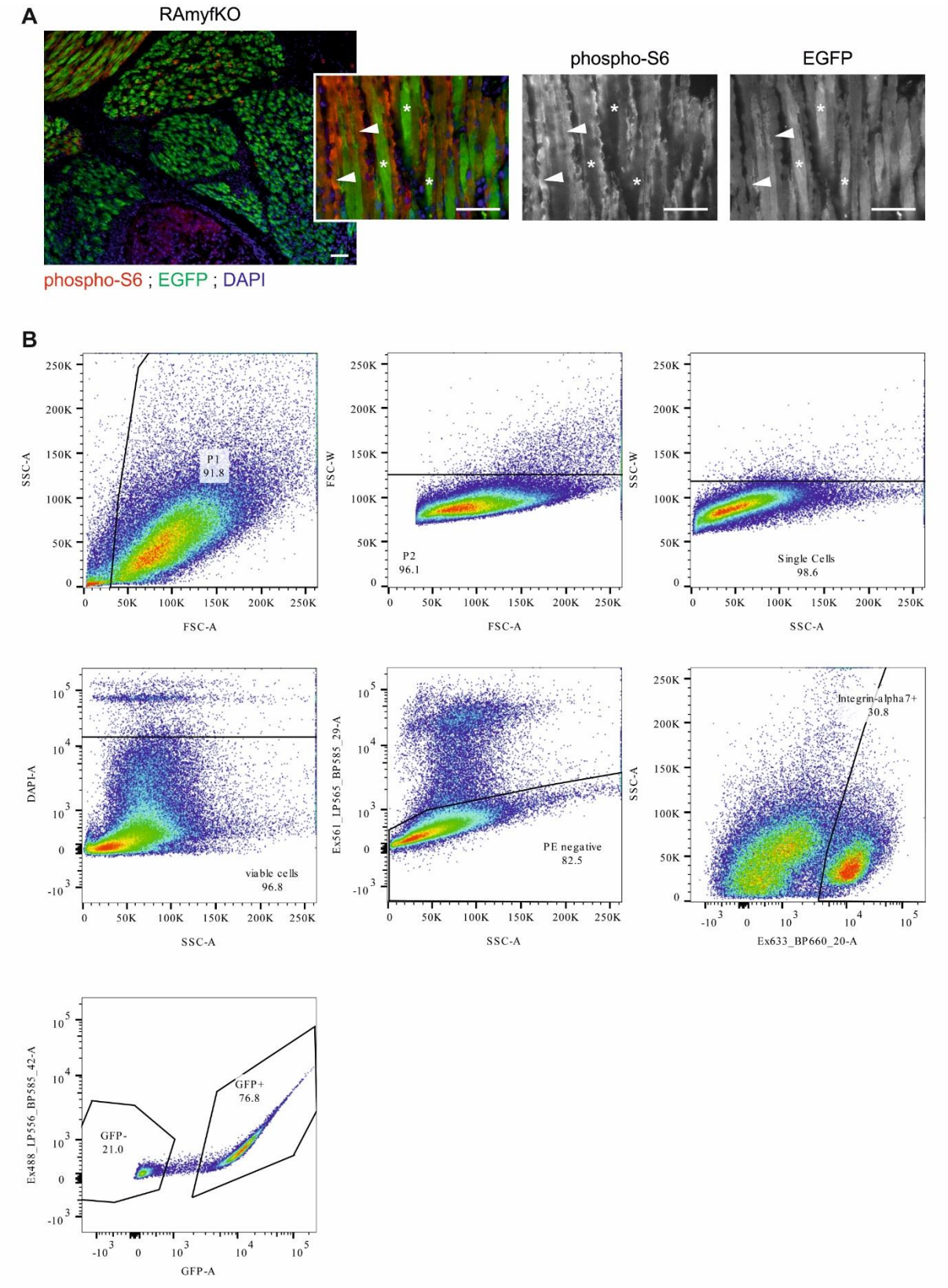

Supplementary Figure 4. EGFP expression and mTORC1 activity in Het-RAmyfKO and RAmyfKO muscle fibers

(A) Immunostaining for phospho-S6 Ser235/236 (red) and EGFP (green) on transverse cross-sections of E18.5 RAmyfKO hindlimbs. With higher magnification a representative

area of longitudinal myofibers are displayed to visualize the absence of co-localized phospho-S6 (arrowhead) and EGFP (star) staining in RAmyfKO muscle. Scale bar, 50 µm. (B) Myogenic cells were isolated from hindlimb and foreleg muscles of E18.5 Het-RAmyfKO embryos. Single cells were selected based on the side and forward scatter profiles (SSC / FSC). Dead cells were excluded using DAPI staining. The cells were purified by selecting Integrin α-7-high (APC, Ex633) and lineage-low (Sca1, CD45, CD31, CD11b; PE, Ex561). The myogenic cells were separated by two-way sorting according to their intrinsic EGFP expression.

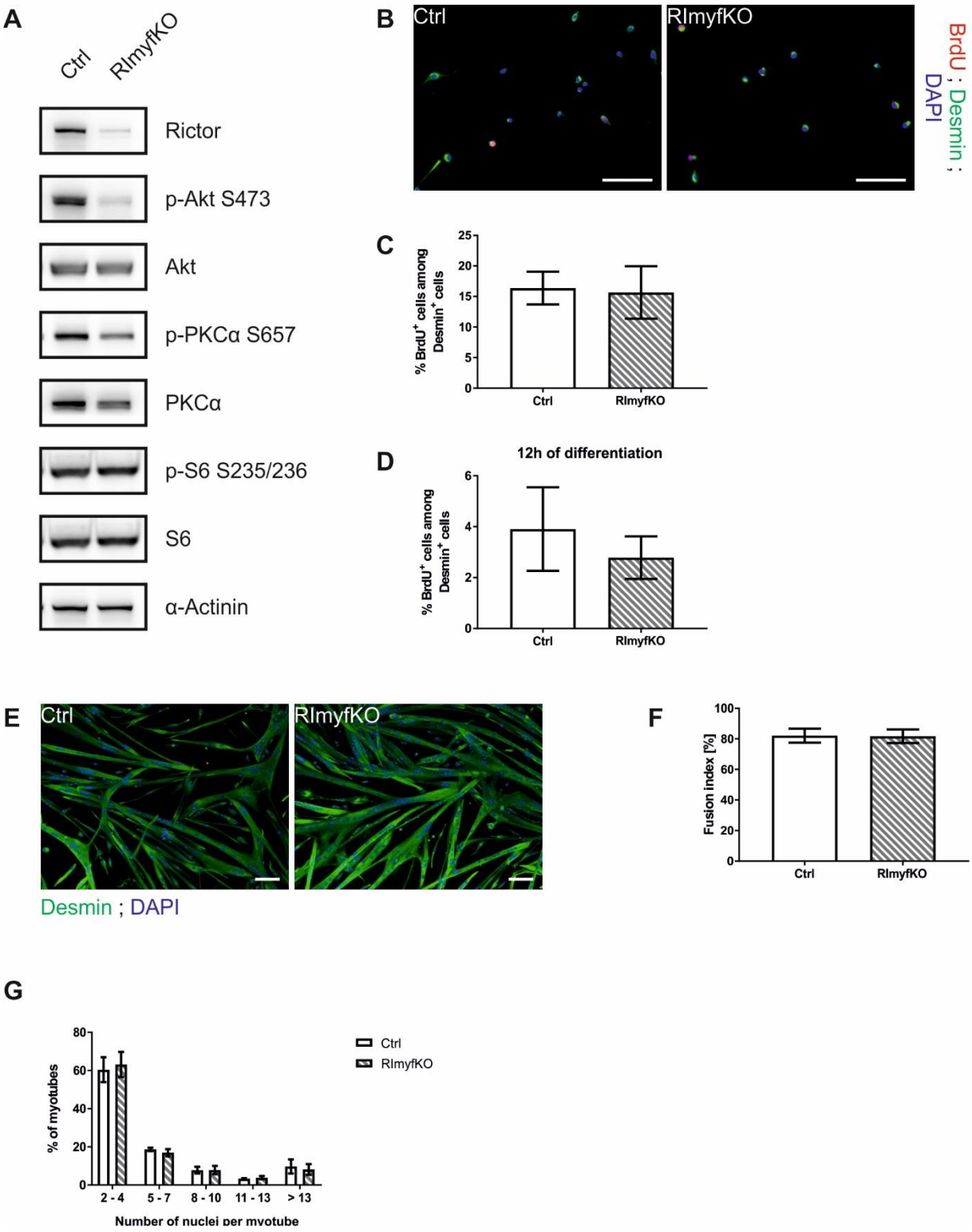

Supplementary Figure 5. mTORC2 signaling is dispensable for proliferation and differentiation of myoblasts

Primary myoblasts were isolated from the EDL muscle of 2 – 3 week-old Ctrl and RImyfKO mice and cultured in growth or differentiation media.

(A) Western blot analysis on proliferating Ctrl and RImyfKO primary myoblasts using antibodies against the proteins indicated. Myoblasts isolated from RImyfKO muscle were

depleted for rictor and show decreased mTORC2 downstream signaling. Equal amount of protein was loaded in each lane. Antibodies to α-actinin were used as loading control (n = 3).

(B) Immunostaining against BrdU (red) and Desmin (green) labels myoblasts in the S-phase during the 1 h BrdU pulse. Scale bar, 50 µm.

(C and D) The percentage of $BrdU^+$ / $Desmin^+$ myoblasts after 48 h of proliferation (C) or 12 h of differentiation (D) was quantified (n = 3).

(E) Immunostaining against Desmin (green) on myotubes after 48 h of differentiation. Scale bar, 100 µm.

(F) The fusion index and size distribution were assessed on 48 h differentiating Ctrl and RImyfKO myotubes (n = 3).

Data represented as mean ± SEM. Student's *t* test.

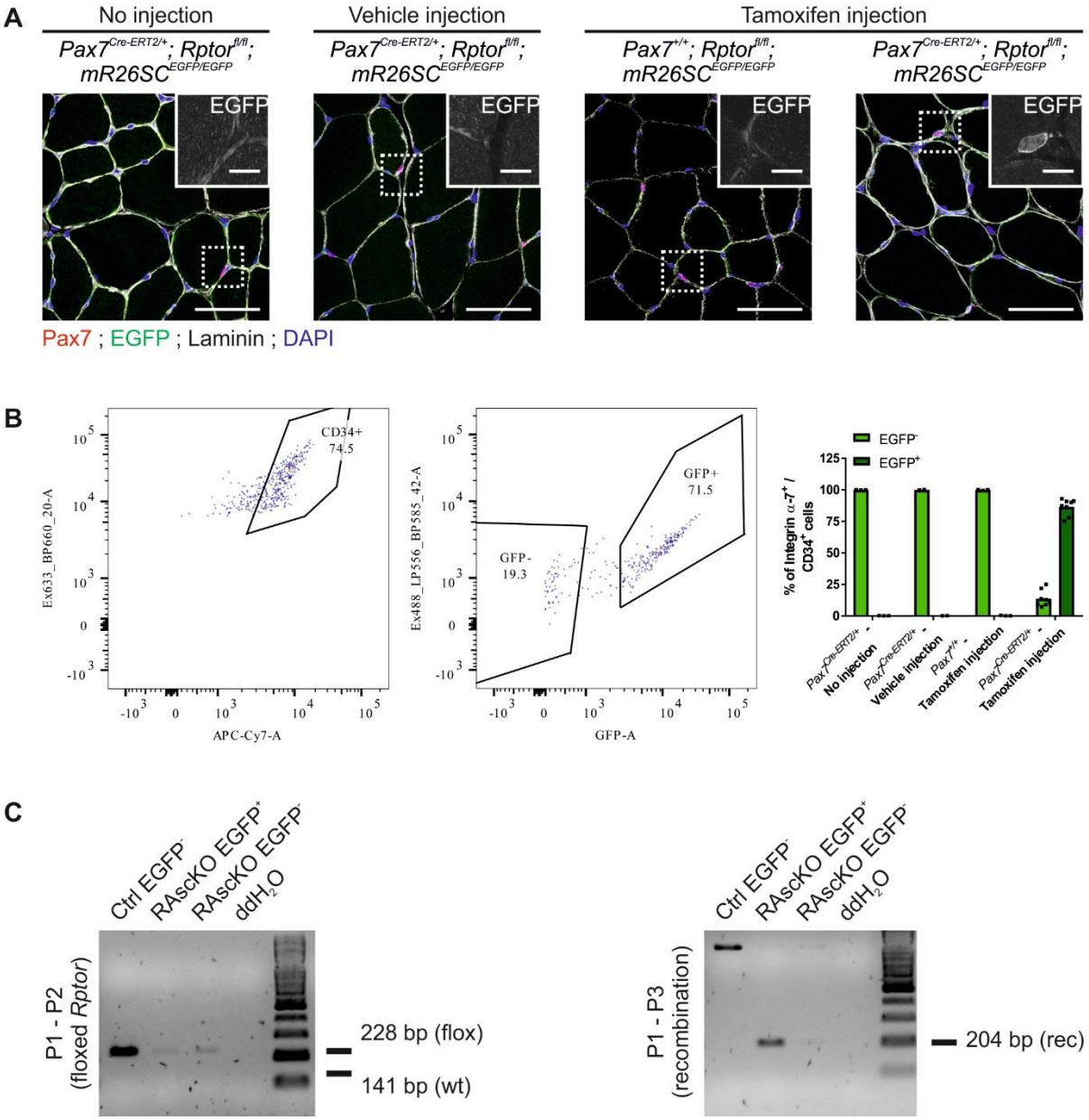

Supplementary Figure 6. EGFP labels raptor-depleted satellite cells of RAscKO mice

(A) Immunostaining against Pax7 (red), EGFP (green) and laminin (white) on TA muscle cross-sections of Ctrl and RAscKO mice after vehicle or tamoxifen treatment. Scale bar, 50 µm and 10 µm at higher magnification.

(B) Representative FACS cytometry blots from hindlimb and foreleg muscles of 3 month-old RAscKO mice 10 days after tamoxifen treatment. Cells were selected based on their lineage-low (Sca1, CD45, CD31, CD11b; PE, Ex561, not shown), Integrin α-7-high (APC, not shown), CD34-high (Alexa-647, Ex633) and EGFP-high signals. All satellite cells isolated from Ctrl (*Pax7$^{+/+}$; Rptor$^{fl/fl}$; mR26CS$^{EGFP/EGFP}$*) and RAscKO (*Pax7$^{Cre-Ert2/+}$; Rptor$^{fl/fl}$; mR26CS$^{EGFP/EGFP}$*) mice treated with / without tamoxifen, respectively, appeared as EGFP-negative. 86.4 % of the satellite cells isolated from tamoxifen-treated RAscKO mice were EGFP-positive (n ≥ 2).

(C) PCR analysis was performed on FACS-isolated satellite cells using primers to distinguish between the wild-type (wt, 141 bp), floxed (flox, 228 bp) or recombined (rec, 204 bp) *Rptor* allele. In Ctrl satellite cells the floxed allele was detected, while in RAscKO satellite cells the recombined *Rptor* allele was amplified (n = 3).

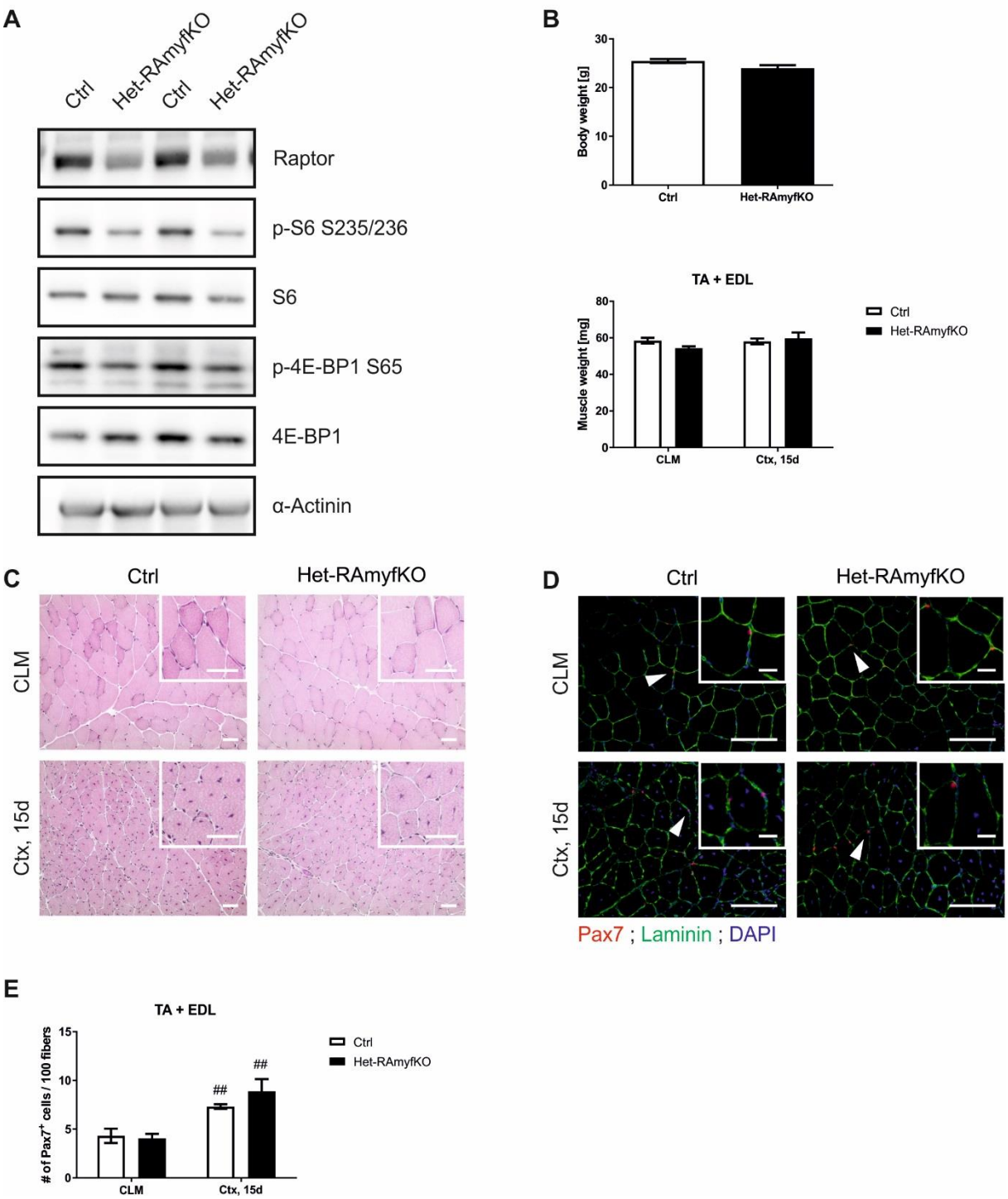

Supplementary Figure 7. 50 % reduction in raptor protein levels does not affect muscle regeneration at young age

(A) Western blot analysis on contralateral (CLM), uninjured gastrocnemius muscle from 3 month-old Ctrl (*Myf5*$^{+/+}$*; Rptor*$^{fl/fl}$) and Het-RAmyfKO (*Myf5*$^{+/Cre}$*; Rptor*$^{+/fl}$) mice using antibodies against the proteins indicated. Equal amount of protein was loaded in each lane. Antibodies to α-actinin were used as loading control (n = 5).

(B) The body and muscle weight of 3 month-old Ctrl and Het-RAmyfKO mice was measured 15 days after cardiotoxin- (Ctx) induced muscle damage. Restoration of the muscle weight

following injury compared to the uninjured, contralateral muscle (CLM) indicates that muscle regeneration was efficient in Het-RAmyfKO mice (n = 5).

(C) H&E coloration on CLM and Ctx, 15d TA cross-sections of Ctrl and Het-RAmyfKO mice. Regenerating fibers are characterized by their centralized nuclei. Scale bar, 50 µm.

(D) Immunostaining against Pax7 (red) and laminin (green) on cross-section of uninjured (CLM) or injured (Ctx, 15d) TA muscles to visualize quiescent $Pax7^+$ satellite cells underneath the basal lamina. Scale bar, 100 µm and 20 µm at higher magnification.

(E) Quantification of the number of $Pax7^+$ satellite cells normalized to 100 myofibers in uninjured and injured TA muscles from Ctrl and Het-RAmyfKO mice (n = 4-5).

Data represented as mean ± SEM. ## $p < 0.01$, represents statistical significance relative to the uninjured condition, Student's *t* test.

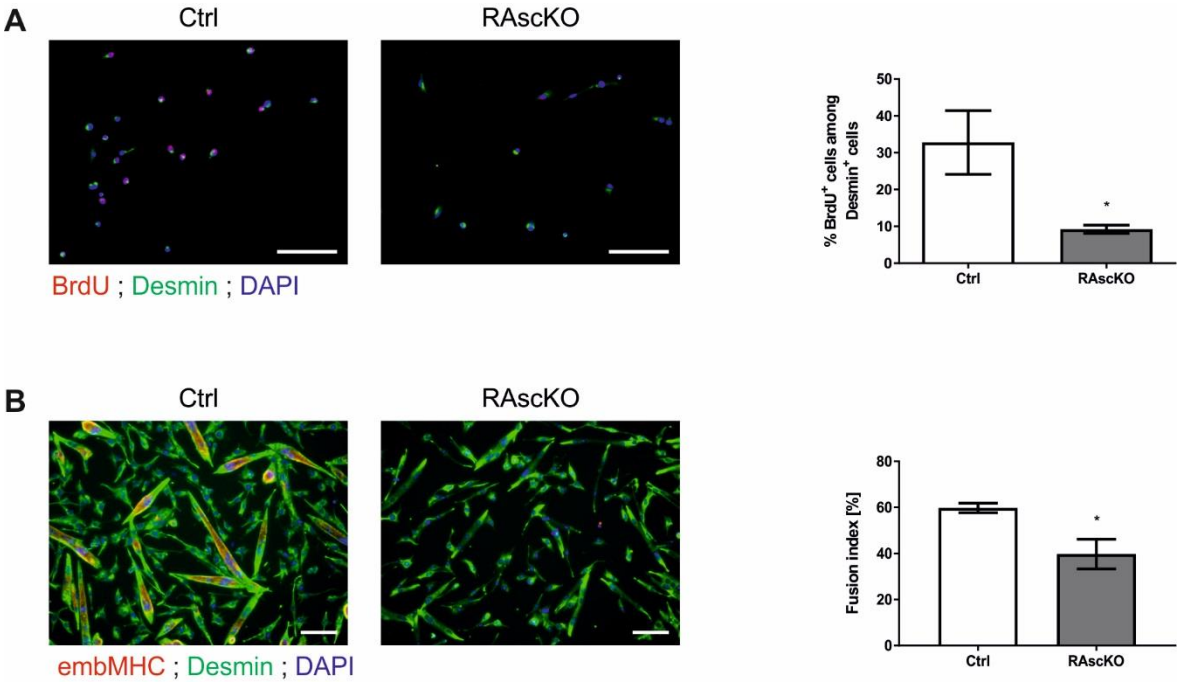

Supplementary Figure 8. Raptor-depleted satellite cells exhibit proliferation and differentiation defects *in vitro*

(A) Freshly sorted satellite cells were cultured in growth media for 48 h and BrdU-labeled 1 h before fixation. Immunostaining against BrdU (red) and desmin (green) visualizes the myoblasts being in the S-phase of the cell cycle during the pulse (n = 3-4). Scale bar, 100 µm.

(B) Immunostaining against embMHC (red) and desmin (green) on myotubes after 4 days of differentiation. The fusion index was quantified after 4 days of differentiation (n = 3). Scale bar, 100 µm.

Data represented as mean ± SEM. * $p < 0.05$, Student's *t* test.

	E18.5 Liver		
	Ctrl	**Het-RAmyfKO**	**RAmyfKO**
Raptor	100 ± 56	138 ± 52	155 ± 56
phospho-S6 Ser235/236	100 ± 23	106 ± 13	145 ± 26
S6	100 ± 17	109 ± 13	124 ± 15

Supplementary Table 1. Quantification of Western blot analysis in liver from E18.5 Ctrl, Het-RAmyfKO and RAmyfKO embryos, related to Figure S2

Protein levels were quantified in liver from E18.5 Ctrl, Het-RAmyfKO and RAmyfKO embryos. The total amount of protein was adjusted according to concentration. Data are represented as the average of grey values ± SEM, after background subtraction and normalization to Pan-Actin and to values from Ctrl mice (n = 3). One-way ANOVA with Tukey's multiple comparisons test.

	Primary myoblasts	
	Ctrl	**RImyfKO**
Rictor	100 ± 11	10 ± 6 **
phospho-PKCα Ser657	100 ± 38	30 ± 6
PKC	100 ± 28	38 ± 16
phospho-Akt Ser473	100 ± 25	18 ± 4 *
Akt	100 ± 32	66 ± 6
phospho-S6 Ser235/236	100 ± 40	70 ± 6
S6	100 ± 26	79 ± 11

Supplementary Table 2. Quantification of Western blot analysis of primary myoblasts isolated from the EDL muscle of Ctrl and RImyfKO mice, related to Figure S5

Protein levels were quantified in primary myoblasts isolated from the EDL muscle of 2-3 week-old Ctrl and RImyfKO mice. The total amount of protein was adjusted according to concentration. Data are represented as the average of grey values ± SEM, after background subtraction and normalization to α-actinin and to values from Ctrl mice (n = 3). Student's *t* test.

	Quadriceps muscle	
	Ctrl	**Het-RAmyfKO**
Raptor	100 ± 15	58 ± 9 *
phoshpo-S6 Ser235/236	100 ± 23	61 ± 13
S6	100 ± 6	106 ± 24
phoshpo-4E-BP1 Ser65	100 ± 18	80 ± 15
4E-BP1	100 ± 11	115 ± 34

Supplementary Table 3. Quantification of Western blot analysis in quadriceps muscle from 3 month-old Ctrl and Het-RAmyfKO mice, related to Figure S7

Protein levels were quantified in uninjured quadriceps muscle from 3 month-old Ctrl and Het-RAmyfKO mice. The total amount of protein was adjusted according to concentration. Data are represented as the average of grey values ± SEM, after background subtraction and normalization to α-actinin and to values from Ctrl mice (n = 5). * $p < 0.05$, Student's *t* test.

	Forward primer	Reverse primer
Pax7	GAG GTG ACA GGA GGC AGA AG	AGC TGC CAG CAA GAT GGT AT
Myf5	AGG AAA AGA AGC CCT GAA GC	GCA AAA AGA ACA GGC AGA GG
MyoD	CAT TCC AAC CCA CAG AAC CT	TGC TGT CTC AAA GGA GCA GA
MyoG	ACT CCC TTA CGT CCA TCG TG	CAG GAC AGC CCC ACT TAA AA
Myh3	GCA CGA AGA AGC CAA GAT TC	TCA GCT GCT CGA TCT CTT CA
Des	GAG GTT GTC AGC GAG GCT AC	CTT CAG GAG GCA GTG AGG AC
β-actin	CAG CTT CTT TGC AGC TCC TT	GCA GCG ATA TCG TCA TCC A

Supplementary Table 4. Primers used for quantitative PCR analysis

6.2 Manuscript 2: "mTORC2 controls the maintenance of the muscle stem cell pool during regeneration and aging"

mTORC2 controls the maintenance of the muscle stem cell pool during regeneration and aging

Nathalie Rion[1], Perrine Castets[1], Shuo Lin[1], Leonie Enderle[2] and Markus A. Rüegg[1]*

[1] Biozentrum, University of Basel, CH-4056 Basel, Switzerland

[2] Lunenfeld-Tanenbaum Research Institute/Mount Sinai Hospital, Toronto, ON M5G 1X5, Canada

* Corresponding author:
markus-a.ruegg@unibas.ch, Tel: +41 61 267 22 23, Fax: +41 61 267 22 08

Abstract

Background: The mammalian target of rapamycin complex 2 (mTORC2), containing the essential protein rictor, regulates cellular metabolism and cytoskeletal organization by phosphorylating protein kinases, such as Akt, PKC and SGK. Inactivation of mTORC2 signaling in adult skeletal muscle affects whole-body metabolism, but not muscle histology and function. However, it is not clear whether mTORC2 is required for the formation of myofibers during development and muscle regeneration.

Methods: We developed a new mouse model depleted for rictor in the Myf5-lineage (RImyfKO) and characterized their muscle phenotype using histological, biochemical and molecular biological methods. The function of muscle stem cells was analyzed during cardiotoxin-induced muscle regeneration *in vivo* and in culture on isolated myofibers.

Results: Skeletal muscle of young and aged RImyfKO mice appeared normal in size, composition and function in respect to their body weight. In young RImyfKO mice, quiescent muscle stem cells exhibited normal functional characteristics, such as proliferation, differentiation and fusion, following one severe muscle damage. However, upon multiple muscle injuries, RImyfKO muscle stem cells failed to replenish the stem cell pool. Moreover, the number of quiescent muscle stem cells in RImyfKO mice decreased during physiological aging, causing a decline in the regenerative capacity of mutant muscle at progressed age.

Conclusions: Our study shows that mTORC2 signaling is dispensable for muscle development, but required for the homeostasis of muscle stem cells. Loss of mTORC2 does not affect the myogenic function of muscle stem cells, but impairs the replenishment of the pool after repeated injuries and during aging. These results point to an essential role of mTORC2 signaling in muscle stem cell maintenance and muscle physiology.

Keywords: mTORC2, rictor, myogenesis, muscle development, muscle regeneration, satellite cells

Background

During development, mesenchymal progenitors from somites, expressing the paired box protein 3 and 7 (Pax3 / Pax7), undergo a multi-step process, called myogenesis, that leads to the formation of skeletal muscle fibers. Myogenesis includes the commitment of the progenitors into the muscle lineage, their proliferation, differentiation and fusion, and is controlled by the sequential expression of myogenic basic-helix-loop-helix (bHLH) transcription factors Myf5, MyoD, Myogenin and Mrf4 [1]. Myogenesis is recapitulated in adult skeletal muscle during muscle regeneration following injury. Adult myogenesis depends on skeletal muscle stem cells, called satellite cells, that originate from progenitor cells expressing Pax7 and Myf5 during fetal embryogenesis [2].

The mammalian (or mechanistic) target of rapamycin (mTOR) associates into two structurally and functionally different complexes called mTOR complex 1 (mTORC1) and mTOR complex 2 (mTORC2). mTORC1, containing the protein raptor, regulates cell growth by controlling the balance between protein synthesis and protein degradation [3]. In contrast, mTORC2, including the essential component rictor, regulates ion transport and cell survival by phosphorylating the serine/threonine protein kinase 1 (SGK1, at the Serine 422) [4], as well as actin cytoskeleton organization via the phosphorylation of protein kinase C α (PKCα, at the Serine 657) [5, 6]. In the last years, mTORC2 has been shown to be a regulator of lipogenesis and glucose homeostasis in insulin-stimulated tissues, *e.g.* in liver, through its downstream substrate Akt, which is phosphorylated within its hydrophobic motif (Serine 473) [7-9]. Genetic inactivation of mTORC2 in adult skeletal muscle, using *HSA-Cre*-induced depletion of rictor (RImKO mice), does not alter muscle organization and function [10], but impairs insulin-stimulated glucose transport and increases glycogen synthase activity in the tissue [11]. Moreover, whole-body metabolism of RImKO mice is perturbed due to a re-partitioning of lean to fat mass and an increase in intramyocellular triglycerides, which resulted in the preferred usage of fat as an energy substrate [12]. However, in those studies, mTORC2 was inactivated in differentiated, mature skeletal muscle, which did not address the role of mTORC2 signaling in the formation of the tissue and the function of satellite cells. Notwithstanding, germline depletion of rictor in mice resulted in embryonic lethality around E11.5 [13, 14], indicating that mTORC2 signaling is required for normal development. Inactivation of rictor in Myf5-expressing cells (*i.e.* progenitors in the dermomyotome giving rise to myoblasts and brown adipocytes) revealed an essential function of mTORC2 in brown adipocyte differentiation and growth: RImyfKO mice displayed a shift to a more oxidative and less lipogenic metabolism in the brown adipose tissue [15]. Even though these mutant mice developed normally and skeletal muscle mass was not altered at young age, long-term consequences of mTORC2

inactivation on muscle tissue homeostasis have not been studied in greater detail. In particular, whether its loss affects the satellite cell pool has not been investigated. Evidence for a specific role of mTORC2 in myogenesis originates from a study in C2C12 myoblasts, in which *Rictor* knock-down caused a blockage in their terminal differentiation [16]. During myoblast differentiation and fusion, Akt downregulates the Rho-associated kinase (ROCK1), involved in the regulation of the actin cytoskeleton, which was prevented in myogenic cells deficient for mTORC2.

Here, we confirm that mTORC2 signaling is not required for the formation of skeletal muscle fibers during development and established that it is dispensable for muscle regeneration. Even though satellite cells are generated and functional in RImyfKO mice, the maintenance of the pool is impaired upon repeated injuries and natural aging, ultimately leading to a reduced satellite cell population in the absence of mTORC2. Hence, we unravel a determinant role of mTORC2 in satellite cell homeostasis and muscle physiology.

Methods

Mice

RImyfKO mice were obtained by crossing *Rictor*-floxed mice [10] with transgenic mice expressing Cre recombinase under the control of the *Myf5* promoter (Jackson Laboratories [17]). Genotyping for conditional *Rictor* and the knock-in of *Cre recombinase* in the *Myf5* locus was performed as described previously [10, 17]. Females or males were used as indicated in the figure legend. No gender-specific differences were observed. *In vitro* force measurements of the *extensor digitorum longus* (EDL) and *soleus* (Sol) muscles were performed as described before [10]. All mice were maintained in standard conditions with a fixed 12 h dark-light cycle and free access to food and water. All animal studies were approved by the veterinary office of the Canton of Basel, in accordance to Swiss regulations.

Muscle injury and regeneration

5 or 14 month-old mice were anesthetized with Ketamine (111 mg/kg, Ketalar) and Xylazine (22 mg/kg, Rompun) by intraperitoneal injection. *Tibialis anterior* (TA) and EDL muscles were unilaterally injected with 6.7 µg cardiotoxin (Ctx; Latoxan) to provoke complete muscle degeneration. Mice were treated with 0.1 mg/kg Buprenorphine, twice a day for at least three days. The second muscle necrosis was induced 30 days after the first Ctx-injury. The injured, regenerating TA and EDL muscles, as well as the uninjured contralateral corresponding muscles, were harvested 15 days after the last injury.

Single myofiber isolation and culture

Single muscle fibers were isolated from the EDL muscle of 5 month-old mice by enzymatic digestion and trituration as previously described [18]. In brief, EDL was digested with 1 mg/ml Collagenase A (Roche) in DMEM Glutamax (Gibco), 1 % penicillin-streptomycin (Thermo Fisher Scientific) for 1.5 h at 37 °C and triturated into single myofibers. Fibers were cultured in DMEM Glutamax supplemented with 1 % pen/strep, 10 % horse serum, 1 % chicken embryo extract and fixed with 4 % PFA at different time points. For immunostaining, fibers were permeabilized with PBS, 0.5 % Triton-X100, and blocked with PBS, 10 % horse serum, 10 % goat serum, 0.35 % Carrageenan (Sigma) for 30 min. Primary antibodies were added overnight at 4 °C. Fibers were washed with PBS, 0.025 % Tween-20, and incubated with secondary antibodies for 1.5 h. They were then mounted on slides coated with 84 % acetone, 16 % (3-aminopropyl)triethoxysilane (Sigma), with Vectashield Dapi (Vector).

Histology and immunofluorescence staining

Muscles were dissected and frozen in nitrogen-cooled isopentane. 8 µm consecutive cryosections were used for standard histological staining. Hematoxylin and eosin staining

(Merck) was performed followed by sequential dehydration with 70 %, 90 % and 100 % ethanol and 100 % xylene. Picrosirius red (1 mg/ml in 1.3 % aqueous solution of picric acid, Sigma) was applied for 1 h, followed by washing in 0.5 % acidic water for 30 min. After dehydration in 100 % ethanol the slides were cleared in xylene. For Oil red O staining, the sections were fixed with 4 % PFA for 1 h and stained with 5 mg/ml Oil red O, 60 % triethyl-phosphate (Sigma) for 30 min. The sections were washed with water and mounted in 10 % glycerol. For immunohistochemistry, cryosections were fixed with 4 % PFA for 6 min, washed in PBS pH7.4, 0.1 M glycine and permeabilized with pre-cooled methanol for 6 min. Antigen retrieval was performed by warming the sections in 0.01 M citric acid. Sections were blocked in 3 % IgG-free BSA (Jackson Immuno Research Laboratories) supplemented with 0.05 mg/ml AffiniPure Mouse IgG, Fab Fragment (Jackson Immuno Research Laboratories). Primary antibodies were incubated overnight at 4 °C. Sections were subsequently washed and incubated with the appropriate fluorescent secondary antibodies for 1.5 h at room temperature. After washing with PBS, the samples were mounted with Vectashield Dapi (Vector laboratories). For MHCIIa staining, PFA-fixation was not performed.

Protein extraction and Western blot

TA muscles were snap-frozen in liquid nitrogen and powdered on dry ice. Samples were lysed in cold RIPA buffer (50 mM Tris-HCl pH8, 150 mM NaCl, 1 % NP-40, 0.5 % sodium deoxycholate, 0.1 % SDS, 1 % Triton X-100, 10 % glycerol) supplemented with phosphatase and protease inhibitor cocktail tablets (Roche), incubated for 2 h, sonicated twice for 10 s, and centrifuged at 16’000 g for 30 min at 4 °C. Total protein amount from cleared lysates were determined according to manufacturer’s protocol (Pierce BCA Protein Assay Kit, Thermo Fisher Scientific). Equal amounts of protein were loaded and separated on 4-12 % Bis-Tris Protein Gels (NuPage Novex, Thermo Fisher Scientific).

Antibodies

Rabbit polyclonal antibodies are as follows: MyoD c-20 (sc-304) and phospho-PKCα (Ser657; sc-12356) from Santa Cruz; laminin (ab11575) from Abcam; Akt (9272), PKCα (2056), phospho-S6 ribosomal protein (Ser235/236; 2211), phospho-4E-BP1 (Ser65; 9451) and 4E-BP1 (9452) from Cell Signaling Technologies (CST). Rabbit monoclonal antibodies are as follows: Rictor (9476), phospho-Akt (Ser473; 4058) and S6 ribosomal protein (2217) from CST. Mouse monoclonal antibodies are as follows: Pax7 and myosin heavy chain (human fast fibers; A4.74) from Developmental Studies Hybridoma Bank (DSHB) and α-actinin (sarcomeric; A7732) from Sigma. Rat monoclonal antibody against laminin α2 (ab11576) was from Abcam.

Statistical analyses

For muscle fiber size quantification, images were acquired using a Leica DM5000B fluorescence microscope with 10x objective, a digital camera (F-View; Olympus Soft Imaging Solutions GmbH) and the analySIS software (Soft Imaging System). The minimum distance of parallel tangents at opposing particle borders (minimal feret's diameter) of muscle fibers from the entire TA / EDL muscle or random fields of the muscles, were measured with the analySIS software as described [19]. All experiments were performed on a minimum of 3 independent biological samples indicated by the n-number (n). In all graphs, data are represented as the mean value and the respective standard error of the mean (SEM, error bars). Student's *t* test was employed to evaluate statistical significance and p-values lower than 0.05 are considered statistically significant.

Results

Depletion of rictor in the Myf5-lineage is dispensable for skeletal muscle development

To examine the function of mTORC2 in muscle progenitors, and their descendent satellite cells and adult myofibers, we generated conditional knockout mice depleted for rictor in Myf5-expressing cells (RImyfKO) by crossing *Myf5-Cre* mice [17] with mice carrying floxed alleles for *Rictor* [10] (*Myf5*$^{+/Cre}$*; Rictor*$^{fl/fl}$). Myf5 is expressed in progenitor cells of the somites from embryonic day (E) 8 [20] and determines cells differentiating into brown adipocytes or skeletal muscle cells [21]. RImyfKO mice were viable and born at the expected Mendelian ratio, but they could be distinguished from their littermate controls (Ctrl; *Myf5*$^{+/+}$*; Rictor*$^{fl/fl}$) by a reduction in their body weight (Figure 1A, 1B). Moreover, the reduction in body weight remained throughout life (Figure 1B). RImyfKO mice showed a normal distribution of fat and lean mass relative to their body weight (Figure 1C) and the mass of various hindlimb muscles, including the *tibialis anterior* (TA), *extensor digitorum longus* (EDL), *soleus* (Sol) and *gastrocnemius* (Gastro), normalized to the body weight was unchanged between Ctrl and mutant mice (Figure 1D). We confirmed that muscle extracts from RImyfKO mice were devoid of rictor and the mTORC2-specific phosphorylation of the downstream target Akt (Serine 473) was strongly decreased in mutant muscle (Figure 1E, Table 1). Total PKCα and its phosphorylated form (Serine 657) were both reduced in mTORC2-deficient muscle (Figure 1E, Table 1), similarly as already observed in RImKO mice [10]. In contrast, mTORC1-specific targets such as S6 ribosomal protein and 4E-BP1 were not affected in RImyfKO mice, confirming that rictor depletion in Myf5-expressing cells only disrupts mTORC2, but not mTORC1, signaling (Figure 1E, Table 1).

Since depletion of rictor in mature muscle fibers does not affect fiber size and cytoskeletal organization [10], we wondered whether mTORC2 inactivation in developing muscle would lead to muscle alterations in adult mice. By hematoxylin and eosin (H&E) staining, we observed no major histological difference in TA muscle from RImyfKO and Ctrl mice, at both 5- and 14-months of age (Figure 2A). Consistently, the fiber size distribution was unchanged in the EDL muscle of 14 month-old RImyfKO compared to Ctrl mice (Figure 2B, C). Additionally, there was no difference concerning fiber type composition and fiber number between genotypes (Figure 2D, E), indicating that RImyfKO muscle do not develop structural changes with age. Furthermore, the specific twitch (sPt) and tetanic (sP0) forces of EDL and Sol muscles were similar in 14 month-old RImyfKO and Ctrl mice (Figure 2F), confirming that mTORC2 inactivation in developing muscle did not cause functional deficits of mature muscle. Thus, deletion of rictor in the Myf5-lineage affects whole-body growth,

but does not interfere with the formation of skeletal muscle during embryogenesis and does not lead to muscle alterations in the adult.

mTORC2 signaling is dispensable for the myogenic function of satellite cells

Since Myf5 is expressed in a subset of quiescent satellite cells in adult skeletal muscle [2, 22, 23], we analyzed the satellite cell pool in RImyfKO muscle under homeostatic and challenging conditions. There was no significant difference in the number of $Pax7^+$ cells in TA and EDL muscles from 5 month-old RImyfKO and Ctrl mice (Figure 3A, B). This result indicates that mTORC2 signaling is dispensable for the generation of the satellite cell population and its maintenance at young age. To directly challenge mTORC2-deficient satellite cells, we injected cardiotoxin (Ctx) into TA and EDL muscles to induce a complete degeneration of the tissue, followed by 15 days of recovery (1x Ctx, 15d). For some mice, muscles were re-injured 30 days after the first Ctx-injection and analyzed 15 days post-injury (2x Ctx, 15d). The contralateral muscle remained uninjured. After one or two rounds of degeneration / regeneration, myofibers in Ctrl muscle were restored and exhibited centralized nuclei, a characteristic of regenerating fibers (Figure 3C). Similarly, an efficient regeneration was observed in muscle from 5 month-old RImyfKO mice; no accumulation of fibrosis, inflammation or adipogenic tissue was detected (Figure 3C). Consistently, the ratio between injured and uninjured TA and EDL muscle mass was not altered in RImyfKO mice, compared to Ctrl, after one or two Ctx-provoked muscle injures (Figure 3D). Furthermore, no difference in the fiber size distribution and in the total number of fibers was detected in RImyfKO muscle after the second muscle damage (Figure 3E-G), therefore providing strong evidence that the process of myofiber restoration was efficient in 5 month-old mice in the absence of mTORC2 signaling. As an efficient myofiber restoration lies on the activation of satellite cells, their proliferation and differentiation [24], we assumed that mTORC2 inactivation did not affect any of these processes. *In vitro* analysis of primary myoblasts isolated from RImyfKO muscle confirmed that mTORC2 is dispensable for muscle cell proliferation, differentiation and fusion [25]. Lastly, we tested whether mTORC2 is involved in the replenishment of the satellite cell pool by analyzing the number of $Pax7^+$ cells underneath the basal lamina after one or two injuries. Interestingly, the pool of $Pax7^+$ cells tended to be reduced and was significantly decreased after one and two Ctx-induced injuries, respectively, in RImyfKO muscle compared to Ctrl (Figure 3H, I). This indicated that mTORC2 signaling is dispensable for the myogenic function of satellite cells, but necessary for the replenishment of the pool following multiple degeneration / regeneration.

Interestingly, we observed an increased proportion of $Pax7^+$ cells with an abnormal, interstitial localization in 5 month-old RImyfKO TA and EDL muscles (Figure 4A). To further

analyze the satellite cell pool in RImyfKO muscle, we isolated single muscle fibers of EDL muscle from 5 month-old mice and analyzed the attached satellite cells either immediately after isolation (t0) or after culturing the fibers for up to 72 hours (t24h, t48h, t72h; Figure 4B-D). Interestingly, the number of $Pax7^+$ cells at t0 in RImyfKO EDL fibers was reduced compared to Ctrl mice (t0; Figure 4B), supporting the observation of an increased proportion of interstitial satellite cells *in vivo* (Figure 4A). After 24 hours in culture (t24h), all Ctrl and RImyfKO satellite cells got activated as indicated by MyoD expression, which was absent at t0 (Figure 4C). Until 72 hours in culture, $Pax7^+/MyoD^+$ activated cells proliferated and formed clones, from which some cells returned into quiescence (characterized by MyoD downregulation; $Pax7^+/MyoD^-$), and some cells entered in differentiation (Pax7 downregulation; $Pax7^-/MyoD^+$). At t48h, the proportion of $Pax7^-/MyoD^+$ cells was significantly increased in RImyfKO culture as compared to Ctrl, suggesting an anticipated commitment of the cells in the differentiation process. However, at t72h, the proportion of $Pax7^+/MyoD^-$, $Pax7^+/MyoD^+$, $Pax7^-/MyoD^+$ cells were similar in RImyfKO and Ctrl cultures (Figure 4C), indicating that mutant satellite cells do not show a defective capacity to return into quiescence. Furthermore, the increase in number of myogenic cells from t0 to t72h was comparable between both genotypes (Figure 4D), confirming that mTORC2 signaling is dispensable for proliferation of satellite cells. Altogether, these results suggest that mTORC2 signaling in satellite cells is dispensable for their myogenic function, but also for their self-renewal capacity.

The satellite cell pool declines during aging in the absence of mTORC2

Since at young age repeated degeneration / regeneration of skeletal muscle reduced the satellite cell pool in the absence of mTORC2 signaling, we wondered whether physiological aging would also alter their maintenance. Interestingly, the number of $Pax7^+$ cells was reduced in TA and EDL muscles from 14 month-old RImyfKO mice, as compared to Ctrl (Figure 5A). To test the function of the remaining satellite cells in mutant muscle, we induced one injury by injecting cardiotoxin in TA and EDL muscles of 14 month-old mice and analyzed their regenerative capacity 15 days post-injury. By H&E staining, we observed that RImyfKO muscle showed a limited regenerative capacity, with smaller newly formed myofibers and an abnormal accumulation of lipid droplets, as compared to Ctrl (Figure 5B). Consistently, the ratio between the mass of injured and uninjured TA / EDL muscles from 14 month-old RImyfKO mice tended to be reduced compared to Ctrl (Figure 5C) and the fiber size distribution in regenerating RImyfKO muscle was shifted towards smaller myofibers (Figure 5D, E). Of note, there was no increase in collagen-rich, fibrotic area in RImyfKO regenerating muscle (Figure 5F). Lipid infiltration in RImyfKO regenerating muscle was confirmed with Oil red O staining, with a significant increase in fat area (Figure 5F, G).

Following muscle regeneration, the satellite cell pool remained smaller in RImyfKO mice compared to Ctrl (Figure 5H). Thus, mTORC2 signaling in satellite cells seems to be essential for the maintenance of the pool, and thereby for the regenerative capacity of muscle tissue, during aging.

Discussion

Our work dissects the role of mTORC2 in embryonic and adult muscle progenitors, by using mice depleted for rictor, the essential component of mTORC2, in the Myf5-lineage. In contrast to RImKO mice, depleted for rictor in adult skeletal muscle [10, 11], RImyfKO mice were lighter compared to littermate Ctrl. Hung et al. previously reported a difference in body weight in mice depleted for rictor in the Myf5-lineage, only between 6 and 15 weeks of age, and they argued that it may be caused by decreased adipose tissue mass and reduced growth [15]. Whole body growth is mediated by the family of insulin-like growth factors (IGFs), in which IGF-II is predominantly active during fetal development [26]. *Igf2*$^{-/-}$ mice and mice carrying a paternally derived mutated *Igf2* gene were smaller and displayed a 40 % body weight reduction compared to littermate controls [27]. Recent reports revealed that in mouse embryonic fibroblasts (MEFs), IGF-II translation is controlled by mTORC2 through the phosphorylation of IGF-II mRNA-binding protein 1 (IMP1) [28]. Even though skeletal muscle is not the only source of circulating IGFs, it may well be that loss of mTORC2 in developing muscle affects whole body growth by reducing the amount of released IGF-II. Importantly, RImyfKO muscles developed normally in respect to their body weight and showed no major alterations in adult, indicating that mTORC2 signaling is not required for embryonic myogenesis and the maintenance of mature muscle.

Myogenesis includes proliferation, differentiation and fusion of muscle progenitors / precursors in order to form multinucleated myotubes that mature into muscle fibers [24]. This process is involved during embryonic muscle development and recapitulated during injury-induced muscle regeneration. RImyfKO muscles were capable to undergo successful muscle regeneration following one or two subsequent muscle injuries at young age. In light of the efficient fiber restoration in RImyfKO mice at young age, we assumed that mTORC2 signaling is not necessary for the myogenic function of adult muscle precursors to proliferate, differentiate and fuse. Consistently, primary myoblasts isolated from RImyfKO muscle efficiently proliferate, differentiate and fuse into multi-nucleated myotubes [25]. Furthermore, mTORC2-deficient satellite cells on single myofibers showed a similar capacity to proliferate and form clones in culture compared to Ctrl cells. These results contrast to a previous report with C2C12 myoblasts silenced for mTORC2 signaling (shRNA directed against *Rictor*), which suggested a potent role of mTORC2 in myoblast differentiation through Akt and ROCK1 [16]. Here, we provide evidence that mTORC2 signaling is dispensable for proliferation, differentiation and fusion of embryonic and adult muscle precursors *in vitro* and *in vivo*.

In this study, we report that inhibition of mTORC2 in satellite cells alters their maintenance. The number of satellite cells was unaffected in muscle from young RImyfKO mice, but we observed an increased proportion of cells located in the interstitial space. This suggests that satellite cells lose their quiescence in the absence of mTORC2, as migration out of the niche is associated to the activation of the cells [29]. This may explain why following repeated injuries, the pool of RImyfKO satellite cells gradually declines. Satellite cells deficient for PTEN, an inhibitor of PI3K and Akt, were found to spontaneously activate and undergo premature differentiation [30]; *Pten*$^{-/-}$ satellite cells were unable to return into quiescence, which results in a depletion of the stem cell pool with age and in regenerative failure [30, 31]. Hence, RImyfKO and *Pten*$^{-/-}$ satellite cells, which are both characterized by a deregulation of Akt (decreased and increased phosphorylation at the site Serine 473, respectively), would also share phenotypic similarities. However, RImyfKO satellite cells did not show reduced capacity to return into quiescence in culture, suggesting that inactivation of mTORC2 signaling, and the subsequent Akt deregulation, did not impair their self-renewal function.

Interestingly, RImyfKO muscle not only lose satellite cells after repeated injuries but also in the absence of external stimuli during physiological aging. Likely as a consequence, the regenerative capacity of muscle from aged RImyfKO mice in response to one injury was reduced. Instead of an efficient fiber restoration, smaller myofibers accompanied with an accumulation of lipid droplets were formed. As an increased number of interstitial satellite cells were observed in RImyfKO muscle and a reduced number of Pax7^{+} cells remained associated to mutant fibers upon dissociation, the precipitated loss of satellite cells during aging may be caused by alterations of their niche or their interaction with myofibers. Adhesion molecules, such as M-cadherin, Mcam, Megf10 and integrin α4β1, mediate the interaction between satellite cells and myofibers and are involved in the colonization of the niche by the satellite cell (“homing”) [29]. Deregulation of the Notch signaling has been shown to cause instable adhesive interactions and homing deficits resulting in an interstitial localization of the stem cell [29]. Similarly, satellite cells deficient for syndecan-3, a transmembrane heparan sulfate proteoglycan, are prone to migrate away from their niche and fail to replenish the quiescent stem cell pool following injury [32-37]. Alterations of the homing capacity of mTORC2-deficient satellite cells may hence contribute to the defects observed. Alternatively, the loss of satellite cells in the absence of mTORC2 signaling may also be caused by an anticipated conversion into a pre-senescent state [38]. In course of natural aging, the number of satellite cells drops [39] and the regenerative potential of individual satellite cells declines [40-42], which have been related to several factors. Senescent satellite cells are marked by impaired autophagy, increased mitochondrial

dysfunction and oxidative stress [43]. Although Akt induction is sufficient to block FoxO3 activation and autophagy [44], it was demonstrated that mTORC2 signaling does not control autophagy in skeletal muscle [45]. Moreover, also age-related alterations in signaling cascades and components of the satellite cell niche affect the homeostasis of their resident stem cell [46]. Since mTORC2-deficient satellite cells did not show any deficits in their myogenic function, it is unlikely that the phenotype appears cell-autonomously and may rather be caused by changes in the interaction between satellite cells and their niche.

Conclusions

Our study demonstrates that mTORC2 is dispensable for the formation and maintenance of skeletal muscle, and for the myogenic function of muscle stem cells. However, with age and after repeated injuries the number of muscle stem cells decreases and the regenerative capacity of the muscle diminishes in the absence of mTORC2. These observations highlight that mTORC2 signaling is essential for muscle stem cell homeostasis and provide evidence for mTORC2 targets required during aging and conditions of multiple rounds of degeneration / regeneration, as in muscular dystrophies.

References

1. Bentzinger, C.F., Y.X. Wang, and M.A. Rudnicki, Building muscle: molecular regulation of myogenesis. Cold Spring Harbor perspectives in biology, 2012. 4(2).

2. Biressi, S., C.R. Bjornson, P.M. Carlig, K. Nishijo, C. Keller, and T.A. Rando, Myf5 expression during fetal myogenesis defines the developmental progenitors of adult satellite cells. Dev Biol, 2013. 379(2): p. 195-207.

3. Saxton, R.A. and D.M. Sabatini, mTOR Signaling in Growth, Metabolism, and Disease. Cell, 2017. 168(6): p. 960-976.

4. Garcia-Martinez, J.M. and D.R. Alessi, mTOR complex 2 (mTORC2) controls hydrophobic motif phosphorylation and activation of serum- and glucocorticoid-induced protein kinase 1 (SGK1). The Biochemical journal, 2008. 416(3): p. 375-85.

5. Jacinto, E., R. Loewith, A. Schmidt, S. Lin, M.A. Ruegg, A. Hall, and M.N. Hall, Mammalian TOR complex 2 controls the actin cytoskeleton and is rapamycin insensitive. Nature cell biology, 2004. 6(11): p. 1122-8.

6. Sarbassov, D.D., S.M. Ali, D.H. Kim, D.A. Guertin, R.R. Latek, H. Erdjument-Bromage, P. Tempst, and D.M. Sabatini, Rictor, a novel binding partner of mTOR, defines a rapamycin-insensitive and raptor-independent pathway that regulates the cytoskeleton. Current biology : CB, 2004. 14(14): p. 1296-302.

7. Sarbassov, D.D., D.A. Guertin, S.M. Ali, and D.M. Sabatini, Phosphorylation and regulation of Akt/PKB by the rictor-mTOR complex. Science, 2005. 307(5712): p. 1098-101.

8. Hagiwara, A., M. Cornu, N. Cybulski, P. Polak, C. Betz, F. Trapani, L. Terracciano, M.H. Heim, M.A. Ruegg, and M.N. Hall, Hepatic mTORC2 Activates Glycolysis and Lipogenesis through Akt, Glucokinase, and SREBP1c. Cell metabolism, 2012. 15(5): p. 725-738.

9. Yuan, M., E. Pino, L. Wu, M. Kacergis, and A.A. Soukas, Identification of Akt-independent regulation of hepatic lipogenesis by mammalian target of rapamycin (mTOR) complex 2. J Biol Chem, 2012. 287(35): p. 29579-88.

10. Bentzinger, C.F., K. Romanino, D. Cloetta, S. Lin, J.B. Mascarenhas, F. Oliveri, J. Xia, E. Casanova, C.F. Costa, M. Brink, F. Zorzato, M.N. Hall, and M.A. Ruegg, Skeletal muscle-specific ablation of raptor, but not of rictor, causes metabolic changes and results in muscle dystrophy. Cell metabolism, 2008. 8(5): p. 411-24.

11. Kumar, A., T.E. Harris, S.R. Keller, K.M. Choi, M.A. Magnuson, and J.C. Lawrence, Jr., Muscle-specific deletion of rictor impairs insulin-stimulated glucose transport and enhances Basal glycogen synthase activity. Molecular and cellular biology, 2008. 28(1): p. 61-70.

12. Kleinert, M., B.L. Parker, R. Chaudhuri, D.J. Fazakerley, A. Serup, K.C. Thomas, J.R. Krycer, L. Sylow, A.M. Fritzen, N.J. Hoffman, J. Jeppesen, P. Schjerling, M.A. Ruegg, B. Kiens, D.E. James, and E.A. Richter, mTORC2 and AMPK differentially regulate muscle triglyceride content via Perilipin 3. Mol Metab, 2016. 5(8): p. 646-55.

13. Guertin, D.A., D.M. Stevens, C.C. Thoreen, A.A. Burds, N.Y. Kalaany, J. Moffat, M. Brown, K.J. Fitzgerald, and D.M. Sabatini, Ablation in mice of the mTORC components raptor, rictor, or mLST8 reveals that mTORC2 is required for signaling to Akt-FOXO and PKCalpha, but not S6K1. Developmental cell, 2006. 11(6): p. 859-71.

14. Shiota, C., J.T. Woo, J. Lindner, K.D. Shelton, and M.A. Magnuson, Multiallelic disruption of the rictor gene in mice reveals that mTOR complex 2 is essential for fetal growth and viability. Developmental cell, 2006. 11(4): p. 583-9.

15. Hung, C.M., C.M. Calejman, J. Sanchez-Gurmaches, H. Li, C.B. Clish, S. Hettmer, A.J. Wagers, and D.A. Guertin, Rictor/mTORC2 loss in the Myf5 lineage reprograms brown fat metabolism and protects mice against obesity and metabolic disease. Cell reports, 2014. 8(1): p. 256-71.

16. Shu, L. and P.J. Houghton, The mTORC2 complex regulates terminal differentiation of C2C12 myoblasts. Molecular and cellular biology, 2009. 29(17): p. 4691-700.

17. Tallquist, M.D., K.E. Weismann, M. Hellstrom, and P. Soriano, Early myotome specification regulates PDGFA expression and axial skeleton development. Development, 2000. 127(23): p. 5059-70.

18. Rosenblatt, J.D., A.I. Lunt, D.J. Parry, and T.A. Partridge, Culturing satellite cells from living single muscle fiber explants. In vitro cellular & developmental biology. Animal, 1995. 31(10): p. 773-9.

19. Briguet, A., I. Courdier-Fruh, M. Foster, T. Meier, and J.P. Magyar, Histological parameters for the quantitative assessment of muscular dystrophy in the mdx-mouse. Neuromuscul Disord, 2004. 14(10): p. 675-82.

20. Ott, M.O., E. Bober, G. Lyons, H. Arnold, and M. Buckingham, Early expression of the myogenic regulatory gene, myf-5, in precursor cells of skeletal muscle in the mouse embryo. Development, 1991. 111(4): p. 1097-107.

21. Seale, P., B. Bjork, W. Yang, S. Kajimura, S. Chin, S. Kuang, A. Scime, S. Devarakonda, H.M. Conroe, H. Erdjument-Bromage, P. Tempst, M.A. Rudnicki, D.R. Beier, and B.M. Spiegelman, PRDM16 controls a brown fat/skeletal muscle switch. Nature, 2008. 454(7207): p. 961-7.

22. Beauchamp, J.R., L. Heslop, D.S. Yu, S. Tajbakhsh, R.G. Kelly, A. Wernig, M.E. Buckingham, T.A. Partridge, and P.S. Zammit, Expression of CD34 and Myf5 defines the majority of quiescent adult skeletal muscle satellite cells. J Cell Biol, 2000. 151(6): p. 1221-34.

23. Crist, C.G., D. Montarras, and M. Buckingham, Muscle satellite cells are primed for myogenesis but maintain quiescence with sequestration of Myf5 mRNA targeted by microRNA-31 in mRNP granules. Cell Stem Cell, 2012. 11(1): p. 118-26.

24. Dumont, N.A., C.F. Bentzinger, M.C. Sincennes, and M.A. Rudnicki, Satellite Cells and Skeletal Muscle Regeneration. Compr Physiol, 2015. 5(3): p. 1027-59.

25. Rion, N., P. Castets, S. Lin, L. Enderle, C. Eickhorst, and M.A. Ruegg, Loss of mTORC1 in muscle progenitors reduces proliferation and differentiation and impairs, but does not abolish, myogenesis. 2017, in preparation.

26. Agrogiannis, G.D., S. Sifakis, E.S. Patsouris, and A.E. Konstantinidou, Insulin-like growth factors in embryonic and fetal growth and skeletal development (Review). Mol Med Rep, 2014. 10(2): p. 579-84.

27. DeChiara, T.M., A. Efstratiadis, and E.J. Robertson, A growth-deficiency phenotype in heterozygous mice carrying an insulin-like growth factor II gene disrupted by targeting. Nature, 1990. 345(6270): p. 78-80.

28. Dai, N., J. Christiansen, F.C. Nielsen, and J. Avruch, mTOR complex 2 phosphorylates IMP1 cotranslationally to promote IGF2 production and the proliferation of mouse embryonic fibroblasts. Genes Dev, 2013. 27(3): p. 301-12.

29. Brohl, D., E. Vasyutina, M.T. Czajkowski, J. Griger, C. Rassek, H.P. Rahn, B. Purfurst, H. Wende, and C. Birchmeier, Colonization of the satellite cell niche by skeletal muscle progenitor cells depends on Notch signals. Developmental cell, 2012. 23(3): p. 469-81.

30. Yue, F., P. Bi, C. Wang, T. Shan, Y. Nie, T.L. Ratliff, T.P. Gavin, and S. Kuang, Pten is necessary for the quiescence and maintenance of adult muscle stem cells. Nat Commun, 2017. 8: p. 14328.

31. Yue, F., P. Bi, C. Wang, J. Li, X. Liu, and S. Kuang, Conditional Loss of Pten in Myogenic Progenitors Leads to Postnatal Skeletal Muscle Hypertrophy but Age-Dependent Exhaustion of Satellite Cells. Cell Rep, 2016. 17(9): p. 2340-2353.

32. Casar, J.C., C. Cabello-Verrugio, H. Olguin, R. Aldunate, N.C. Inestrosa, and E. Brandan, Heparan sulfate proteoglycans are increased during skeletal muscle regeneration: requirement of syndecan-3 for successful fiber formation. J Cell Sci, 2004. 117(Pt 1): p. 73-84.

33. Cornelison, D.D., M.S. Filla, H.M. Stanley, A.C. Rapraeger, and B.B. Olwin, Syndecan-3 and syndecan-4 specifically mark skeletal muscle satellite cells and are implicated in satellite cell maintenance and muscle regeneration. Dev Biol, 2001. 239(1): p. 79-94.

34. Cornelison, D.D., S.A. Wilcox-Adelman, P.F. Goetinck, H. Rauvala, A.C. Rapraeger, and B.B. Olwin, Essential and separable roles for Syndecan-3 and Syndecan-4 in skeletal muscle development and regeneration. Genes Dev, 2004. 18(18): p. 2231-6.

35. Fuentealba, L., D.J. Carey, and E. Brandan, Antisense inhibition of syndecan-3 expression during skeletal muscle differentiation accelerates myogenesis through a basic fibroblast growth factor-dependent mechanism. J Biol Chem, 1999. 274(53): p. 37876-84.

36. Pisconti, A., D.D. Cornelison, H.C. Olguin, T.L. Antwine, and B.B. Olwin, Syndecan-3 and Notch cooperate in regulating adult myogenesis. J Cell Biol, 2010. 190(3): p. 427-41.

37. Pisconti, A., G.B. Banks, F. Babaeijandaghi, N.D. Betta, F.M. Rossi, J.S. Chamberlain, and B.B. Olwin, Loss of niche-satellite cell interactions in syndecan-3 null mice alters muscle progenitor cell homeostasis improving muscle regeneration. Skelet Muscle, 2016. 6: p. 34.

38. Brack, A.S. and P. Munoz-Canoves, The ins and outs of muscle stem cell aging. Skelet Muscle, 2016. 6: p. 1.

39. Shefer, G., D.P. Van de Mark, J.B. Richardson, and Z. Yablonka-Reuveni, Satellite-cell pool size does matter: defining the myogenic potency of aging skeletal muscle. Dev Biol, 2006. 294(1): p. 50-66.

40. Sadeh, M., Effects of aging on skeletal muscle regeneration. J Neurol Sci, 1988. 87(1): p. 67-74.

41. Grounds, M.D., Age-associated changes in the response of skeletal muscle cells to exercise and regeneration. Ann N Y Acad Sci, 1998. 854: p. 78-91.

42. Barani, A.E., A.C. Durieux, O. Sabido, and D. Freyssenet, Age-related changes in the mitotic and metabolic characteristics of muscle-derived cells. J Appl Physiol (1985), 2003. 95(5): p. 2089-98.

43. Garcia-Prat, L., M. Martinez-Vicente, E. Perdiguero, L. Ortet, J. Rodriguez-Ubreva, E. Rebollo, V. Ruiz-Bonilla, S. Gutarra, E. Ballestar, A.L. Serrano, M. Sandri, and P. Munoz-Canoves, Autophagy maintains stemness by preventing senescence. Nature, 2016. 529(7584): p. 37-42.

44. Mammucari, C., G. Milan, V. Romanello, E. Masiero, R. Rudolf, P. Del Piccolo, S.J. Burden, R. Di Lisi, C. Sandri, J. Zhao, A.L. Goldberg, S. Schiaffino, and M. Sandri, FoxO3 controls autophagy in skeletal muscle in vivo. Cell Metab, 2007. 6(6): p. 458-71.

45. Castets, P., S. Lin, N. Rion, S. Di Fulvio, K. Romanino, M. Guridi, S. Frank, L.A. Tintignac, M. Sinnreich, and M.A. Ruegg, Sustained activation of mTORC1 in skeletal muscle inhibits constitutive and starvation-induced autophagy and causes a severe, late-onset myopathy. Cell metabolism, 2013. 17(5): p. 731-44.

46. Sousa-Victor, P. and P. Munoz-Canoves, Regenerative decline of stem cells in sarcopenia. Mol Aspects Med, 2016. 50: p. 109-17.

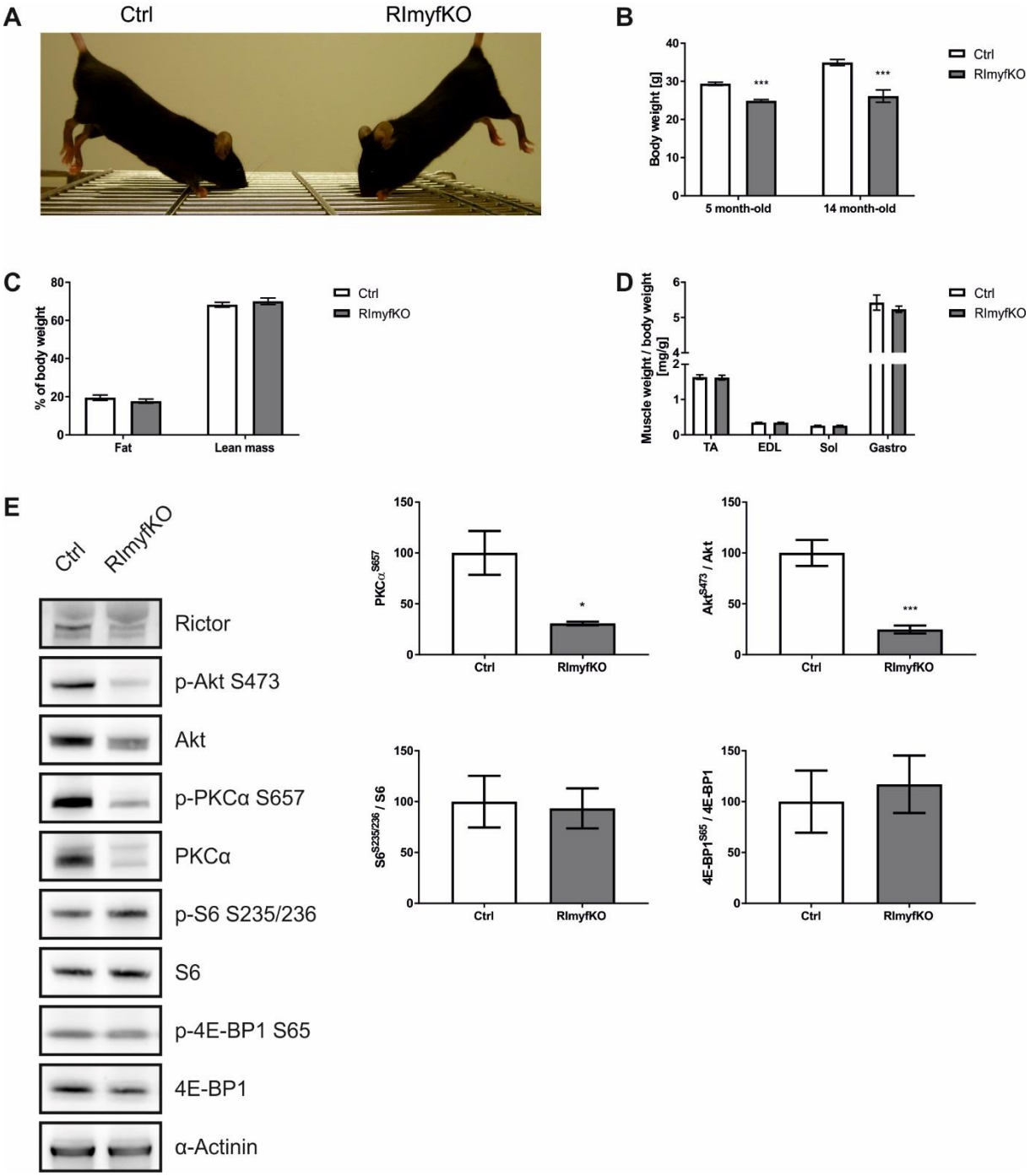

Figure 1. Depletion of rictor in the Myf5-lineage affects whole-body growth

a Photograph of Ctrl (*Myf5*$^{+/+}$*; Rictor*$^{fl/fl}$) and RImyfKO (*Myf5*$^{+/Cre}$*; Rictor*$^{fl/fl}$) mice at the age of 5 months. **b** The body weight of Ctrl and RImyfKO male mice was measured at 5 and 14 month of age (n = 6-8). **c** The fat mass and lean mass of 5 month-old, male Ctrl and RImyfKO mice was analyzed by EchoMRI (n = 4-6). **d** The mass of TA, EDL, Sol and Gastro muscles from 5 month-old RImyfKO males is unchanged compared to Ctrl littermates (n = 4-6). **e** Western blot analysis of the proteins indicated in TA muscle from 5 month-old, male Ctrl and RImyfKO mice. Equal amount of protein was loaded in each lane. α-Actinin was used as loading control (n =5).

Data represent mean ± SEM. * p < 0.05, *** p < 0.001, Student's *t* test.

	TA muscle	
	Ctrl	**RImyfKO**
Rictor	100 ± 7	72 ± 4 *
phospho-Akt Ser473	100 ± 12	18 ± 2 ***
Akt	100 ± 7	76 ± 9
phospho-PKCα Ser657	100 ± 22	31 ± 2 *
PKC	100 ± 10	29 ± 2 ***
phospho-S6 Ser235/236	100 ± 24	101 ± 27
S6	100 ± 13	106 ± 16
phospho-4E-BP1 Ser65	100 ± 24	98 ± 17
4E-BP1	100 ± 10	81 ± 12
Ratio phospho-Akt Ser473 / Akt	100 ± 13	25 ± 4 ***
Ratio phospho-S6 Ser235/236 / S6	100 ± 25	93 ± 20
Ratio phospho-4E-BP1 Ser65 / 4E-BP1	100 ± 31	117 ± 28

Table 1. Quantification of Western blot analysis in TA muscle from 5 month-old, male RImyfKO and Ctrl mice, related to Figure 1

Protein levels were quantified in TA muscle from 5 month-old, male RImyfKO and Ctrl mice. The total amount of protein was adjusted according to concentration. Data are represented as the average of grey values ± SEM, after background subtraction and normalization to α-Actinin and to values from Ctrl mice (n = 5). * p < 0.05, *** p < 0.001, Student's *t* test.

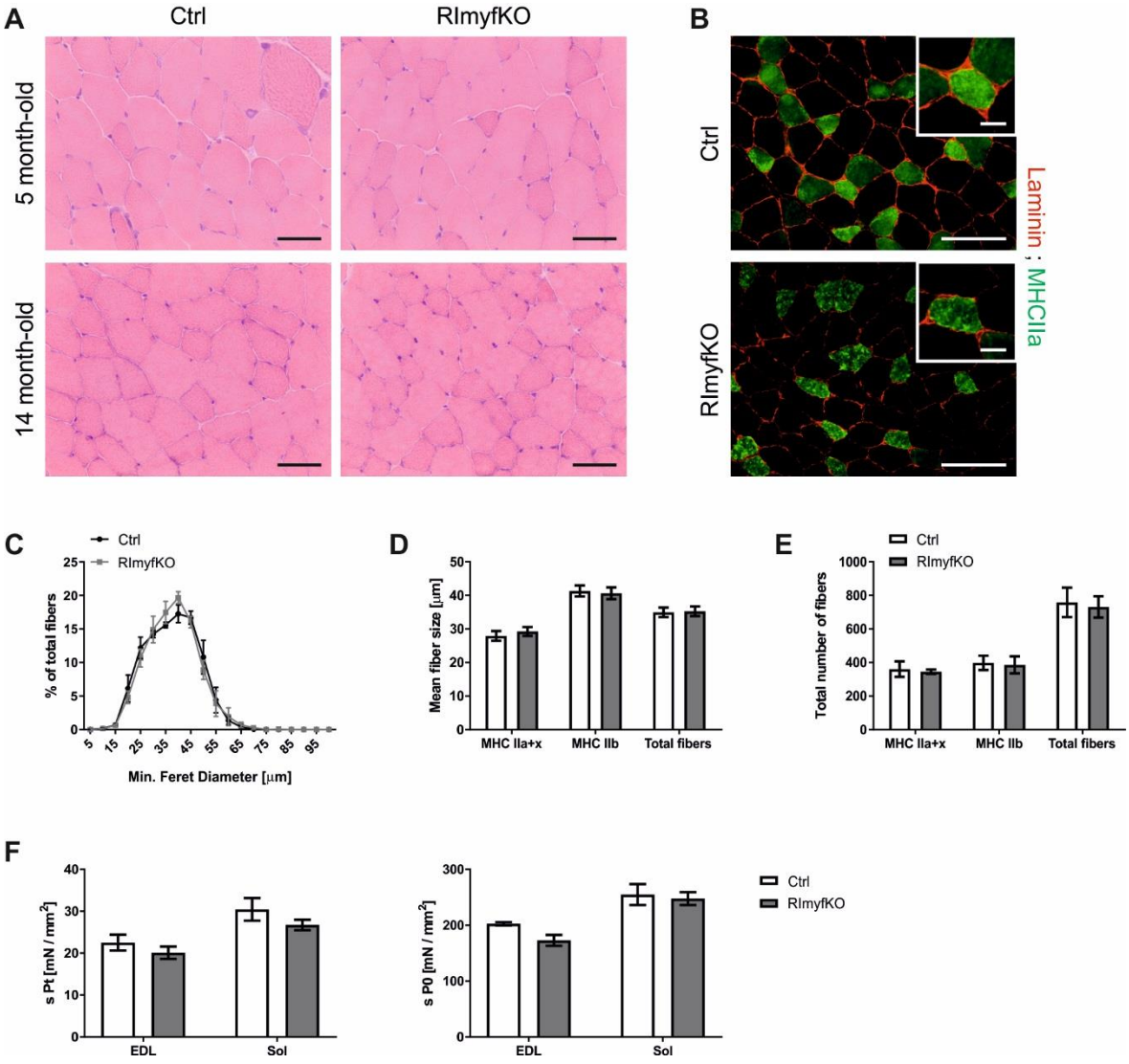

Figure 2. mTORC2 is not required for adult skeletal muscle homeostasis

a Hematoxylin and eosin (H&E) coloration on TA cross-sections of 5 and 14 month-old Ctrl and RImyfKO mice. No alteration in muscle histology and fiber organization was detected in RImyfKO muscle. Scale bar, 50 µm. **b** Immunostaining against laminin (red) and myosin heavy chain IIa (MHCIIa, green) on EDL cross-section from 14 month-old, female Ctrl and RImyfKO mice. Type IIa fibers are labeled in bright green, type IIx in mild green and IIb fibers appear unstained. Scale bar, 100 µm and 20 µm at higher magnification. **c – e** Fiber size distribution (**c**), mean fiber size (**d**) and total number of fibers (**e**) was analyzed in the EDL muscle of 14 month-old Ctrl and RImyfKO mice (n = 3). **f** Specific twitch force and specific tetanic force of the EDL and Sol muscle from 14 month-old Ctrl and RImyfKO mice was measured (n = 4-7).

Data represent mean ± SEM. Student's *t* test.

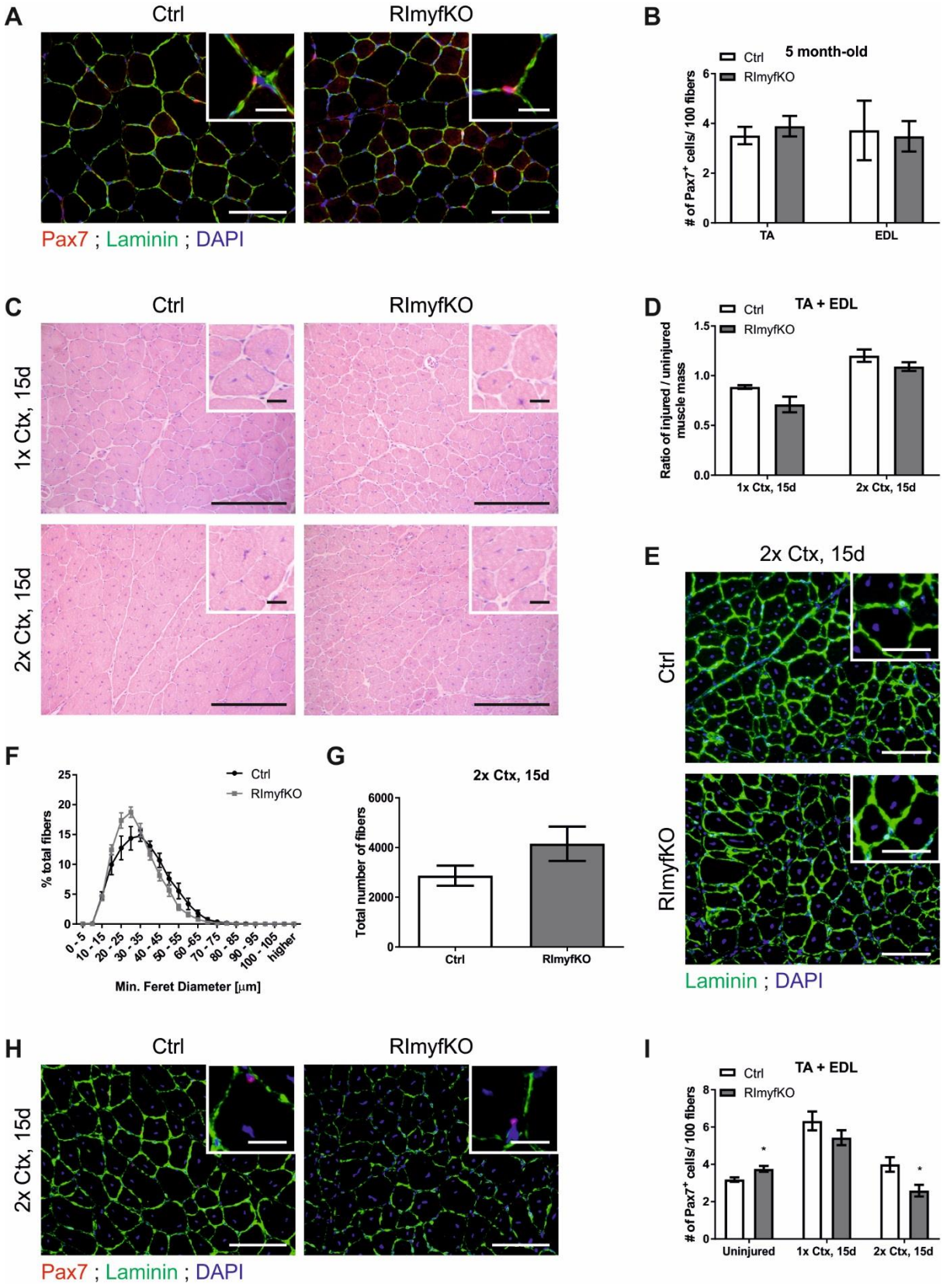

Figure 3. Satellite cells of RImyfKO mice fail to replenish the pool after repeated injuries

a Immunostaining against Pax7 (red) and laminin (green) on TA muscle cross-sections from 5 month-old Ctrl and RImyfKO mice. Scale bar, 100 µm and 20 µm at higher magnification.

b The number of $Pax7^+$ cells underneath the basal lamina was counted in TA and EDL muscles from 5 month-old, male Ctrl and RImyfKO mice and normalized to 100 myofibers (n = 4-5). **c – i** Cardiotoxin (Ctx) was injected into TA and EDL muscles of 5 month-old, male Ctrl and RImyfKO mice. Muscle analysis was performed 15 days post-injury (1x Ctx). Contralateral muscles were not injured. Some mice were re-injured 30 days after the first injury (2x Ctx). **c** H&E staining on 1x Ctx or 2x Ctx TA muscle cross-sections from Ctrl and RImyfKO mice. Centralized nuclei are characteristics of regenerating myofibers. Scale bar, 100 µm and 10 µm at higher magnification. **d** The ratio between the mass of the injured and uninjured TA and EDL muscles was calculated after 1x Ctx or 2x Ctx (n = 3-4). A ratio of 1 implies successful restoration of the injured muscle 15 days after the induction of muscle damage. **e** Immunostaining against laminin (green) on cross-sections of regenerating TA muscle following two Ctx-injuries. Scale bar, 100 µm and 50 µm at higher magnification. **f – g** The fiber size distribution (**f**) and total number of myofibers (**g**) was quantified in 2x Ctx TA muscle (n =3). **h** Immunostaining against Pax7 (red) and laminin (green) on regenerating TA and EDL muscle following 2x Ctx. Scale bar, 100 µm and 20 µm at higher magnification. **i** Quantification of the number of $Pax7^+$ cells normalized to 100 myofibers fibers in the uninjured, 1x Ctx and 2x Ctx TA and EDL muscles (n = 3-7).
Data represent mean ± SEM. * $p > 0.05$, Student's *t* test.

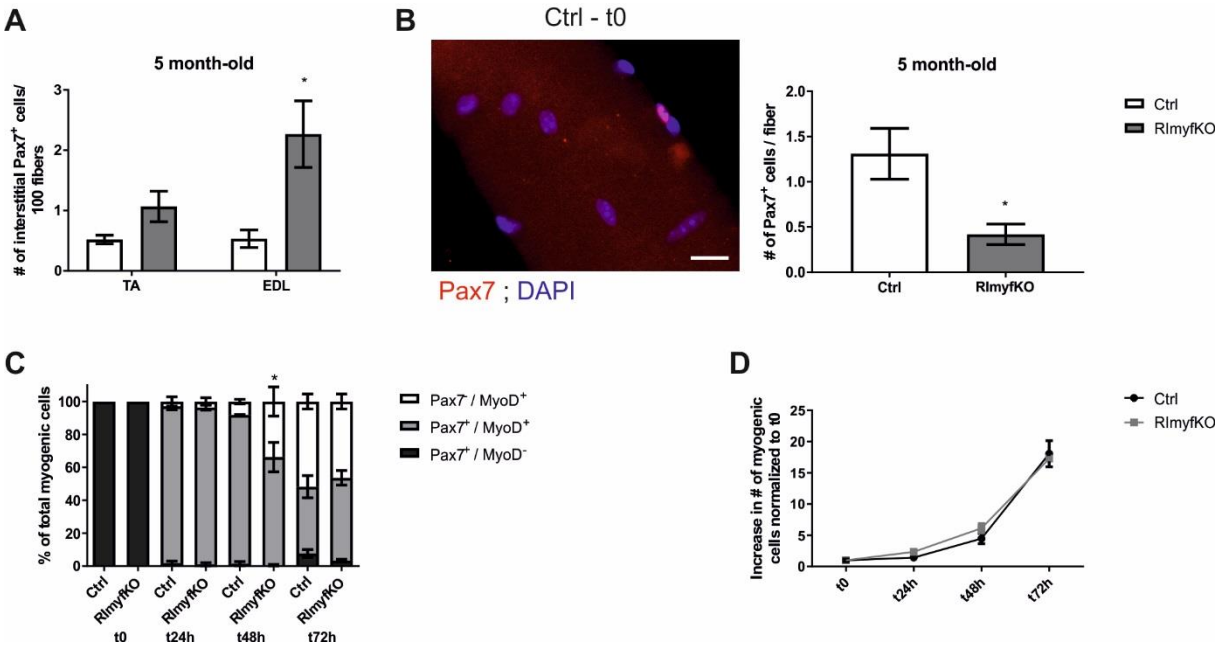

Figure 4. mTORC2 signaling is dispensable for satellite cell quiescence and differentiation

a Quantification of the number of interstitial Pax7$^+$ cells normalized to 100 myofibers in the TA and EDL muscles of 5 month-old, male mice (n = 4-5). **b** Immunostaining against Pax7 on freshly isolated myofibers from the EDL muscle of 5 month-old mice. Scale bar, 20 µm. Quantification of the number of Pax7$^+$ cells associated on freshly isolated myofibers (t0) from the EDL muscle of 5 month-old male Ctrl and RImyfKO mice (n = 3-8, 10-30 myofibers per animal). **c – d** Single EDL myofibers were isolated from 5 month-old Ctrl and RImyfKO female mice and their associated satellite cells analyzed directly after isolation (t0) or after 24, 48 or 72 h in culture (t24h, t48h, t72h). **c** The number of Pax7- and / or MyoD-positive cells was quantified and normalized to the total number of myogenic cells on single isolated myofibers at t0, t24h, t48h and t72h (n = 3, 10-30 myofibers per animal). **d** The total number of myogenic cells per myofiber was counted at t24h, t48h and t72h and normalized to t0 (n = 3, 10-30 myofibers per animal).

Data represent mean ± SEM. * p > 0.05, Student's *t* test.

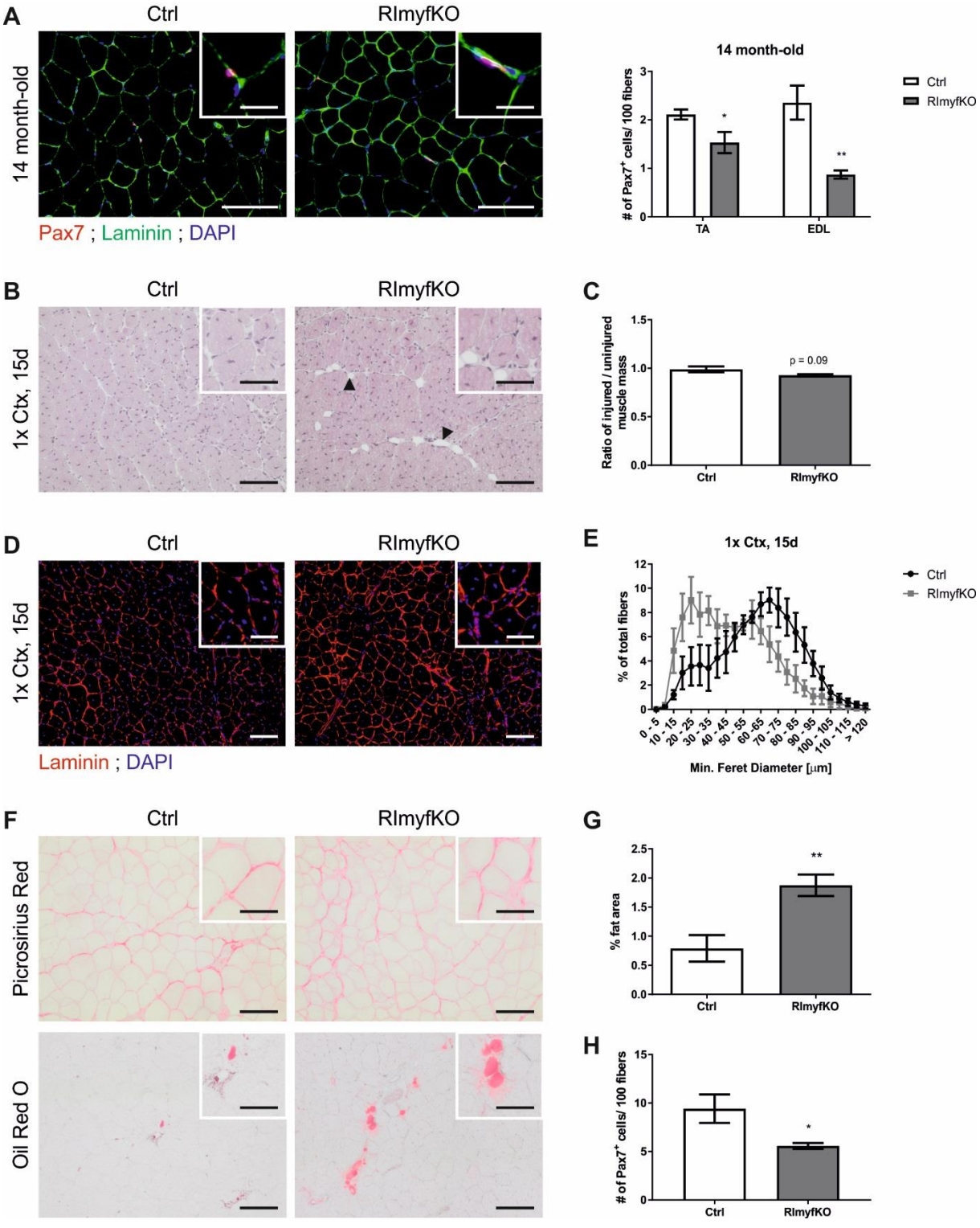

Figure 5. The satellite cell pool decreases with age in the absence of mTORC2

a Immunostaining against Pax7 (red) and laminin (green) on TA and EDL muscle cross-sections from 14 month-old, female Ctrl and RImyfKO mice. The number of $Pax7^+$ cells underneath the basal lamina was counted and normalized to 100 myofibers (n = 3-5). Scale bar, 100 µm and 20 µm at higher magnification. **b – h** Ctx was injected into TA and EDL muscles of 14 month-old, male Ctrl and RImyfKO mice. Muscle analysis was performed 15 days post-injury (1x Ctx). Contralateral muscles were not injured. **b** H&E coloration on TA

muscle cross-sections from 14 month-old Ctrl and RImyfKO mice 15 days after one Ctx-injury. Centralized nuclei are a characteristic of regenerating myofibers. Arrowheads point to adipocytes generated in regenerating RImyfKO muscle. Scale bar, 100 µm and 50 µm at higher magnification. **c** The mass ratio between injured and uninjured TA and EDL muscles was calculated after 15 days of recovery (n = 5). **d** Immunostaining against laminin (red) on cross-sections of regenerating TA muscles following 1x Ctx. Scale bar, 100 µm and 50 µm at higher magnification. **e** The fiber size distribution was quantified in TA muscle 15 days after Ctx-injury (n = 3). **f** Picrosirius Red coloration (upper panel) on regenerating TA muscle stains collagens in the extracellular matrix between myofibers of Ctrl and RImyfKO mice. Oil red O staining (lower panel) visualizes lipid droplets in the regenerating muscle of RImyfKO mice. Scale bar, 100 µm and 50 µm at higher magnification. **g** Quantification of the adipocyte area normalized to the total muscle area after 1x Ctx (n = 5). **h** Quantification of the number of $Pax7^+$ cells normalized to 100 myofibers in Ctx-injured TA and EDL muscles after 15 days recovery (n = 5).

Data represent mean ± SEM. * $p > 0.05$, ** $p > 0.01$, Student's *t* test.

7. Discussion

The mTOR signaling pathway functions as a central hub controlling homeostasis and growth of adult skeletal muscle. Before my thesis, several reports pointed to an important role of the signaling in muscle fiber formation during embryogenesis and muscle regeneration. Because most of these studies were conducted *in vitro* and / or using pharmacological inhibitors, in-depth analysis of the role of mTOR signaling *in vivo* needed to be done to sort-out the different views. Therefore, we generated conditional knockout mice depleted for raptor or rictor under the control of the *Myf5* promoter, in order to inactivate mTORC1 or mTORC2, respectively, in muscle progenitors and precursors (RAmyfKO and RImyfKO). Additionally, we generated a tamoxifen-inducible mouse model deficient for raptor in Pax7-expressing cells, resulting in the loss of mTORC1 in muscle stem cells (RAscKO). My PhD work provides strong evidence that loss of mTORC1, but not mTORC2, in muscle progenitors impairs, but does not abolish, embryonic and adult myogenesis. Furthermore, I established that mTORC2 signaling regulates the maintenance of the satellite cell pool.

7.1 Inactivation of mTORC1, but not mTORC2, in developing muscle affects viability of mice

RAmyfKO embryos died perinatally due to respiratory failure, while RImyfKO mice were viable and were born at the expected Mendelian ratio. Interestingly, both mouse models exhibited reduced body weight compared to their wild-type littermates. The skeleton, in particular the long bones of hindlimbs and forelegs, of RAmyfKO embryos was unchanged in size, indicating that whole-body growth was normal in the absence of mTORC1 in developing muscle. Muscle mass in RAmyfKO embryos was reduced, which most likely contributed to the decrease in the overall body weight. In contrast, RImyfKO mice appeared smaller in size, although whole-body growth of mutant mice was not analyzed in further details. As RImKO mice, depleted for rictor in adult muscle tissue, did not show growth retardation (Bentzinger et al., 2008), I concluded that loss of mTORC2 in developing, but not mature, muscle affects body size. Fetal growth is controlled by the family of insulin-like growth factors (IGFs), including IGF-I and IGF-II. Interestingly, *Igf-1*$^{-/-}$ and *Igf-2*$^{-/-}$ mice exhibit a growth deficiency of about 60 % compared to wild-type mice (DeChiara et al., 1990; Liu et al., 1993), confirming their specific role in fetal growth. IGF-II is abundant during fetal development, while its serum concentrations drop in the first days after birth (Agrogiannis et al., 2014). Inversely, IGF-I concentrations increase during postnatal development, primarily produced by the liver. Notably, in mouse embryonic fibroblasts (MEFs), IGF-II translation is controlled by mTORC2, via the phosphorylation of the *Igf2* mRNA-binding

protein 1 (IMP1) at the Serine 181 (Dai et al., 2013). Binding of phosphorylated IMP1 to the *Igf2* untranslated region leads to ribosomal entry and subsequent *Igf2* translation. In light of this, in depth characterization of circulating and muscle-specific IGFs, in particular of IGF-II, in RImyfKO embryos and adult mice will give further insights on the mechanisms linking mTORC2 deficiency in developing muscle to altered growth.

Surprisingly, skeleton analyses revealed that the thoracic cage of RAmyfKO embryos is smaller compared to littermate heterozygous and control embryos. Previously, it was demonstrated that mice lacking Myf5 show severe rib defects, causing death of the mutant mice immediately after birth (Braun et al., 1992). Similarly, ablation of Myf5-expressing cells, achieved by the insertion of a DTA transgene in the *Myf5* locus, caused malformations of the ribs and vertebrae (Gensch et al., 2008). Thus, one can hypothesize that altered development of the myotome, as observed upon mTORC1 inactivation in Myf5-expressing cells, may affect the adjacent sclerotome forming the rib cage. However, it was suggested that the rib phenotype in Myf5-mutant mice is independent from the formation of the myotome, and rather depends on *cis* effects on a yet unknown gene (Kaul et al., 2000). Moreover, it was demonstrated that, at the thoracic level, *Hox* genes regulate *Myf5* and *Mrf4* myotomal expression, promoting rib specification through FGF and platelet-derived growth factor (PDGF) signaling, although the exact regulatory mechanisms are not yet known (Vinagre et al., 2010). Lastly, it is unlikely that 50 % reduction of *Myf5*, resulting from the knock-in of the *Cre* cDNA into one allele, affected rib cage development in RAmyfKO embryos, since Het-RAmyfKO embryos, which also have the *Cre* transgene integrated at the *Myf5* locus, did not show a rib phenotype. These observations highlight the importance of considering the formation of surrounding tissue in the study of muscle development, as the generation of embryonic muscle structures tightly depends on cell-cell interactions and secreted factors.

7.2 mTORC1 is crucial for the myogenic function of embryonic and adult muscle progenitors

Proliferation, differentiation and fusion of myoblasts is restricted in the absence of mTORC1 signaling

Myogenesis corresponds to the process leading to the formation of muscle fibers that occurs during embryonic muscle development and during muscle regeneration at the adult age. Interestingly, RAmyfKO, but not RImyfKO, embryos exhibited strongly reduced skeletal muscle mass relative to their whole-body size, suggesting that mTORC1, but not mTORC2 signaling is crucial for embryonic muscle development. Nevertheless, in RAmyfKO embryos, all muscles were formed and they normally expressed myogenic regulatory

factors at E18.5. Furthermore, a proportion of myofibers in RAmyfKO muscle expressed EGFP, indicative of mTORC1 inactivation, hence providing evidence that myofiber formation still occurred in the absence of mTORC1. These observations indicated that mTORC1 is not absolutely required for the myogenic process, but that inactivation of the signaling severely impacts on the myogenic efficiency and consequently the viability of the mice.

The myogenic process consists of major, sequential steps including the commitment of muscle progenitors, their proliferation, differentiation and subsequent fusion into multi-nucleated myotubes. Embryonic and adult muscle progenitors from RAmyfKO and RAscKO mice, respectively, showed severe defects in proliferation and a reduced efficiency to differentiate and fuse (Figure 4). Notwithstanding, no increase in programmed cell death was observed in mTORC1-deficient muscle progenitors and precursors. Consistent with our findings, mTORC1 has been previously implicated in proliferation of other cell types, such as β-cells of the pancreas and MEF cells (Blandino-Rosano et al., 2017; Dowling et al., 2010). Interestingly, it was proposed that mTORC1 controls proliferation through 4E-BP, while cell growth regulation is mediated by the S6K1 branch (Dowling et al., 2010; Ohanna et al., 2005). In parallel, I demonstrated that RImyfKO precursors efficiently proliferated *in vitro* and *in vivo*, indicating that mTORC2 signaling does not play a determinant role in muscle cell proliferation (Figure 4). Similarly, the differentiation and fusion capacity of muscle precursors was normal in the absence of mTORC2 in tissue culture and during muscle regeneration *in vivo*. These results contrasted with previous reports suggesting that differentiation of myoblasts is controlled by both mTORC1 and mTORC2 pathways, although contradictory results were obtained from the different studies. Inhibition of mTORC1 by the application of rapamycin blocked myogenic differentiation and fusion of rat and mouse myoblasts (Conejo et al., 2001; Coolican et al., 1997; Cuenda and Cohen, 1999). Inversely, shRNA-mediated knockdown of *Rptor*, leading to inhibition of mTORC1, in C2C12 myoblasts resulted in increased differentiation due to the release of feedback inhibition of S6K1 on IRS1, hence leading to further activation of the PI3K / Akt pathway (Ge et al., 2011). Similarly, it was reported that inhibition of mTORC2, achieved by shRNA-mediated silencing of *Rictor*, in C2C12 myoblasts prevented myotube formation in an Akt and ROCK1-dependent way, suggesting a potent role of mTORC2 in myoblast differentiation (Shu and Houghton, 2009). Recently, mTORC2 has also been implicated in C2C12 differentiation by phosphorylating SGK1 (at the Serine 422) (Chen et al., 2017). Hence, while previous studies, performed *in vitro* or using pharmacological inhibition of the signaling, have highlighted potential functions of mTORC1 and mTORC2 in the myogenic process, I provided strong evidence by using genetic approaches that mTORC1, but not

mTORC2, is required for the myogenic function of muscle cells, and thereby for the development of muscle tissue during embryogenesis.

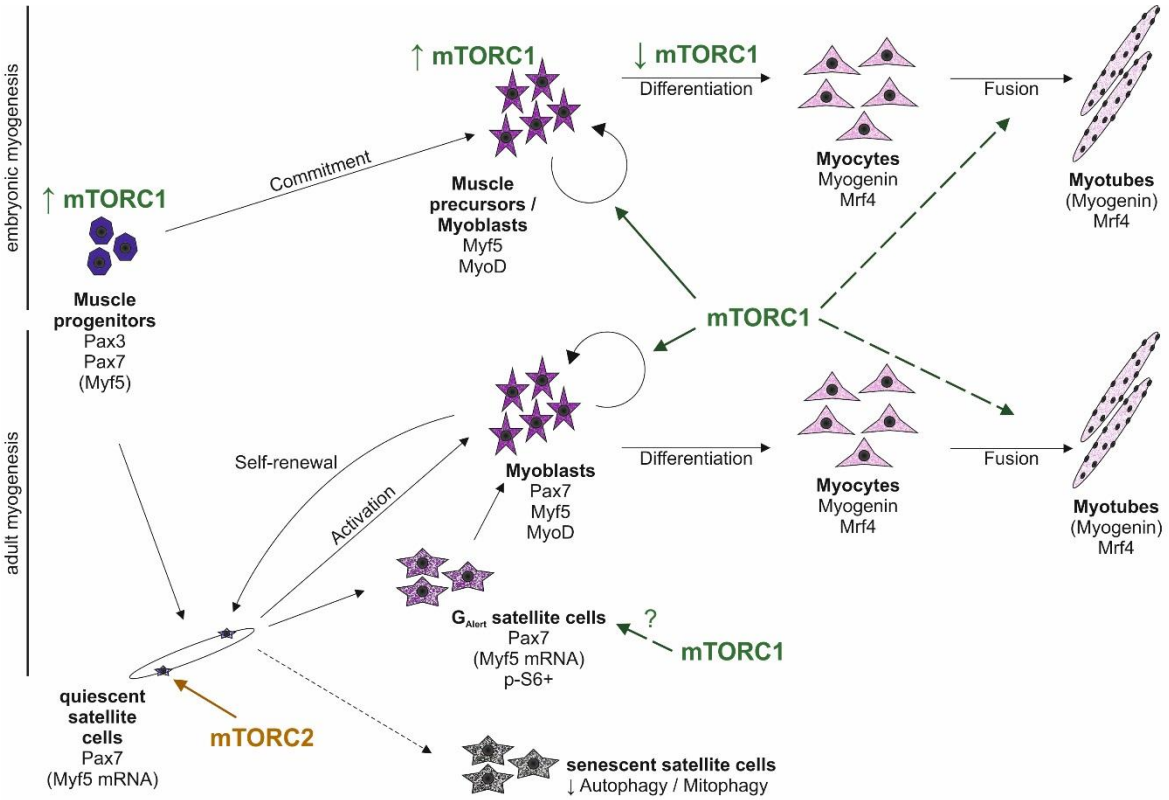

Figure 4. mTORC1, but not mTORC2, controls proliferation and differentiation of myoblasts during embryonic and adult myogenesis. mTORC2 signaling is crucial for the maintenance of quiescent satellite cells.

Does mTORC1 control proliferation and differentiation of myoblasts by affecting protein synthesis?

One potential mechanism of how mTORC1 controls proliferation is *via* its downstream substrates S6K1 and 4E-BP1, which regulate translation initiation (Brunn et al., 1997; Gingras et al., 1999; Holz et al., 2005). I confirmed that raptor-depleted myoblasts exhibited reduced rates of protein synthesis, which may likely be the limiting factor for their proliferation and differentiation in the absence of mTORC1. Surprisingly, in Het-RAmyfKO myoblasts, which express only 50 % of the raptor levels, mTORC1 downstream signaling, *i.e.* phosphorylation of the 40S ribosomal S6 protein (S6) and of 4E-BP1, was not significantly altered. Consequently, the rates of protein synthesis of Het-RAmyfKO myoblasts was comparable to control, suggesting that 50 % raptor protein is sufficient to maintain mTORC1 signaling and to efficiently drive translation initiation. Similarly,

haploinsufficiency of eIF4E is still compatible with normal mouse development and general induction of protein synthesis (Truitt et al., 2015). Therefore, it seems that regulators of protein synthesis are abundant in excess, although the dose requirements and the translational landscape of genome-wide mRNAs during embryonic muscle development need further investigation. Additionally, it would be interesting to analyze through which downstream substrate mTORC1 controls protein synthesis and the myogenic process. Thus, the use of specific pharmacological inhibitors or shRNAs targeting S6K1 or 4E-BP1 in satellite cells may unravel through which branch mTORC1 controls the different steps in myogenesis.

mTORC1, but not mTORC2, is necessary for myofiber restoration following muscle injury

Myofiber formation, as a result of the myogenic process, is recapitulated during muscle regeneration of the adult tissue upon damage, and is thus considered as adult myogenesis. Young RImyfKO mice were capable to restore myofibers following one or two subsequent muscle injuries, indicating that mTORC2-deficient satellite cells efficiently proliferate, differentiate and fuse to generate new myofibers. In contrast, regenerating RAscKO muscle, depleted for raptor in satellite cells, failed to restore myofibers after one cardiotoxin-injury and only few, small embryonic MHC-positive myofibers were formed in the mutant muscle. Thus, similar to embryonic muscle development, adult myogenesis is severely impaired in RAscKO, but not in RImyfKO mice, indicating that mTORC1, but not mTORC2 signaling is required for the myogenic function of satellite cells following muscle injury. Consistently, *in vivo* application of rapamycin, inhibiting mTORC1 signaling, impaired the regenerative capacity of skeletal muscle (Ge et al., 2009; Miyabara et al., 2010): rapamycin delayed myofiber restoration but also limited the extend of myofiber cross-sectional area recovery one month after injury-induced muscle degeneration (Ge et al., 2009). Nevertheless, the regenerative failure in RAscKO muscle was more prominent compared to regenerating muscles treated with rapamycin, consistent with the idea that genetic inactivation of mTORC1 in satellite cells provokes a stronger phenotype than pharmacological inhibition of the signaling, which does not specifically target satellite cells in the muscle tissue. Remarkably, fat and fibrotic tissue accumulated in regenerating RAscKO muscle, indicating that FAPs differentiated into fibroblasts and adipocytes upon the regenerative failure of mTORC1-deficient satellite cells. FAPs are the source of fibrosis and adipogenesis in dystrophic muscles undergoing chronic degeneration / regeneration, *e.g.* in Duchenne muscular dystrophy, which further limits the potential of the remaining satellite cells in the regenerative process (Cordani et al., 2014; Mozzetta et al., 2013). One can hypothesize that FAP differentiation in regenerating RAscKO muscle contributed to the abrogation of the

myogenic capacity of raptor-depleted satellite cells. It would be, therefore, of interest to study the role of mTORC1 signaling for the interaction and communication of satellite cells with other cells, in particular FAPs, residing in the stem cell niche. To this purpose, co-culture of raptor-depleted satellite cells in the presence of non-targeted FAPs may give further insights on whether FAPs further limit their myogenic capacity, including proliferation, differentiation and fusion. Additionally, satellite cells cultured with conditioned medium from FAP cells may unravel whether the interaction is driven by direct cell-cell contact or secreted factors. Lastly, since cardiotoxin-induced muscle injury induces complete necrosis of myofibers, it will be interesting to study the myogenic capacity of mTORC1-deficient satellite cells in more physiological conditions as in muscular dystrophy (by breeding RAscKO mice with mdx mice, a mouse model for Duchenne muscular dystrophy), or upon acute exercise-induced muscle damages (by submitting RAscKO mice to downhill treadmill exercise). This may give further insights into the regenerative capacity of mTORC1-deficient satellite cells, activated by sporadically damaged myofibers, in the presence of an intact stem cell niche.

7.3 The controlled transition between quiescence and activation of satellite cells requires both mTORC1 and mTORC2

Quiescent satellite cells reside in their niche tightly associated to myofibers underneath the basal lamina. Satellite cell quiescence is regulated by cell intrinsic signaling pathways, but it is also controlled by external stimuli in the close environment of the satellite cell, called the niche. Whether satellite cell quiescence and the maintenance of the pool are regulated by mTORC1 or mTORC2 signaling has not yet been investigated. During my PhD work, I unraveled that RImyfKO muscle lose satellite cells following repeated injuries and during physiological aging, indicating that mTORC2 contributes to the maintenance and homeostasis of satellite cells (Figure 4). Results obtained so far in RAscKO mice indicated that the satellite cell pool is maintained in mutant muscle three months after mTORC1 inactivation, which suggests that mTORC1 signaling is dispensable for satellite cell quiescence. However, to confirm this hypothesis, the analysis of the stem cell pool in RAscKO muscle at later time points, *e.g.* one year after tamoxifen-induced mTORC1 inactivation in satellite cells, is required.

The decline of the stem cell pool in RImyfKO muscle was not caused by an impairment in satellite cell self-renewal, as verified with single isolated muscle fibers. Notably, I observed that already at young age, fewer Pax7-positive cells remained associated to freshly isolated RImyfKO myofibers. Concomitantly, an increased proportion of satellite cells failed to maintain their typical anatomical localization underneath the basal

lamina, and relocated to the interstitial space in RImyfKO muscle. In light of these observations, it could be that loss of mTORC2 in satellite cells affects their interaction and adhesion to the niche. Previously, it was demonstrated that deregulation of Notch components in satellite cells causes instable adhesive interactions between the satellite cell and the myofiber, resulting in an interstitial localization of the stem cell and in the loss of its quiescent features (Brohl et al., 2012). Similarly, satellite cells deficient for syndecan-3, a transmembrane heparan sulfate proteoglycan acting as a co-receptor for Notch signaling, were prone to migrate away from their niche and showed defective ability to replenish the pool following injury-induced muscle regeneration (Pisconti et al., 2016; Pisconti et al., 2010). Interestingly, syndecan-3 depletion in satellite cells still allowed efficient fiber restoration in conditions of chronic degeneration and regeneration due to an enlarged number of activated stem cells remaining in the interstitial space (Pisconti et al., 2016). In line with this, it will be interesting to investigate whether the loss of mTORC2 in satellite cells affects their interaction with their niche. To do so, satellite cell homing should be analyzed in RImyfKO embryos during late fetal development, paying special attention to adhesion molecules, such as M-cadherin, Mcam, Megf10 and integrin α4β1 (Brohl et al., 2012). In adult RImyfKO mice, it will also be interesting to analyze the activation state of satellite cells, especially those located in the interstitial space, in uninjured muscle, to confirm that they prematurely lose their quiescent properties upon migration. Lastly, the satellite cell niche is also involved in the homeostasis of the stem cell pool by controlling the occurrence of asymmetric and symmetric cell divisions, the latter mainly ensuring the maintenance of cells with stemness characteristics (Le Grand et al., 2009). Symmetric cell division is controlled by the non-canonical Wnt pathway, which induces the cytoplasmic scaffolding protein Dishevelled to activate Rac/JNK and Rho/ROCK pathways, subsequently leading to cytoskeletal remodeling and changes in gene expression (Dumont et al., 2015). In light of the role of mTORC2 in cytoskeleton organization (Jacinto et al., 2004; Sarbassov et al., 2004), it will be relevant to study whether deregulation of mTORC2 affects cytoskeleton organization in satellite cells, which could impact on symmetric cell division and the replenishment of the stem cell pool. To distinguish between a satellite cell-autonomous effect and changes upon mTORC2-deficiency in myofibers, the phenotype of RImyfKO mice, depleted for rictor in satellite cells and myofibers, and RImKO mice, in which only myofibers are targeted for mTORC2 inactivation, should be compared. Overall, my results pave the way for additional experiments, which may unravel the mechanisms underlying the function of mTORC2 in satellite cell maintenance.

Loss of mTORC1 in adult muscle progenitors delays their activation

Quiescent satellite cells quickly respond to external stimuli and enter activation by boosting their metabolism and changing gene expression. In particular, upon activation, satellite cells induce translation of sequestered *Myf5* mRNA and promote *MyoD* transcription, both processes being hallmarks of an activated state (Crist et al., 2012). In my PhD work, I determined that RImyfKO satellite cells showed no impairments in the transition from quiescence to activation upon stimulation / injury, thus confirming that mTORC2 is dispensable for their myogenic function. Inversely, MyoD expression in RAscKO satellite cells was delayed upon external, activating stimuli. Nevertheless, RAscKO satellite cells still entered the myogenic program at later time points, suggesting that mTORC1 signaling is important, but not absolutely required, for satellite cell activation. Consistently, it was demonstrated that mTORC1 activity is low in quiescent satellite cells, but that the signaling is induced in the G_{Alert} and activated states (Rodgers et al., 2014). Interestingly, Rodgers et al. showed that upon a systemic injury, satellite cells enter the G_{Alert} state, mainly characterized by a faster cell cycle entry and an increase in energy levels (Rodgers et al., 2014). As it was claimed that the G_{Alert} state is dependent on mTORC1, the analysis of the uninjured, contralateral muscle in regenerating RAscKO mice will be of particular interest, to confirm or invalidate this hypothesis, and to get further insights on the characteristics of the G_{Alert} state. In particular, the mechanisms linking mTORC1 to satellite cell activation are not yet known. As I observed that mTORC1-deficient myoblasts exhibit reduced rates of protein synthesis in culture, delayed expression of determination factors, such as MyoD, during satellite cell activation, may be caused by limited translation initiation in the absence of mTORC1. Previously, it was described that a general boost in mRNA translation, controlled by eIF2α dephosphorylation, accompanies satellite cell activation (Zismanov et al., 2016). In light of these results, the function of mTORC1 in promoting protein synthesis may underlie the decisive role of the signaling in the control of the transition between quiescence and activation of satellite cells. Hence, in the long-term, analysis of the proteins, which are specifically translated under the control of mTORC1 during the different phases of the myogenic process, will be of interest.

Does deregulation of mTOR signaling drive quiescent satellite cells to enter senescence?

During aging, satellite cells undergo geroconversion, which corresponds to the transition from quiescence into senescence, a process that has been related to impaired autophagy, increased mitochondrial dysfunction and oxidative stress (Garcia-Prat et al., 2016; Sousa-Victor et al., 2014). Interestingly, in skeletal muscle of RAmKO mice autophagy is constantly induced and the flux with subsequent degradation steps are reduced (Castets et al., 2013).

Concomitantly, protein synthesis is expected to be decreased in RAmKO muscle, hence resulting in imbalanced proteostasis. Since proteostasis seems to play a role in satellite cell maintenance, by controlling geroconversion, I hypothesized that the loss of mTORC1 and consequently the perturbed proteostasis in satellite cells may affect their quiescent state and their transition to senescence. In line with this hypothesis, mTORC1-deficient satellite cells showed an impaired myogenic potential during muscle regeneration. Therefore, it will be important, as mentioned above, to study the long-term effects of mTORC1 inactivation in satellite cells by analyzing mutant mice one year after tamoxifen treatment. At the same time, analysis of senescent markers, such as p21, $p16^{INK4a}$ and pH2AX, may unravel premature, or alternatively delayed, geroconversion of RAscKO satellite cells. On the other hand, mTORC2 has not been linked to autophagy dysfunction or cellular senescence, but considering the decline of the satellite cell pool in aged RImyfKO muscle, it could be that inactivation of mTORC2 prematurely converts satellite cells into a senescent state by cell intrinsic or extrinsic changes. As for RAscKO cells, it will be of particular interest to analyze senescence markers in satellite cells from RImyfKO mice at different ages, to identify potential anticipated geroconversion, in the absence of mTORC2. In the future, single cell RNA sequencing and proteomic studies on isolated, quiescent satellite cells from RAscKO and RImyfKO muscles should also give further insights on the consequences of mTOR deregulation in the maintenance of satellite cell quiescence.

7.4 Concluding remarks

My PhD thesis establishes that mTORC1 signaling is predominantly active in proliferating muscle progenitors and precursors, while decreasing upon differentiation and fusion of myocytes during the embryonic wave of myogenesis. In line with this, I demonstrated that mTORC1, but not mTORC2, is crucial for proliferation, differentiation and fusion of muscle cells *in vitro* and *in vivo*. Consequently, mice deficient for mTORC1 in developing muscle die perinatally, while mTORC2 inactivation in muscle progenitors does not affect survival of the mice. The limited capacity of mTORC1-deficient myoblasts to enter the myogenic process may be caused by the reduced rates of protein synthesis. Similarly, mTORC1 is crucial for the activation of adult muscle progenitors, and essential for the regeneration of the adult muscle tissue. Although mTORC2 is dispensable for the myogenic function of myoblasts, I unraveled that the signaling is necessary for the maintenance of the satellite cell pool after repeated injuries and during aging.

In light of my observations, it will be of major importance to further understand the distinct roles and to identify the molecular functions of mTORC1 and mTORC2 signaling in

the myogenic process, since mTOR signaling is often deregulated in pathological conditions. Chronic muscle degeneration is a major hallmark of dystrophic muscle, such as in Duchenne muscular dystrophy or in merosin-deficient congenital muscular dystrophy, in which the limited regenerative capacity of the diseased muscle ultimately leads to the deterioration of the tissue. Therefore, understanding the mechanisms involved in muscle regeneration, and controlling the maintenance and renewal of satellite cells, is crucial to limit muscle alterations and improve muscle homeostasis in pathological context. Furthermore, myogenesis not only occurs during development and regeneration of the tissue, but is also involved in the spontaneous activation, differentiation and fusion of satellite cells to myofibers naturally occurring over time. Even though it has been suggested that the decline in satellite cell content is not the main driver of sarcopenia, analysis of the mechanisms controlling the balance between quiescence, activation and senescence, is essential to understand the exact relationship between age-dependent muscle dysfunction and satellite cell decline, and thereby to identify potential strategies to limit alterations of skeletal muscle with age.

8. References

Agrogiannis, G.D., S. Sifakis, E.S. Patsouris, and A.E. Konstantinidou. 2014. Insulin-like growth factors in embryonic and fetal growth and skeletal development (Review). *Mol Med Rep*. 10:579-584.

Alessi, D.R., S.R. James, C.P. Downes, A.B. Holmes, P.R. Gaffney, C.B. Reese, and P. Cohen. 1997. Characterization of a 3-phosphoinositide-dependent protein kinase which phosphorylates and activates protein kinase Balpha. *Curr Biol*. 7:261-269.

Ben-Yair, R., and C. Kalcheim. 2005. Lineage analysis of the avian dermomyotome sheet reveals the existence of single cells with both dermal and muscle progenitor fates. *Development*. 132:689-701.

Bentzinger, C.F., K. Romanino, D. Cloetta, S. Lin, J.B. Mascarenhas, F. Oliveri, J. Xia, E. Casanova, C.F. Costa, M. Brink, F. Zorzato, M.N. Hall, and M.A. Ruegg. 2008. Skeletal muscle-specific ablation of raptor, but not of rictor, causes metabolic changes and results in muscle dystrophy. *Cell Metab*. 8:411-424.

Bentzinger, C.F., Y.X. Wang, and M.A. Rudnicki. 2012. Building muscle: molecular regulation of myogenesis. *Cold Spring Harb Perspect Biol*. 4.

Bernet, J.D., J.D. Doles, J.K. Hall, K. Kelly Tanaka, T.A. Carter, and B.B. Olwin. 2014. p38 MAPK signaling underlies a cell-autonomous loss of stem cell self-renewal in skeletal muscle of aged mice. *Nat Med*. 20:265-271.

Biressi, S., M. Molinaro, and G. Cossu. 2007. Cellular heterogeneity during vertebrate skeletal muscle development. *Dev Biol*. 308:281-293.

Bjornson, C.R., T.H. Cheung, L. Liu, P.V. Tripathi, K.M. Steeper, and T.A. Rando. 2012. Notch signaling is necessary to maintain quiescence in adult muscle stem cells. *Stem Cells*. 30:232-242.

Blandino-Rosano, M., R. Barbaresso, M. Jimenez-Palomares, N. Bozadjieva, J.P. Werneck-de-Castro, M. Hatanaka, R.G. Mirmira, N. Sonenberg, M. Liu, M.A. Ruegg, M.N. Hall, and E. Bernal-Mizrachi. 2017. Loss of mTORC1 signalling impairs beta-cell homeostasis and insulin processing. *Nat Commun*. 8:16014.

Bodine, S.C., T.N. Stitt, M. Gonzalez, W.O. Kline, G.L. Stover, R. Bauerlein, E. Zlotchenko, A. Scrimgeour, J.C. Lawrence, D.J. Glass, and G.D. Yancopoulos. 2001. Akt/mTOR pathway is a crucial regulator of skeletal muscle hypertrophy and can prevent muscle atrophy in vivo. *Nat Cell Biol*. 3:1014-1019.

Brack, A.S., and P. Munoz-Canoves. 2016. The ins and outs of muscle stem cell aging. *Skelet Muscle*. 6:1.

Braun, T., E. Bober, B. Winter, N. Rosenthal, and H.H. Arnold. 1990. Myf-6, a new member of the human gene family of myogenic determination factors: evidence for a gene cluster on chromosome 12. *Embo J*. 9:821-831.

Braun, T., G. Buschhausen-Denker, E. Bober, E. Tannich, and H.H. Arnold. 1989. A novel human muscle factor related to but distinct from MyoD1 induces myogenic conversion in 10T1/2 fibroblasts. *Embo J*. 8:701-709.

Braun, T., M.A. Rudnicki, H.H. Arnold, and R. Jaenisch. 1992. Targeted inactivation of the muscle regulatory gene Myf-5 results in abnormal rib development and perinatal death. *Cell*. 71:369-382.

Brohl, D., E. Vasyutina, M.T. Czajkowski, J. Griger, C. Rassek, H.P. Rahn, B. Purfurst, H. Wende, and C. Birchmeier. 2012. Colonization of the satellite cell niche by skeletal muscle progenitor cells depends on Notch signals. *Dev Cell*. 23:469-481.

Brown, E.J., M.W. Albers, T.B. Shin, K. Ichikawa, C.T. Keith, W.S. Lane, and S.L. Schreiber. 1994. A mammalian protein targeted by G1-arresting rapamycin-receptor complex. *Nature*. 369:756-758.

Brunn, G.J., C.C. Hudson, A. Sekulic, J.M. Williams, H. Hosoi, P.J. Houghton, J.C. Lawrence, Jr., and R.T. Abraham. 1997. Phosphorylation of the translational repressor PHAS-I by the mammalian target of rapamycin. *Science*. 277:99-101.

Buckingham, M., L. Bajard, T. Chang, P. Daubas, J. Hadchouel, S. Meilhac, D. Montarras, D. Rocancourt, and F. Relaix. 2003. The formation of skeletal muscle: from somite to limb. *J Anat*. 202:59-68.

Buckingham, M., and F. Relaix. 2007. The role of Pax genes in the development of tissues and organs: Pax3 and Pax7 regulate muscle progenitor cell functions. *Annu Rev Cell Dev Biol*. 23:645-673.

Cafferkey, R., P.R. Young, M.M. McLaughlin, D.J. Bergsma, Y. Koltin, G.M. Sathe, L. Faucette, W.K. Eng, R.K. Johnson, and G.P. Livi. 1993. Dominant missense mutations in a novel yeast

protein related to mammalian phosphatidylinositol 3-kinase and VPS34 abrogate rapamycin cytotoxicity. *Mol Cell Biol*. 13:6012-6023.

Castets, P., S. Lin, N. Rion, S. Di Fulvio, K. Romanino, M. Guridi, S. Frank, L.A. Tintignac, M. Sinnreich, and M.A. Ruegg. 2013. Sustained activation of mTORC1 in skeletal muscle inhibits constitutive and starvation-induced autophagy and causes a severe, late-onset myopathy. *Cell Metab*. 17:731-744.

Chakkalakal, J.V., K.M. Jones, M.A. Basson, and A.S. Brack. 2012. The aged niche disrupts muscle stem cell quiescence. *Nature*. 490:355-360.

Chal, J., and O. Pourquie. 2017. Making muscle: skeletal myogenesis in vivo and in vitro. *Development*. 144:2104-2122.

Charge, S.B., and M.A. Rudnicki. 2004. Cellular and molecular regulation of muscle regeneration. *Physiol Rev*. 84:209-238.

Chen, S.E., B. Jin, and Y.P. Li. 2007. TNF-alpha regulates myogenesis and muscle regeneration by activating p38 MAPK. *Am J Physiol Cell Physiol*. 292:C1660-1671.

Chen, W.Y., C.L. Lin, J.H. Chuang, F.Y. Chiu, Y.Y. Sun, M.C. Liang, and Y. Lin. 2017. Heterogeneous nuclear ribonucleoprotein M associates with mTORC2 and regulates muscle differentiation. *Sci Rep*. 7:41159.

Cheung, T.H., N.L. Quach, G.W. Charville, L. Liu, L. Park, A. Edalati, B. Yoo, P. Hoang, and T.A. Rando. 2012. Maintenance of muscle stem-cell quiescence by microRNA-489. *Nature*. 482:524-528.

Cheung, T.H., and T.A. Rando. 2013. Molecular regulation of stem cell quiescence. *Nat Rev Mol Cell Biol*. 14:329-340.

Comai, G., R. Sambasivan, S. Gopalakrishnan, and S. Tajbakhsh. 2014. Variations in the Efficiency of Lineage Marking and Ablation Confound Distinctions between Myogenic Cell Populations. *Dev Cell*. 31:654-667.

Comai, G., and S. Tajbakhsh. 2014. Molecular and cellular regulation of skeletal myogenesis. *Curr Top Dev Biol*. 110:1-73.

Conejo, R., A.M. Valverde, M. Benito, and M. Lorenzo. 2001. Insulin produces myogenesis in C2C12 myoblasts by induction of NF-kappaB and downregulation of AP-1 activities. *J Cell Physiol*. 186:82-94.

Conerly, M.L., Z. Yao, J.W. Zhong, M. Groudine, and S.J. Tapscott. 2016. Distinct Activities of Myf5 and MyoD Indicate Separate Roles in Skeletal Muscle Lineage Specification and Differentiation. *Dev Cell*. 36:375-385.

Coolican, S.A., D.S. Samuel, D.Z. Ewton, F.J. McWade, and J.R. Florini. 1997. The mitogenic and myogenic actions of insulin-like growth factors utilize distinct signaling pathways. *J Biol Chem*. 272:6653-6662.

Cordani, N., V. Pisa, L. Pozzi, C. Sciorati, and E. Clementi. 2014. Nitric oxide controls fat deposition in dystrophic skeletal muscle by regulating fibro-adipogenic precursor differentiation. *Stem Cells*. 32:874-885.

Cornelison, D.D., B.B. Olwin, M.A. Rudnicki, and B.J. Wold. 2000. MyoD(-/-) satellite cells in single-fiber culture are differentiation defective and MRF4 deficient. *Dev Biol*. 224:122-137.

Crist, C.G., D. Montarras, and M. Buckingham. 2012. Muscle satellite cells are primed for myogenesis but maintain quiescence with sequestration of Myf5 mRNA targeted by microRNA-31 in mRNP granules. *Cell Stem Cell*. 11:118-126.

Cuenda, A., and P. Cohen. 1999. Stress-activated protein kinase-2/p38 and a rapamycin-sensitive pathway are required for C2C12 myogenesis. *J Biol Chem*. 274:4341-4346.

Dai, N., J. Christiansen, F.C. Nielsen, and J. Avruch. 2013. mTOR complex 2 phosphorylates IMP1 cotranslationally to promote IGF2 production and the proliferation of mouse embryonic fibroblasts. *Genes Dev*. 27:301-312.

DeChiara, T.M., A. Efstratiadis, and E.J. Robertson. 1990. A growth-deficiency phenotype in heterozygous mice carrying an insulin-like growth factor II gene disrupted by targeting. *Nature*. 345:78-80.

Deries, M., and S. Thorsteinsdottir. 2016. Axial and limb muscle development: dialogue with the neighbourhood. *Cell Mol Life Sci*. 73:4415-4431.

Dorrello, N.V., A. Peschiaroli, D. Guardavaccaro, N.H. Colburn, N.E. Sherman, and M. Pagano. 2006. S6K1- and betaTRCP-mediated degradation of PDCD4 promotes protein translation and cell growth. *Science*. 314:467-471.

Dowling, R.J., I. Topisirovic, T. Alain, M. Bidinosti, B.D. Fonseca, E. Petroulakis, X. Wang, O. Larsson, A. Selvaraj, Y. Liu, S.C. Kozma, G. Thomas, and N. Sonenberg. 2010. mTORC1-mediated cell proliferation, but not cell growth, controlled by the 4E-BPs. *Science*. 328:1172-1176.

Duchesne, E., M.H. Tremblay, and C.H. Cote. 2011. Mast cell tryptase stimulates myoblast proliferation; a mechanism relying on protease-activated receptor-2 and cyclooxygenase-2. *BMC Musculoskelet Disord*. 12:235.

Dumont, N.A., C.F. Bentzinger, M.C. Sincennes, and M.A. Rudnicki. 2015. Satellite Cells and Skeletal Muscle Regeneration. *Compr Physiol*. 5:1027-1059.

Duvel, K., J.L. Yecies, S. Menon, P. Raman, A.I. Lipovsky, A.L. Souza, E. Triantafellow, Q.C. Ma, R. Gorski, S. Cleaver, M.G.V. Heiden, J.P. MacKeigan, P.M. Finan, C.B. Clish, L.O. Murphy, and B.D. Manning. 2010. Activation of a Metabolic Gene Regulatory Network Downstream of mTOR Complex 1. *Mol Cell*. 39:171-183.

Edmondson, D.G., and E.N. Olson. 1989. A gene with homology to the myc similarity region of MyoD1 is expressed during myogenesis and is sufficient to activate the muscle differentiation program. *Genes Dev*. 3:628-640.

Esner, M., S.M. Meilhac, F. Relaix, J.F. Nicolas, G. Cossu, and M.E. Buckingham. 2006. Smooth muscle of the dorsal aorta shares a common clonal origin with skeletal muscle of the myotome. *Development*. 133:737-749.

Evans, D., H. Baillie, A. Caswell, and P. Wigmore. 1994. During fetal muscle development, clones of cells contribute to both primary and secondary fibers. *Dev Biol*. 162:348-353.

Evans, W.J., and W.W. Campbell. 1993. Sarcopenia and Age-Related-Changes in Body-Composition and Functional-Capacity. *J Nutr*. 123:465-468.

Fry, C.S., J.D. Lee, J. Mula, T.J. Kirby, J.R. Jackson, F. Liu, L. Yang, C.L. Mendias, E.E. Dupont-Versteegden, J.J. McCarthy, and C.A. Peterson. 2015. Inducible depletion of satellite cells in adult, sedentary mice impairs muscle regenerative capacity without affecting sarcopenia. *Nat Med*. 21:76-80.

Gangloff, Y.G., M. Mueller, S.G. Dann, P. Svoboda, M. Sticker, J.F. Spetz, S.H. Um, E.J. Brown, S. Cereghini, G. Thomas, and S.C. Kozma. 2004. Disruption of the mouse mTOR gene leads to early postimplantation lethality and prohibits embryonic stem cell development. *Mol Cell Biol*. 24:9508-9516.

Ganley, I.G., H. Lam du, J. Wang, X. Ding, S. Chen, and X. Jiang. 2009. ULK1.ATG13.FIP200 complex mediates mTOR signaling and is essential for autophagy. *J Biol Chem*. 284:12297-12305.

Garcia-Martinez, J.M., and D.R. Alessi. 2008. mTOR complex 2 (mTORC2) controls hydrophobic motif phosphorylation and activation of serum- and glucocorticoid-induced protein kinase 1 (SGK1). *Biochem J*. 416:375-385.

Garcia-Prat, L., M. Martinez-Vicente, E. Perdiguero, L. Ortet, J. Rodriguez-Ubreva, E. Rebollo, V. Ruiz-Bonilla, S. Gutarra, E. Ballestar, A.L. Serrano, M. Sandri, and P. Munoz-Canoves. 2016. Autophagy maintains stemness by preventing senescence. *Nature*. 529:37-42.

Ge, Y., A.L. Wu, C. Warnes, J. Liu, C. Zhang, H. Kawasome, N. Terada, M.D. Boppart, C.J. Schoenherr, and J. Chen. 2009. mTOR regulates skeletal muscle regeneration in vivo through kinase-dependent and kinase-independent mechanisms. *Am J Physiol Cell Physiol*. 297:C1434-1444.

Ge, Y., M.S. Yoon, and J. Chen. 2011. Raptor and Rheb negatively regulate skeletal myogenesis through suppression of insulin receptor substrate 1 (IRS1). *J Biol Chem*. 286:35675-35682.

Gensch, N., T. Borchardt, A. Schneider, D. Riethmacher, and T. Braun. 2008. Different autonomous myogenic cell populations revealed by ablation of Myf5-expressing cells during mouse embryogenesis. *Development*. 135:1597-1604.

Gingras, A.C., B. Raught, and N. Sonenberg. 1999. eIF4 initiation factors: effectors of mRNA recruitment to ribosomes and regulators of translation. *Annu Rev Biochem*. 68:913-963.

Glass, D.J. 2005. Skeletal muscle hypertrophy and atrophy signaling pathways. *Int J Biochem Cell Biol*. 37:1974-1984.

Guertin, D.A., D.M. Stevens, C.C. Thoreen, A.A. Burds, N.Y. Kalaany, J. Moffat, M. Brown, K.J. Fitzgerald, and D.M. Sabatini. 2006. Ablation in mice of the mTORC components raptor, rictor, or mLST8 reveals that mTORC2 is required for signaling to Akt-FOXO and PKCalpha, but not S6K1. *Dev Cell*. 11:859-871.

Guridi, M., B. Kupr, K. Romanino, S. Lin, D. Falcetta, L. Tintignac, and M.A. Ruegg. 2016. Alterations to mTORC1 signaling in the skeletal muscle differentially affect whole-body metabolism. *Skelet Muscle*. 6:13.

Guridi, M., L.A. Tintignac, S. Lin, B. Kupr, P. Castets, and M.A. Ruegg. 2015. Activation of mTORC1 in skeletal muscle regulates whole-body metabolism through FGF21. *Science signaling*. 8:ra113.

Gwinn, D.M., D.B. Shackelford, D.F. Egan, M.M. Mihaylova, A. Mery, D.S. Vasquez, B.E. Turk, and R.J. Shaw. 2008. AMPK phosphorylation of raptor mediates a metabolic checkpoint. *Mol Cell*. 30:214-226.

Hagiwara, A., M. Cornu, N. Cybulski, P. Polak, C. Betz, F. Trapani, L. Terracciano, M.H. Heim, M.A. Ruegg, and M.N. Hall. 2012. Hepatic mTORC2 Activates Glycolysis and Lipogenesis through Akt, Glucokinase, and SREBP1c. *Cell Metab*. 15:725-738.

Haldar, M., G. Karan, P. Tvrdik, and M.R. Capecchi. 2008. Two cell lineages, myf5 and myf5-independent, participate in mouse skeletal myogenesis. *Dev Cell*. 14:437-445.

Halevy, O., B.G. Novitch, D.B. Spicer, S.X. Skapek, J. Rhee, G.J. Hannon, D. Beach, and A.B. Lassar. 1995. Correlation of terminal cell cycle arrest of skeletal muscle with induction of p21 by MyoD. *Science*. 267:1018-1021.

Hara, T., A. Takamura, C. Kishi, S. Iemura, T. Natsume, J.L. Guan, and N. Mizushima. 2008. FIP200, a ULK-interacting protein, is required for autophagosome formation in mammalian cells. *J Cell Biol*. 181:497-510.

Harrington, L.S., G.M. Findlay, A. Gray, T. Tolkacheva, S. Wigfield, H. Rebholz, J. Barnett, N.R. Leslie, S. Cheng, P.R. Shepherd, I. Gout, C.P. Downes, and R.F. Lamb. 2004. The TSC1-2 tumor suppressor controls insulin-PI3K signaling via regulation of IRS proteins. *J Cell Biol*. 166:213-223.

Hasty, P., A. Bradley, J.H. Morris, D.G. Edmondson, J.M. Venuti, E.N. Olson, and W.H. Klein. 1993. Muscle deficiency and neonatal death in mice with a targeted mutation in the myogenin gene. *Nature*. 364:501-506.

Hinterberger, T.J., D.A. Sassoon, S.J. Rhodes, and S.F. Konieczny. 1991. Expression of the muscle regulatory factor MRF4 during somite and skeletal myofiber development. *Dev Biol*. 147:144-156.

Hollenberg, S.M., P.F. Cheng, and H. Weintraub. 1993. Use of a conditional MyoD transcription factor in studies of MyoD trans-activation and muscle determination. *Proc Natl Acad Sci U S A*. 90:8028-8032.

Holz, M.K., B.A. Ballif, S.P. Gygi, and J. Blenis. 2005. mTOR and S6K1 mediate assembly of the translation preinitiation complex through dynamic protein interchange and ordered phosphorylation events. *Cell*. 123:569-580.

Hosokawa, N., T. Sasaki, S. Iemura, T. Natsume, T. Hara, and N. Mizushima. 2009. Atg101, a novel mammalian autophagy protein interacting with Atg13. *Autophagy*. 5:973-979.

Hsu, P.P., S.A. Kang, J. Rameseder, Y. Zhang, K.A. Ottina, D. Lim, T.R. Peterson, Y. Choi, N.S. Gray, M.B. Yaffe, J.A. Marto, and D.M. Sabatini. 2011. The mTOR-regulated phosphoproteome reveals a mechanism of mTORC1-mediated inhibition of growth factor signaling. *Science*. 332:1317-1322.

Hung, C.M., C.M. Calejman, J. Sanchez-Gurmaches, H. Li, C.B. Clish, S. Hettmer, A.J. Wagers, and D.A. Guertin. 2014. Rictor/mTORC2 loss in the Myf5 lineage reprograms brown fat metabolism and protects mice against obesity and metabolic disease. *Cell Rep*. 8:256-271.

Hutcheson, D.A., J. Zhao, A. Merrell, M. Haldar, and G. Kardon. 2009. Embryonic and fetal limb myogenic cells are derived from developmentally distinct progenitors and have different requirements for beta-catenin. *Genes Dev*. 23:997-1013.

Inoki, K., Y. Li, T. Xu, and K.L. Guan. 2003a. Rheb GTPase is a direct target of TSC2 GAP activity and regulates mTOR signaling. *Genes Dev*. 17:1829-1834.

Inoki, K., Y. Li, T. Zhu, J. Wu, and K.L. Guan. 2002. TSC2 is phosphorylated and inhibited by Akt and suppresses mTOR signalling. *Nat Cell Biol*. 4:648-657.

Inoki, K., T. Zhu, and K.L. Guan. 2003b. TSC2 mediates cellular energy response to control cell growth and survival. *Cell*. 115:577-590.

Izumiya, Y., T. Hopkins, C. Morris, K. Sato, L. Zeng, J. Viereck, J.A. Hamilton, N. Ouchi, N.K. LeBrasseur, and K. Walsh. 2008. Fast/Glycolytic muscle fiber growth reduces fat mass and improves metabolic parameters in obese mice. *Cell Metab*. 7:159-172.

Jacinto, E., R. Loewith, A. Schmidt, S. Lin, M.A. Ruegg, A. Hall, and M.N. Hall. 2004. Mammalian TOR complex 2 controls the actin cytoskeleton and is rapamycin insensitive. *Nat Cell Biol*. 6:1122-1128.

Joe, A.W., L. Yi, A. Natarajan, F. Le Grand, L. So, J. Wang, M.A. Rudnicki, and F.M. Rossi. 2010. Muscle injury activates resident fibro/adipogenic progenitors that facilitate myogenesis. *Nat Cell Biol*. 12:153-163.

Jones, D.L., and A.J. Wagers. 2008. No place like home: anatomy and function of the stem cell niche. *Nat Rev Mol Cell Biol*. 9:11-21.

Jones, N.C., Y.V. Fedorov, R.S. Rosenthal, and B.B. Olwin. 2001. ERK1/2 is required for myoblast proliferation but is dispensable for muscle gene expression and cell fusion. *J Cell Physiol*. 186:104-115.

Jung, J., H.M. Genau, and C. Behrends. 2015. Amino Acid-Dependent mTORC1 Regulation by the Lysosomal Membrane Protein SLC38A9. *Mol Cell Biol*. 35:2479-2494.

Kanisicak, O., J.J. Mendez, S. Yamamoto, M. Yamamoto, and D.J. Goldhamer. 2009. Progenitors of skeletal muscle satellite cells express the muscle determination gene, MyoD. *Dev Biol*. 332:131-141.

Kassar-Duchossoy, L., B. Gayraud-Morel, D. Gomes, D. Rocancourt, M. Buckingham, V. Shinin, and S. Tajbakhsh. 2004. Mrf4 determines skeletal muscle identity in Myf5:Myod double-mutant mice. *Nature*. 431:466-471.

Kassar-Duchossoy, L., E. Giacone, B. Gayraud-Morel, A. Jory, D. Gomes, and S. Tajbakhsh. 2005. Pax3/Pax7 mark a novel population of primitive myogenic cells during development. *Genes Dev*. 19:1426-1431.

Kaul, A., M. Koster, H. Neuhaus, and T. Braun. 2000. Myf-5 revisited: loss of early myotome formation does not lead to a rib phenotype in homozygous Myf-5 mutant mice. *Cell*. 102:17-19.

Kawabe, Y., Y.X. Wang, I.W. McKinnell, M.T. Bedford, and M.A. Rudnicki. 2012. Carm1 regulates Pax7 transcriptional activity through MLL1/2 recruitment during asymmetric satellite stem cell divisions. *Cell Stem Cell*. 11:333-345.

Keefe, A.C., J.A. Lawson, S.D. Flygare, Z.D. Fox, M.P. Colasanto, S.J. Mathew, M. Yandell, and G. Kardon. 2015. Muscle stem cells contribute to myofibres in sedentary adult mice. *Nat Commun*. 6:7087.

Kim, J., M. Kundu, B. Viollet, and K.L. Guan. 2011. AMPK and mTOR regulate autophagy through direct phosphorylation of Ulk1. *Nat Cell Biol*. 13:132-141.

Kleinert, M., B.L. Parker, R. Chaudhuri, D.J. Fazakerley, A. Serup, K.C. Thomas, J.R. Krycer, L. Sylow, A.M. Fritzen, N.J. Hoffman, J. Jeppesen, P. Schjerling, M.A. Ruegg, B. Kiens, D.E. James, and E.A. Richter. 2016. mTORC2 and AMPK differentially regulate muscle triglyceride content via Perilipin 3. *Mol Metab*. 5:646-655.

Kuang, S., K. Kuroda, F. Le Grand, and M.A. Rudnicki. 2007. Asymmetric self-renewal and commitment of satellite stem cells in muscle. *Cell*. 129:999-1010.

Kumar, A., T.E. Harris, S.R. Keller, K.M. Choi, M.A. Magnuson, and J.C. Lawrence, Jr. 2008. Muscle-specific deletion of rictor impairs insulin-stimulated glucose transport and enhances Basal glycogen synthase activity. *Mol Cell Biol*. 28:61-70.

Kunz, J., R. Henriquez, U. Schneider, M. Deuter-Reinhard, N.R. Movva, and M.N. Hall. 1993. Target of rapamycin in yeast, TOR2, is an essential phosphatidylinositol kinase homolog required for G1 progression. *Cell*. 73:585-596.

Lamming, D.W., L. Ye, P. Katajisto, M.D. Goncalves, M. Saitoh, D.M. Stevens, J.G. Davis, A.B. Salmon, A. Richardson, R.S. Ahima, D.A. Guertin, D.M. Sabatini, and J.A. Baur. 2012. Rapamycin-induced insulin resistance is mediated by mTORC2 loss and uncoupled from longevity. *Science*. 335:1638-1643.

Laplante, M., and D.M. Sabatini. 2009. mTOR signaling at a glance. *J Cell Sci*. 122:3589-3594.

Laplante, M., and D.M. Sabatini. 2012. mTOR signaling in growth control and disease. *Cell*. 149:274-293.

Le Grand, F., A.E. Jones, V. Seale, A. Scime, and M.A. Rudnicki. 2009. Wnt7a activates the planar cell polarity pathway to drive the symmetric expansion of satellite stem cells. *Cell Stem Cell*. 4:535-547.

Leu, M., E. Bellmunt, M. Schwander, I. Farinas, H.R. Brenner, and U. Muller. 2003. Erbb2 regulates neuromuscular synapse formation and is essential for muscle spindle development. *Development*. 130:2291-2301.

Liu, J.P., J. Baker, A.S. Perkins, E.J. Robertson, and A. Efstratiadis. 1993. Mice carrying null mutations of the genes encoding insulin-like growth factor I (Igf-1) and type 1 IGF receptor (Igf1r). *Cell*. 75:59-72.

Long, X., Y. Lin, S. Ortiz-Vega, K. Yonezawa, and J. Avruch. 2005. Rheb binds and regulates the mTOR kinase. *Curr Biol*. 15:702-713.

Manning, B.D., A.R. Tee, M.N. Logsdon, J. Blenis, and L.C. Cantley. 2002. Identification of the tuberous sclerosis complex-2 tumor suppressor gene product tuberin as a target of the phosphoinositide 3-kinase/akt pathway. *Mol Cell*. 10:151-162.

Massari, M.E., and C. Murre. 2000. Helix-loop-helix proteins: regulators of transcription in eucaryotic organisms. *Mol Cell Biol*. 20:429-440.

Matsumoto, A., A. Pasut, M. Matsumoto, R. Yamashita, J. Fung, E. Monteleone, A. Saghatelian, K.I. Nakayama, J.G. Clohessy, and P.P. Pandolfi. 2017. mTORC1 and muscle regeneration are regulated by the LINC00961-encoded SPAR polypeptide. *Nature*. 541:228-232.

McKinnell, I.W., J. Ishibashi, F. Le Grand, V.G. Punch, G.C. Addicks, J.F. Greenblatt, F.J. Dilworth, and M.A. Rudnicki. 2008. Pax7 activates myogenic genes by recruitment of a histone methyltransferase complex. *Nat Cell Biol*. 10:77-84.

Menon, S., C.C. Dibble, G. Talbott, G. Hoxhaj, A.J. Valvezan, H. Takahashi, L.C. Cantley, and B.D. Manning. 2014. Spatial control of the TSC complex integrates insulin and nutrient regulation of mTORC1 at the lysosome. *Cell*. 156:771-785.

Messina, G., S. Biressi, S. Monteverde, A. Magli, M. Cassano, L. Perani, E. Roncaglia, E. Tagliafico, L. Starnes, C.E. Campbell, M. Grossi, D.J. Goldhamer, R.M. Gronostajski, and G. Cossu. 2010. Nfix regulates fetal-specific transcription in developing skeletal muscle. *Cell*. 140:554-566.

Miner, J.H., and B. Wold. 1990. Herculin, a fourth member of the MyoD family of myogenic regulatory genes. *Proc Natl Acad Sci U S A*. 87:1089-1093.

Miyabara, E.H., T.C. Conte, M.T. Silva, I.L. Baptista, C. Bueno, Jr., J. Fiamoncini, R.H. Lambertucci, C.S. Serra, P.C. Brum, T. Pithon-Curi, R. Curi, M.S. Aoki, A.C. Oliveira, and A.S. Moriscot. 2010. Mammalian target of rapamycin complex 1 is involved in differentiation of regenerating myofibers in vivo. *Muscle Nerve*. 42:778-787.

Mourikis, P., R. Sambasivan, D. Castel, P. Rocheteau, V. Bizzarro, and S. Tajbakhsh. 2012. A critical requirement for notch signaling in maintenance of the quiescent skeletal muscle stem cell state. *Stem Cells*. 30:243-252.

Mozzetta, C., S. Consalvi, V. Saccone, M. Tierney, A. Diamantini, K.J. Mitchell, G. Marazzi, G. Borsellino, L. Battistini, D. Sassoon, A. Sacco, and P.L. Puri. 2013. Fibroadipogenic progenitors mediate the ability of HDAC inhibitors to promote regeneration in dystrophic muscles of young, but not old Mdx mice. *EMBO Mol Med*. 5:626-639.

Murakami, M., T. Ichisaka, M. Maeda, N. Oshiro, K. Hara, F. Edenhofer, H. Kiyama, K. Yonezawa, and S. Yamanaka. 2004. mTOR is essential for growth and proliferation in early mouse embryos and embryonic stem cells. *Mol Cell Biol*. 24:6710-6718.

Murphy, M., and G. Kardon. 2011. Origin of vertebrate limb muscle: the role of progenitor and myoblast populations. *Curr Top Dev Biol*. 96:1-32.

Nabeshima, Y., K. Hanaoka, M. Hayasaka, E. Esumi, S. Li, I. Nonaka, and Y. Nabeshima. 1993. Myogenin gene disruption results in perinatal lethality because of severe muscle defect. *Nature*. 364:532-535.

Nishiyama, T., I. Kii, and A. Kudo. 2004. Inactivation of Rho/ROCK signaling is crucial for the nuclear accumulation of FKHR and myoblast fusion. *J Biol Chem*. 279:47311-47319.

Ohanna, M., A.K. Sobering, T. Lapointe, L. Lorenzo, C. Praud, E. Petroulakis, N. Sonenberg, P.A. Kelly, A. Sotiropoulos, and M. Pende. 2005. Atrophy of S6K1(-/-) skeletal muscle cells reveals distinct mTOR effectors for cell cycle and size control. *Nat Cell Biol*. 7:286-294.

Pallafacchina, G., E. Calabria, A.L. Serrano, J.M. Kalhovde, and S. Schiaffino. 2002. A protein kinase B-dependent and rapamycin-sensitive pathway controls skeletal muscle growth but not fiber type specification. *Proc Natl Acad Sci U S A*. 99:9213-9218.

Pisconti, A., G.B. Banks, F. Babaeijandaghi, N.D. Betta, F.M. Rossi, J.S. Chamberlain, and B.B. Olwin. 2016. Loss of niche-satellite cell interactions in syndecan-3 null mice alters muscle progenitor cell homeostasis improving muscle regeneration. *Skelet Muscle*. 6:34.

Pisconti, A., D.D. Cornelison, H.C. Olguin, T.L. Antwine, and B.B. Olwin. 2010. Syndecan-3 and Notch cooperate in regulating adult myogenesis. *J Cell Biol*. 190:427-441.

Potter, C.J., L.G. Pedraza, and T. Xu. 2002. Akt regulates growth by directly phosphorylating Tsc2. *Nat Cell Biol*. 4:658-665.

Rebsamen, M., L. Pochini, T. Stasyk, M.E. de Araujo, M. Galluccio, R.K. Kandasamy, B. Snijder, A. Fauster, E.L. Rudashevskaya, M. Bruckner, S. Scorzoni, P.A. Filipek, K.V. Huber, J.W. Bigenzahn, L.X. Heinz, C. Kraft, K.L. Bennett, C. Indiveri, L.A. Huber, and G. Superti-Furga. 2015. SLC38A9 is a component of the lysosomal amino acid sensing machinery that controls mTORC1. *Nature*. 519:477-481.

Relaix, F., D. Rocancourt, A. Mansouri, and M. Buckingham. 2004. Divergent functions of murine Pax3 and Pax7 in limb muscle development. *Genes Dev*. 18:1088-1105.

Relaix, F., D. Rocancourt, A. Mansouri, and M. Buckingham. 2005. A Pax3/Pax7-dependent population of skeletal muscle progenitor cells. *Nature*. 435:948-953.

Rhodes, S.J., and S.F. Konieczny. 1989. Identification of MRF4: a new member of the muscle regulatory factor gene family. *Genes Dev*. 3:2050-2061.

Rodgers, J.T., K.Y. King, J.O. Brett, M.J. Cromie, G.W. Charville, K.K. Maguire, C. Brunson, N. Mastey, L. Liu, C.R. Tsai, M.A. Goodell, and T.A. Rando. 2014. mTORC1 controls the adaptive transition of quiescent stem cells from G0 to G(Alert). *Nature*. 510:393-396.

Romanino, K., L. Mazelin, V. Albert, A. Conjard-Duplany, S. Lin, C.F. Bentzinger, C. Handschin, P. Puigserver, F. Zorzato, L. Schaeffer, Y.G. Gangloff, and M.A. Ruegg. 2011. Myopathy caused by mammalian target of rapamycin complex 1 (mTORC1) inactivation is not reversed by restoring mitochondrial function. *Proc Natl Acad Sci U S A*. 108:20808-20813.

Rommel, C., S.C. Bodine, B.A. Clarke, R. Rossman, L. Nunez, T.N. Stitt, G.D. Yancopoulos, and D.J. Glass. 2001. Mediation of IGF-1-induced skeletal myotube hypertrophy by PI(3)K/Akt/mTOR and PI(3)K/Akt/GSK3 pathways. *Nat Cell Biol*. 3:1009-1013.

Rudnicki, M.A., T. Braun, S. Hinuma, and R. Jaenisch. 1992. Inactivation of MyoD in mice leads to up-regulation of the myogenic HLH gene Myf-5 and results in apparently normal muscle development. *Cell*. 71:383-390.

Rudnicki, M.A., P.N. Schnegelsberg, R.H. Stead, T. Braun, H.H. Arnold, and R. Jaenisch. 1993. MyoD or Myf-5 is required for the formation of skeletal muscle. *Cell*. 75:1351-1359.

Ryall, J.G., S. Dell'Orso, A. Derfoul, A. Juan, H. Zare, X. Feng, D. Clermont, M. Koulnis, G. Gutierrez-Cruz, M. Fulco, and V. Sartorelli. 2015. The NAD(+)-dependent SIRT1 deacetylase translates a metabolic switch into regulatory epigenetics in skeletal muscle stem cells. *Cell Stem Cell*. 16:171-183.

Sabatini, D.M., H. Erdjument-Bromage, M. Lui, P. Tempst, and S.H. Snyder. 1994. RAFT1: a mammalian protein that binds to FKBP12 in a rapamycin-dependent fashion and is homologous to yeast TORs. *Cell*. 78:35-43.

Sabers, C.J., M.M. Martin, G.J. Brunn, J.M. Williams, F.J. Dumont, G. Wiederrecht, and R.T. Abraham. 1995. Isolation of a protein target of the FKBP12-rapamycin complex in mammalian cells. *J Biol Chem*. 270:815-822.

Sancak, Y., T.R. Peterson, Y.D. Shaul, R.A. Lindquist, C.C. Thoreen, L. Bar-Peled, and D.M. Sabatini. 2008. The Rag GTPases bind raptor and mediate amino acid signaling to mTORC1. *Science*. 320:1496-1501.

Sancak, Y., C.C. Thoreen, T.R. Peterson, R.A. Lindquist, S.A. Kang, E. Spooner, S.A. Carr, and D.M. Sabatini. 2007. PRAS40 is an insulin-regulated inhibitor of the mTORC1 protein kinase. *Mol Cell*. 25:903-915.

Sarbassov, D.D., S.M. Ali, D.H. Kim, D.A. Guertin, R.R. Latek, H. Erdjument-Bromage, P. Tempst, and D.M. Sabatini. 2004. Rictor, a novel binding partner of mTOR, defines a rapamycin-insensitive and raptor-independent pathway that regulates the cytoskeleton. *Curr Biol*. 14:1296-1302.

Sarbassov, D.D., D.A. Guertin, S.M. Ali, and D.M. Sabatini. 2005. Phosphorylation and regulation of Akt/PKB by the rictor-mTOR complex. *Science*. 307:1098-1101.

Saxton, R.A., and D.M. Sabatini. 2017. mTOR Signaling in Growth, Metabolism, and Disease. *Cell*. 168:960-976.

Scadden, D.T. 2006. The stem-cell niche as an entity of action. *Nature*. 441:1075-1079.

Schwander, M., M. Leu, M. Stumm, O.M. Dorchies, U.T. Ruegg, J. Schittny, and U. Muller. 2003. Beta1 integrins regulate myoblast fusion and sarcomere assembly. *Dev Cell*. 4:673-685.

Seale, P., L.A. Sabourin, A. Girgis-Gabardo, A. Mansouri, P. Gruss, and M.A. Rudnicki. 2000. Pax7 is required for the specification of myogenic satellite cells. *Cell*. 102:777-786.

Serrano, A.L., B. Baeza-Raja, E. Perdiguero, M. Jardi, and P. Munoz-Canoves. 2008. Interleukin-6 is an essential regulator of satellite cell-mediated skeletal muscle hypertrophy. *Cell Metab*. 7:33-44.

Shah, O.J., Z. Wang, and T. Hunter. 2004. Inappropriate activation of the TSC/Rheb/mTOR/S6K cassette induces IRS1/2 depletion, insulin resistance, and cell survival deficiencies. *Curr Biol*. 14:1650-1656.

Shaw, R.J., N. Bardeesy, B.D. Manning, L. Lopez, M. Kosmatka, R.A. DePinho, and L.C. Cantley. 2004. The LKB1 tumor suppressor negatively regulates mTOR signaling. *Cancer Cell*. 6:91-99.

Shea, K.L., W. Xiang, V.S. LaPorta, J.D. Licht, C. Keller, M.A. Basson, and A.S. Brack. 2010. Sprouty1 regulates reversible quiescence of a self-renewing adult muscle stem cell pool during regeneration. *Cell Stem Cell*. 6:117-129.

Sheehan, S.M., and R.E. Allen. 1999. Skeletal muscle satellite cell proliferation in response to members of the fibroblast growth factor family and hepatocyte growth factor. *J Cell Physiol*. 181:499-506.

Shefer, G., D.P. Van de Mark, J.B. Richardson, and Z. Yablonka-Reuveni. 2006. Satellite-cell pool size does matter: defining the myogenic potency of aging skeletal muscle. *Dev Biol*. 294:50-66.

Shimobayashi, M., and M.N. Hall. 2016. Multiple amino acid sensing inputs to mTORC1. *Cell Res*. 26:7-20.

Shiota, C., J.T. Woo, J. Lindner, K.D. Shelton, and M.A. Magnuson. 2006. Multiallelic disruption of the rictor gene in mice reveals that mTOR complex 2 is essential for fetal growth and viability. *Dev Cell*. 11:583-589.

Shu, L., and P.J. Houghton. 2009. The mTORC2 complex regulates terminal differentiation of C2C12 myoblasts. *Mol Cell Biol*. 29:4691-4700.

Sousa-Victor, P., and P. Munoz-Canoves. 2016. Regenerative decline of stem cells in sarcopenia. *Molecular aspects of medicine*. 50:109-117.

Sousa-Victor, P., E. Perdiguero, and P. Munoz-Canoves. 2014. Geroconversion of aged muscle stem cells under regenerative pressure. *Cell Cycle*. 13:3183-3190.

Stokoe, D., L.R. Stephens, T. Copeland, P.R. Gaffney, C.B. Reese, G.F. Painter, A.B. Holmes, F. McCormick, and P.T. Hawkins. 1997. Dual role of phosphatidylinositol-3,4,5-trisphosphate in the activation of protein kinase B. *Science*. 277:567-570.

Tee, A.R., B.D. Manning, P.P. Roux, L.C. Cantley, and J. Blenis. 2003. Tuberous sclerosis complex gene products, Tuberin and Hamartin, control mTOR signaling by acting as a GTPase-activating protein complex toward Rheb. *Curr Biol*. 13:1259-1268.

Thedieck, K., P. Polak, M.L. Kim, K.D. Molle, A. Cohen, P. Jeno, C. Arrieumerlou, and M.N. Hall. 2007. PRAS40 and PRR5-like protein are new mTOR interactors that regulate apoptosis. *PLoS One*. 2:e1217.

Troy, A., A.B. Cadwallader, Y. Fedorov, K. Tyner, K.K. Tanaka, and B.B. Olwin. 2012. Coordination of satellite cell activation and self-renewal by Par-complex-dependent asymmetric activation of p38alpha/beta MAPK. *Cell Stem Cell*. 11:541-553.

Truitt, M.L., C.S. Conn, Z. Shi, X. Pang, T. Tokuyasu, A.M. Coady, Y. Seo, M. Barna, and D. Ruggero. 2015. Differential Requirements for eIF4E Dose in Normal Development and Cancer. *Cell*. 162:59-71.

Uezumi, A., S. Fukada, N. Yamamoto, S. Takeda, and K. Tsuchida. 2010. Mesenchymal progenitors distinct from satellite cells contribute to ectopic fat cell formation in skeletal muscle. *Nat Cell Biol*. 12:143-152.

Vander Haar, E., S.I. Lee, S. Bandhakavi, T.J. Griffin, and D.H. Kim. 2007. Insulin signalling to mTOR mediated by the Akt/PKB substrate PRAS40. *Nat Cell Biol*. 9:316-323.

Vinagre, T., N. Moncaut, M. Carapuco, A. Novoa, J. Bom, and M. Mallo. 2010. Evidence for a myotomal Hox/Myf cascade governing nonautonomous control of rib specification within global vertebral domains. *Dev Cell*. 18:655-661.

Wan, M., X. Wu, K.L. Guan, M. Han, Y. Zhuang, and T. Xu. 2006. Muscle atrophy in transgenic mice expressing a human TSC1 transgene. *FEBS Lett*. 580:5621-5627.

Wang, L., T.E. Harris, R.A. Roth, and J.C. Lawrence, Jr. 2007. PRAS40 regulates mTORC1 kinase activity by functioning as a direct inhibitor of substrate binding. *J Biol Chem*. 282:20036-20044.

Wang, S., Z.Y. Tsun, R.L. Wolfson, K. Shen, G.A. Wyant, M.E. Plovanich, E.D. Yuan, T.D. Jones, L. Chantranupong, W. Comb, T. Wang, L. Bar-Peled, R. Zoncu, C. Straub, C. Kim, J. Park, B.L. Sabatini, and D.M. Sabatini. 2015. Metabolism. Lysosomal amino acid transporter SLC38A9 signals arginine sufficiency to mTORC1. *Science*. 347:188-194.

Weintraub, H., R. Davis, S. Tapscott, M. Thayer, M. Krause, R. Benezra, T.K. Blackwell, D. Turner, R. Rupp, S. Hollenberg, and et al. 1991. The myoD gene family: nodal point during specification of the muscle cell lineage. *Science*. 251:761-766.

Wick, M.J., L.Q. Dong, R.A. Riojas, F.J. Ramos, and F. Liu. 2000. Mechanism of phosphorylation of protein kinase B/Akt by a constitutively active 3-phosphoinositide-dependent protein kinase-1. *J Biol Chem*. 275:40400-40406.

Wood, W.M., S. Etemad, M. Yamamoto, and D.J. Goldhamer. 2013. MyoD-expressing progenitors are essential for skeletal myogenesis and satellite cell development. *Dev Biol*. 384:114-127.

Yablonka-Reuveni, Z., R. Seger, and A.J. Rivera. 1999. Fibroblast growth factor promotes recruitment of skeletal muscle satellite cells in young and old rats. *J Histochem Cytochem*. 47:23-42.

Yang, G., D.S. Murashige, S.J. Humphrey, and D.E. James. 2015. A Positive Feedback Loop between Akt and mTORC2 via SIN1 Phosphorylation. *Cell Rep*. 12:937-943.

Yennek, S., M. Burute, M. Thery, and S. Tajbakhsh. 2014. Cell adhesion geometry regulates non-random DNA segregation and asymmetric cell fates in mouse skeletal muscle stem cells. *Cell Rep*. 7:961-970.

Yu, Y., S.O. Yoon, G. Poulogiannis, Q. Yang, X.M. Ma, J. Villen, N. Kubica, G.R. Hoffman, L.C. Cantley, S.P. Gygi, and J. Blenis. 2011. Phosphoproteomic analysis identifies Grb10 as an mTORC1 substrate that negatively regulates insulin signaling. *Science*. 332:1322-1326.

Yuan, M., E. Pino, L. Wu, M. Kacergis, and A.A. Soukas. 2012. Identification of Akt-independent regulation of hepatic lipogenesis by mammalian target of rapamycin (mTOR) complex 2. *J Biol Chem*. 287:29579-29588.

Zhang, W., R.R. Behringer, and E.N. Olson. 1995. Inactivation of the myogenic bHLH gene MRF4 results in up-regulation of myogenin and rib anomalies. *Genes Dev*. 9:1388-1399.

Zinzalla, V., D. Stracka, W. Oppliger, and M.N. Hall. 2011. Activation of mTORC2 by association with the ribosome. *Cell*. 144:757-768.

Zismanov, V., V. Chichkov, V. Colangelo, S. Jamet, S. Wang, A. Syme, A.E. Koromilas, and C. Crist. 2016. Phosphorylation of eIF2alpha Is a Translational Control Mechanism Regulating Muscle Stem Cell Quiescence and Self-Renewal. *Cell Stem Cell*. 18:79-90.

Zoncu, R., L. Bar-Peled, A. Efeyan, S. Wang, Y. Sancak, and D.M. Sabatini. 2011. mTORC1 senses lysosomal amino acids through an inside-out mechanism that requires the vacuolar H(+)-ATPase. *Science*. 334:678-683.

9. Appendix

9.1 Research highlight: "LncRNA-encoded peptides: More than translational noise?"

Cell Research (2017) 27:604-605.

www.nature.com/cr

RESEARCH HIGHLIGHT

LncRNA-encoded peptides: More than translational noise?

Cell Research (2017) **27**:604-605. doi:10.1038/cr.2017.35; published online 14 March 2017

Long non-coding RNAs (lncRNAs) belong to the ever-increasing number of transcripts that are thought not to encode proteins. A recent study has now identified a small polypeptide encoded by the lncRNA LINC00961 that inhibits amino acid-induced mTORC1 activation in skeletal muscle.

LncRNAs are non-coding RNAs with a transcript length > 200 nucleotides. They are transcribed by RNA polymerase II, capped, spliced, and polyadenylated. They are expressed in a tissue- and development-specific manner and have been shown to directly regulate a large variety of functions [1]. LncRNAs can also code for short open reading frames (ORFs), which were considered, until very recently, not to be translated. However, recent studies in *Drosophila melanogaster* and zebrafish have uncovered functionally relevant "hidden polypeptides" encoded by lncRNAs [2-4]. Furthermore, in mammalian skeletal muscle, the recently identified, lncRNA-encoded micropeptides myoregulin and DWORF regulate Ca^{2+} handling by directly modulating the activity of the calcium pump SERCA [5, 6]. Despite increasing evidence of the important functional role of lncRNAs, our understanding of the biology and the potential of such small molecules remains in its infancy. In a recent study, Matsumoto and colleagues [7] uncovered a new "hidden polypeptide", termed "small regulatory polypeptide of amino acid response" (SPAR), which suppresses activation of the mammalian (or mechanistic) target of rapamycin complex 1 (mTORC1) in response to amino acids.

Activation of mTORC1 (Figure 1) is controlled by several mechanisms, including growth factors (through the PI3K/Akt pathway), energy levels (via AMP-dependent kinase, AMPK) and the availability of amino acids [8]. Of those, availability of amino acids, in particular of leucine, arginine and glutamine, is dominant for mTORC1 activation. Through its key downstream targets, ribosomal protein S6 kinase 1 (S6K1) and the eukaryotic translation initiation factor 4E-binding protein 1 (4E-BP1), mTORC1 promotes protein translation and lipid and nucleotide synthesis. Simultaneously, mTORC1 inhibits the unc-51-like autophagy activating kinase 1 (Ulk1), thereby inhibiting autophagy induction. Amino acids activate mTORC1, mediating its translocation to the lysosome. At the lysosomal membrane, the vacuolar H^+-ATPase (v-ATPase), best known for controlling acidification of the lysosomal lumen, interacts with the pentameric protein complex Ragulator and serves as an anchoring scaffold for the Rag GTPases. High levels of amino acids weaken the interaction between the v-ATPase and Ragulator, thereby activating the heterodimeric protein Rag by loading RagA/B with GTP and hydrolyzing RagC/D-GTP. The now active RagA/B-RagC/D heterodimers then recruit mTORC1 from the cytoplasm to the lysosome where it becomes fully activated by Rheb-GTP, the downstream target of growth factor signaling [8].

This regulatory network has now been extended by the work of Matsumoto *et al.* who demonstrate that SPAR, a polypeptide translated from lncRNA LINC00961, inhibits amino acid-mediated mTORC1 activation at the lysosomal membrane [7]. SPAR was discovered by proteomics aimed at identifying polypeptides encoded by lncRNAs. LINC00961 is conserved across species and is most highly expressed in lung, heart and skeletal muscle. It codes for three putative ORFs, but only one of them generates the 90 amino acid-long SPAR polypeptide. SPAR harbors an N-terminal transmembrane domain and binds to all four subunits of the v-ATPase complex at the lysosomal membrane. Knockdown and overexpression approaches revealed that SPAR inhibits the recruitment and subsequent activation of mTORC1 at the lysosome by binding to the v-ATPase complex.

The function of SPAR *in vivo* was approached with the generation of mice unable to synthesize SPAR but still expressing its lncRNA by removing the translation initiation codon. Surprisingly, despite pronounced activation of mTORC1 in skeletal muscle, *SPAR*$^{-/-}$ mice showed no obvious phenotype. Only challenging the mice by injection of cardiotoxin into muscle, revealed differences between *SPAR*$^{-/-}$ and littermate controls. Cardiotoxin destroys muscle fibers, which is followed by muscle regeneration. This paradigm was chosen as (1) muscle regeneration is accompanied by increased mTORC1 signaling, (2) the mTORC1 inhibitor rapamycin delays muscle regeneration and (3) supplementation of leucine, which activates mTORC1, accelerates injury-induced muscle regeneration [9, 10]. Indeed, *SPAR*$^{-/-}$ muscles exhibited an increased regenerative capacity due to accelerated stem cell proliferation, differentiation and myofiber maturation.

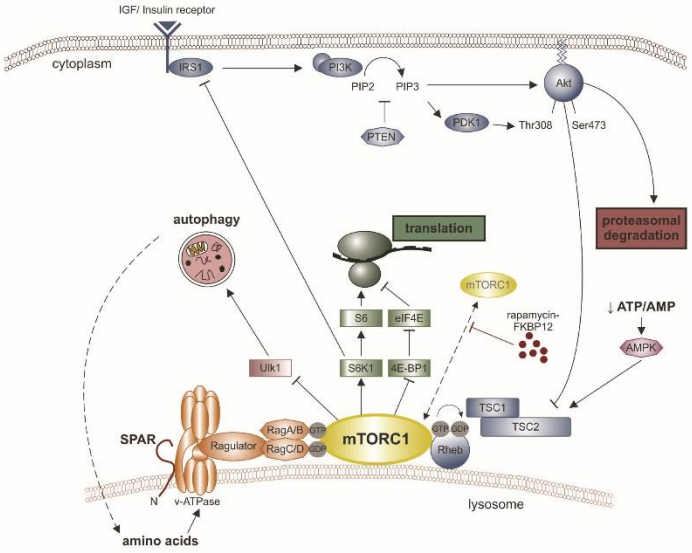

Figure 1 mTORC1 controls cell growth and is regulated by the lncRNA-encoded polypeptide SPAR. mTORC1 signaling induces protein translation through S6K1/S6 and 4E-BP1/eIF4E. The negative feedback from S6K1 to IRS1 reduces PI3K/Akt signaling, thereby promoting proteasomal degradation. mTORC1 is stimulated by growth factors that induce the PI3K/Akt pathway and thereby inhibit the TSC1/TSC2 complex which functions as a GTPase-activating protein for Rheb. GTP-bound Rheb recruits mTORC1 from the cytoplasm to the lysosome. Activation of mTORC1 is also achieved by free amino acids that weaken the interaction between the v-ATPase and Ragulator, consequently transforming the Rag proteins into their active form. SPAR, a polypeptide encoded by lncRNA LINC00961, directly binds to v-ATPase and blunts mTORC1 activation by amino acids. Other regulators of mTORC1 include AMPK that is activated upon low cellular energy levels (reduced ATP/AMP ratio) and stabilizes the TSC1/TSC2 complex, thereby increasing mTORC1 inhibition.

This effect was abrogated in the *SPAR*$^{-/-}$ mice when fed a leucine-free diet, consistent with the idea that the inhibitory effect of SPAR towards mTORC1 is specific for the amino acid-sensing arm (see Figure 1).

In summary, the findings of Matsumoto and colleagues define an additional level of mTORC1 control through the conserved lncRNA-encoded polypeptide SPAR. This study elegantly highlights that "hidden polypeptides" encoded by lncRNAs are not just "translational noise" but serve important biological functions. Interestingly, the SPAR-encoding lncRNA LINC00961 is expressed in a tissue- and age-specific manner, suggesting that the control of mTORC1 signaling is strongly context- and tissue-dependent. Understanding the mechanism of how expression of protein-coding lncRNAs is regulated might give further insights into the role of such polypeptides.

The discovery that SPAR modulates the amino acid-dependent activation of mTORC1 and the correlation with muscle regeneration are interesting aspects that need further investigation. Even though the pharmacological mTORC1 inhibitor rapamycin prevents muscle fiber restoration following severe muscle damage [9], the exact mechanisms of how mTORC1 regulates muscle regeneration are yet to be identified. As regenerative capacity of skeletal muscle declines during physiological aging and mTORC1-controlled autophagy appears to be an important aspect of muscle stem cell aging [11], it would be interesting to investigate the regulation of LINC00961 during aging and to test whether depletion of SPAR in aged mice has a similar beneficial effect on muscle regeneration as in young mice. Moreover, sustained activation of mTORC1 in skeletal muscle by depletion of the upstream inhibitor TSC1, causes a late-onset myopathy [12]. In light of these findings, it will also be important to study the long-term effects of SPAR inhibition *in vivo* and to investigate to what extent mTORC1 hyperactivation may be beneficial in clinical and therapeutic strategies.

Nathalie Rion[1],
Markus A Rüegg[1]

[1]*Biozentrum, University of Basel, Basel, Switzerland*
Correspondence: Markus A Rüegg
E-mail: markus-a.ruegg@unibas.ch

References

1 Quinn JJ, Chang HY. *Nat Rev Genet* 2016; **17**:47-62.
2 Pauli A, Norris ML, Valen E, *et al. Science* 2014; **343**:1248636.
3 Magny EG, Pueyo JI, Pearl FM, *et al. Science* 2013; **341**:1116-1120.
4 Kondo T, Plaza S, Zanet J, *et al. Science* 2010; **329**:336-339.
5 Anderson DM, Anderson KM, Chang CL, *et al. Cell* 2015; **160**:595-606.
6 Nelson BR, Makarewich CA, Anderson DM, *et al. Science* 2016; **351**:271-275.
7 Matsumoto A, Pasut A, Matsumoto M, *et al. Nature* 2017; **541**:228-232.
8 Shimobayashi M, Hall MN. *Cell Res* 2016; **26**:7-20.
9 Miyabara EH, Conte TC, Silva MT, *et al. Muscle Nerve* 2010; **42**:778-787.
10 Pereira MG, Silva MT, da Cunha FM, *et al. Exp Gerontol* 2015; **72**:269-277.
11 Sousa-Victor P, Munoz-Canoves P. *Mol Aspects Med* 2016; **50**:109-117.
12 Castets P, Lin S, Rion N, *et al. Cell Metab* 2013; **17**:731-744.

9.2 Publication 3: "Targeting deregulated AMPK/mTORC1 pathways improves muscle function in myotonic dystrophy type I"

The Journal of Clinical Investigation RESEARCH ARTICLE

Targeting deregulated AMPK/mTORC1 pathways improves muscle function in myotonic dystrophy type I

Marielle Brockhoff,[1] Nathalie Rion,[2] Kathrin Chojnowska,[2] Tatiana Wiktorowicz,[1] Christopher Eickhorst,[2] Beat Erne,[1] Stephan Frank,[3] Corrado Angelini,[4] Denis Furling,[5] Markus A. Rüegg,[2] Michael Sinnreich,[1] and Perrine Castets[1,2]

[1]Neuromuscular Research Group, Departments of Neurology and Biomedicine, University of Basel, University Hospital Basel, Basel, Switzerland. [2]Biozentrum, University of Basel, Basel, Switzerland. [3]Institute of Pathology, Division of Neuropathology, University of Basel, University Hospital Basel, Basel, Switzerland. [4]Fondazione San Camillo Hospital IRCCS, Venice Lido, Italy. [5]Sorbonne Universités, University Pierre and Marie Curie (UPMC) Paris 06, Inserm, CNRS, Centre de Recherche en Myologie, Institut de Myologie, GH Pitié-Salpêtrière, Paris, France.

Myotonic dystrophy type I (DM1) is a disabling multisystemic disease that predominantly affects skeletal muscle. It is caused by expanded CTG repeats in the 3′-UTR of the dystrophia myotonica protein kinase (*DMPK*) gene. RNA hairpins formed by elongated *DMPK* transcripts sequester RNA-binding proteins, leading to mis-splicing of numerous pre-mRNAs. Here, we have investigated whether DM1-associated muscle pathology is related to deregulation of central metabolic pathways, which may identify potential therapeutic targets for the disease. In a well-characterized mouse model for DM1 (HSA^{LR} mice), activation of AMPK signaling in muscle was impaired under starved conditions, while mTORC1 signaling remained active. In parallel, autophagic flux was perturbed in HSA^{LR} muscle and in cultured human DM1 myotubes. Pharmacological approaches targeting AMPK/mTORC1 signaling greatly ameliorated muscle function in HSA^{LR} mice. AICAR, an AMPK activator, led to a strong reduction of myotonia, which was accompanied by partial correction of misregulated alternative splicing. Rapamycin, an mTORC1 inhibitor, improved muscle relaxation and increased muscle force in HSA^{LR} mice without affecting splicing. These findings highlight the involvement of AMPK/mTORC1 deregulation in DM1 muscle pathophysiology and may open potential avenues for the treatment of this disease.

Introduction

Myotonic dystrophy type I (DM1; OMIM #160900) is a multisystemic neuromuscular disorder, which represents the most common form of muscular dystrophy in adults (1). In particular, DM1 patients suffer from muscle wasting, weakness, and myotonia. DM1 is an autosomal dominant disease caused by an expansion of unstable CTG repeats located within the 3′-UTR of the dystrophia myotonica protein kinase (*DMPK*) gene. Toxic expanded transcripts containing RNA hairpins formed by the triplet repeats accumulate as RNA foci in the nuclei of affected cells (2, 3). These mutant transcripts are thought to sequester RNA-binding proteins, such as muscleblind-like 1 (MBNL1), and to increase CUG triplet repeat RNA-binding protein 1 (CUGBP1) levels. The resulting splicing defects are considered the primary cause of DM1 symptoms (4–6). HSA^{LR} mice, which carry a CTG repeat expansion in the human skeletal actin (*HSA*) gene, constitute a well-characterized mouse model for DM1 (5). These mice express (CUG)n-expanded transcripts specifically in skeletal muscle and reiterate the dystrophic phenotype and myotonic discharges observed in muscle of patients. HSA^{LR} mice also recapitulate DM1 molecular characteristics such as foci accumulation, MBNL1 sequestration, and splicing abnormalities (5, 7, 8). Therapeutic strategies have mainly focused on targeting DM1-associated mis-splicing and mRNA toxicity (9–11), although a more complete understanding of pathogenic pathways would clearly be of interest for the development of alternative or additional therapeutic options.

Recently, deregulation of cellular processes and signaling pathways important for maintaining proper muscle homeostasis has been reported in DM1. This includes abnormal activation of the ubiquitin-proteasome system and increased autophagic flux, which were both related to muscle atrophy and weakness in DM1 (12–14). In parallel, perturbation in the PKB/Akt pathway may arise from altered expression of the insulin receptor, which correlates with glucose intolerance in DM1 patients (15). Although PKB/Akt deregulation has been reported in *Dmpk*-deficient mice (16), in DM1 flies (13), and in DM1 human neural stem cells (17), contradictory results have been obtained in human muscle cells (18, 19).

To obtain further insight into the pathomechanisms associated with the disease, we investigated whether deregulated metabolic pathways may be involved in muscle alterations in DM1. We uncovered that muscles from HSA^{LR} mice do not efficiently respond to fasting by displaying impaired activation of AMPK and delayed inhibition of the mTOR complex 1 (mTORC1) pathway. Moreover, we observed mild perturbations of the autophagic flux in both HSA^{LR} muscle and myotubes from DM1 patients, which may arise from AMPK/mTORC1 deregulation. Importantly, we established that treatments normalizing these pathways improved

Conflict of interest: M. Sinnreich owns shares of Novartis and is coinventor on a patent application for drug discovery in DM1 (EP 16/166212.7). M. Sinnreich's institution (University Hospital Basel) has received research support from CSL Behring and Roche, not in relation to this study. C. Angelini is part of the European Board of Genzyme-Sanofi.
Submitted: July 19, 2016; **Accepted:** November 17, 2016.
Reference information: *J Clin Invest*. 2017;127(2):549–563.
https://doi.org/10.1172/JCI89616.

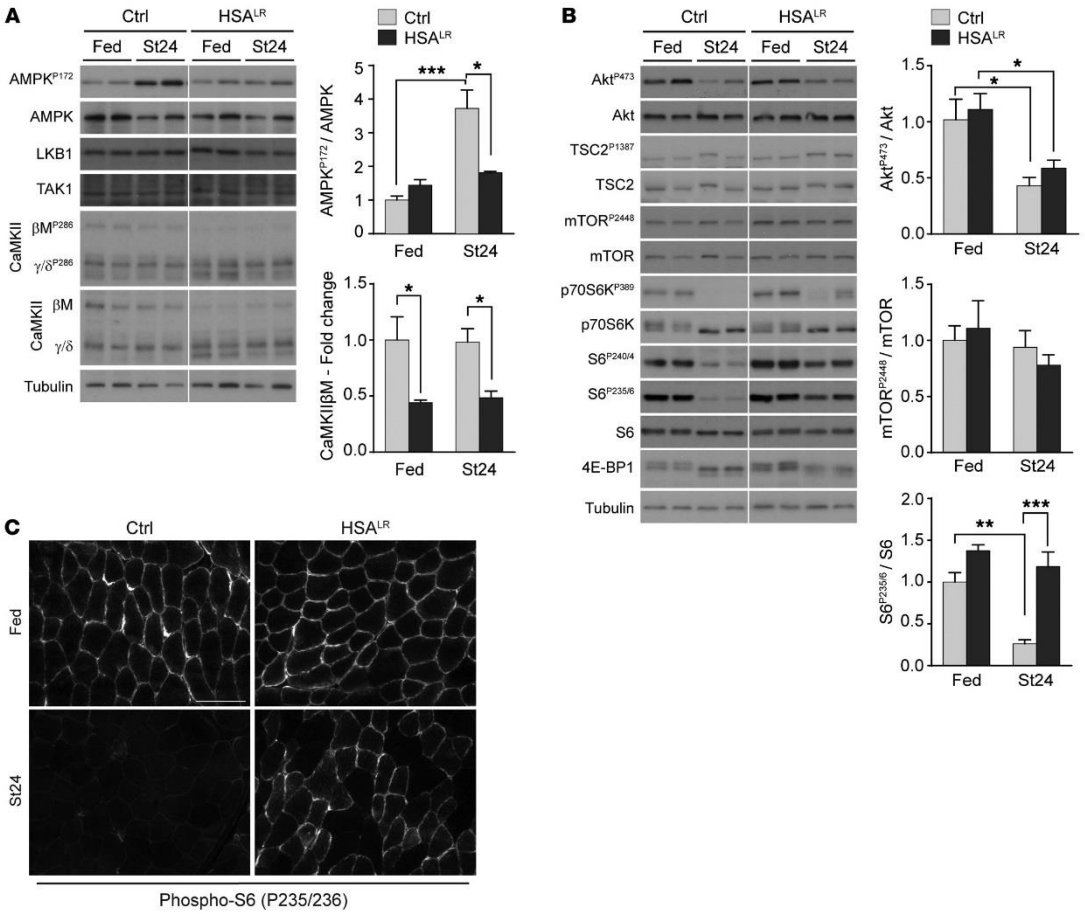

Figure 1. AMPK and mTORC1 pathways do not respond to starvation in HSA^{LR} muscle. (**A** and **B**) Two-month-old HSA^{LR} and control (Ctrl) mice were examined in fed conditions and after 24 hours of starvation (St24). Immunoblots for phospho- (P) and total proteins of the AMPK (**A**) and mTORC1 (**B**) pathways reveal reduced AMPK activation and increased phosphorylation of some mTORC1 targets upon starvation in mutant muscle. Samples were run on the same gel but were noncontiguous. Protein quantification is given for AMPK^{P172} (n = 4 Ctrl and 3 HSA^{LR}), CaMKIIβM, Akt^{P473}, mTOR^{P2448} (Fed, n = 3; St24, n = 4), and S6$^{P235/6}$ (Fed, n = 3; St24, n = 7 Ctrl and 6 HSA^{LR}). Data are relative to fed control mice and are mean ± SEM. *P < 0.05, **P < 0.01, ***P < 0.001, 2-way ANOVA with Tukey's multiple comparisons test correction. (**C**) Immunostaining on muscle cross sections from fed and starved (St24) HSA^{LR} and control (Ctrl) mice shows high levels of phospho-S6 in mutant muscle upon starvation. Scale bar: 100 μm.

skeletal muscle strength and strongly reduced the myotonia in HSA^{LR} mice. Our data provide evidence for the pathological role of metabolic pathways in DM1 and may open interesting avenues for alternative therapeutic strategies for the disease.

Results

AMPK and mTORC1 pathways are deregulated in HSA^{LR} muscle. To identify pathomechanisms involved in DM1-related muscle alterations, we examined the potential deregulation of metabolic pathways in HSA^{LR} mice (Supplemental Figure 1A; supplemental material available online with this article; doi:10.1172/JCI89616DS1). To this purpose, the activation state of key proteins was compared in muscle from 2-month-old mice analyzed in fed conditions or subjected to a physiological stimulus like fasting (20). No major difference was observed in the activation state of AMPK, PKB/Akt, and mTORC1 pathways in muscle from fed mutant and control mice, as reflected by the similar phosphorylation levels of AMPK (AMPK^{P172}), PKB/Akt (Akt^{P473}), and the mTORC1 targets ribosomal protein S6 kinase (p70S6K^{P389}) and S6 ribosomal protein (S6$^{P235/6}$ and S6$^{P240/4}$) (Figure 1, A and B). After 24 hours of starvation, HSA^{LR} mice showed impaired activation of the AMPK pathway, as revealed by the reduced levels of AMPK^{P172} in tibialis anterior (TA) mutant muscle (Figure 1A). Regardless of the nutritional status, protein expression of the known AMPK regulatory kinases

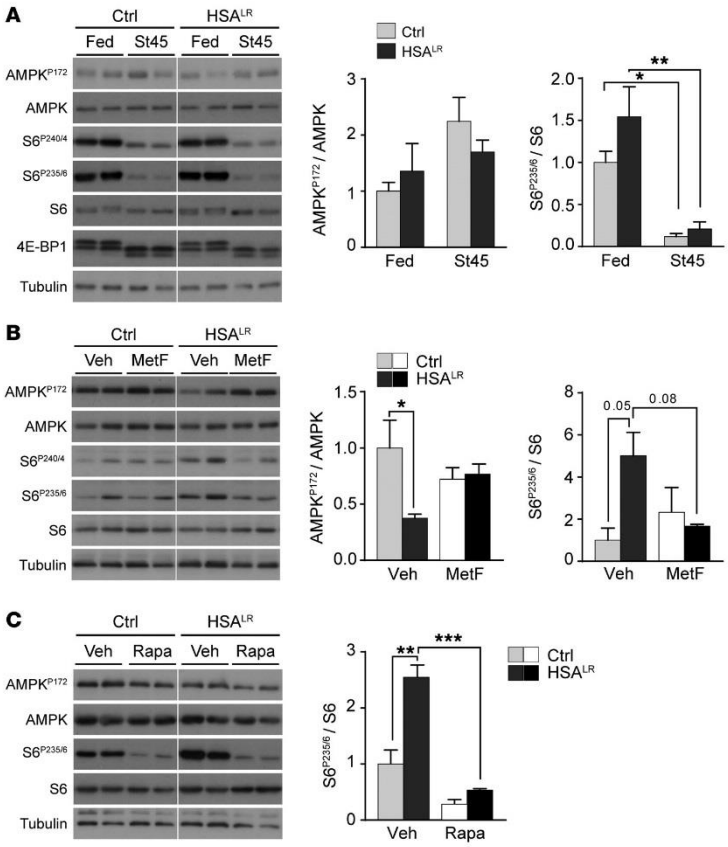

Figure 2. AMPK and mTORC1 pathways can be modulated by caloric and pharmacological treatments in HSA^{LR} muscle. Immunoblots for phospho- (P) and total AMPK and S6 proteins reveal efficient inhibition of mTORC1 signaling upon 45 hours of starvation (St45, **A**) and with metformin (MetF, **B**) or rapamycin (Rapa, **C**) treatment in muscle from HSA^{LR} mice. AMPK activation shows a trend toward increase in mutant muscle with metformin treatment (**B**). Samples were run on the same gel but were noncontiguous. Protein quantification is shown for AMPK^{P172} and S6$^{P235/6}$ (Fed, n = 3; St45, n = 4 Ctrl and 3 HSA^{LR}; Veh [**B**], n = 3; MetF, n = 4; Veh [**C**], n = 4 Ctrl and 3 HSA^{LR}; Rapa, n = 3 per genotype). Data are relative to fed (**A**) or vehicle-treated (**B** and **C**) control mice and are mean ± SEM. $^*P < 0.05$, $^{**}P < 0.01$, $^{***}P < 0.001$, 2-way ANOVA with Tukey's multiple comparisons test correction.

liver kinase B1 (LKB1) and TGF-β–activated kinase 1 (TAK1) was unchanged in HSA^{LR} muscle compared with control (Figure 1A). In contrast, mutant muscle displayed an altered expression profile for Ca^{2+}-calmodulin–dependent kinase II (CaMKII) isoforms, with marked reduction in levels of the CaMKIIβM muscle-specific form and of its phosphorylated, active form (Figure 1A). Such deregulation was consistent with splicing defects in the *Camk2* genes previously described in tissues from DM1 patients and mouse models (11, 21–23). We confirmed by quantitative PCR that splicing of *Camk2b* was altered in muscle from HSA^{LR} mice (exon 13 exclusion; Supplemental Figure 1B), while overall expression of *Camk2* transcripts was unchanged in comparison with controls (Supplemental Figure 1C). As CaMKII regulates AMPK (24–26), these results suggest that impaired AMPK activation in HSA^{LR} muscle may rely on mis-splicing–dependent CaMKII deficiency.

In parallel, higher phosphorylation of p70S6K and S6 was detected upon starvation in HSA^{LR} muscle compared with control muscle (Figure 1B). Accumulation of phosphorylated S6 in muscle from starved mutant mice was further confirmed by immunostaining (Figure 1C), suggesting an abnormal activation of the mTORC1 signaling in HSA^{LR} mice. The specificity of the staining was confirmed by use of the S6$^{P235/6}$ blocking peptide and by immunostaining of sections from muscles with a constant activation (TSCmKO; ref. 27) or depletion (RAmKO; ref. 28) of mTORC1 (Supplemental Figure 1D). Notably, no major change in the phosphorylation of mTOR was observed in mutant and control muscles from fed versus starved mice (Figure 1B). Moreover, upon starvation, changes in 4E-BP1 levels were similar between HSA^{LR} and control muscles (Figure 1B), consistent with previous reports indicating differential regulation of mTORC1 targets (29). Interestingly, mTORC1 deregulation was not related to abnormal activity of PKB/Akt, since levels of the active phosphorylated form of PKB/Akt were efficiently decreased upon starvation in mutant mice (Figure 1B). Accordingly, we did not detect any changes in the splicing (exon 11, mis-spliced in DM1 patients) or expression of the gene encoding insulin receptor (*Insr*) in TA muscle from 2-month-old HSA^{LR} mice (Supplemental Figure 1E). Moreover, mTORC1 and AMPK activation state in nonmuscle tissue, such as liver, was similar in control and mutant mice (Supplemental Figure 1F), indicating that deregulation of these pathways is confined to skeletal muscles, which specifically express (CUG)n-expanded transcripts.

In an attempt to normalize mTORC1/AMPK pathways, control and HSA^{LR} mice were subjected to starvation for 45 hours. Mutant mice lost less weight than controls after prolonged starvation (Supplemental Figure 2). Moreover, upon 45 hours of star-

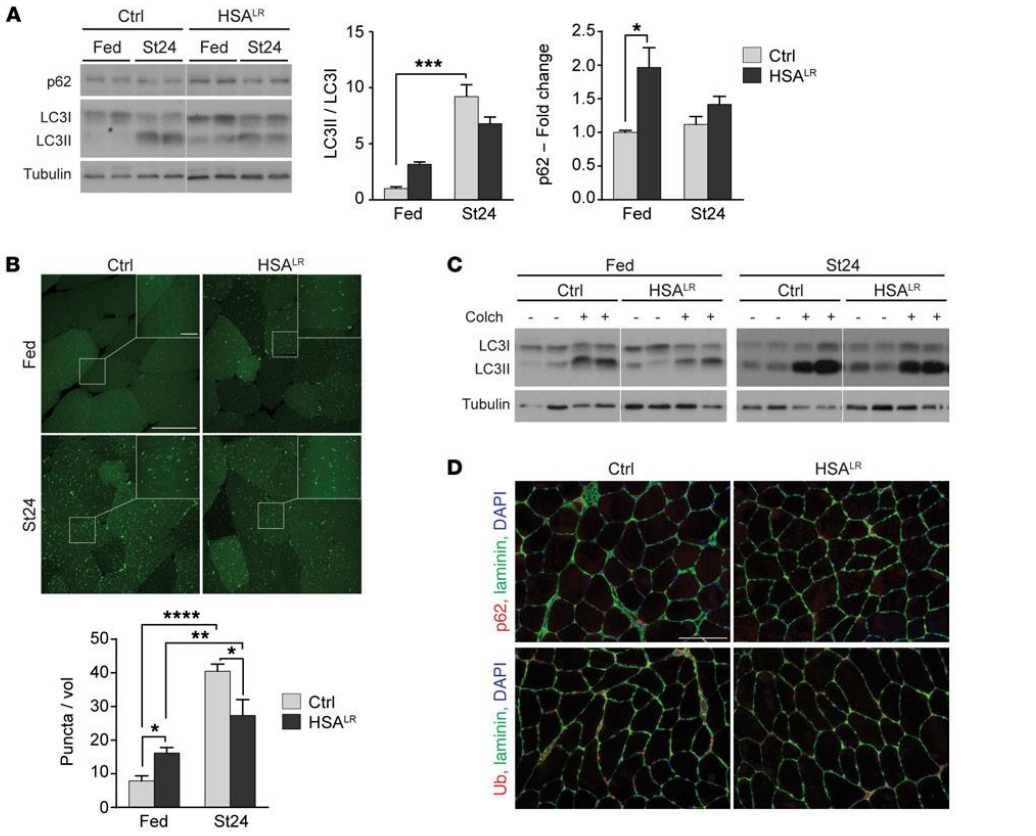

Figure 3. HSA^{LR} muscles show mild deregulation of the autophagic flux. (**A**) Immunoblots for autophagy-related proteins show accumulation of autophagic substrates in HSA^{LR} TA muscle in fed conditions. A reduced LC3I-to-LC3II switch is observed in mutant muscle upon 24 hours of starvation (St24), compared with control (Ctrl). Samples were run on the same gel but were noncontiguous. (Fed, $n = 3$; St24, $n = 7$ Ctrl and 6 HSA^{LR} for LC3 ratio, $n = 4$ for p62.) For LC3I and LC3II levels, see Supplemental Figure 3A. (**B**) HSA^{LR} mice expressing GFP-LC3 display increased number of GFP-positive puncta in TA muscle compared with control (Ctrl) in fed conditions ($n = 3$ Ctrl and 4 HSA^{LR}), but reduced accumulation after 24 hours of starvation (St24, $n = 3$). Scale bar: 50 μm; 10 μm for insets. A volume unit (vol) corresponds to 2.8×10^3 μm^3. (**C**) Treatment with colchicine (Colch) leads to milder changes in LC3II levels in TA muscle from fed and starved HSA^{LR} mice, compared with control (Ctrl) mice. For LC3II/LC3I quantification, see Supplemental Figure 3C. (**D**) Immunostaining of muscle sections from starved control (Ctrl) and HSA^{LR} mice reveals no major accumulation of p62 or ubiquitinated proteins in mutant muscle. Scale bar: 100 μm. Data are relative to control fed mice and represent mean ± SEM. *$P < 0.05$, **$P < 0.01$, ***$P < 0.001$, ****$P < 0.0001$, 2-way ANOVA with Tukey's multiple comparisons test correction.

vation, 4E-BP1 and phospho-S6 levels were similar in mutant and control muscles, while AMPK phosphorylation showed only a trend toward increase in HSA^{LR} muscle (Figure 2A). We next addressed whether pharmacological treatments would be sufficient to modulate AMPK/mTORC1 pathways in HSA^{LR} mice. Control and mutant mice were treated for 5 days with metformin, a drug known to induce AMPK signaling. The treatment slightly activated AMPK in muscle from starved HSA^{LR} mice, which was accompanied by a decrease in phospho-S6 levels (Figure 2B). Conversely, a single injection of rapamycin, a canonical inhibitor of mTORC1, strongly reduced S6$^{P235/6}$ levels in muscle from HSA^{LR} mice, to levels similar to those in controls. This further confirmed that S6 deregulation is dependent on mTORC1/p70S6K and does not involve ERK/p90S6K, which can also phosphorylate S6 at Ser235/6 (30). Levels of AMPK^{P172} remained unchanged in rapamycin-treated mice (Figure 2C). Although no obvious change was detected in AMPK-dependent phosphorylation of TSC2 (TSC2^{P1387}), an upstream inhibitor of mTORC1 (Figure 1B), these results suggest that AMPK deregulation may primarily be responsible for the defective response to starvation and for mTORC1 signaling perturbation in HSA^{LR} muscle.

Autophagic flux is perturbed in HSA^{LR} muscle. It is well established that mTORC1 and AMPK are key regulators of autophagy and that perturbation of their activities can lead to severe tissue alterations, especially in skeletal muscle (31–33). To determine whether the expression of the CUG repeats impairs the autophagy process, we

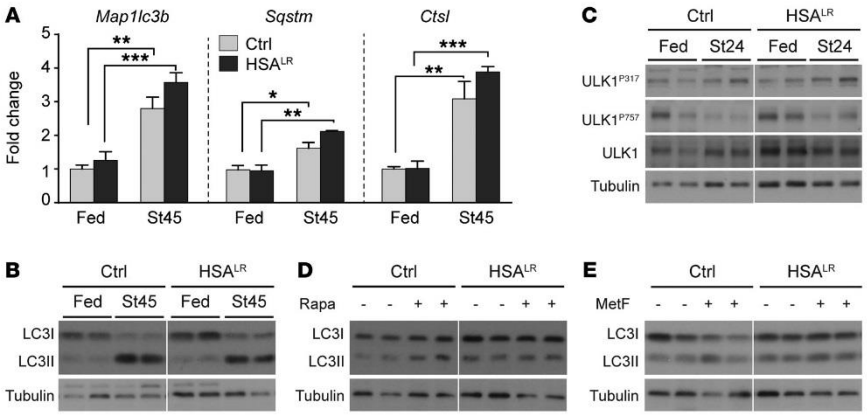

Figure 4. HSA^{LR} muscles display perturbed response of autophagy to caloric and pharmacological treatments. (**A**) Expression of autophagy-related genes is efficiently upregulated after 45 hours of starvation (St45) in HSA^{LR} TA muscle. Data are normalized to *Actn2* levels (Fed, $n = 4$; St45, $n = 4$ Ctrl and 3 HSA^{LR}). Data are relative to control fed mice and represent mean ± SEM. $^*P < 0.05$, $^{**}P < 0.01$, $^{***}P < 0.001$, 2-way ANOVA with Tukey's multiple comparisons test correction. (**B**) Immunoblots reveal limited switch from LC3I to LC3II in HSA^{LR} muscle upon 45 hours of starvation (St45) compared with controls (Ctrl). Samples were run on the same gel but were noncontiguous. For LC3II/LC3I quantification, see Supplemental Figure 4B. (**C**) Levels of the inhibited phosphorylated form of ULK1 (Ser^{P757}) remain slightly higher upon starvation in HSA^{LR} muscle, compared with control (Ctrl) muscle. For quantification, see Supplemental Figure 4C. (**D** and **E**) Immunoblots for LC3 show blunted induction of LC3II upon rapamycin (Rapa, **D**) or metformin (MetF, **E**) treatments, compared with controls (Ctrl). For LC3II/LC3I quantification, see Supplemental Figure 4, D and E. Samples were run on the same gel but were noncontiguous.

assessed the ability of HSA^{LR} muscle to induce autophagy when the mice were subjected to starvation. First, we evaluated levels of the soluble (LC3I) and autophagosome-associated (LC3II) forms of the widely used LC3B (MAP1LC3 for microtubule-associated protein light chain 3) autophagy marker. The amount of LC3II correlates with the intracellular accumulation of autophagic vesicles (34). Under fed conditions, LC3II levels were increased, although not significantly, in mutant muscle, which reflects either a slight increase in autophagy induction or a mild defect in the degradation steps (Figure 3A and Supplemental Figure 3A). After 24 hours of starvation, a clear switch from LC3I to LC3II occurred in control muscle, while HSA^{LR} muscle displayed reduced changes in LC3 levels and LC3II/LC3I ratio (Figure 3A and Supplemental Figure 3A). To confirm these results, we starved HSA^{LR} and control mice expressing the GFP-LC3 fusion protein for 24 hours. In control muscle, a striking increase in the number of GFP-LC3–positive puncta, representing autophagic vesicles, was observed upon starvation (Figure 3B and Supplemental Figure 3B). In HSA^{LR} mice, the number of puncta was higher under fed conditions, but was significantly less increased upon starvation as compared with control muscle (Figure 3B and Supplemental Figure 3B). These results confirmed that autophagy is perturbed in HSA^{LR} muscle, which may rely on impaired induction and/or degradation steps.

To assess the status of the autophagic flux, mice were treated for 2 days with colchicine, a drug preventing degradation of the autophagic content. Under both fed and starved conditions, colchicine induced a major switch from LC3I to LC3II in control muscle (Figure 3C). Comparing colchicine-treated and untreated mice, we observed that the fold change in the LC3II/LC3I ratio was less in HSA^{LR} muscle compared with controls, in both fed and starved conditions (Figure 3C and Supplemental Figure 3C). This result ruled out that elevated LC3II levels in fed conditions were due to increased autophagy induction in HSA^{LR} muscle; accumulation of autophagic vesicles was therefore likely related to restricted degradation. Consistently, levels of the autophagosome cargo protein p62 were higher in muscle from fed mutant mice than in controls (Figure 3A). However, we detected neither p62 aggregates nor accumulation of ubiquitinated proteins in muscle from fed and starved HSA^{LR} mice (Figure 3D), indicating that autophagy is only mildly affected. Similarly, distribution of lysosomal vesicles, visualized by LAMP1 immunostaining, was unchanged between 2-month-old mutant and control mice (Supplemental Figure 3D). Together, these results suggest that autophagy is slightly deregulated in DM1 muscle, which results from reduced degradation in combination with attenuated autophagy induction upon starvation.

Under fed conditions, increased amounts of p62 and LC3II were not due to abnormal transcript expression in HSA^{LR} muscle (Figure 4A). Moreover, expression of the *Map1lc3b*, *Sqstm* (encoding p62), and *Ctsl* (encoding cathepsin L) genes was unchanged after 24 hours of fasting, but we observed an efficient induction of the genes upon 45 hours of starvation in both mutant and control muscles (Figure 4A and Supplemental Figure 4A). It should be noted that following prolonged starvation, autophagy induction remained weaker in mutant muscle compared with control muscle (Figure 4B and Supplemental Figure 4B). To gain further insight into autophagy deregulation, we assessed the phosphorylation state of Unc-51–like kinase 1 (ULK1), as mTORC1 and AMPK phosphorylate and thereby inhibit or activate ULK1, respectively (31). Upon starvation, levels of the inactive form of ULK1 (ULK1^{P757}) remained slightly higher in mutant muscle as compared with control muscle, while no major difference was observed for its active form (ULK1^{P317}; Figure 4C and Supplemental Figure 4C). Interestingly, rapamycin and metformin treatments were both sufficient

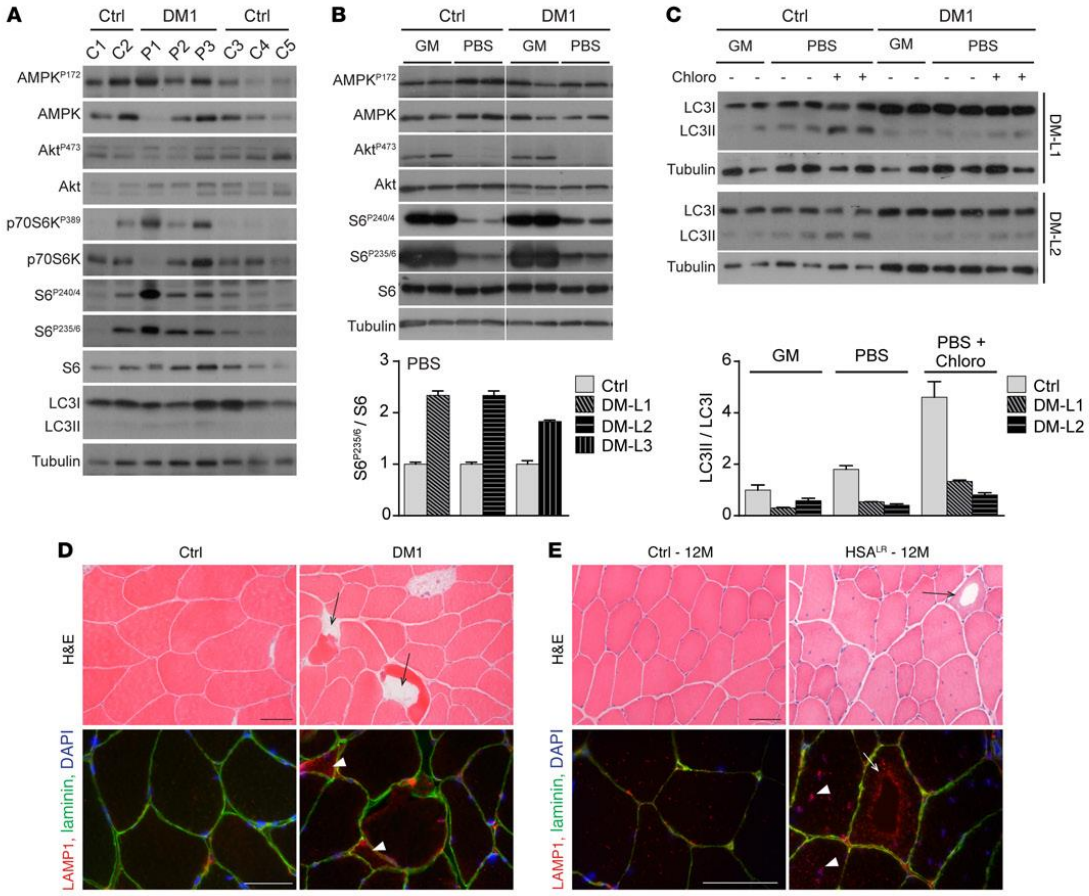

Figure 5. Autophagy perturbation contributes to muscle alterations in DM1. (**A**) Protein lysates from muscle biopsies of control individuals (C1–5) and DM1 patients (P1–3) were analyzed for phospho- (P) and total proteins of the AMPK and PKB/Akt–mTORC1 pathways. (**B**) MyoD-transduced fibroblasts from controls (Ctrl) and DM1 patients were differentiated to myotubes and subjected to growth medium (GM) or deprived conditions (PBS) for 3 hours. Immunoblots for phospho- (P) and total proteins reveal increased phospho-S6 levels upon deprivation in the 3 cell lines of DM1 patients (DM-L1–3), compared with controls. Samples were run on the same gel but were noncontiguous. Quantification is given for deprived conditions; values are mean ± SEM of technical replicates. (**C**) Immunoblots for LC3 marker show defective accumulation of LC3II in DM1 myotubes upon energy and amino acid deprivation (PBS) as well as with deprived conditions and chloroquine treatment (Chloro), compared with control cells (Ctrl). Quantification of LC3II/LC3I ratio is shown for 2 DM1 cell lines (DM-L1/2) in enriched (GM) and deprived conditions; values are mean ± SEM of technical replicates. (**D**) H&E stain reveals the presence of vacuolated fibers (arrows) in muscle biopsy from 1 DM1 patient, together with lysosomal accumulation (arrowheads) observed by immunostaining in some affected muscle fibers (red, bottom panel). Scale bars: 50 μm. (**E**) Vacuoles (arrows) are observed in muscle from aging HSA^{LR} mice; the periphery of the vacuoles is strongly reactive with anti-LAMP1 antibodies (red, bottom panel), indicating accumulation of lysosomal structures in these regions. High density of lysosomes is also observed in nonvacuolated muscle fibers from 12-month-old (12M) mutant mice (arrowheads), compared with muscle from age-matched control mice (Ctrl). Scale bars: 50 μm.

to increase LC3II levels in control muscle, but did not induce autophagy in HSA^{LR} muscle (Figure 4, D and E, and Supplemental Figure 4, D and E). Hence, mTORC1/AMPK deregulation in conjunction with mTORC1/AMPK-independent mechanisms likely contributes to autophagy perturbation in HSA^{LR} muscle.

Lastly, upon starvation, expression of the atrogenes *Trim63* and *Fbxo32* was similarly induced in HSA^{LR} and control muscles (Supplemental Figure 4F). However, caspase- and trypsin-like activities associated with the proteasome system were increased in muscle from fed and starved mutant mice, compared with control animals (Supplemental Figure 4G). This is consistent with a previous report showing higher proteasome activity in muscle from a DM1 mouse model expressing 550 CTG triplets (12).

Involvement of AMPK/mTORC1 deregulation in DM1 pathology. To ascertain the relevance of the changes observed in HSA^{LR} mice for DM1 pathology, we evaluated the activation state of AMPK/

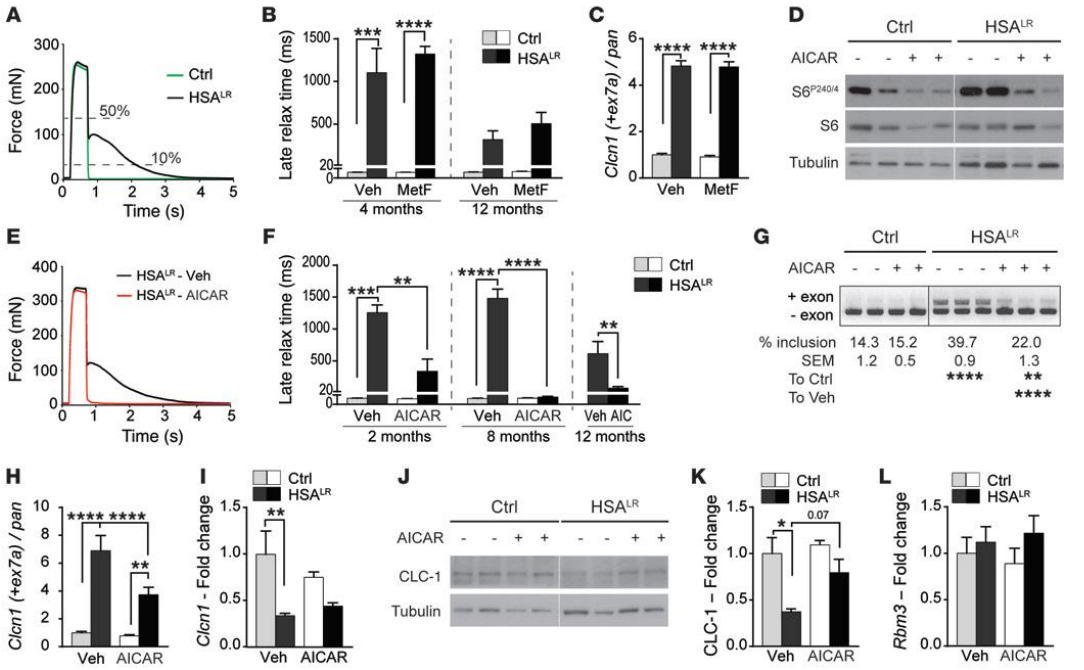

Figure 6. AICAR markedly decreases myotonia in HSA^{LR} mice and reduces mis-splicing in mutant muscle. (**A**) In vitro tetanic stimulation of EDL muscle reveals strongly increased relaxation time in HSA^{LR} muscle. (**B**) Metformin (MetF) treatment does not reduce muscle late relaxation time in 4-month-old (Ctrl, n = 5; HSA^{LR}, n = 6 Veh and 8 MetF) and 12-month-old (Ctrl, n = 3; HSA^{LR}, n = 7 Veh and 8 MetF) HSA^{LR} mice, as compared with vehicle-treated mutant mice. (**C**) Inclusion of exon 7a of the *Clcn1* gene is not changed in muscle from metformin-treated (MetF) HSA^{LR} mice, compared with vehicle-treated mice (n = 3). (**D**) Immunoblots for phospho- and total S6 protein reveal efficient inhibition of indirect AMPK target in muscle from control (Ctrl) and mutant mice treated with AICAR. Samples were run on the same gel but were noncontiguous. (**E**) AICAR treatment normalizes the time to relax of HSA^{LR} muscle upon tetanic stimulation, compared with muscle from vehicle-treated (Veh) mutant mice. (**F**) Late relaxation time is significantly reduced in EDL muscle from 2-month-old (n = 3 Ctrl and 4 HSA^{LR}), 8-month-old (Ctrl, n = 3; HSA^{LR}, n = 6 Veh and 7 AICAR), and 12-month-old (n = 4 Veh and 5 AICAR) HSA^{LR} mice that were treated with AICAR, as compared with age-matched vehicle-treated (Veh) mutant mice. (**G**–**K**) End-point PCR (**G**) and quantitative PCR (**H** and **I**) reveal strong reduction in exon 7a inclusion of the *Clcn1* gene in muscle from HSA^{LR} mice treated with AICAR, compared with vehicle-treated (Veh) mutant mice (Ctrl, n = 3; HSA^{LR}, n = 5 Veh and 4 AICAR [**G**], n = 5 [**I**]). Protein levels of CLC-1 are also increased in mutant muscle from AICAR-treated mice (**J** and **K**, n = 3 Ctrl and 4 HSA^{LR}). (**L**) Quantitative PCR shows similar transcript levels of *Rbm3* in muscle from AICAR-treated and untreated mice (n = 3 Ctrl and 4 HSA^{LR}). Data represent mean ± SEM. *P < 0.05, **P < 0.01, ***P < 0.001, ****P < 0.0001, 2-way ANOVA with Tukey's multiple comparisons test correction (except 12M AICAR, unpaired 2-tailed Student's t test).

mTORC1 signaling in muscle biopsies from 3 DM1 patients (P1–3) of 33, 34, and 49 years of age. There was no major difference in total and phosphorylated levels of PKB/Akt and AMPK proteins in muscle from DM1 patients compared with age-matched control individuals (C1/2 and C3–5 aged 30 and 50 years, respectively) (Figure 5A). Notwithstanding, we noticed that levels of the active phosphorylated forms of p70S6K and S6 were increased in muscle biopsies from DM1 patients compared with control individuals (Figure 5A). However, the nutritive status of the patients at the time of the biopsy could not be ascertained and may have influenced the results. For this reason, we next tested the ability of DM1 human muscle cells to modulate mTORC1/AMPK signaling in response to energy and nutrient deprivation. Fibroblasts of 3 DM1 patients (DM-L1–3) were transduced with MyoD and differentiated for 10 days into myotubes, before being subjected to growth medium or to amino acid– and glucose-deprived conditions (i.e., PBS) for 3 hours. Upon deprivation, levels of the active phosphorylated forms of PKB/Akt and S6 were strongly reduced in control muscle cells; there was no major activation of AMPK in comparison with enriched conditions (Figure 5B). A similar response was observed in DM1 muscle cells, although they retained higher phosphorylation of S6 in deprived conditions compared with control cells (Figure 5B). In parallel, a major switch from LC3I to LC3II occurred in control muscle cells upon deprivation. LC3II levels were further increased in control cells treated with chloroquine, consistent with high autophagy induction in deprived cells (Figure 5C). In contrast, LC3II levels were only slightly changed when DM1 myotubes were subjected to deprivation, even in the presence of chloroquine, indicating that the autophagic flux is blocked at the induction steps (Figure 5C). Together, these data indicate that DM1 human muscle cells do not efficiently respond to nutrient/energy deprivation and display deregulation of the autophagy process.

Table 1. Changes in muscle cross-sectional area and tetanic forces upon treatments in HSA^{LR} and control mice

	Ctrl		HSA^{LR}	
	Vehicle	AICAR	Vehicle	AICAR
CSA EDL (mm^2)				
2M	1.38 ± 0.02	1.31 ± 0.03	1.65 ± 0.05^C	1.62 ± 0.01^C
8M	1.52 ± 0.00	1.70 ± 0.2	1.86 ± 0.07	1.70 ± 0.04
12M	–	–	2.46 ± 0.07	2.32 ± 0.02
Po (mN)				
2M	185.20 ± 9.01	255.79 ± 9.09^D	197.91 ± 13.96	279.97 ± 17.25^E
8M	285.37 ± 33.67	273.71 ± 36.71	288.31 ± 15.15	274.39 ± 12.27
12M	–	–	260.90 ± 26.53	339.42 ± 24.22$^{0.07}$
sPo (mN/mm^2)				
2M	134.58 ± 4.84	194.73 ± 2.67^D	121.23 ± 12.16	173.60 ± 11.05^D
8M	187.58 ± 22.01	168.80 ± 34.37	156.89 ± 11.95	161.94 ± 7.34
12M	–	–	107.33 ± 13.02	146.46 ± 10.51$^{0.06}$
	Vehicle	Rapamycin	Vehicle	Rapamycin
CSA EDL (mm^2)				
4M	1.69 ± 0.12	1.61 ± 0.07	2.04 ± 0.07^B	1.96 ± 0.02^B
12M	1.67 ± 0.09	1.50 ± 0.10	1.90 ± 0.06	1.77 ± 0.09
Po (mN)				
4M	180.94 ± 26.37	170.07 ± 3.91	193.80 ± 13.01	274.48 ± 16.11^{B,E}
12M	226.14 ± 28.30	245.67 ± 16.07	209.59 ± 30.94	240.28 ± 18.95
sPo (mN/mm^2)				
4M	114.98 ± 21.53	111.32 ± 8.79	99.41 ± 7.64	144.37 ± 8.32^E
12M	137.66 ± 23.49	168.87 ± 20.50	109.78 ± 15.01	137.12 ± 12.41
	Vehicle	AZD8055	Vehicle	AZD8055
CSA EDL (mm^2)	1.24 ± 0.42	1.67 ± 0.03	2.09 ± 0.09^A	2.06 ± 0.04
Po (mN)	185.19 ± 76.17	241.13 ± 80.46	257.96 ± 28.02	353.06 ± 8.90
sPo (mN/mm^2)	190.13 ± 23.13	192.38 ± 6.94	124.30 ± 13.88^A	171.96 ± 5.22^D

CSA, cross-sectional area; M, month; Po, tetanic muscle force; sPo, specific tetanic muscle force. CSA = weight/(1.06 * length * 0.44), where 1.06 corresponds to the density of the muscle and 0.44 the correction factor for EDL muscle. AICAR, 2-month-old (n = 3 Ctrl and 4 HSALR), 8-month-old (Ctrl, n = 3; HSALR, n = 6 Veh and 7 AICAR), 12-month-old (HSALR, n = 4 Veh and 5 AICAR) mice; rapamycin, 4-month-old (Ctrl, n = 4; HSALR, n = 8 Veh and 10 Rapa), 12-month-old (Ctrl, n = 3; HSALR, n = 5 Veh and 6 Rapa) mice; AZD8055, 8-month-old (Ctrl, n = 3; HSALR, n = 5 Veh and 8 AZD) mice. Values are mean ± SEM. $^AP < 0.05$, $^BP < 0.01$, $^CP < 0.001$ compared with control mice with same treatment; $^DP < 0.05$, $^EP < 0.01$, compared with same genotype treated with vehicle; 2-way ANOVA with Tukey's multiple comparisons test correction; for 12-month-old AICAR-treated mice, unpaired 2-tailed Student's t test.

To test the relevance of autophagy changes in DM1, we looked for muscle alterations related to autophagy defects in muscle biopsies from DM1 patients and in muscle from aged HSA^{LR} mice. As previously reported (14, 35–37), vacuolated fibers were observed in muscle biopsy of 1 DM1 patient, out of the 3 examined (Figure 5D). Lysosome accumulation was also detected in affected fibers from DM1 muscle (Figure 5D). However, in contrast to biopsies from an inclusion body myositis (IBM) patient, there was no accumulation of LC3, ubiquitinated proteins, or p62 in DM1 patient muscles (Supplemental Figure 5A). Consistently, LC3 levels detected by Western blot were similar in DM1 and control biopsies (Figure 5A). Interestingly, we observed some intracellular vacuoles in muscle from 12-month-old HSA^{LR} mice, as well as accumulation of the lysosomal marker LAMP1 near the vacuolar structures and myonuclei (Figure 5E). Secondary antibodies alone did not react with the vacuoles, and we did not observe such features in muscle from age-matched control mice (Figure 5E and Supplemental Figure 5B). Electron microscopy confirmed the presence of vacuoles in mutant mouse muscle: they were surrounded by dense, disorganized areas of contractile elements and usually limited by a single, discontinuous membrane (Supplemental Figure 5C). Together with the lysosome staining, these features argue for the presence of autophagic vacuoles in muscle from older HSA^{LR} mice. These results suggest that autophagy perturbation may contribute to the alteration of muscle tissue in DM1, but is unlikely to be a predominant feature of the disease.

AICAR, an AMPK agonist, abrogates myotonia in HSA^{LR} mice. In light of the deregulation of AMPK signaling in HSA^{LR} muscle, we investigated whether AMPK normalization would have a beneficial effect on muscle function in mutant mice. As readout of the disease, we evaluated myotonia by measuring the late relaxation time of skeletal muscle (i.e., time to reduce the maximal force from 50% to 10%) after ex vivo tetanic stimulation (8). As reported previously, we observed no change in the late relaxation time of soleus muscle from HSA^{LR} mice compared with controls (Supplemental Figure 6A), whereas this parameter was strongly increased in extensor digitorum longus (EDL) mutant muscle (Figure 6A). Since AMPK activation by metformin has recently been shown to correct mis-splicing in human DM1 cells in vitro (38), 4- and 12-month-old control and HSA^{LR} mice were treated with metformin for 10 days. Despite using high doses of metformin, we observed only a limited and nonreproducible effect of the treatment on AMPK/S6 activation state in these groups of mice analyzed under basal nutritive conditions (Supplemental Figure 6B). Besides, the treatment failed to reduce the late relaxation time of EDL muscle in mutant mice (Figure 6B), and it did not modify the expression and splicing of genes affected in DM1, including *Clcn1* (encoding CLC-1, chloride channel protein 1; inclusion of exon 7a) and *Atp2a1* (encoding sarcoplasmic/endoplasmic reticulum Ca^{2+}-ATPase 1; exclusion of exon 22) (Figure 6C and Supplemental Figure 6C).

As we did not detect any effect of metformin on HSA^{LR} muscle, we tested whether 5-aminoimidazole-4-carboxamide ribonucleotide (AICAR), an agonist of AMPK, may constitute an alternative strategy to target AMPK activation in muscle. Following a 7-day treatment with AICAR, control and mutant muscles showed a clear reduction in phospho-S6 levels (Figure 6D). We further confirmed that AICAR increased phosphorylated levels of AMPK and those of its direct target acetyl-CoA carboxylase shortly after the last injection (30 minutes), while inhibition of the indirect AMPK target S6 was detected only after 2 hours in control muscle (Supplemental Figure 6D). Importantly, following tetanic stimuli, a strong and significant reduction in the late

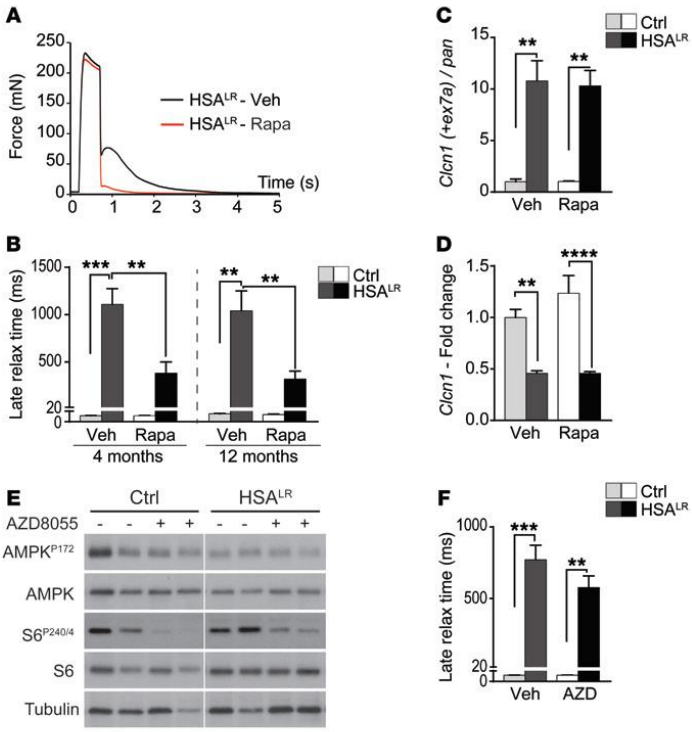

Figure 7. Rapamycin improves muscle function in HSA^{LR} mice via splicing-independent mechanisms. (**A**) Rapamycin treatment strongly reduces the time to relax of HSA^{LR} muscle upon tetanic stimulation, compared with muscle from vehicle-treated (Veh) mutant mice. (**B**) Rapamycin (Rapa) treatment significantly reduces late relaxation time of muscle from 4-month-old (Ctrl, $n = 4$; HSA^{LR}, $n = 8$ Veh and 10 Rapa) and 12-month-old (Ctrl, $n = 3$; HSA^{LR}, $n = 5$ Veh and 6 Rapa) HSA^{LR} mice, as compared with age-matched, vehicle-treated mutant mice. (**C** and **D**) Splicing (**C**) and overall transcript expression (**D**) of the *Clcn1* gene are not modified in muscle from rapamycin-treated (Rapa) HSA^{LR} mice, compared with vehicle-treated (Veh) mutant mice. Values are relative to vehicle-treated control mice ($n = 3$ Ctrl and 4 Veh-treated and 5 Rapa-treated HSA^{LR}). (**E**) Treatment with AZD8055 for 10 days efficiently reduces phosphorylation of mTORC1 target, S6, in control (Ctrl) and HSA^{LR} muscle, but does not change AMPK activation. Samples were run on the same gel but were noncontiguous. (**F**) AZD8055 (AZD) does not reduce late relaxation time of EDL mutant muscle, compared with vehicle-treated (Veh) mutant mice. ($n = 3$ Ctrl and 5 Veh and 8 AZD HSA^{LR} mice.) Data represent mean ± SEM. $^{**}P < 0.01$, $^{***}P < 0.001$, $^{****}P < 0.0001$, 2-way ANOVA with Tukey's multiple comparisons test correction.

relaxation time of EDL muscle was detected in 2- and 12-month-old AICAR-treated mutant mice, and myotonia was completely abrogated with AICAR in the group of 8-month-old HSA^{LR} mice (Figure 6, E and F). Normalization of the half-relaxation time (i.e., time to reduce the maximal force from 100% to 50%) of mutant muscle was also observed upon treatment (Supplemental Figure 6E). As mis-splicing of the *Clcn1* gene is thought to be the primary cause of myotonia in DM1 (7, 39–41), we investigated whether the effect of AICAR was related to changes in *Clcn1* splicing. By end-point PCR, a significant improvement of the misregulated *Clcn1* splicing was detected upon AICAR treatment (Figure 6G). We confirmed by quantitative PCR that the expression of the mis-spliced *Clcn1* transcript (containing exon 7a) was strongly reduced in muscle from AICAR-treated HSA^{LR} mice, while overall transcript levels of *Clcn1* were unchanged compared with those in untreated mutant mice (Figure 6, H and I). Furthermore, AICAR led to a slight increase in CLC-1 protein levels in mutant muscle (Figure 6, J and K). It is worth noting that AICAR did not change splicing of the *Atp2a1* and *Camk2b* genes in HSA^{LR} muscle (Supplemental Figure 6, F and G). Moreover, we did not detect any reduction in transcript levels of *Rbm3*, encoding RNA-binding protein 3 (Figure 6L), previously suggested to mediate the effect of AMPK activation on splicing (38).

Besides its effect on myotonia, we wondered whether AICAR treatment would change muscle force in mutant mice. As initially reported (5), we detected neither muscle wasting nor reduction in total twitch (Pt) and tetanic (Po) muscle forces in HSA^{LR} mice compared with controls (Table 1 and Supplemental Table 1). Nonetheless, as cross-sectional area [CSA: mass/(density * length * correction factor)] of EDL muscle was increased in mutant mice, specific muscle forces (sPt and sPo), representative of the contractile capacity of the myofibers, were reduced in HSA^{LR} mice compared with control animals (Table 1 and Supplemental Table 1). Upon AICAR treatment, we observed that both total and specific forces of EDL muscle were increased in 2-month-old HSA^{LR} and control mice, but not in older mice (Table 1 and Supplemental Table 1). Altogether, these results indicate that targeting AMPK activation by AICAR improves muscle function in HSA^{LR} mice by reducing myotonia and potentially increasing muscle force, at least in part, through splicing correction.

Rapamycin treatment improves muscle function in HSA^{LR} mice. Based on the abnormal activation of mTORC1 signaling detected in HSA^{LR} muscle, we wondered whether indirect mTORC1 inhibition was part of the effect of AICAR and whether direct mTORC1 inhibition would improve muscle function in mutant mice. To this purpose, we subjected 4- and 12-month-old mice to rapamycin treatment for 7 and 10 days, respectively. Rapamycin treatment efficiently inhibited mTORC1 signaling, as shown by reduced phospho-S6 levels in muscle from control and HSA^{LR} mice (Supplemental Figure 7A). Rapamycin did not affect muscle half-relaxation time (Supplemental Figure 7B), but significantly reduced the late relaxation time of EDL muscle from 4- and 12-month-old HSA^{LR} mice (Figure 7, A and

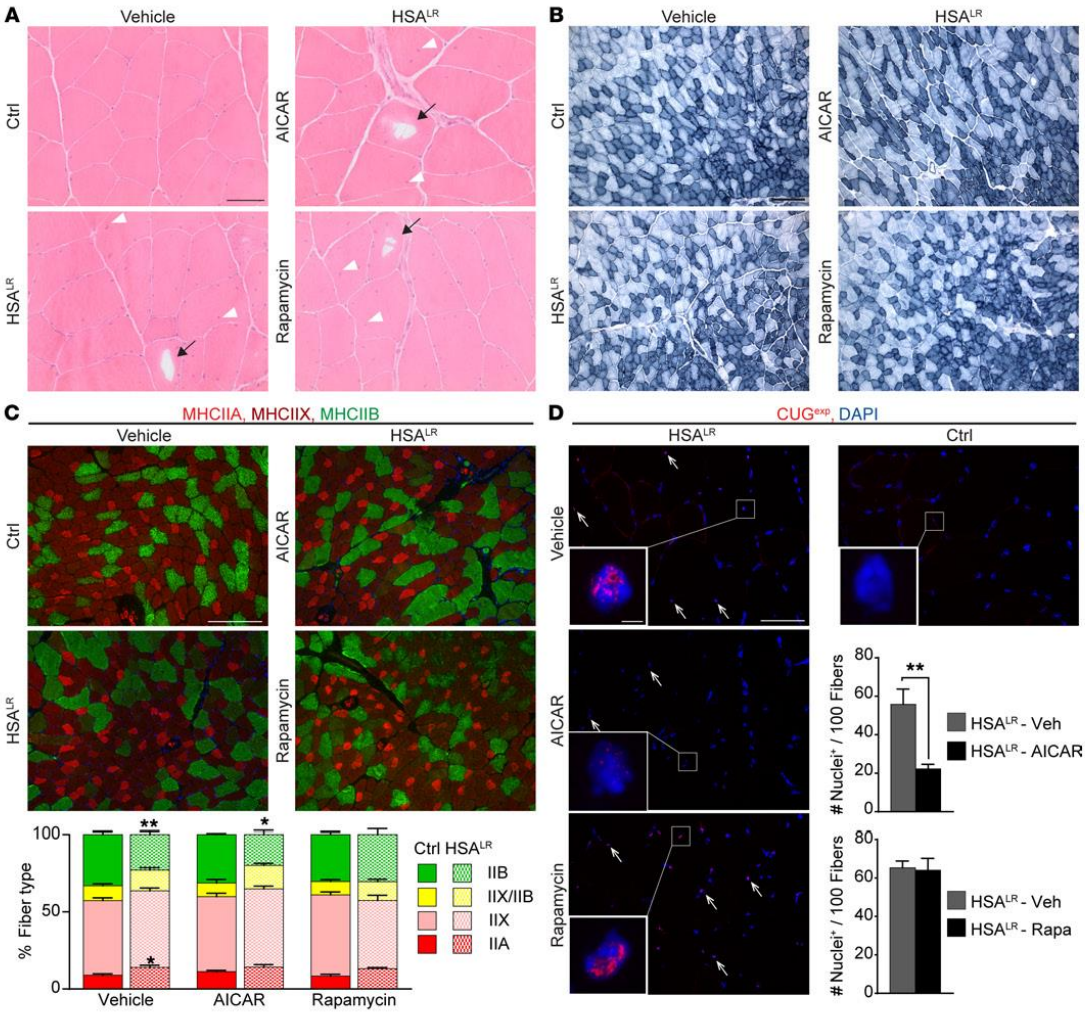

Figure 8. AMPK activation by AICAR leads to nuclear foci dispersion in HSA^{LR} muscle. (**A** and **B**) H&E (**A**) and NADH (**B**) stains reveal no major change in muscle histopathology and oxidative capacity upon AICAR or rapamycin treatment in HSA^{LR} mice. Arrowheads and arrows show internalized nuclei and vacuoles, respectively. Scale bars: 50 μm (**A**), 200 μm (**B**). (**C**) Immunostaining for type IIA (bright red), IIX (dark red), and IIB (green) myosin heavy chains (MHC) reveals no significant change in the respective proportion of fiber types in TA mutant muscle upon AICAR (n = 3 Ctrl and 4 HSA^{LR}) or rapamycin (n = 4) treatment, compared with vehicle-treated HSA^{LR} mice (n = 6 Ctrl and 7 HSA^{LR}). Scale bar: 200 μm. (**D**) FISH on TA muscle sections with a Cy3-CAG$_{10}$ DNA probe shows accumulation of nuclear foci in HSA^{LR} muscle (arrows). The number of stained nuclei is significantly decreased upon AICAR treatment (n = 4), but not with rapamycin (Rapa, n = 3), compared with vehicle-treated (Veh) mutant mice. Foci are not detected in control (Ctrl) muscle. Scale bar: 50 μm; 2 μm for insets. Data in **C** and **D** represent mean ± SEM. *P < 0.05, **P < 0.01, 2-way ANOVA with Tukey's multiple comparisons test correction.

B). Moreover, we detected a significant increase in total and specific muscle forces in young rapamycin-treated mutant mice compared with vehicle-treated animals. Forces remained unchanged upon treatment in older mice (Table 1 and Supplemental Table 1).

To test whether the effect of rapamycin on muscle function relied on splicing improvement, we assessed *Clcn1* mis-splicing (i.e., exon 7a inclusion) by quantitative PCR. Interestingly, rapamycin affected neither *Clcn1* splicing (Figure 7C) nor the overall transcript expression of the gene (Figure 7D) in mutant muscle. Consistently, splicing of the *Atp2a1* gene was also not restored in rapamycin-treated HSA^{LR} mice (Supplemental Figure 7C). Together, these data suggest that mTORC1 inhibition by rapamycin is sufficient to improve muscle function in HSA^{LR} mice likely through splicing-independent mechanisms.

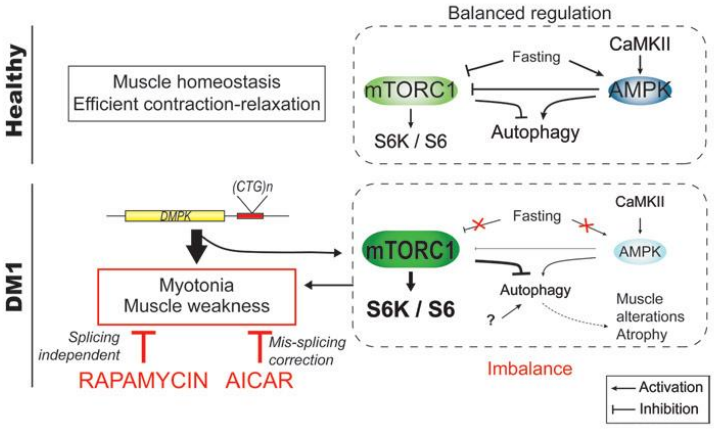

Figure 9. Scheme depicting the deregulation of AMPK/mTORC1 signaling pathways in DM1 muscle. In healthy muscle, the pathways are tightly regulated depending on external and internal stimuli (e.g., growth factors, energy, nutrients). Upon fasting, mTORC1 is inhibited, while AMPK is activated, leading to the induction of autophagy. In DM1, skeletal muscle does not respond to fasting conditions. Deregulation of the AMPK/mTORC1 signaling likely contributes to muscle dysfunction: rapamycin, an inhibitor of mTORC1, and AICAR, an AMPK agonist, both lead to marked reduction of myotonia and normalize muscle weakness in DM1 mice. The underlying mechanisms include RNA splicing–dependent and –independent mechanisms.

Since rapamycin has been shown to impact on channel function (e.g., ryanodine receptor 1, RyR1) via its binding to FKBP12, we wondered whether mTORC1 inhibition or the drug itself mediated the effect of the treatment on myotonia. Hence, control and HSA^{LR} mice were treated for 10 days with AZD8055, an ATP-competitive inhibitor of mTORC1. We confirmed that AZD8055 strongly decreased phospho-S6 levels in control and mutant muscle, while the activation state of AMPK remained unchanged (Figure 7E). In contrast to rapamycin, AZD8055 had no effect on late relaxation time of mutant muscle (Figure 7F). Nonetheless, total and specific forces of EDL muscle were increased in AZD8055-treated mutant mice, as observed with rapamycin (Table 1 and Supplemental Table 1). Together, these results indicate that mTORC1 inhibition may ameliorate the contractile capacity of muscle in HSA^{LR} mice and suggest that improvement of muscle relaxation upon rapamycin and AICAR treatments may be independent of mTORC1.

AICAR, but not rapamycin, leads to nuclear foci dispersion in HSA^{LR} muscle. To further understand the beneficial effect of AICAR and rapamycin in HSA^{LR} mice, we investigated whether the treatments improved muscle function by affecting the properties of the diseased muscle. First, we did not observe major changes in the histopathology of HSA^{LR} muscle upon 7-day AICAR or 10-day rapamycin treatment, compared with untreated conditions (Figure 8A). Notably, vacuoles remained present in muscle fibers from 12-month-old AICAR- or rapamycin-treated HSA^{LR} mice (Figure 8A), indicating that the treatments were not sufficient to reverse muscle alterations related to impaired autophagy in aging mice. As no myotonia was detected in the slow, soleus muscle of HSA^{LR} mice and as AICAR and rapamycin were previously shown to alter muscle fiber types (42, 43), we tested whether changes in muscle function upon treatments were related to modification of muscle metabolic and contractile capacities. By reduced nicotinamide adenine dinucleotide (NADH) staining, we first observed that the overall oxidative property of TA muscle was unchanged in AICAR- and rapamycin-treated mutant mice, compared with untreated animals (Figure 8B). Immunostaining against type I, IIA/X, and IIB myosin heavy chains (MHCs) was then conducted in TA muscle from HSA^{LR} and control mice to identify changes in muscle contractile properties upon treatment. Few type I fibers were present in all the muscles analyzed (data not shown). Mutant muscle displayed a switch to slower fibers (i.e., increased and reduced proportion of IIA and IIB fibers, respectively) compared with control muscle (Figure 8C). However, upon AICAR or rapamycin, there was no significant change in the proportion of the different fiber types in comparison with vehicle-treated mice (Figure 8C).

Since aggregation of (CUG)n-expanded RNA in nuclear foci is a histological hallmark in DM1 diseased muscle, we next wondered whether the treatments affected their accumulation in HSA^{LR} muscle. To this purpose, we performed FISH using a CAG_{10} DNA probe on TA muscle sections from mutant untreated and treated mice. Numerous foci were observed in HSA^{LR} muscle, while none were detected in control muscle (Figure 8D). Interestingly, the number of nuclei showing foci was significantly decreased in muscle from AICAR-treated mutant mice, while no change was observed with rapamycin (Figure 8D). Moreover, foci appeared more diffuse in positive nuclei from mutant muscle upon AICAR treatment, compared with untreated conditions (Figure 8D). Altogether, these results indicate that changes in muscle metabolic and contractile properties do not account for the beneficial effect of the short treatments applied to HSA^{LR} mice, while reduced muscle pathology upon AICAR-mediated acute AMPK activation likely involves nuclear foci dispersion in the mutant muscle.

Discussion

The pathogenic mechanisms underlying DM1 disease are still not well understood, and most investigations so far have focused on splicing defects caused by mRNA toxicity. In this study, we uncovered that in DM1, the AMPK and the mTORC1 pathways are deregulated and that the autophagic flux is perturbed in skeletal muscle. Most importantly, we established that AICAR and rapamycin, which interfere with AMPK/mTORC1 signaling, ameliorate DM1 muscle function (Figure 9).

AMPK signaling and PKB/Akt–mTORC1 signaling are central metabolic pathways in muscle cells, and their deregulation has been related to muscle alterations and disease (27, 32, 44).

We found that DM1 muscle shows an altered response to energy/nutrient-deprived conditions, with impaired AMPK activation and abnormal activation of mTORC1 signaling. Although we have not studied the upstream mechanisms involved in this deregulation, mis-splicing–dependent CaMKII deficiency could well account for the limited AMPK activation in DM1 muscle (21, 23–26). Interestingly, Jones et al. recently reported increased GSK3β levels and activity in HSA^{LR} muscle (45), which may also contribute to the perturbation of AMPK in DM1 muscle (46). In parallel, AMPK constitutes an upstream regulator of mTORC1 (47), and its deregulation could thus be responsible for abnormal mTORC1 activation in DM1 muscle cells. Nonetheless, as we did not detect changes in 4E-BP1 levels or mTOR phosphorylation in mutant muscle, evidence that the state of mTORC1 is modified in DM1 muscle and not only the activation of its downstream axis p70S6K/S6 is missing. Previous reports suggested that mTORC1 is inhibited in DM1 human neural and muscle cells (14, 17), although results were only obtained in vitro and the underlying mechanisms have not been investigated. On the basis of the abnormal splicing and protein trafficking of the insulin receptor in metabolic tissues in DM1 (15, 16), it has also been hypothesized that PKB/Akt–mTORC1 may be less responsive to insulin. However, results regarding the activation state of PKB/Akt signaling in DM1 human muscle biopsies or cells are conflicting (18, 19). In our experiments, we did not detect changes in PKB/Akt activation or in the expression of *Insr* in HSA^{LR} muscle, suggesting that AMPK/mTORC1 deregulation is independent of insulin receptor deficiency.

Autophagy as a major catabolic process essential for proteostasis has also been suggested to contribute to muscle alterations in DM1 (48). The involvement of autophagy in DM1 was largely deduced from the presence of autophagic vesicles and/or accumulation of autophagic markers in DM1 cells, but usually without dynamic measurement of the autophagic flux (13, 14, 17, 19, 36, 37, 49). In our study, we combined several methods to establish that mild changes in autophagic markers in muscle from HSA^{LR} mice are caused by autophagic flux limitation during the degradation steps. Further, we showed that even prolonged starvation did not fully induce autophagy in mutant muscle. We hypothesize that AMPK- and mTORC1-independent mechanisms contribute to autophagy perturbation, as rapamycin and metformin were not sufficient to normalize the flux in HSA^{LR} mice. Although this autophagy deregulation may contribute to muscle atrophy in DM1, it is unlikely to be the main pathogenic event, as autophagic features were scarce in DM1 muscle biopsies, compared with diseases primarily related to autophagy defects, such as vacuolar myopathies.

Importantly, we identified that AMPK/mTORC1 deregulation likely contributes to alteration of muscle function in DM1. Myotonia, which is due to membrane hyperexcitability, is thought to be caused primarily by mis-splicing and thereby deficiency in the CLC-1 (5, 7, 39, 41). In contrast to a recent report studying cultured human DM1 cells (38), we did not find any effect of metformin on the mis-splicing of DM1-affected genes or on the severe myotonia observed in HSA^{LR} mice. While we cannot rule out that changes in dosage and administration may lead to different results, much higher concentrations may be required to efficiently stimulate AMPK in rodent muscle tissue. Although metformin is commonly used to treat diabetes, clinical evaluation of its effect on muscle function in DM1 patients is lacking. In contrast to metformin, we found a profound effect of AICAR, a more potent AMPK agonist. AICAR led to a strong reduction of myotonia in HSA^{LR} mice, which correlated with improved splicing of the *Clcn1* gene and increased protein levels of the channel. While AMPK activation was related to repression of the RNA-binding protein *Rbm3* in vitro, *Rbm3* expression was unchanged in HSA^{LR} muscle upon AICAR treatment. As we observed dispersion of the nuclear foci formed by the (CUG)n-expanded RNA aggregation after AICAR treatment, the effect of AMPK activation on splicing may be mediated by its interaction with other RNA-binding proteins, such as hnRNP H, which were implicated in foci stability in DM1 (50, 51). Hence, one may argue that AMPK deregulation likely contributes to pathogenesis in DM1 muscle by perturbing RNA-binding proteins and thereby accentuating foci stability and mis-splicing events (52–54). Notably, we cannot rule out that amelioration of muscle relaxation also relies on splicing-independent mechanisms. In particular, changes in sodium- and calcium-activated potassium channels or in Ca^{2+} homeostasis, which have also been suggested to contribute to myotonia in DM1 (55–60), may mediate some of the observed effect. Consistently, AMPK has been shown to modulate chloride and potassium channels in several cell types, including cardiomyocytes (61, 62). Such mechanisms may also contribute to the beneficial effect of rapamycin, as it occurs in the absence of splicing changes. Rapamycin could influence intracellular calcium mobilization by dissociating FKBPs (FK506-binding protein) from RyR1, thereby modifying channel activity (63–65). Although AZD8055-dependent mTORC1 inhibition did not improve muscle relaxation, further investigations are required to rule out the involvement of mTORC1 signaling in myotonia reduction, given the complexity of the signaling.

While muscle weakness is observed in DM1 patients, it was initially not reported in HSA^{LR} mice (5). Consistently, in our study, total muscle force was not affected in mutant mice but we observed reduced specific strength of EDL muscle in HSA^{LR} mice. Both specific and total muscle forces were increased upon AICAR, rapamycin, and AZD8055 treatments in young mutant mice, which may be mediated by mTORC1 inhibition as the signaling was shown to modulate Ca^{2+} homeostasis and excitation-contraction coupling in skeletal muscle (66). Myotonia reduction and increase in muscle force were not caused by modified metabolic and contractile properties of the mutant muscle upon the applied short-term treatments. However, one can hypothesize that the changes expected upon long-term administration of these drugs (i.e., switch toward slower fibers) may further positively affect DM1 muscle function.

In conclusion, we identified that deregulation of AMPK/mTORC1 signaling, together with mild autophagy perturbation, contributes to DM1-associated muscle alterations. We showed that treatments targeting the AMPK/mTORC1 imbalance are beneficial for muscle function, though to varying degrees. Whether alternative AMPK/mTORC1-targeting compounds, as well as changes in the dosage, administration mode, or treatment duration, may further improve muscle function remains to be investigated. As the drugs used in our study can target the pathways body-wide, they may also be beneficial in other tissues and thus may represent new treatment options for DM1.

Methods

Mice. Homozygous mice of the mouse line LR20b carrying about 250 (CTG) repeats within the *HSA* transgene (HSA^{LR}) were obtained from Thornton and colleagues (University of Rochester Medical Center, Rochester, New York, USA) (5). Mice of the corresponding background strain (FVB/N) were used as control. GFP-LC3 HSA^{LR} and GFP-LC3 FVB/N mice were obtained by crossing of GFP-LC3–expressing mice (20) with HSA^{LR} or FVB/N mice. Mice were genotyped for HSA^{LR} transgenes by quantification of *ACTA1* levels normalized to endogenous actin (mouse *Acta1*) in genomic DNA. Mice were maintained in a conventional specific-pathogen–free facility with a fixed light cycle (23°C, 12-hour dark-light cycle). Mice were injected i.p. with colchicine (Sigma-Aldrich; 0.4 mg/kg) for 2 days, rapamycin (LC Laboratories) for 1 day (4 mg/kg) or 7 or 10 days (2 mg/kg), AICAR (Toronto Research Chemicals; 500 mg/kg) for 7 days, or AZD8055 (LC Laboratories; 10 mg/kg) for 10 days. Mice were treated with metformin (Sigma-Aldrich; 300 mg/kg) by gavage for 5 or 10 days. For starvation experiments, mice were sacrificed after 12 hours of food deprivation followed by 4 hours of free access to food (fed), or after 24 or 45 hours of food deprivation but free access to water (starved). In vitro force measurement of EDL and soleus muscles was conducted as previously described (32). Half- and late relaxation times were calculated according to Moyer et al. (8).

Human muscle cells and biopsy samples. Muscle biopsies frozen in nitrogen-cooled isopentane from 3 DM1 patients, aged 33, 34, and 49 years, and from an IBM patient were analyzed and compared with 5 control muscle samples from age-matched individuals showing no clinical signs of DM1 and normal muscle histology. MyoD-transduced fibroblasts from control individuals and patients were cultured in growth medium (DMEM, 10% FBS, 50 μg/ml gentamicin) at 37°C under 5% CO_2. At confluence, transduction into myoblasts was induced by differentiation medium (DMEM, 50 μg/ml gentamicin, 3 μg/ml doxycycline hyclate, 10 μg/ml human recombinant insulin) (67). Myotubes obtained after 10 days were incubated for 3 hours in growth medium (refed), PBS (starved), or PBS supplemented with chloroquine (100 μM).

Western blotting. Cell pellets and muscles powdered in liquid nitrogen were lysed in cold RIPA+ buffer (50 mM Tris-HCl pH 8, 150 mM NaCl, 1% NP-40, 0.5% sodium deoxycholate, 0.1% SDS, 1% Triton X, 10% glycerol, phosphatase and protease inhibitors). Following dosage (BCA Protein Assay, Sigma-Aldrich), proteins were separated on SDS-polyacrylamide gels and transferred to nitrocellulose membrane. Blots were blocked in TBS, 3% BSA, 0.1% Tween-20, and incubated overnight at 4°C with primary antibodies, then for 2 hours with HRP-labeled secondary antibodies. Immunoreactivity was detected using the ECL Western blot detection reagent LumiGLO (KPL) and exposed to Super RX-N films (Fujifilm). Protein expression was normalized to α-actinin, α-tubulin, or the total protein of the corresponding phosphorylated form. Antibodies used are listed in Supplemental Methods.

Polymerase chain reaction. Total RNAs were extracted with the RNeasy Mini Kit (Qiagen), reverse transcribed with the SuperScript III First-Strand Synthesis System (Invitrogen), and amplified with the Power SYBR Green Master Mix (Applied Biosystems) or the Hot FirePol EvaGreen qPCR Mix (Solis BioDyne). Expression of specific spliced or pan transcripts was analyzed by end-point PCR and electrophoresis, or by quantitative PCR with Step One software and normalization to *Actn2* expression. Primers are listed in Supplemental Table 2.

Histology and immunofluorescence. Muscles were frozen in liquid nitrogen–cooled isopentane. Eight-micrometer muscle sections were stained with H&E or NADH, and observed with an upright microscope (DMR, Leica). For immunostaining, sections were unfixed or fixed with 4% paraformaldehyde (PFA), cold acetone, or methanol; for some, microwave antigen retrieval was used. Sections were then blocked in PBS, 3% BSA, incubated sequentially with primary and appropriate secondary fluorescent antibodies (Invitrogen), mounted with Vectashield medium (Vector), and observed with a Leica fluorescent microscope.

GFP-LC3 puncta analysis. For GFP-LC3 detection, mice were perfused with 4% PFA, and muscles were incubated in 30% sucrose overnight. Cryosections were washed and mounted. Images were recorded using a Leica confocal microscope with ×63 or ×100 objectives. The number of GFP-LC3 puncta was counted on the 3D reconstructed images with Imaris (version 8.1.2) software. Seven to twelve image stacks were quantified for each muscle, and the average number of GFP-LC3 puncta per volume unit defined within a single fiber ($20.8 \times 20.8 \times 6.5\ \mu m^3$) was used for statistical analyses. All GFP quantifications were done in a blinded way.

Fluorescence in situ hybridization. FISH was conducted on muscle cryosections as previously described by Batra et al. (68), using a Cy3-CAG_{10} DNA probe. Nuclear foci were observed with a Leica confocal microscope with ×40 and ×100 objectives.

Statistics. Quantitative data are displayed as mean ± SEM of independent samples, with n (number of individual experiments) ≥ 3. Statistical analysis of values was performed using Student's t test or 2-way ANOVA test with Tukey's multiple comparisons test correction, with a 0.05 level of confidence accepted for statistical significance.

Study approval. Muscle biopsies from DM1 patients were obtained from the Neuromuscular Tissue Bank (Department of Neurosciences, University of Padova, Padova, Italy) through the Telethon Network of Genetic Biobanks and the EuroBioBank, in accordance with European recommendation and Italian legislation on ethics. Control and IBM human muscle biopsies were from the Department of Pathology, University Hospital Basel (Basel, Switzerland); their use was approved by the Ethical Committee of the University Hospital Basel. Human fibroblast cell lines were obtained from the platform for immortalization of human cells at the Institut de Myologie (Paris, France). Fibroblasts derived from skin biopsies were obtained from the MyoBank-AFM bank of tissues for research at the Institut de Myologie, a partner in the European Union network EuroBioBank, in accordance with European recommendation and French legislation on ethics. All animal studies were performed in accordance with the European Union guidelines for animal care and approved by the Veterinary Office of the Canton of Basel city (application number 2601).

Author contributions

MB and PC performed most of the experiments, analyzed the data, and wrote the paper with input from all authors. NR, KC, TW, CE, and BE conducted quantitative PCR and Western blot analyses, GFP-LC3 quantification, muscle dissection, cryosections and inorganic staining, and electron microscopy analyses, respectively. SF and CA provided human muscle biopsies. DF developed and provided transduced fibroblasts from DM1 patients. MAR and MS helped conceive the project and edited the manuscript. MS secured funding. PC designed and directed the research project.

Acknowledgments

We thank C.A. Thornton for the generous gift of HSA^{LR} mice, and J. Hench and G. Schweighauser (Institute of Pathology, University of Basel, University Hospital Basel) for their help in preparing electron microscopy samples. We are grateful to S. Lin (Biozentrum, University of Basel) for his technical expertise on muscle force measurement and Imaris software, and to J. Kinter and L. Tintignac (Neuromuscular Research Group, University of Basel, University Hospital Basel) for their constructive comments on the project. We also thank the platform for immortalization of human cells from the Institut de Myologie (Paris, France) for providing human transduced fibroblasts. MHC antibodies, developed by H.M. Blau and S. Schiaffino, were obtained from the Developmental Studies Hybridoma Bank (University of Iowa, Iowa City, Iowa, USA). This work was supported by EuroBioBank and Telethon Network of Genetic Biobanks (grant GTB 12001D to CA), the University of Basel and University Hospital Basel (MS), the University of Basel–Stadt and Basel-Landschaft (MAR), the Neuromuscular Research Association Basel (MS, PC), the Swiss Foundation for Research on Muscle Diseases (MAR, MS), and the Swiss National Science Foundation (PC, MS).

Address correspondence to: Perrine Castets, Biozentrum, University of Basel, Klingelbergstrasse 50/70, CH-4056 Basel, Switzerland. Phone: 41.61.260.22.25; E-mail: perrine.castets@unibas.ch. Or to: Michael Sinnreich, Neuromuscular Research Group, Departments of Neurology and Biomedicine, University of Basel, University Hospital Basel, Klingelbergstrasse 50/70, CH-4056 Basel, Switzerland. Phone: 41.61.265.25.25; E-mail: michael.sinnreich@unibas.ch.

1. Machuca-Tzili L, Brook D, Hilton-Jones D. Clinical and molecular aspects of the myotonic dystrophies: a review. *Muscle Nerve*. 2005;32(1):1–18.
2. Brook JD, et al. Molecular basis of myotonic dystrophy: expansion of a trinucleotide (CTG) repeat at the 3′ end of a transcript encoding a protein kinase family member. *Cell*. 1992;69(2):385.
3. Mahadevan M, et al. Myotonic dystrophy mutation: an unstable CTG repeat in the 3′ untranslated region of the gene. *Science*. 1992;255(5049):1253–1255.
4. Lin X, et al. Failure of MBNL1-dependent post-natal splicing transitions in myotonic dystrophy. *Hum Mol Genet*. 2006;15(13):2087–2097.
5. Mankodi A, et al. Myotonic dystrophy in transgenic mice expressing an expanded CUG repeat. *Science*. 2000;289(5485):1769–1773.
6. Philips AV, Timchenko LT, Cooper TA. Disruption of splicing regulated by a CUG-binding protein in myotonic dystrophy. *Science*. 1998;280(5364):737–741.
7. Mankodi A, et al. Expanded CUG repeats trigger aberrant splicing of ClC-1 chloride channel pre-mRNA and hyperexcitability of skeletal muscle in myotonic dystrophy. *Mol Cell*. 2002;10(1):35–44.
8. Moyer M, Berger DS, Ladd AN, Van Lunteren E. Differential susceptibility of muscles to myotonia and force impairment in a mouse model of myotonic dystrophy. *Muscle Nerve*. 2011;43(6):818–827.
9. Herrendorff R, et al. Identification of plant-derived alkaloids with therapeutic potential for myotonic dystrophy type I. *J Biol Chem*. 2016;291(33):17165–17177.
10. Wheeler TM, et al. Reversal of RNA dominance by displacement of protein sequestered on triplet repeat RNA. *Science*. 2009;325(5938):336–339.
11. Sobczak K, Wheeler TM, Wang W, Thornton CA. RNA interference targeting CUG repeats in a mouse model of myotonic dystrophy. *Mol Ther*. 2013;21(2):380–387.
12. Vignaud A, et al. Progressive skeletal muscle weakness in transgenic mice expressing CTG expansions is associated with the activation of the ubiquitin-proteasome pathway. *Neuromuscul Disord*. 2010;20(5):319–325.
13. Bargiela A, Cerro-Herreros E, Fernandez-Costa JM, Vilchez JJ, Llamusi B, Artero R. Increased autophagy and apoptosis contribute to muscle atrophy in a myotonic dystrophy type1 Drosophila model. *Dis Model Mech*. 2015;8(7):679–690.
14. Beffy P, et al. Altered signal transduction pathways and induction of autophagy in human myotonic dystrophy type 1 myoblasts. *Int J Biochem Cell Biol*. 2010;42(12):1973–1983.
15. Savkur RS, Philips AV, Cooper TA. Aberrant regulation of insulin receptor alternative splicing is associated with insulin resistance in myotonic dystrophy. *Nat Genet*. 2001;29(1):40–47.
16. Llagostera E, et al. Role of myotonic dystrophy protein kinase (DMPK) in glucose homeostasis and muscle insulin action. *PLoS One*. 2007;2(11):e1134.
17. Denis JA, et al. mTOR-dependent proliferation defect in human ES-derived neural stem cells affected by myotonic dystrophy type 1. *J Cell Sci*. 2013;126(pt 8):1763–1772.
18. Li X, Zhang W, Lv H, Wang ZX, Yuan Y. [Activities of Akt pathway and their correlation with pathological changes in myotonic dystrophy]. *Beijing Da Xue Xue Bao*. 2010;42(5):526–529.
19. Loro E, et al. Normal myogenesis and increased apoptosis in myotonic dystrophy type-1 muscle cells. *Cell Death Differ*. 2010;17(8):1315–1324.
20. Mizushima N, Yamamoto A, Matsui M, Yoshimori T, Ohsumi Y. In vivo analysis of autophagy in response to nutrient starvation using transgenic mice expressing a fluorescent autophagosome marker. *Mol Biol Cell*. 2004;15(3):1101–1111.
21. Suenaga K, et al. Muscleblind-like 1 knockout mice reveal novel splicing defects in the myotonic dystrophy brain. *PLoS One*. 2012;7(3):e33218.
22. Du H, et al. Aberrant alternative splicing and extracellular matrix gene expression in mouse models of myotonic dystrophy. *Nat Struct Mol Biol*. 2010;17(2):187–193.
23. Nakamori M, et al. Splicing biomarkers of disease severity in myotonic dystrophy. *Ann Neurol*. 2013;74(6):862–872.
24. Hart PC, et al. MnSOD upregulation sustains the Warburg effect via mitochondrial ROS and AMPK-dependent signalling in cancer. *Nat Commun*. 2015;6:6053.
25. Lee H, et al. NQO1-induced activation of AMPK contributes to cancer cell death by oxygen-glucose deprivation. *Sci Rep*. 2015;5:7769.
26. Raney MA, Turcotte LP. Evidence for the involvement of CaMKII and AMPK in Ca^{2+}-dependent signaling pathways regulating FA uptake and oxidation in contracting rodent muscle. *J Appl Physiol*. 2008;104(5):1366–1373.
27. Bentzinger CF, et al. Differential response of skeletal muscles to mTORC1 signaling during atrophy and hypertrophy. *Skelet Muscle*. 2013;3(1):6.
28. Bentzinger CF, et al. Skeletal muscle-specific ablation of raptor, but not of rictor, causes metabolic changes and results in muscle dystrophy. *Cell Metab*. 2008;8(5):411–424.
29. Kang SA, et al. mTORC1 phosphorylation sites encode their sensitivity to starvation and rapamycin. *Science*. 2013;341(6144):1236566.
30. Roux PP, et al. RAS/ERK signaling promotes site-specific ribosomal protein S6 phosphorylation via RSK and stimulates cap-dependent translation. *J Biol Chem*. 2007;282(19):14056–14064.
31. Kim J, Kundu M, Viollet B, Guan KL. AMPK and mTOR regulate autophagy through direct phosphorylation of Ulk1. *Nat Cell Biol*. 2011;13(2):132–141.
32. Castets P, et al. Sustained activation of mTORC1 in skeletal muscle inhibits constitutive and starvation-induced autophagy and causes a severe, late-onset myopathy. *Cell Metab*. 2013;17(5):731–744.
33. Masiero E, et al. Autophagy is required to maintain muscle mass. *Cell Metab*. 2009;10(6):507–515.
34. Klionsky DJ, et al. Guidelines for the use and interpretation of assays for monitoring autophagy. *Autophagy*. 2012;8(4):445–544.
35. Ueda H, et al. Decreased expression of myotonic dystrophy protein kinase and disorganization of sarcoplasmic reticulum in skeletal muscle of myotonic dystrophy. *J Neurol Sci*. 1999;162(1):38–50.
36. Swash M, Fox KP. Abnormal intrafusal muscle fibres in myotonic dystrophy: a study using serial sections. *J Neurol Neurosurg Psychiatr*. 1975;38(1):91–99.
37. Ludatscher RM, Kerner H, Amikam S, Gellei B. Myotonia dystrophica with heart involvement: an electron microscopic study of skeletal, cardiac, and smooth muscle. *J Clin Pathol*. 1978;31(11):1057–1064.
38. Laustriat D, et al. In vitro and in vivo modulation of alternative splicing by the biguanide metformin. *Mol Ther Nucleic Acids*. 2015;4:e262.

39. Wheeler TM, Lueck JD, Swanson MS, Dirksen RT, Thornton CA. Correction of ClC-1 splicing eliminates chloride channelopathy and myotonia in mouse models of myotonic dystrophy. *J Clin Invest*. 2007;117(12):3952–3957.
40. Lueck JD, et al. Chloride channelopathy in myotonic dystrophy resulting from loss of posttranscriptional regulation for CLCN1. *Am J Physiol Cell Physiol*. 2007;292(4):C1291–C1297.
41. Charlet-BN, Savkur RS, Singh G, Philips AV, Grice EA, Cooper TA. Loss of the muscle-specific chloride channel in type 1 myotonic dystrophy due to misregulated alternative splicing. *Mol Cell*. 2002;10(1):45–53.
42. Pauly M, et al. AMPK activation stimulates autophagy and ameliorates muscular dystrophy in the mdx mouse diaphragm. *Am J Pathol*. 2012;181(2):583–592.
43. Lee CS, et al. Ligands for FKBP12 increase Ca^{2+} influx and protein synthesis to improve skeletal muscle function. *J Biol Chem*. 2014;289(37):25556–25570.
44. Grumati P, et al. Autophagy is defective in collagen VI muscular dystrophies, and its reactivation rescues myofiber degeneration. *Nat Med*. 2010;16(11):1313–1320.
45. Jones K, et al. GSK3β mediates muscle pathology in myotonic dystrophy. *J Clin Invest*. 2012;122(12):4461–4472.
46. Suzuki T, et al. Inhibition of AMPK catabolic action by GSK3. *Mol Cell*. 2013;50(3):407–419.
47. Inoki K, Zhu T, Guan KL. TSC2 mediates cellular energy response to control cell growth and survival. *Cell*. 2003;115(5):577–590.
48. Castets P, Frank S, Sinnreich M, Rüegg MA. "Get the balance right": pathological significance of autophagy perturbation in neuromuscular disorders. *J Neuromuscul Dis*. 2016;3(2):127–155.
49. Dunne PW, Ma L, Casey DL, Harati Y, Epstein HF. Localization of myotonic dystrophy protein kinase in skeletal muscle and its alteration with disease. *Cell Motil Cytoskeleton*. 1996;33(1):52–63.
50. Kim N, et al. AMPKα2 translocates into the nucleus and interacts with hnRNP H: implications in metformin-mediated glucose uptake. *Cell Signal*. 2014;26(9):1800–1806.
51. Kim DH, Langlois MA, Lee KB, Riggs AD, Puymirat J, Rossi JJ. HnRNP H inhibits nuclear export of mRNA containing expanded CUG repeats and a distal branch point sequence. *Nucleic Acids Res*. 2005;33(12):3866–3874.
52. Zou T, et al. Polyamines modulate the subcellular localization of RNA-binding protein HuR through AMP-activated protein kinase-regulated phosphorylation and acetylation of importin alpha1. *Biochem J*. 2008;409(2):389–398.
53. Wang W, et al. AMP-activated kinase regulates cytoplasmic HuR. *Mol Cell Biol*. 2002;22(10):3425–3436.
54. Finley J. Alteration of splice site selection in the LMNA gene and inhibition of progerin production via AMPK activation. *Med Hypotheses*. 2014;83(5):580–587.
55. Santoro M, et al. Alternative splicing alterations of Ca^{2+} handling genes are associated with Ca^{2+} signal dysregulation in myotonic dystrophy type 1 (DM1) and type 2 (DM2) myotubes. *Neuropathol Appl Neurobiol*. 2014;40(4):464–476.
56. Vihola A, et al. Altered expression and splicing of Ca(2+) metabolism genes in myotonic dystrophies DM1 and DM2. *Neuropathol Appl Neurobiol*. 2013;39(4):390–405.
57. Kimura T, et al. Alternative splicing of RyR1 alters the efficacy of skeletal EC coupling. *Cell Calcium*. 2009;45(3):264–274.
58. Kimura T, et al. Altered mRNA splicing of the skeletal muscle ryanodine receptor and sarcoplasmic/endoplasmic reticulum Ca^{2+}-ATPase in myotonic dystrophy type 1. *Hum Mol Genet*. 2005;14(15):2189–2200.
59. Tang ZZ, et al. Muscle weakness in myotonic dystrophy associated with misregulated splicing and altered gating of Ca(V)1.1 calcium channel. *Hum Mol Genet*. 2012;21(6):1312–1324.
60. Franke C, Hatt H, Iaizzo PA, Lehmann-Horn F. Characteristics of Na^+ channels and Cl^- conductance in resealed muscle fibre segments from patients with myotonic dystrophy. *J Physiol (Lond)*. 1990;425:391–405.
61. Andersen MN, Rasmussen HB. AMPK: a regulator of ion channels. *Commun Integr Biol*. 2012;5(5):480–484.
62. Sukhodub A, et al. AMP-activated protein kinase mediates preconditioning in cardiomyocytes by regulating activity and trafficking of sarcolemmal ATP-sensitive K(+) channels. *J Cell Physiol*. 2007;210(1):224–236.
63. Kaftan E, Marks AR, Ehrlich BE. Effects of rapamycin on ryanodine receptor/Ca(2+)-release channels from cardiac muscle. *Circ Res*. 1996;78(6):990–997.
64. Avila G, Dirksen RT. Rapamycin and FK506 reduce skeletal muscle voltage sensor expression and function. *Cell Calcium*. 2005;38(1):35–44.
65. Brillantes AB, et al. Stabilization of calcium release channel (ryanodine receptor) function by FK506-binding protein. *Cell*. 1994;77(4):513–523.
66. Lopez RJ, et al. Raptor ablation in skeletal muscle decreases Cav1.1 expression and affects the function of the excitation-contraction coupling supramolecular complex. *Biochem J*. 2015;466(1):123–135.
67. Chaouch S, et al. Immortalized skin fibroblasts expressing conditional MyoD as a renewable and reliable source of converted human muscle cells to assess therapeutic strategies for muscular dystrophies: validation of an exon-skipping approach to restore dystrophin in Duchenne muscular dystrophy cells. *Hum Gene Ther*. 2009;20(7):784–790.
68. Batra R, et al. Loss of MBNL leads to disruption of developmentally regulated alternative polyadenylation in RNA-mediated disease. *Mol Cell*. 2014;56(2):311–322.